University of Stavanger

Faculty of Science and Technology

MASTER'S THESIS

Study program/Specialization: Petroleum Engineering / Drilling and Well Technology	Spring semester, 2016 Open
Writer: Shirin Charlotte Forthun	…… (Writer's signature)
Faculty supervisor: Mesfin Belayneh	
Thesis title: **Effect of Nano Additives on Friction in a Bentonite Water Based System**	
Credits (ECTS): 30	
Key words: Rheology Friction reduction Nano TiN Nano MoS_2 Nano Graphene Hydraulics Torque and Drag Viscoelasticity Polymers: XG, CMC	Pages: 176 + enclosure: 38 Stavanger, 13/06/2016 Date/year

Acknowledgements

First of all, I would like to thank my supervisor Mesfin Belayneh for his never-ending guidance and care for the students. Your knowledge and support through the entire process of writing and working on my thesis has been of very great help, and has motivated me to stay on the right track the entire time.

I would also like to thank the University of Stavanger for providing me with their facilities for laboratory and simulation works. Furthermore, I would like to express my gratitude towards my family who has supported me through my entire degree and always helped me when I was in need of it.

Finally, I would like to thank my proof readers Elham Baghestan and Sigrunn Lund for taking the time to read through my thesis and give me pointers. Your time and effort has been very much appreciated.

Abstract

This thesis will present relevant literature study and theory for the experimental and simulation parts. Several water based drilling fluids containing high and low concentrations of TiN, MoS_2 and Graphene in nano-size were formulated and characterised in terms of rheology, frictional behaviour, viscoelasticity and filtrate loss. A performance simulation study on torque, drag and hydraulics were executed for the best selected fluid systems. From overall studies, the results show among others that:

- The nano type and concentration in various polymers improve the conventional drilling fluid system in terms such as rheology, lubricity and viscoelastic properties.
- The addition of 0.04 wt% and 0.16 wt% of MoS_2 in the conventional fluid system resulted in a friction reduction of 34.8% and 44.7% respectively. In terms of torque and drag reduction, the simulation results exhibited that the fluids allow for 15.2% and 25.9% extended drilling as compared to the conventional nano-free system.
- The addition of 0.03 wt% and 0.04 wt% of TiN in the conventional fluid system resulted in a friction reduction of 23.6% and 16.7% respectively. In terms of torque and drag reduction, the simulation results exhibited that the fluids allow for 9.9% and 14.5% extended drilling as compared to the conventional nano-free system.
- The addition of 0.01 wt% and 0.02 wt% of Graphene in the conventional fluid system resulted in a friction reduction of 8.3% and 10.1% respectively. In terms of torque and drag reduction, the simulation results exhibited that this fluid allows for 4.0% and 4.7% extended drilling as compared to the conventional nano-free system.
- All of the tested fluids exhibited the best friction reduction with low concentrations of nano. Rheology testing exhibited that the filtrate loss decreased for very low concentrations of TiN and MoS_2, while it increased for higher concentrations. The filtrate loss increased for all concentrations of Graphene.

The objective of this thesis was to investigate if it was possible to improve the rheology and the lubricating effect of conventional water based mud by adding nanoparticles to the fluid system. The results show that the application of nano in a bentonite water based system could have the potential to replace the oil based mud in terms of low friction performance.

Table of Contents

1 Introduction

Drilling fluids are essential for a drilling operation, and always applied when drilling oil and gas wells. The two most commonly used drilling fluid types are water based mud (WBM) and oil based mud (OBM). Three key factors to determine the type of fluid used to drill a well are technical performance, environmental impact and cost. WBM is the most commonly applied fluid when drilling, as it is cheaper and more environmentally friendly. With the right additives, WBM may perform just as well as OBM in order to prevent critical drilling problems. But OBM lubricates the drill-string and the bit better and may provide an increased rate of penetration (ROP) compared to WBM. It is also a known fact that the coefficient of friction in OBMs is of a lower value than WBM's.

With maturing fields and a rapid growth in technology, operators are increasingly drilling wells of more challenging profiles. Wells in harsher environments such as extreme water depth and drilling depth, high pressure high temperature (HPHT) formations and long reach inclined and/or horizontal sections are becoming more common [1]. From a technical performance perspective, OBM may be preferable for a drilling operation compared to WBM, but the fluid system possesses some environmental challenges. The environmental policies in Norway allow the use of OBM, but the mud should be properly disposed. This is time-consuming and costly.

As of today, the application of nanotechnology has proven results in several fields of science and in several industries such as biomedicine. Nanotechnology has also been implemented in the petroleum industry, and preliminary tests show positive effect in cement, drilling fluids and on enhanced oil recovery. This thesis will present an investigation of the effect of nanoparticles in two bentonite based fluid systems. Several conventional and nano-enhanced WBM systems were formulated and tested. The systems were evaluated with various concentrations of nano, and with two types of polymers. The main objective of this thesis was to improve the conventional WBM system by the use of nanoparticles to provide possible lubricity properties. The formulated fluids rheology, frictional coefficient and viscoelasticity were investigated by experiments. Additionally, a simulation study of torque, drag and hydraulic performance was executed.

1.1 Background

The purpose of drilling a well is to connect the reservoir to the surface and recover potential hydrocarbons. The objective when drilling a well is to drill the hole as fast as possible without encountering any drilling problems or accidents. Drilling the wellbore is the first and most expensive step when connecting the reservoir to surface. The drilling process represents as much as 25% of the total exploitation cost, while the drilling fluid represents about 15-18% of the total drilling cost [58]. Three important qualities that the drilling fluid should comply with is that it should not be too expensive, it should play several functions simultaneously and it should be environmentally friendly. It is therefore of interest to develop solutions that make the total operation cost cheaper and more friendly to the environment.

During conventional drilling operations, high-pressure mud pumps contribute to circulate the drilling fluid through the well circulation system. It is pumped from mud pits through the standpipe, rotary house and swivel. Further, it flows through the Kelly, drill-string, drill collar and across the bit. When it enters the annulus, it flows up the annular clearance to the surface. The circulation system is illustrated in Figure 1.1.

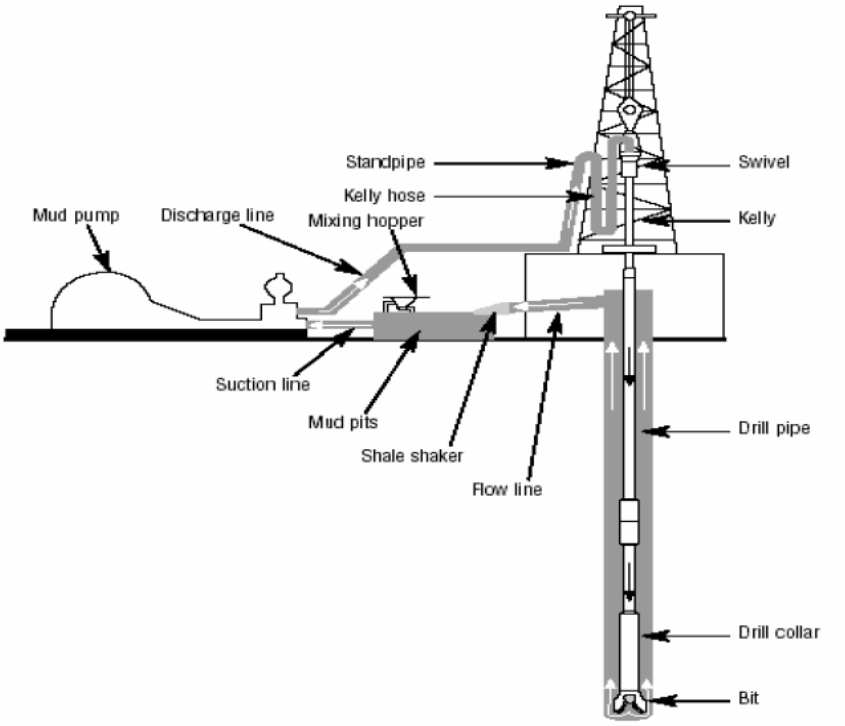

Figure 1.1: Drilling fluid circulation system [57]

The circulation process is essential for well cleaning, as the drilling fluid transport cuttings from the bottom of the well to the surface. The fluid has other important tasks as lubricating and cooling of the bit, prevent formation damage and maintain the pressure in the borehole within the safe operational window. The safe operational window is limited by the pore pressure gradient and the fracture pressure gradient. If the well pressure is lower or equal to the formation pore pressure, formation fluids may influx the well due to the pressure differentials. The well is also in risk of collapse. If the well pressure is higher than the formation fracture pressure, situations such as formation fracturing or differential sticking may occur. It is therefore crucial to maintain the well pressure within the allowable operational window. The operational window will be affected by harsher environments such as HPHT environments, extreme water and drilling depths and by horizontal or inclined wells. The well pressure is determined by the equivalent circulation density. This is more thorough described in chapter 3.8.

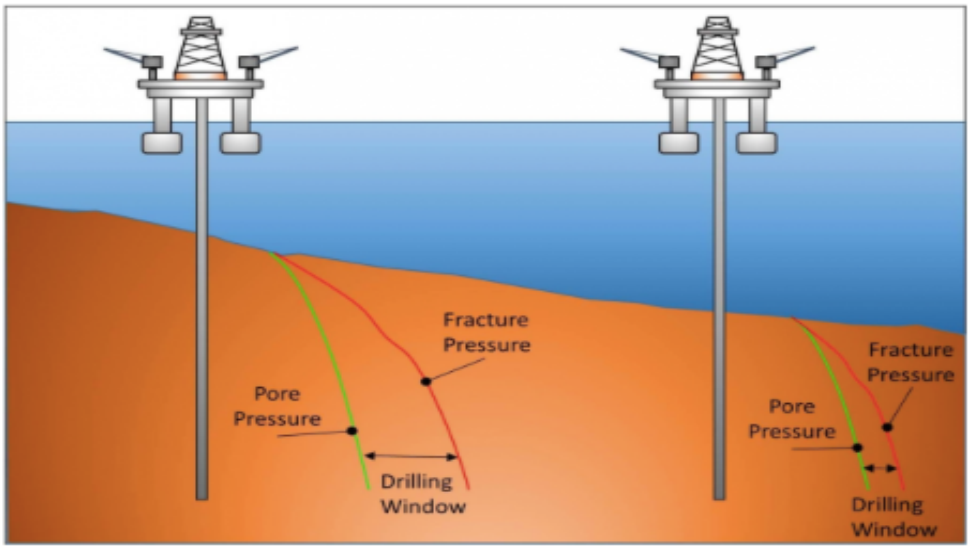

Figure 1.2: Illustration of the drilling window and a narrower window with greater depths [58]

A properly designed fluid makes a good filter cake on the wellbore walls. The optimal cake should be thin, firm and impenetrable. This prevents too much fluid from entering the formation, increase the well strength and avoid well stability issues. If the designed mud possesses a friction coefficient of lower values, the fluid will act lubricating on the materials used for the operation, and reduce the probability of differential sticking. A lower coefficient of friction also makes it easier to break the pull force that keeps the pipe stuck. It is therefore important to gain knowledge about the drilling fluid, as it is essential to avoid drilling problems.

1.2 Problem formulation

Nanotechnology may improve the performance of conventional technology. The research within the petroleum industry is still in its early stages. Authors and experimental studies have illustrated the effect of implementing nanoparticles in both WBM and OBM systems. Since the environmental and cost impact of applying OBM on the Norwegian Continental Shelf (NCS) poses challenges, the application of nanoparticles in conventional WBM to improve the system properties creates a potential research activity.

This thesis consists primarily of laboratory work. Water based fluid systems were created realistically with both salt, clay and polymers added to the solution. Some types of nanoparticles were added to the fluid systems. These were Titanium Nitride (TiN), Molybdenum Disulphide (MoS_2) and Graphene of different concentrations. This thesis will address issues such as:

- Effect of nano on the rheology of the drilling fluids.
- Effect of nano on the friction of the drilling fluids.
- Effect of nano on the viscoelastic behaviour of the fluid systems.

1.3 Scope and Objective

The primary objective of this thesis is to formulate nano-based fluid systems containing TiN, MoS_2 and Graphene to enhance the frictional properties of the conventional WBM system. The scope of this thesis is limited to experimental and simulation activities. The activities are:

- Literature review the different water based mud components.
- Review the rheology and hydraulics model to be used for evaluation of the formulated drilling fluids.
- Formulate nano-based drilling fluids and characterise their rheological, filtrate, pH and viscoelastic behaviour.
- Characterise the frictional behaviour of the nano-enhanced drilling fluids.
- Perform torque, drag and hydraulic simulation studies on the best formulated drilling fluids according to the experimental tests.

1.4 Investigation methodology

The effect of nanoparticles in a conventional, non-weighted drilling fluid system will be investigated. To meet the thesis objectives, the investigation method consists of mainly two parts:

- Part 1: Experimental studies.
- Part 2: Performance simulation.

The idea of the experimental part was to formulate mud systems containing nanoparticles that exhibited favourable friction properties. The rheology, filtrate and frictional properties were to be studied, followed by the viscoelastic properties of the best mud systems in terms of friction. The performance of the mud was tested and simulated with respect to torque, drag and hydraulics. Different rheology models were analysed to find the most suitable model for the drilling fluids formulated.

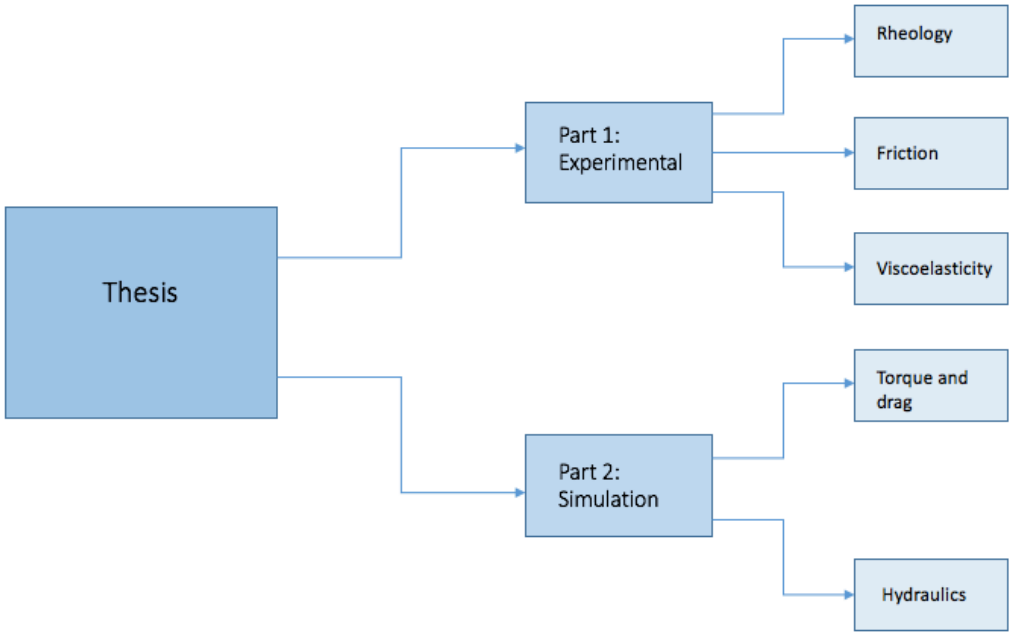

Figure 1.3: Thesis methodology

2 Literature Study

This chapter will present literature that is associated with drilling fluids and additives. It also includes sections with case studies that are relevant for further experimental and simulation work in this thesis.

2.1 Drilling Fluid

The term drilling fluid describes all of the compositions used to drill and remove cuttings from a wellbore [1]. Some typical types of drilling fluids are water, brine and mud. Drilling mud is most frequently used, especially for less shallow sections where the pore pressure gradient value of the formation exceeds the density value of fresh- and/or seawater and where there is a need of a filtrate cake.

Some of the essential functions and features of the drilling fluid are [2]:

- Prevent a kick, or formation fluid influx in the borehole and prevent fraction/collapse of the borehole by maintaining a stable well pressure.
- Transport drill cuttings from the well to surface and prevent cuttings bedding.
- Prevent loss of drilling fluid to formation by forming a thin and impenetrable filtrate cake on the formation wall.
- Keeping weight material and cuttings floating during circulation stop.
- Lubricate and cool the drill-string and drill-bit.
- Protect and stabilise the formation.
- Provide the casing and drill-string with buoyancy.
- Corrosion control.
- Ensure maximal borehole information.

As described, WBM and OBM are the two most commonly used drilling fluid types. In OBM's, the oil function as the continuous phase while the water is in a dispersed state. This is also called an invert-emulsion system. The amount of water in OBM's may vary from 0.1% to 50% [2]. The WBM's may contain oil as an additive, with an emulsion system where oil is dispersed in the water.

2.2 Drilling Problems

It is usual to encounter foreseen and unforeseen problems during the drilling process. These problems may lead to increased costs partly due to non-productive time (NPT). Some drilling problems with description are presented in Table 2.1 [3]. Differential-pressure sticking and drill-pipe failure are further explained in section 2.2.1 and 2.2.2. Table 2.1 describes some common drilling problems.

Drilling problem	Description
Mechanical pipe sticking	A stuck pipe due to mechanical reasons such as drill cut beddings, borehole instabilities and key seating. Clay swelling may also contribute to mechanical pipe sticking.
Differential-pressure sticking	A portion of the drill-string becomes embedded in the mud-cake due to the mud pressure exceeding the formation pore pressure.
Lost circulation	Uncontrolled flow of mud into the formation. This may happen partially or in total depending on the returns to surface (some return and no return respectively). This is a regular problem when encountering high permeability zones and formations that are inherently fractured. It may also happen during improper drilling conditions with induced fractures.
Hole deviation	The reason for this drilling problem is not exactly known, but it occurs when the drill bit deviates from it's intended path unintentionally. Some factors like hole inclination, bit hydraulics and improper hole cleaning is thought to be the reason.
Drill-pipe failure	May occur due to excessive torque, burst and/or collapse due to excessive external and/or internal pressure, excessive drag or fatigue due to mechanical cyclic loads
Borehole instability	Borehole instability is the definition of an open-hole drilled section that does not maintain its structural integrity and/or its gauge size and shape. It is important with proper circulation and proper mud-weight to keep the wellbore from collapse, washouts and fracturing. Encountering salt formations may also be a problem as salt is highly soluble in water.

Table 2.1: Listing of some frequently encountered drilling problems [3].

2.2.1 Differential-Pressure Pipe Sticking

The encountered complications related to a stuck pipe may account for almost a half of the total well costs. The drilling problem is often related to improper well control and loss of circulation, and it is a significant risk of differential-pressure pipe sticking to occur in highly inclined or in horizontal wells [4].

Differential-pressure pipe sticking occurs when drilling through depleted zones, and the annulus pressure exceeds the formation pressure. The drill-string will be pulled against the borehole wall and embedded in the present filtrate cake. The pressures in the contact zone between the filtrate cake and the drill-string will decrease, and the pipe will be held against the wall by the differential pressure [4].

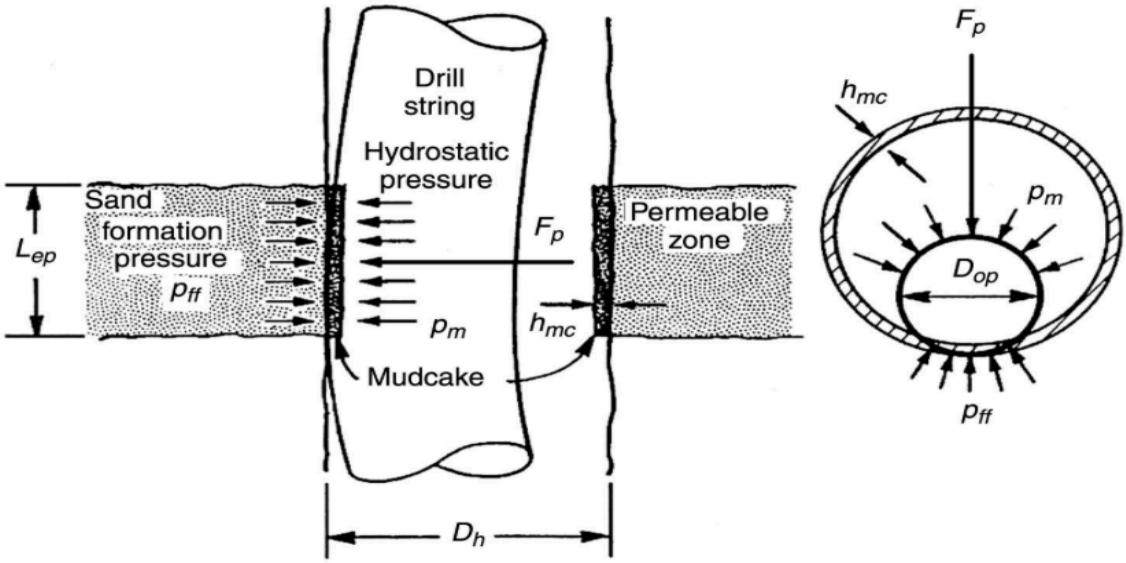

Figure 2.1: Illustration of a stuck pipe with related parameters [3]

The differential pressure may be expressed as the following [3]:

$$\Delta P = P_m - P_{ff} \tag{2.1}$$

Where ΔP equals the differential pressure, P_m equals the hydrostatic well pressure and P_{ff} equals the formation fluid pressure [3].

The pull force that is required to free the stuck pipe is expressed as the following [3]:

$$F_p = \mu_f \Delta P A_c \quad (2.2)$$

Where F_p equals the pull force, μ_f equals the coefficient of friction, A_c equals the contact area between the pipe and filtrate cake surface and ΔP equals the differential pressure [3].

From these equations it is possible to see that the lower the friction coefficient, the less required pull force to free the pipe from the filtrate cake. To prevent or to mitigate the differential sticking as a drilling problem, it is essential to select a mud system that will yield a filtrate cake that is smooth. This is obtained by a mud system with a low coefficient of friction [3]. As OBM acts lubricating it may mitigate this very costly, and more frequently occurring, problem more efficiently then regular WBM.

2.2.2 Drill-Pipe Failure

Some of the parameters that may lead to drill-pipe failure are twist-off caused by excessive torque (torque is further explained in section 3.7.2) or parting due to excessive tension (tension and drag are further explained in section 3.7.1).

A twist-off is a type of pipe failure caused by induced shear stress due to high torque. This happens if the torque exceeds the ultimate shear stress of the material, and this excessive torque is mainly a problem during directional- and extended reach drilling [3].

A pipe-parting failure will occur if the tensile stress of the pipe exceeds the ultimate tensile stress of the pipe-material This is a condition that may occur with pipe-sticking, and an over-pull is applied in addition to the effective weight of suspended pipe in the hole above the stuck point [3]. The drilling fluid must act lubricating to reduce the risk of pipe-sticking and over-pull. This to ensure minimal occurrence of pipe-parting failure.

2.3 Clays in Drilling Fluids

Clay is encountered in two different scenarios in the petroleum industry; drilling in argillaceous formations and as an additive in drilling fluids. Clay is an important colloidal additive in drilling fluids and is added to provide wanted viscosity, increase the density and modify the filtrate loss properties [5]. It is used in almost every form of WBM's, but is frequently also used in OBM's [6].

For this thesis, bentonite is the only clay additive used in the formulated drilling fluids. Bentonite will be further described in the next sections.

2.3.1 Bentonite

As an industrial material, bentonite is defined as a clay consisting of Smectite group minerals [7]. These minerals were earlier referred to as Montmorillonite, and the name is still used in the petroleum industry today [2]. The bentonite name was first proposed by Knight in 1898, and is named after Benton Shale where the clay was thought to have occurred [7].

Bentonite is classified in two categories, swelling (sodium) or non-swelling (calcium). Bentonite clay containing Na^+ ions as the dominant and exchangeable cat ion will swell in water, while there will be a significant swelling decrease in bentonite clays containing Ca^{2+} as the dominant and exchangeable cation [7]. The bentonite type classified as swelling have extensive water absorption properties and the swelled particles obtain the ability to remain suspended in water dispersions for great amounts of time [8]. As an additive in fluid this may help to increase the fluid viscosity. When bentonite swells, the clay particles increase its size several times the original particle volume and it forms thixotropic gels with water [8]. Thixotropic gel is pertained to the drilling fluid's ability to develop gel strength when it is not exposed to shearing [9]. In the petroleum industry, bentonite is one of the additives used in drilling fluids to obtain wanted viscosity and to control filtrate losses to formation [2]. Bentonite is not considered a weight material as it does not increase the fluid density significantly.

2.3.2 Bentonite Structure

As mentioned, the dominating mineral in bentonite is Montmorillonite, but bentonite may also contain up to 50% of the minerals Illitt and Kaolinitt. Non-clay minerals may also be represented in quantities up to 10-30% [2]. The thixotropic and swelling properties are caused by the Montmorillonite minerals present in the Bentonite. In Figure 2.2 the chemical composition of commercial bentonite is presented.

Chemical composition in %			
	Wyoming "Volclay"	*Panther Creek Mississippi*	*Ponza, Italy*
Silica, SiO_2	64.32	64.00	67.42
Alumina, Al_2O_3	20.74	17.10	15.83
Ferric oxide, Fe_2O_3	3.03	} 4.70 {	0.88
Ferous oxide, FeO	0.46		-
Titanium dioxide, TiO_2	0.14	1.50	-
Lime, CaO	0.50	3.80	2.64
Magnesia, MgO	2.30	0.50	1.09
Potash, K_2O	0.39	0.20	}1.09
Soda, Na_2O	2.59	-	
Phosphoric anhydride, P_2O_5	0.01	-	-
Sulfuric anhydride, SO_3	0.35	0.20	0.01
Other minor constituents	0.01	8.00	-
Combined water	5.14	64.00	10.88

Figure 2.2: Composition of commercial bentonite [8]

Most of the clay minerals are constructed using two fundamental building structures. The clay mineral properties are represented by the combination of building structures and chemical modification. These fundamental structures are called the octahedral layer and the tetrahedral layer [2].

The octahedral layer is a two-plane structure packed with either hydroxyl molecules (OH) or oxygen (O). The OH molecules or O atoms surrounds Alumina (A) and builds up an octahedral structure [2]. The tetrahedral layer consists of OH or O in the corners of a tetrahedral structure, with a Silica (Si) atom placed in the gravity centre of the tetrahedral. Several of these structures may be combined in larger aggregates in a hexagonal structure [2]. A sketch of the Montmorillonite crystalline structure is presented in Figure 2.3. Both the tetrahedral and octahedral layer structure is represented in this Figure [6].

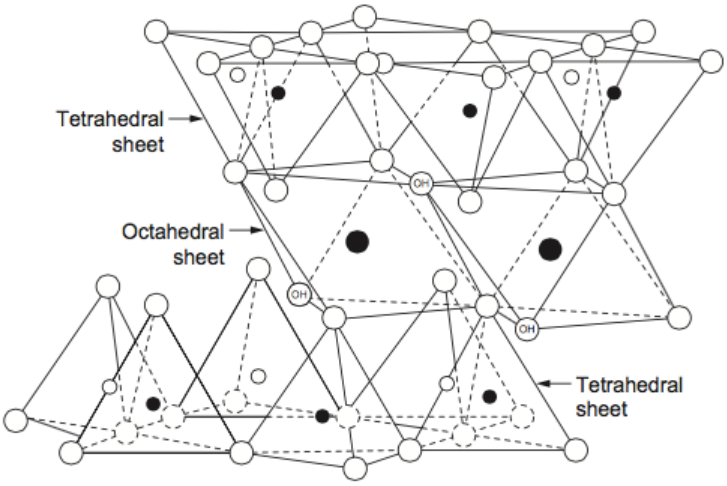

Figure 2.3: Montmorillonite crystalline structure [6]

2.3.3 Bentonite Particle Associations

The clay particle behaviour in the drilling fluid is important as it may influence important drilling fluid parameters such as the viscosity, yield point and the filtrate loss [5]. There are four typical states of clay particle behaviour in the drilling fluid. These particle arrangements will be described in the following section and illustrated in Figure 2.4.

2.3.3.1 Flocculated system

A system where the particles are suspended and contains net attractive forces will be called flocculated. The particles are formed in clusters where they are connected end-to-end or surface-to-surface. The particles will form a three dimensional, loose network between themselves. When the bentonite system is flocculated, the viscosity will increase and the yield point will increase significantly. Dispersed drilling fluid systems may flocculate [5].

2.3.3.2 Deflocculated system

A fluid system is deflocculated when the net forces in the system only consist of repelling forces between the particles. It is possible to obtain a deflocculated system by implementing particles of the same charge or by adding deflocculating chemicals. These chemicals will neutralize the particles and disperse the clay plates. Alkaline conditions will create a negative net charge in the fluid systems. The yield point values of a deflocculated bentonite drilling fluid will be low [5].

2.3.3.3 Dispersed system

A solute with particles in suspension is dispersed when all the particles are split from packing. The particles may have negative and positive end-charges which depends on the pH value. A dispersed system may be both flocculated and deflocculated. When bentonite swells in water, the clay is close to a dispersed state. This is ideal, as a good bentonite drilling fluid is dispersed and deflocculated [5].

2.3.3.4 Aggregated system

In an aggregated system, the particles are bound together in aggregates. The sheet structure of the clay is assembled and packed together. When the clay is in contact with water, the hydration process and the mechanical influence might separate the clay sheets. The clay sheets may be flocculated or deflocculated as a result [5].

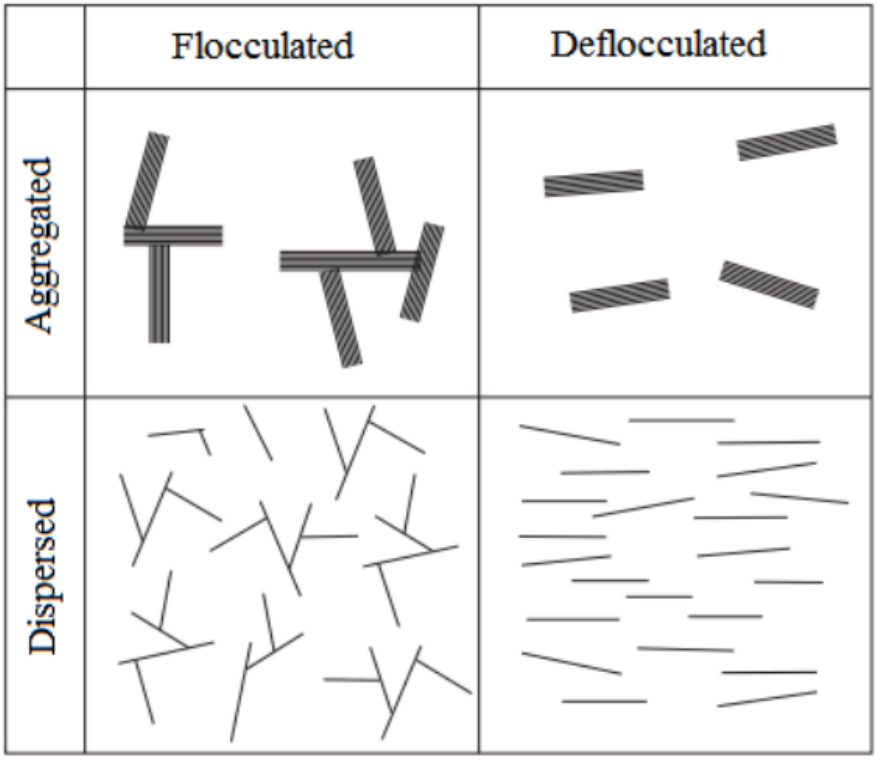

Figure 2.4: Clay particle arrangement in drilling fluids [5]

2.4 Polymers

The history of using polymers as an additive in drilling fluid formulations goes as far back as to the 1930s when corn starch was added in a formulation for fluid loss control. This has resulted in polymers being applicable in nearly all the water based drilling fluid systems today, and some systems are solely dependent on polymers. Adding polymers to clay suspensions is of great interest in the petroleum industry due to the polymer's capacity to modify the drilling fluid's colloidal and rheological properties [10].

A polymer is defined as a large molecule where small and identical units are repeated [10]. The units are called monomers, and a polymer consists of several monomers that are combined and joined together. The polymerization degree is represented by the number of monomers present in the polymer structure [10]. The polymer additives in drilling fluids may be classified according to their chemistry, by their function or by their origin. Some examples are illustrated in Table 2.2.

Chemistry	Function	Origin
· Anionic · Nonionic	· Viscosifier · Filtration control	· Naturally occurring · Synthetically derived · Modified naturally occurring

Table 2.2: Classification of polymers [10]

The polymer structures are also divided into three categories: Linear, branched or crosslinked. The possible structural variations of the polymers are infinite, and some of the variations that may affect the polymer's performance are [10]:

- The type of monomer or monomers.
- The molecular weight.
- Type of subsequent chemical polymer modification.
- Extent of subsequent chemical polymer modification.
- The number of branching or crosslinking groups in the polymer chain.

The three categories of polymer structures are illustrated in Figure 2.5.

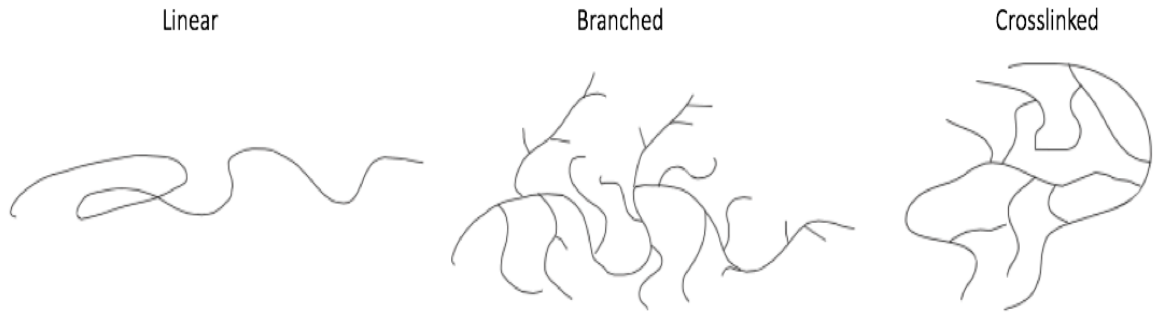

Figure 2.5: Illustration of polymer structures [10]

Polymer additives in drilling fluids may also possess the ability to reduce formation clay swelling by behaving inhibitive. Clay particles can adsorb larger molecule units and the polymer molecule units may plug cracks and pores in the clay formation. This restricts the clay formation from adsorbing water and swell [5]. The next sections will describe the polymers used as an additive for the experimental studies

2.4.1 CMC

Cellulose is an insoluble natural polymer that is modified to be useful as an additive in drilling fluids. Cellulose derivatives in drilling fluids are used due to the biodegradable properties and it being compatible with other materials [11]. It is added as a viscosifier and a fluid loss additive [10]. Cellulose is modified to Carboxymethylcellulose (CMC) by introducing anionic carboxymethyl to the cellulose ring structure. The sodium salt part of monochloroacetic acid (ClCH2COONa) will react with the cellulose and create CMC by a substitution, most often at the $–CH_2OH$ group of the cellulose structure. This modification makes the additive a water-soluble polyelectrolyte [10]. The structure of CMC is linear and the molecular formula is $[C_6H_7O_2(OH)_2CH_2COONa]_n$. The cellulose and CMC structure is illustrated in Figure 2.6 [10].

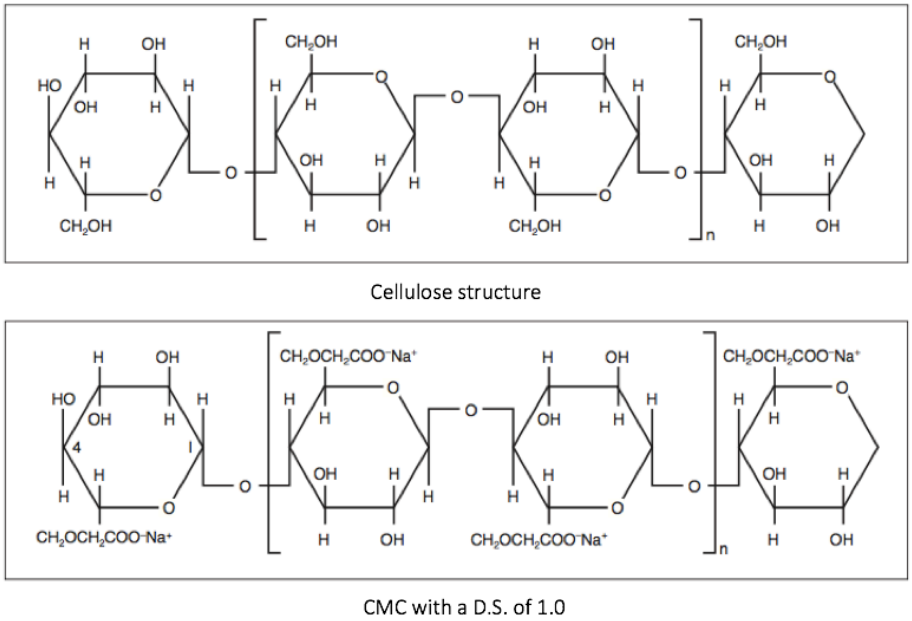

Figure 2.6: Cellulose and CMC structure [10]

The repeated ring structure defines the polymer, and the degree of polymerisation (D.P.) represents the number of times the ring structure is repeated. The molecular weight of the polymer will increase with a larger value of D.P.; hence the viscosity will increase. This means that high-viscosity CMC will have a higher molecular weight than low-viscosity CMC [10].

The number of substitutions that occur on a single ring structure represents the degree of substitution (D.S.). In the CMC structure illustrated in Figure 2.6, one substitution per ring structure occurs, hence the D.S. of 1.0. If there was a substitution of the two –OH groups in the middle sections of the ring structures, the D.S. would be defined as 3.0. The polymer will be water-soluble when the D.S. reaches a value of 0.45 [10]. The D.S. will not impact the viscosity properties of the polymer [10].

2.4.2 Xanthan Gum

By origin, xanthan gum (XG) is characterized as a naturally occurring polymer but is in reality bacterially produced [10]. The polymer is produced through a complex enzymatic process during the lifecycle of the bacteria Xanthomonas campestris [10]. Xanthomonas campestris excrete a polysaccharide gum that works as a preventive layer on the bacteria. This layer creates a physical barrier and prevents dehydration [12]. In addition to being naturally occurring, XG is categorised as slightly anionic. It is also water soluble, but it is hard to dissolve it in water due to its complexity and therefore needs to be pre-treated [5]. The molecular weight of XG is relatively high for the use in drilling fluids as it ranges from two to three million and the polymer structure is highly branched. It is mainly added to drilling fluids as a viscosifier in saltwater where there is a requirement for suspension properties [10]. XG is not known as the best polymer to control filtrate loss, and does not contain significant inhibition skills [5]. As with the CMC polymer, XG is composed of repeating ring structures but is a five-ring structure composed of a two-ring backbone and three-ring side chain [10]. This is shown in Figure 2.7.

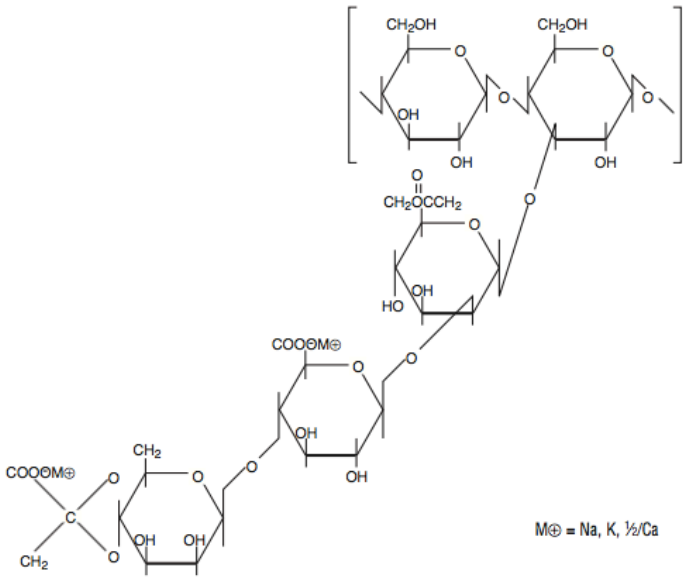

Figure 2.7: Xanthan gum structure [10]

XG is a heteropolysaccharide [10]. The backbone of the structure consists of glucose that is identical to the ring structures in CMC. Additional sugar residue is branched of to the side chains where various groups such as carboxyl and hydroxyl (and others) are attached. It is the structure and these functional groups that give XG viscosifying properties [10].

After a concentration limit of XG is reached a weak, hydrogen bonding between the branches of the polymers will occur and a complex, tangled polymer network is created. When shear forces are applied to the system, the hydrogen bonding will break and the fluid will thin. When shear is removed the chains will resume their interaction and the viscosity will decrease to its original state [10]. When the fluid is exposed to high shear rate conditions like flowing in the drill-string and through the bit-nozzles, it will thin and with very high shear rates the fluid behaviour may be close to the behaviour of water. For low shear rate conditions like flowing in the annulus, the viscosity will increase again. The XG polymers produces gel structures of thixotropic characteristics when the fluid is static [10]. This is an important drilling fluid quality as it will prevent drill cuttings from sinking with the help of gravity and prevent cuttings bedding in the annulus.

2.5 Salt Systems

Shale is a sedimentary rock laid down in marine basins. The most sensitive shale formations contain concentrations as high as 80% of montmorillonites, illites and other interlayered clay varieties [13]. The clay present in shale contain exchangeable cat-ions, most commonly Na^+. Salts consisting of metal ions with a greater bonding strength will exchange their cat ion with Na^+ if they are divalent and able to bond to the surface of clay crystals. If the exchanged cat ions reduce the water penetration, the salt system added to the drilling fluid are characterised as inhibitive [5]. The inhibition mechanism for monovalent ions like K^+ is the particle size. The small size of the ion makes it able to penetrate the void space in the hexagonal structure of the clay's tetrahedral layer. This will result in a tighter bonding between the clay particles, hence less hydration [5]. In complex salt rock formations there may be a need for a multi-salt system, where more than one type of salt is present in the drilling fluid solution to ensure no washouts [5]. Typically, the multi-salt system is saturated with Na^+, K^+ and Mg^{2+} ions. The next section will describe the salt system used for the experimental work in this thesis.

2.5.1 KCl

Potassium chloride is mainly used in WBM as a shale inhibitor. In the KCl salt system, the inhibitive ion is K^+. The salt is added to WBM so that the K^+ ions can compete with the exchangeable ions in the drilled clay section [13]. The ion exchange will keep possible clay formations from swelling and causing borehole instability. To control the filtrate in WBM's containing KCL, polymers such as Drispac or starch are usually applied. During the well drilling, it is important that the concentration of K^+ ions and the added polymers is kept constant. With a concentration decrease of the polymers, the drill cuttings ability to stay dispersed will decrease as well [2]. The density of KCl as an additive varies from 6 to 170kg/m^3.

2.6 Nano Sized Additives

Nanotechnology is the use of small material pieces by themselves or their manipulation to create large-scale materials. Nanoparticles are defined as matter at dimensions of 1-100 nanometers, and have in later years been implemented in the Oil and Gas industry. In simpler terms, nanotechnology may be described as the science, engineering and technology that is conducted at nano-scale [14].

Quite useful characteristics may be drawn from nanoparticles due to their tiny nature, such as an increased surface area. This makes other materials able to bond in ways that make stronger or more lightweight materials [14]. This is illustrated in Figure 2.8.

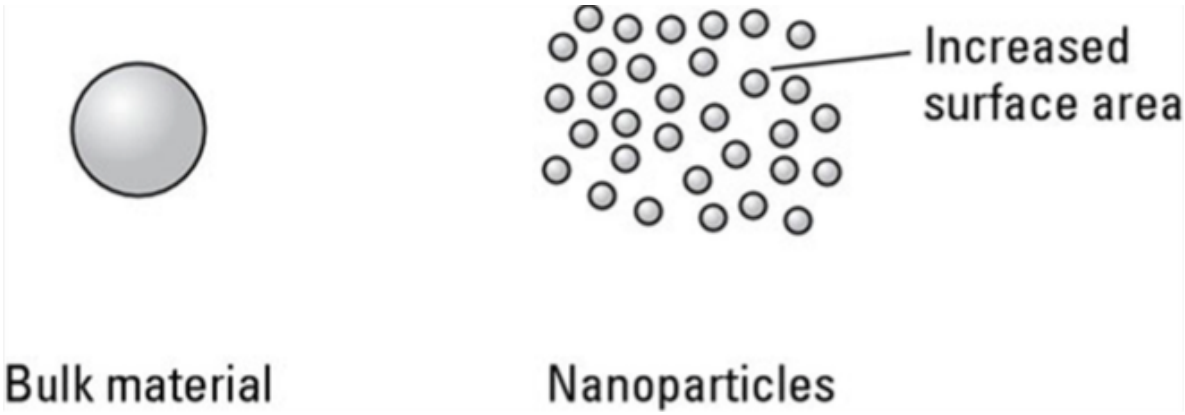

Figure 2.8: Increased surface area with nanoparticles [14]

Nanoparticles might be in suspension if the interaction between the particle surface and the solvent is strong enough to overcome density differences. This usually results in a material either sinking or floating in a liquid, forming nano-fluid. In the Oil and Gas industry, a nano-fluid is defined as any fluid containing a nano-sized additive used in the exploration and exploitation of oil and gas [14].

In the following sections, the nano-sized additives used for the experimental study in this thesis are described. A literature study of previous executed experiments with nano-sized additives has been conducted and summarised in section 2.7.

2.6.1 Titanium Nitride (TiN)

TiN is an important tribological material due to its superior mechanical properties. It is a widely and commonly chosen coating material, with a hardness lever that is useful for material protection [15]. It is chemically characterised as a substance, with a melting point of 2950°C and a density of 5.22 g/cm^3 (43.561 lbs/gal) [16]. TiN is chemically unaffected in many environments, and more noble than certain metals. This makes the material adequate for coating protection against corrosion. Nano-sized TiN was used as an additive in bentonite water based drilling fluid for further experimental studies.

2.6.2 Molybdenum Disulphide (MoS_2)

MoS_2 is a naturally occurring substance in large quantities as the mineral molybdenite. The substance was recorded of use in both Greek and Roman civilisations of 2000 years ago, and was often confused with graphite [17]. It has a specific gravity varying from 4.6 to 4.75 and a melting point of 1185°C. It has been used as a lubrication material for various sciences since it was distinguished from graphite in 1778. These industries include military, aircraft and automotive fields. The most important area of application today is in the automotive fields [17]. Nano-sized MoS_2 was used as an additive in bentonite water based drilling fluid for further experimental studies.

2.6.3 Graphene

Graphene is a two dimensional material that is referred to as the mother of all graphitic forms. It is a sheet of carbon atoms arranged in hexagonal cells, and the the thinnest known material [18]. It is one hundred times stronger than steel by weight, and contains superior mechanical properties such as a tensile strength of 130 GPa. Its melting point is set to 4510K (4237°C). In the Oil and Gas industry, graphene has been implemented into drilling fluids with the main focus on improving fluid loss control while Scomi has worked partners to develop a product to provide lubricity and thermal stability to a conventional drilling fluid system [19]. Nano-sized Graphene was used as an additive in bentonite water based drilling fluid for further experimental studies.

2.7 Effect of Nanoparticles in Drilling Fluids

Long L. et al. (2012) [20] presented a literature review which evaluated the applications of nanomaterial in drilling fluids, as well as the technical exploration and production benefits of the applications. They reviewed important developed nanomaterials in drilling fluid and reservoir protection applications. This review concluded the following:

- Nanomaterials in drilling fluids offer many potential solutions to resolve drilling problems that are hard to solve with conventional fluids.
- It may contribute in good economical and technical solutions for a drilling operation.
- Nanomaterials can enhance wellbore stability, reservoir protection and avoid severe drilling problems.
- It may improve drilling efficiency and help keep the drilling operation safe.
- New wells are more complex. Nanomaterials may help meet specific requirements drilling deviated, horizontal wells and complex deep wells.
- In the future, nanomaterials will play an essential part in preparation of additives, drilling fluids and materials for reservoir protection.

Abdo J. and Haneef M.D. (2013) [21] presented an approach to stabilise the rheology of drilling fluids exposed to harsh HPHT environments using nanoparticles. Palygorskite (PAL) was tested in nanoform and micronform to establish if it could tailor the drilling fluid rheology. They formulated samples containing as much as 40g of PAL in 500ml of water. They obtained the following results:

- When PAL was added in nano-size, the PV and YP deviated compared to the fluids containing fine grinded and micron PAL particles. PV increased from 9-9.5cP to 11cP while YP increased from 7.5lb/100sqft to 8lb/100sqft.
- The gel strength measurements indicated an improvement in the gelling characteristics of 200%.
- Most of the test samples failed to sustain a temperature above 100°C.
- The fluid loss was significantly reduced using nano-sized PAL as an additive. After 30 minutes the fluid loss with and without nanoparticles were set to 7.1ml and 13ml respectively.
- From the lubricant test, the reduction in torque was calculated and tested to be 68%.

Ponami S. et al. (2014) [22] prepared nano-fluids of both CuO and ZnO. The solutions were prepared with 0.1, 0.3 and 0.5wt% of CuO and ZnO. They were added to an aqueous solution containing 0.4wt% of XG, which acts as a dispersant. The nanofluid was used as an additive in WBM as 1% of the total solution, and the effect on thermal and electrical properties were studied in both fluids. They also studied the rheology with varying pressures and temperatures to understand the nano influence on rheology of the fluid exposed to those conditions. The change in rheological properties were studied, and they used rheological models to develop the experimental data. This resulted in:

- The thermal conductivity in WBM containing CuO or ZnO increased from 20% to 38% and 17% to 34% respectively. Increased thermal conductivity means that the mud is able to cool down more quickly and better maintain its viscosity.
- It was observed that with the concentration increase of nanoparticles from 0.1wt% to 0.5wt%, the electrical conductivity was enhanced.

Barry M. et al. (2015) [23] investigated the fluid filtration and the rheological properties of low solid content (LSC) bentonite fluids. Iron oxide, nanoparticle additives and two different clay hybrids intercalated with iron oxide (ICH) and aluminosilicate (ASCH) were added to the bentonite fluids. A control fluid was established as a reference. The fluids were tested in LPLT conditions and HPHT conditions. A pressurised and rotational viscometer was used for testing. LPLT filtration testing was executed with a filter-press regulated by CO_2, while for the HPHT filtration testing, N_2 was used. The filtrate cakes for both the tests were freeze-dried at -45°C before characterizations. The testing resulted in the following conclusions:

- The filtrate of the ICH samples exhibited less filtrate compared to the bentonite sample in both LPLT and HPHT testing.
- The fluid platelets formed a strong coagulated network less sensitive to pressure and temperature for the ICH samples.
- ASCH samples exhibited less filtrate loss compared to the control sample.
- Nanosized iron-oxide as an additive in the drilling fluids resulted in increased filtrate losses with LPLT conditions, but decreased filtrate losses with HPHT conditions.

Hareland G. et al. (2013) [24] used drilling fluid blend containing loss circulation material (LCM) to achieve wellbore strengthening in permeable and impermeable formations. They used micron sized graphite and $CaCO_3$ (A and B respectively) in combination with nano sized Iron(III)hydroxide and calcium (NP1 and NP2 respectively) as additives in the drilling fluids and ran hydraulic fracture experiments on sandstone and impermeable concrete core samples. They used both WBM and diesel based OBM when conducting the experiments. This gave the following results:

- The optimal WBM blend was obtained using LCM A in combination with NP2, which increased the fracture breakdown pressure by 1668psi, 70% increase compared to the control sample.
- The optimal OBM blend was obtained using a combination of LCM A and NP2, where the fracture breakdown pressure increased by 586psi, a 36% increase compared to the control sample.
- LCM A interacted better with the NP's compared to LCM B, the WBM fracture breakdown pressure was 47% higher compared to the OBM system.

Amanullah MD. et al. (2011) [25] presented a paper that described formulation and preliminary test results of several nano-based drilling fluids. The filtration and rheological properties were evaluated for oil and gas field application. Three commercial nanomaterials were used in a bentonite micron-sized control fluid. The concentration of nano was set to 0.5ppb. No surfactants were used. They added a polymeric viscosifier to the solution to enhance viscosity properties, fluid loss behaviour and nano shielding. The fluids were evaluated by both long term and short term behaviour. They measured the rheological properties immediately after preparation, and static aging after 18, 48 and 72 hours. API fluid loss measurements were also conducted. They came to the following conclusions:

- Nano-based fluids may help controlling loss of circulation when combining micro, macro and nano-sized particles in the system.
- Low concentration nano-additives demonstrated the potential of improving mud properties such as viscosity and fluid loss, but only with low concentrations.
- Spurt loss was eliminated with the nano-based fluids, which may lead to a reduction in formation damage.
- No mud cake formation with the nano-based fluids may lead to better cleaning of the borehole wall before completion operations, and ROP in hard rock formations may be enhanced due to low solid contents in the nano-based fluids.

Sabbaghi. et al. (2014) [26] tried to improve WBM properties using TiO_2 or polyacrylamide (PAM) as nano-sized additives to the fluid. From the study, they obtained the following results:

- The viscosity of the base fluids increased with larger quantities of TiO_2 and PAM. The viscosity increased from 1-2cP with 1g of additive to 46-47cP with 14g of additive.
- The fluid viscosity stayed constant with 1g of additive for 9 weeks, but decreased to 17cP for the fluid with 14g of additive after 9 weeks.
- Fluid loss decreased for the nano-enhanced WBM, from 53ml after 30 minutes to 19ml after 30 minutes with 14g of additive.

Lee S. et al. (2015) [27] developed a product enhanced with nano-sized graphene to cater to more challenging drilling and production conditions. Graphene enhanced drilling fluids have been successfully applied in field trial and showed superior lubricity and improves the thermal stability in WBM. The graphene particles penetrate the microscopic sized pores of the tubular metal and crystalizes under high pressure. This forms a protective film that improves the lubricity, prevent bit balling, improves the ROP and may extend the life span of bottom hole assemblies (BHA's). They used a standard 10lb/gal salt polymer mud and enhanced it with graphene and ester as lubricants. 5% of the total fluid volume contained either graphene or ester. They did the same with a standard 13.5lb/gal HPHT WBM. To test in the laboratory they used a lubricity tester, while for field testing the fluids were applied in a HPHT onshore well with temperatures reaching 176°C and hard formation. A Shale dispersion and linear swelling test was also conducted on the salt polymer and the HPHT WBM to evaluate if the product would affect shale inhibition. Both of the base muds did not contain any swelling reducing additives or any shale inhibitors. With this they came to the following conclusions:

- The graphene enhanced WBM reduced the torque value with 80% while the ester enhanced WBM reduced the torque with 30-40%.
- Decreasing the concentrations to 4,3,2 and 1% still showed that the graphene lubricant outperformed the ester based lubricant with a torque reduction twice as high every single time.
- The rheology readings of the base mud enhanced with graphene showed a reading increase of 40-60%. The API fluid loss improved when adding graphene.
- The shale swelling test resulted in a swelling percentage of 40-50% with graphene as an additive for borth the 10lb/gal and 13.5lb/gal muds. The percentage of swelling was calculated assuming that swelling occurrence in the base mud was 100%.
- The results indicate 60-70% of shale dispersion into the drilling mud containing graphene as an additive.
- Field trials showed that that 2-3% of the product had improved the ROP of 125%. The actual torque reduction was set to 20% and improved the life span of the bit of more than 75%. A fluid loss reduction was set to 30%.

2.8 A Study of the Friction Coefficient in Drilling Fluids

Deng Z. et al. (2015) [28] presented a novel solution to overcome the issues of unconsolidated oil sands. Bitumen is common in oil sands, and will increase the torque and drag, and decrease the ROP. A common method when encountering bitumen has been to dissolve it into the drilling fluid. This will contaminate the drilling fluid and jeopardise the wellbore stability. To overcome these issues, they formulated a new oil sands drilling fluid system containing a multifunctional polymer additive as a diffuser for the bitumen. They presented an exemplary formulation of WBM for oil sands, given in Figure 2.9:

Components	Quantities	
	lb/bbl	Kg/m^3
Water	0.97 bbl	0.97 m^3
Xanthan gum	1	3
Starch	5	15
Bridging agent	9	25
pH modifier	1	2
Bitumen inhibitor	3	9
Corrosion inhibitor	6	17
Drilling solids	2	5

Figure 2.9: Formulation of water-based oil sands drilling fluid [28]

They performed a friction test of the WBM with and without the bitumen inhibitor using a Falex Pin-vee tribometer. They measured the friction coefficient with the tribometer and came to the following conclusion:

- The coefficient of friction was reduced when the bitumen inhibitor was added to the control fluid.
- The average friction coefficient of the control fluid was set to be between 0.2 and 0.25.
- The average friction coefficient of the testing mud with the bitumen inhibitor was set to be between 0.15 and 0.2.

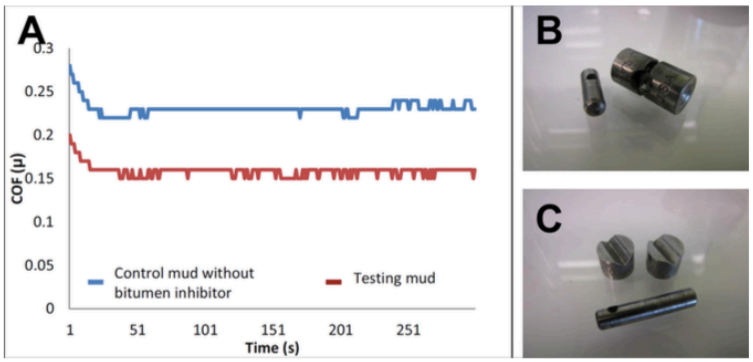

Figure 2.10: Falex Pin-vee test results [28]

Robello S. (2010) [29] presented the adoption of "mechanical friction factor" that is unique to the drilling industry. Robello described the term as a proxy for the coefficient of friction that is used to estimate torque, drag and side force for the string, moving pipe and transient swab/surge pressure estimation. In his paper he presented a table with typical ranges of downhole friction factors for several types of well fluids. These are described in Table 2.3:

Range of friction factors		
Fluid Type	Cased Hole	Open Hole
Oil based	0.16-0.20	0.17-0.25
Water based	0.25-0.35	0.25-0.40
Brine	0.30-0.40	0.30-0.40
Polymer based	0.15-0.22	0.20-0.30
Synthetic based	0.12-0.18	0.15-0.25
Foam	0.30-0.40	0.35-0.55
Air	0.35-0.55	0.40-0.60

Table 2.3: Range of friction factors [29]

Xu L. et al. (2014) [30] presented a flat rheology WBM with a conducted evaluation on the design system. Inhibition and lubricity performance was tested on the formulated system. From the inhibition and lubricity tests, they stated that the common friction coefficient for WBM systems were set from 0.20 to 0.35 and reported the following results:

- The designed WBM yielded a lower friction coefficient of 0.11 which is parallel to the friction coefficient values of the OBM systems.

Vos B. et al. (2000) [31] presented a paper that elaborates on the benefits of real-time torque and drag monitoring. In the paper they compared the ECD to friction factor trends using case studies. In Figure 2.11 they plotted the friction factor and ECD over a measured depth range of 3300m to 5500m to relate the ECD to the friction factor.

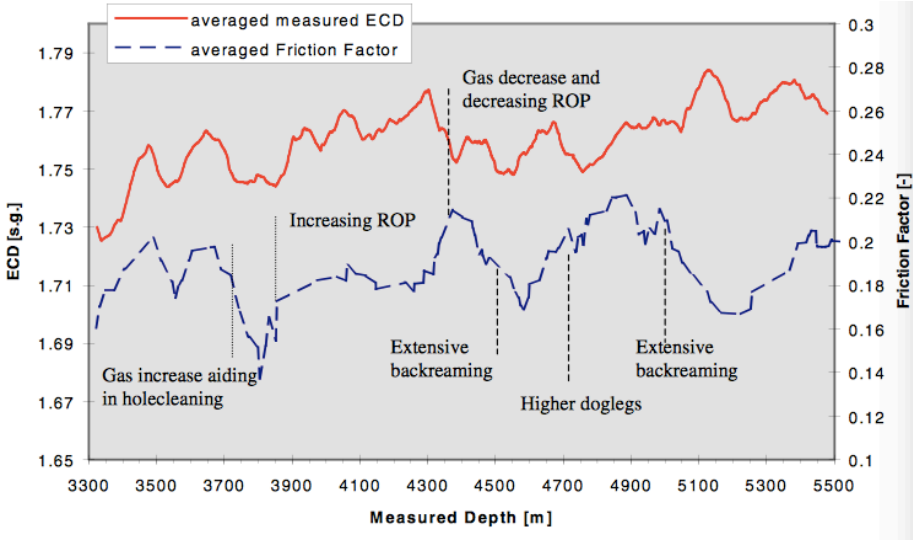

Figure 2.11: Comparison of ECD and friction factor [31]

Mud containing different components were investigated in similar offset wells. The coefficient of frictions for the different mud types were plotted against the measured depth of the well as illustrated in Figure 2.12.

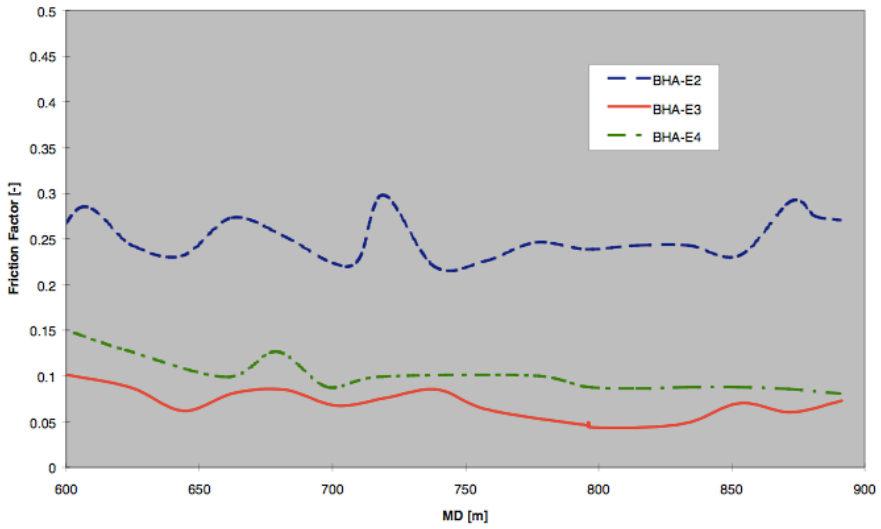

Figure 2.12: Different friction factors for different mud types in similar offset wells [31]

Hereby, the following conclusion was made:

- The correlation between ECD and calculated friction shows that they are both a function of hole cleaning. The friction coefficient showed a 10% increase as the mud-weight was raised from 1.10s.g to 1.13s.g.

Seireg A.A (1998) [32] wrote about an experiment conducted by Furey and Appeldoorn where the effect of lubricant viscosity on metallic contact was tested. The testing system consisted of a fixed steel ball on a rotating cylinder. They obtained the following results:

- Friction generally decreased with increasing viscosity because the more viscous oils gave less metal-to-metal contact. For low viscosity oils, the friction coefficient was set to 0.13 whilst for the higher viscosity fluids it dropped to 0.08.

2.9 Effect of Lubricity on Torque, Drag and Extended Reach Drilling

A publication by Abbassian F. et al. (1997) [33] addresses the issues related to torque and drag predictions in extended reach drilling (ERD) wells. They stated that frictional torque is generated by the contact loads between the drill-string and the casing/open hole. The magnitude of the contact loads is determined by the tension or compression of the drill-string, the dogleg severities, the drill-pipe and the hole size. They stated the following, relevant information in their paper:

- Lubricity is important to control friction, and is largely controlled by the drilling mud and the formation types.
- From historical well data they stated a cased hole and open hole friction factor of 0.24 and 0.29 respectively for WBM.
- From historical well data they stated a cased hole and open hole friction factor of 0.17 and 0.21 respectively for OBM.

McCormick J.E. et al. (2011) [34] presented a paper with a focus on torque and drag reduction methods utilised in the past and how they have proven to be worthwhile for use in engineering. The methods they discussed in the paper included well-path design, lightweight string components, lubricants, hole cleaning, co-polymer beads and mechanical friction reduction tools. With a focus on the lubricants section, they presented the following:

- Lubricants are commonly used in the drilling mud to reduce torque and drag forces and cool the bit and string.
- Many different additives have been implemented to reduce the friction coefficient, and these additives may reduce the coefficient up to 30% - 40%.

Estes B.L. et al. (2006) [35] presented a paper where it was raised concern regarding the feasibility of being able to drill a longer well later in the well development, as sufficiently high torque was experienced. It was documented that the use of liquid lubricants added to an oil base system reduced the torque, which was sufficient to drill the longest throw wells. They obtained the following results:

- Liquid lubricants that were added at concentrations from 2% to 6% reduced the torque with 5% to 15% respectively. However, the lubricants needed to be added continuously.
- Higher concentrations did not yield additional torque reductions.

Kaarstad E. et al. (2009) [36] conducted a friction research to further understand mechanical, viscous, temperature and material frictional effects in the wellbore, as the wellbore friction plays a central role in increased well reach. The provided paper presented some of the results of this work. The instrument used for the experiments was a tribometer from CMI Instruments that is based on the ball on disc technology. The experiment was designed to investigate parameters such as drilling fluid with different properties and the variation in the coefficient of friction. They also included temperature effects and tested the fluids for several temperatures. With this they came to the following conclusions:

- The coefficient of friction increases with increasing temperature.
- The coefficient of friction was significantly lower for oil based drilling fluids compared to water.

2.10 Evaluation of Hydraulic Models

There are several hydraulic models available in literature. To select the proper model for further analysis in this thesis, a research performed by Sagidov was reviewed.

Sagidov J. (2013) [37] performed a hydraulic analysis on two drilling fluids (drilling fluid-A and drilling fluid-B), and compared the predictive power of several hydraulic models. Among the models, he analysed the Unified model and the Herschel-Buckley model. For the analysis of fluid-A, he illustrated the results with the following model:

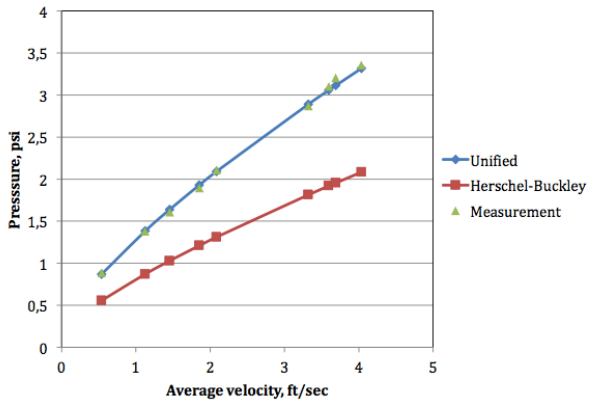

Figure 2.13: Prediction of the Herschel Bulkley and Unified model for fluid-A in annulus [26]

He also analysed fluid-B when it was flowing through the annulus, and the results are presented in Figure 2.14.

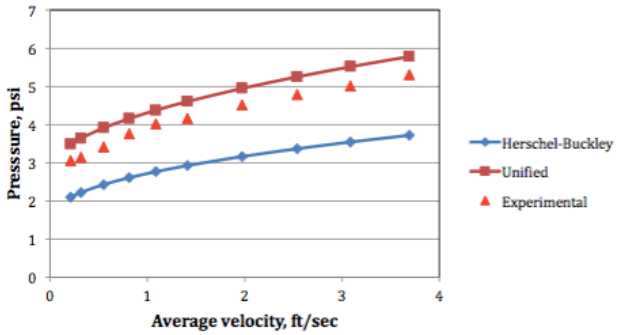

Figure 2.14: Prediction of the Herschel Bulkley and Unified model for fluid-B in annulus [26]

The Unified model works well based on the given information, and is used for further simulation studies.

3 Theory

This chapter will review relevant theories for the laboratory investigation and further laboratory analysis. The theories are rheology, viscoelasticity, torque and drag, friction and hydraulics.

3.1 Rheology

Rheology may be defined as the study of flow and deformation of matter [38]. The functions of the drilling fluid rely on the rheological properties of the mud. The rheological properties may contribute and help the mud to [5]:

- Remove and transport cuttings from the bottom hole section.
- Keep the cuttings floating and keep the weight material in a state of suspension during circulation stop.
- Separate cuttings at surface.
- Minimise the pump friction.
- Minimise formation damage while drilling.

The fluid rheology is important for the drilling process, and is also used in the following applications [39]:

- Frictional pressure loss calculations in the annuli and pipes.
- Determining flow regimes in the annulus.
- Estimate the ECD of the fluid under downhole conditions.
- Estimate the efficiency of hole cleaning.
- Estimating the surge and swab pressures.
- Optimize the circulating system to improve the drilling efficiency.

The drilling mud, both water based and oil based, consist of colloidal particles that may affect the viscosity of the fluid. Viscosity is further explained in section 3.2.1. When the colloidal particles are inconsistent in size, the viscosity will become dependent on the fluids flowrate [2].

3.2 Fluid properties

This section will present relevant theory about fluid properties used for evaluation during experimental and simulation studies later in this thesis.

3.2.1 Viscosity

The viscosity of the drilling fluid is expressed as the fluids floating resistance. This resistance occurs due to the frictional forces between the additives in the mud, and/or due to electrostatic forces between particles or ions in the mud. The viscosity is a parameter that is dependent of temperature, pressure, shear stress and time. The shear stress of a fluid is expressed as τ [lbf/100ft^2] and describes the relation between force and area. The shear rate of a fluid is expressed as $\dot{\gamma}$ [s^{-1}] and describes the relation between velocity and distance [5].

The Newtonian viscosity of a fluid is expressed by the symbol μ, and may be stated as [5]:

$$\mu = \frac{\tau}{\dot{\gamma}} \tag{3.1}$$

To characterise the floating ability and the viscosity characteristics of the formulated fluids in the experimental study, the following parameters were analysed:

- Plastic viscosity (PV)
- Yield point (YP)
- Gel strength

3.2.2 Plastic Viscosity PV

The mechanical friction that occurs in the drilling fluid is characterised by the plastic viscosity. The friction is caused by the particles itself, the particles and the water phase as well as the liquid elements itself. The PV will vary with particle concentration, size and shape and the fluids viscosity.

3.2.3 Yield Point YP

The yield point is the part of the viscosity created due to electrostatic forces between particles in the drilling fluid. Applied pressure should exceed the yield strength of the drilling fluid for flow to be initiated.

3.2.4 Gel-strength

The gel strength is expressed the thixotropic abilities of the fluid. It is an important quality of the drilling fluid, as it holds the particles and cuttings in suspension during circulation stop. It is measured as a function of time, and the shear stress is not constant for a specific velocity, but it will vary with time. The gel structure may also prevent invasion of drilling fluids into the formation, and stop lost circulation problems [40]. The gel structure is formed under static conditions.

3.2.5 Optimum system

An optimum drilling fluid system is dispersed and flocculated. When using additives in the drilling fluid system, PV and YS may be used to determine the properties of the drilling fluid. This is illustrated in Figure 3.1.

- If a decreasing PV, increasing filtration rate and reduced water bonding is experienced, the system may go from dispersed to aggregated.
- If increasing YP and gel strength is experienced, the fluid may go from deflocculated to flocculated.
- If increasing PV, decreasing filtration rate and increasing water bonding is experienced, the fluid may go from aggregated and flocculated to dispersed and flocculated.

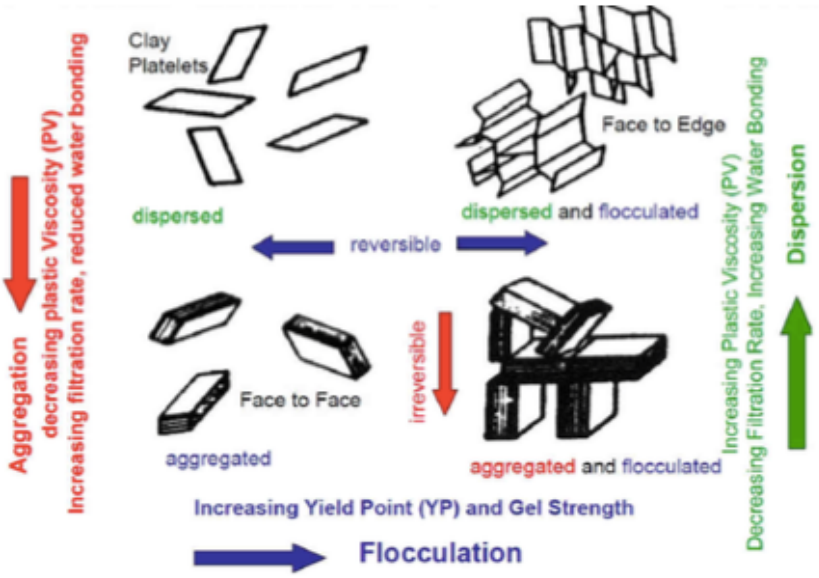

Figure 3.1: Description of the YS and PV influence on the different particle associations

3.3 Flow and flow behaviour

As mentioned, a fluids viscosity will become dependent of the fluids flowrate if it contains colloidal particles that are inconsistent in size. The flow pattern is characterised by the Reynolds number. The flow behaviour may have an impact on parameters of the drilling process like ROP and the cutting transport. The Reynolds number is a dimensional number, given by the following equation:

$$Re = \frac{\rho \bar{V} D}{\mu} \tag{3.2}$$

Where ρ [kg/m^3] is the fluid density, D [m] is the diameter of the pipe, $\bar{V}$ [m/s] Is the mean fluid velocity and μ is the dynamic fluid viscosity [Pa·s]. Inserting these parameters in Equation 3.2 makes you able to state the flow regime of a fluid, hence if the flow behaviour is laminar, transitional or turbulent.

A flow is described as laminar when the velocity is higher at the centre of the pipe the fluid is flowing through. The pattern is uniform, and laminar flow occurs with lower flow rates, lower pipe diameters and for fluids of lower density, typically when the Re number is smaller than 2000.

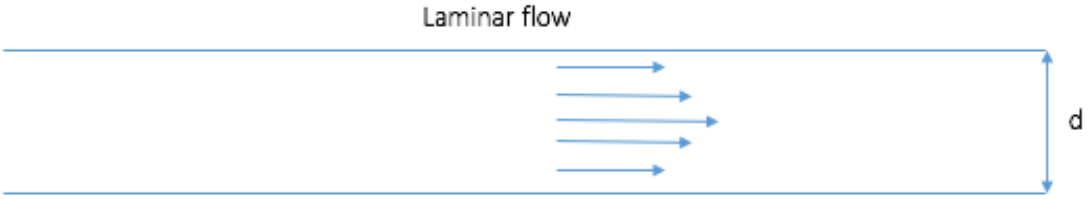

Figure 3.2: Laminar flow in a pipe

The transitional phase is described as the period where flow velocity increases and the flow pattern changes from uniform to a pattern of more chaotic state. The Re number associated with transitional flow varies from 2000 to 4000.

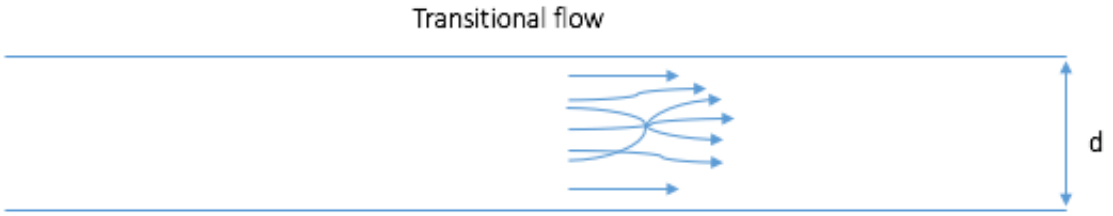

Figure 3.3: Transitional flow in a pipe

A turbulent flow is chaotic and often random, and is associated with Re numbers greater than 4000. Turbulent flow occurs for greater fluid velocities, greater fluid densities and a narrower pipe diameter.

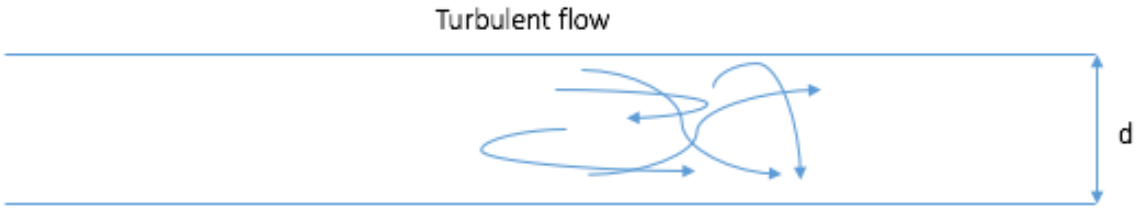

Figure 3.4: Turbulent flow

3.4 Fluid types

Fluids may be split into groups according to their rheological properties and behaviours. There are two main groups of fluids, these are [5]:

- Newtonian fluids.
- Non Newtonian fluids.

The difference is presented in Table 3.1:

Fluid types	
Newtonian	Non Newtonian
The viscosity is independent of the shear rate and does not contain particles larger than molecule size. Some examples may be oil, water and glycol.	The viscosity is dependent on the shear rate. It is possible for the fluid to contain larger particles.

Table 3.1: Newtonian and Non Newtonian fluid descriptions [5]

The Non Newtonian fluids are split into either plastic, pseudo plastic or dilatant fluids. Most of the drilling fluids will behave either plastic or pseudo plastic. For plastic fluids you need to break the yield point for flow to be initiated. The fluid behaves shear thinning with increasing shear rates. Pseudo plastic fluids does not obtain a yield point, but does also behave shear thinning with increasing shear rates.

3.5 Rheological Models

There has been developed several mathematical models to describe a fluid using rheology parameters. The models relate the shear stress to the shear rate, and one is able to extract both the gel strength and flow viscosity from the results, which may help further analysis for hole cleaning and flow behaviour of the fluid. Fluids are exposed to a wide range of shear rates, and a detailed understanding of the fluid rheology and influence of the shear is necessary to optimize the fluid design. As explained in the fluid properties section, high viscosity is desirable under low shear rate conditions to keep e.g. cuttings floating, and the viscosity should decrease under greater shear rate conditions. The upcoming sections will describe the models used for analysis and investigation of the experimental study results.

To analyse and provide examples for the different models, a set of viscometer data was retrieved from the experimental study and is exhibited in Table 3.2.

RPM (θ)	Reading (V)
600	42
300	36
200	34
100	30
6	21
3	20

Table 3.2: Viscometer data retrieved from the experimental study

To transform the obtained laboratory data to field units, one has to apply conversion factors and calculate the shear stress and shear rate from Equation 3.3 and Equation 3.4:

$$\tau = 1.067V \tag{3.3}$$

$$\dot{\gamma} = 1.703\theta \tag{3.4}$$

Using Table 3.2 and Equation 3.3 and Equation 3.4 we obtain the following parameters

$\dot{\gamma}$ [s^{-1}]	τ [lbf/100ft^2]
1022	44.8
511	38.4
341	36.3
170	32
10	22.4
5	21.3

Table 3.3: Converted viscometer data

3.5.1 The Newtonian model

This model is mostly used for Newtonian fluids, and may be described by a one-parameter rheological model [38]. The equation used to describe a Newtonian fluid is given by:

$$\tau = \mu\dot{\gamma} \tag{3.5}$$

Where τ is the shear stress, μ the Newtonian viscosity and γ is the shear rate. The straight trend-line through the origin coordinates when the shear stress is plotted against the shear rate is described as the Newtonian model. The Newtonian viscosity is the slope of the shear rate versus the shear rate data [38]. It is possible to calculate the Newtonian viscosity in cP from the slope using the following equation:

$$\mu = \frac{47880 \cdot slope}{100} \tag{3.6}$$

The slope of the Newtonian model is retrieved from a trend-line using a linear regression technique, and set to be 0.0576. From this, μ was calculated to the following value in cP:

$$\mu = \frac{47880 \cdot 0{,}0576}{100} = 27.6\ cP$$

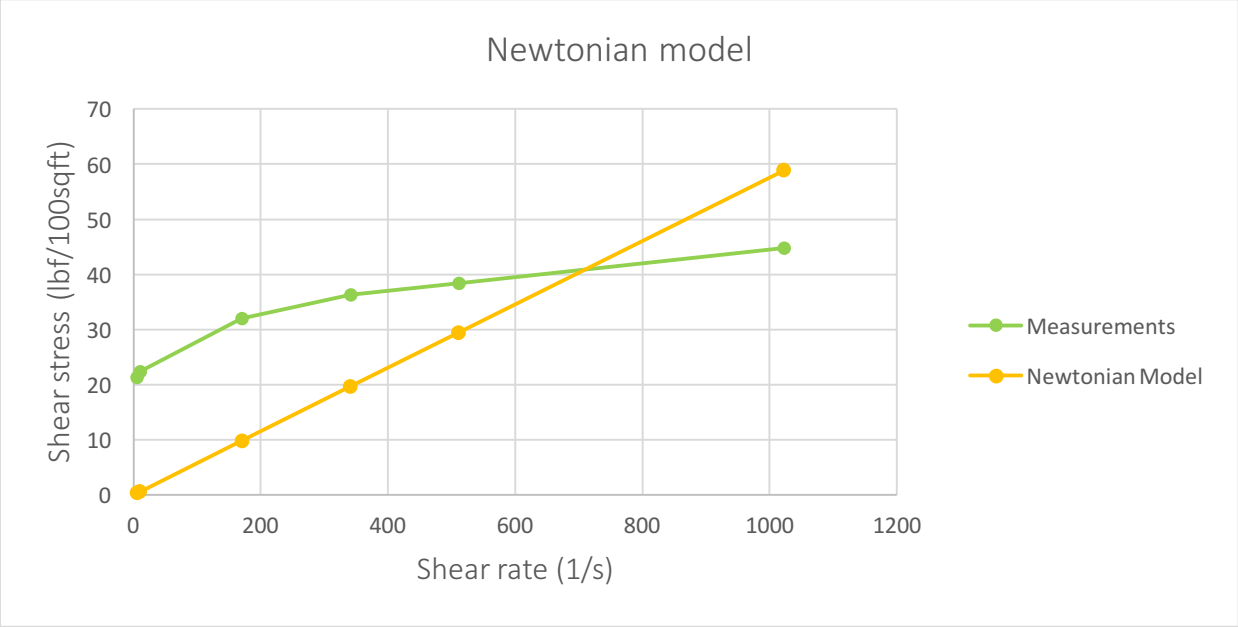

Figure 3.5: An illustration of the Newtonian fluid model

Table 3.4 presents data including the % deviation between the Newtonian fluid model and the real measurements. The Figure 3.5 and Table 3.4 shows that the model does not capture the measured data to describe the fluid behaviour well enough.

Model	Equation	μ slope	μ cP	Deviation in %
Newtonian	$0.0576 \cdot \gamma$	0.0576	27.6	61.0%

Table 3.4: Data for the Newtonian model example

3.5.2 Non Newtonian Models

3.5.2.1 Bingham Plastic Model

This model gained widespread acceptance in the drilling industry, and was the first two parameter model stated. The model is simple to visualize, but does not represent the drilling fluid behaviour at low (in the annulus) and high (at the bit) shear rates accurately considering it is linear. The equation used to describe the Bingham model is given by [38]:

$$\tau = \mu_p \dot{\gamma} + \tau_y \tag{3.7}$$

Where τ is the shear stress, μ_p is the plastic viscosity (PV), γ is the shear rate and τ_y is the yield point (YP). YP and PV may be calculated using the following equations [5]:

$$\mu_p = \theta_{600} - \theta_{300} \tag{3.8}$$

$$\tau_y = \theta_{300} - \mu_p = 2 \cdot \theta_{300} - \theta_{600} \tag{3.9}$$

Where θ_{600} represents the shear rate 600RPM and θ_{300} represents the shear rate 300RPM. Linear regression techniques are used to retrieve the parameters for the Bingham plastic model, and the measurements are compared to the model in Figure 3.6.

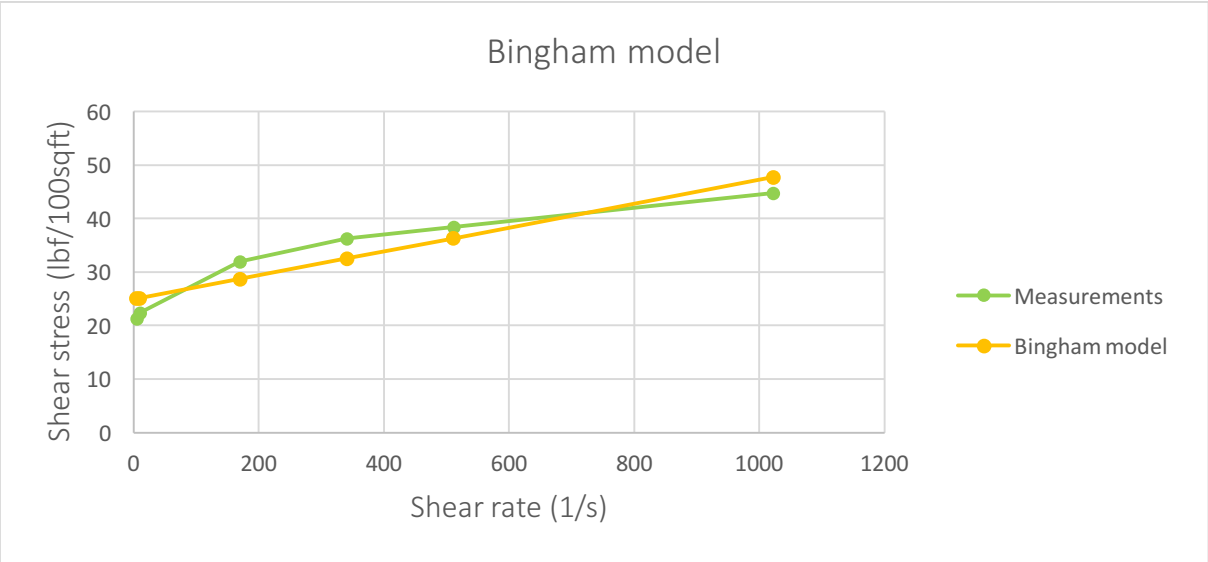

Figure 3.6: An illustration of the Bingham plastic model

Table 3.5 presents data including the % deviation between the Bingham plastic model and the real measurements. The Figure 3.6 and Table 3.5 shows that the model does not capture the measured data to describe the fluid behaviour well enough, but the model captures the data better than the one presented for the Newtonian model as the deviation percentage has decreased significantly. μ_p was calculated by equation 3.6.

Model	Equation	τ_y	μ_p slope	μ_p cP	Model deviation in %
Bingham	0.0223· γ+24,904	24.904	0.0223	10.7	10.4%

Table 3.5: Data for the Bingham plastic model example

3.5.2.2 Power Law Model

The Bingham plastic model assumes a linear relationship between the shear rate and shear stress of the fluid. According to the measurement data it is easier to see that this may not be the case. A better representation can be a logarithmic relationship, which the power law model is based on. The equation used to describe the Power law model is presented as [38]:

$$\tau = k\gamma^n \tag{3.10}$$

Where k is the consistency index and n is the flow behaviour or power law index. These parameters may be estimated from the following equations [5]:

$$n = 3.32 \log\left(\frac{\theta_{600}}{\theta_{300}}\right) \quad (3.11)$$

$$k = \frac{\theta_{600}}{1022^n} = \frac{\theta_{300}}{511^n} \quad (3.12)$$

The power-law model index indicates the type of fluid by its value. When:

- n < 1 → Pseudo plastic fluid
- n = 1 → Newtonian fluid
- n > 1 → Dilatant fluid

Drilling fluids does often have a shear thinning effect, which is when the effective viscosity decreases with increasing shear rate. This is typical for a pseudo plastic fluid, or when the n value is below 1. The measured data was compared to the modelled Power law model, and is illustrated in Figure 3.7. One can tell that with this logarithmic model, the percentage of deviation has decreased significantly compared to the Newtonian model.

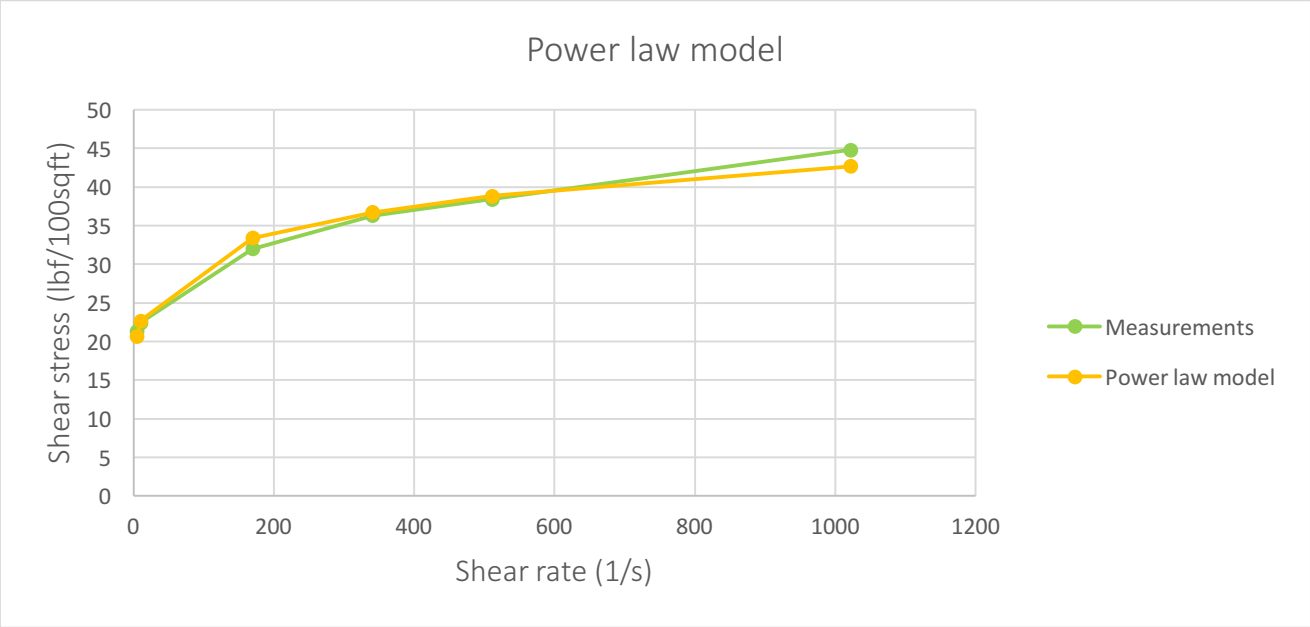

Figure 3.7: An illustration of the Power law model

Model	Equation	k	n	Model deviation in %
Power law	$16.552 \cdot \gamma^{0.1367}$	16.552	0.1367	2.7%

Table 3.6: Data for the Power law model example

3.5.5.3 Herschel-Bulkley Model

This model defines the fluid by three parameters and is a modified yield power law. The model characterises the mud behaviour more accurately across the shear rate range, and offers advantages compared to the Bingham and Power law models [41]. Similar to the Bingham model, this model states that the fluid requires pressure to initiate flow at zero shear strain and that the viscosity decreases with increasing shear rate. It is similar to the Bingham model and the Power law model as it is logarithmic but also considers the yield stress. The model is expressed by the following equation [38]:

$$\tau = \tau_o + k\gamma^n \tag{3.13}$$

Where τ [lbf/100ft^2] is the shear stress, τ_o [lbf/100ft^2] is the yield stress, k [lbf/100ft^2] is the consistency factor, γ [s^{-1}] is the shear rate and n is the flow index, or the power law exponent.

The k and n values are determined graphically. The yield stress is determined by the following equation [38]:

$$\tau_0 = \frac{\tau^{*2} - \tau_{min}\tau_{max}}{2\tau^* - \tau_{min} - \tau_{max}} \tag{3.14}$$

Where $\tau^*$is determined from the geometric mean corresponding to the shear rate, γ^*. γ^* may be determined by the following equation [38]:

$$\gamma^* = \sqrt{\gamma_{min}\gamma_{max}} \tag{3.15}$$

Figure 3.8 illustrates the comparison between the modelled Herschel-Bulkley model and the measurements. The model deviation decreased by 0.2% compared to the Power law model.

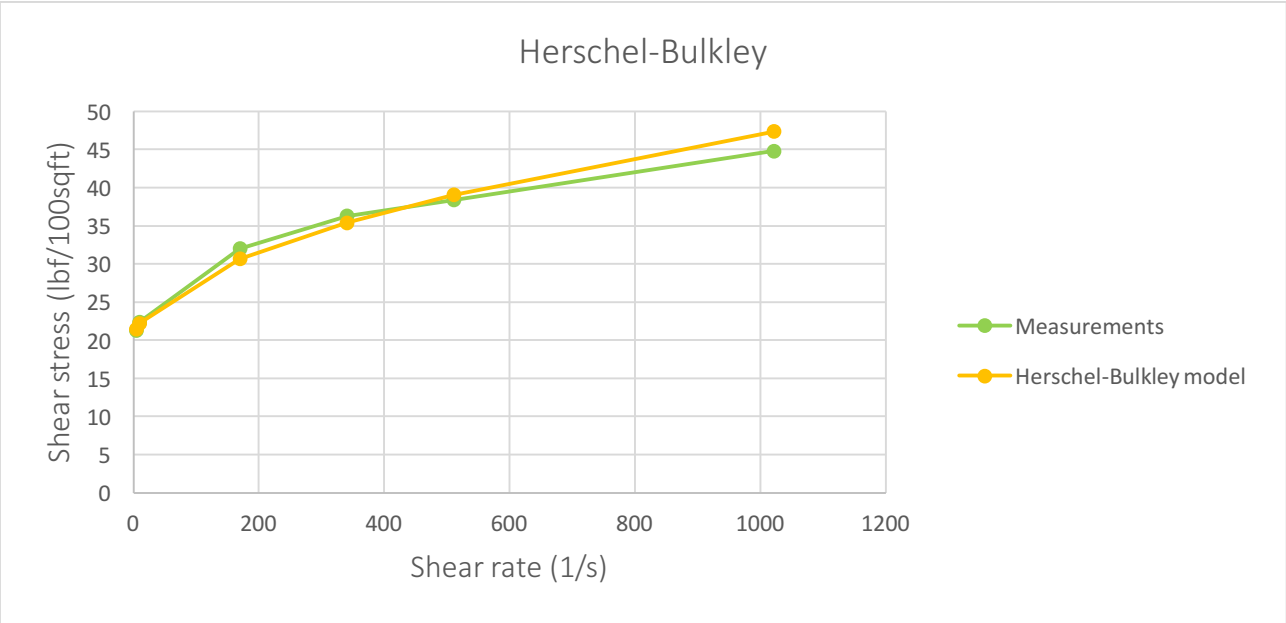

Figure 3.8: An illustration of the Herschel-Bulkley model

Model	Equation	Parameters			Model deviation in %
		τ_0	k	n	
Herschel-Bulkley	$19.69+0.7794\gamma^{0.5151}$	19.69	0.7794	0.5151	2.5%

Table 3.7: Data for the Herschel-Bulkley model example

3.5.5.4 Unified Model

The Unified model is a yield Power law model, or in other words, a simplified Herschel-Bulkley model. This model was established by the drilling industry several years ago [38], but the model uses the yield stress point derived from the Fann 6 RPM and 3 RPM data readings. The model is given as [42]:

$$\tau = \tau_{yL} + k\gamma^n \quad (3.16)$$

Where τ_{yL} [lbf/100ft^2] is the lower shear yield point. The other parameters have been described earlier. To calculate the lower shear yield point, one may use the following equation [38]:

$$\tau_{yL} = 2\theta_3 - \theta_6 \quad (3.17)$$

To convert the lower shear yield point to field units [lbf/100ft^2], one may multiply Equation 3.7 with 1.066. Figure 3.9 illustrates the comparison between the measured data and the modelled Unified model. For the provided example, the model deviated more than both the Herschel-Bulkley and Power law models.

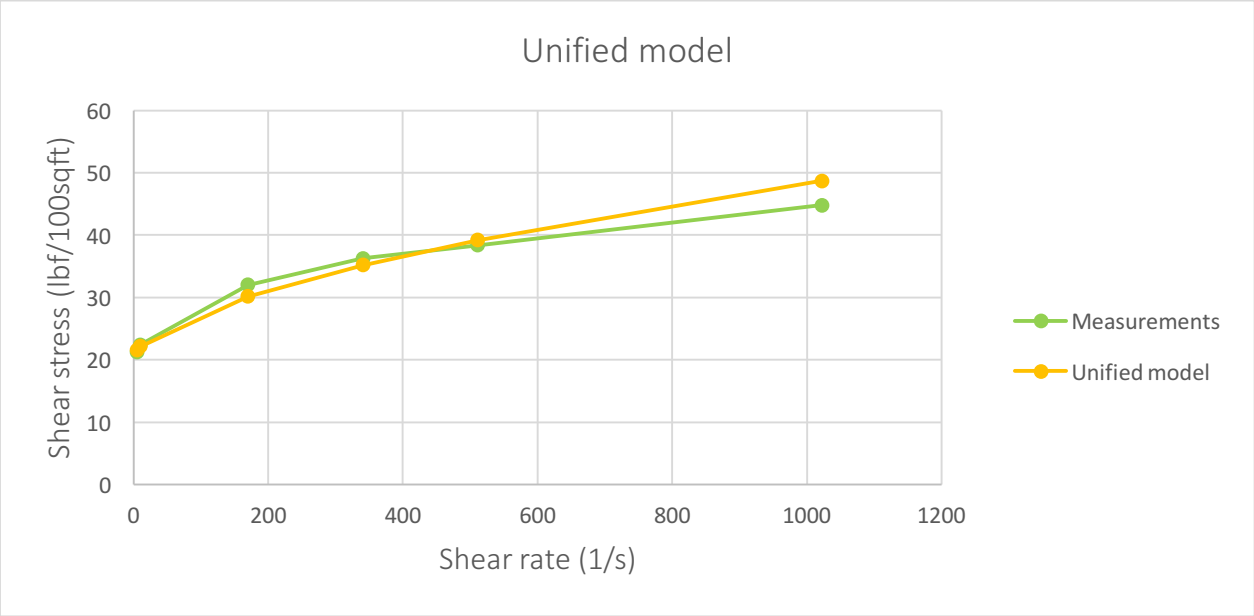

Figure 3.9: An illustration of the Unified model

Model	Equation	Parameters			Model deviation in %
		τ_0	k	n	
Unified	20.273+0.4841 $\gamma^{0.5878}$	20.273	0.4841	0.5878	3.6%

Table 3.8: Data for the Unified model example

3.5.5.5 Robertson and Stiff Model

This model is a relatively complex model [38] with three model parameters. This model is a Power law logarithmic model that includes a correction factor to the shear rate. It is mainly used to describe the rheological behaviour of both drilling fluids and cement slurries, and the basic equation is given as [38]:

$$\tau = A(\gamma + C)^B \tag{3.18}$$

Where A and B may be considered similar to the k and n parameters of the power law mode. Parameter C is the correction factor, and the term $(\gamma + C)$ is described as the effective shear rate. The correction factor is given as [38]:

$$C = \frac{(\gamma_{min}\gamma_{max} - \gamma^{*^2})}{2\gamma^{*} - \gamma_{min}\gamma_{max}} \quad (3.19)$$

Where γ^* is a parameter determined by interpolation. This parameter corresponds to the geometrical shear stress that is stated as [38]:

$$\tau^* = \sqrt{\tau_{min}\tau_{max}} \quad (3.20)$$

Figure 3.10 illustrates the comparison between the measured data and the modelled Robertson and Stiff model. This model deviated the least compared to the measured data.

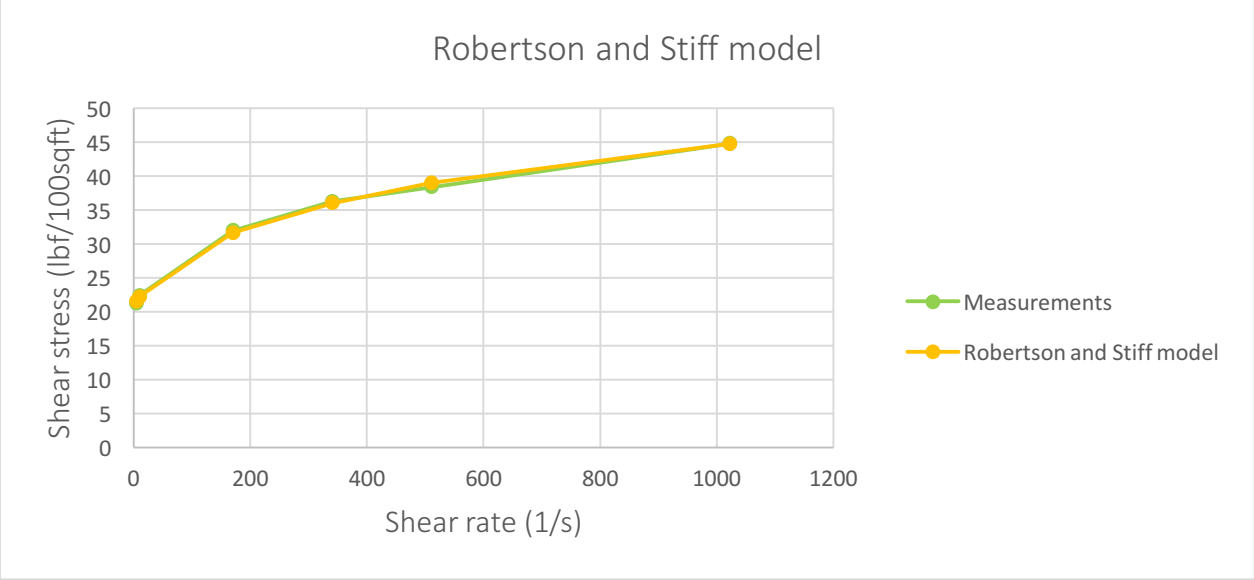

Figure 3.10: An illustration of the Robertson and Stiff model

Model	Equation	Parameters			Model deviation in %
		A	C	B	
Robertson Stiff	$10.721(24.839+\gamma)^{0.2055}$	10.721	24.839	0.2055	0.8%

Table 3.9: Data for the Robertson and Stiff model example

3.6 Viscoelasticity

The viscoelastic behaviour of selected fluid systems from experimental works will be examined and presented in the experimental study. This section will present useful theory for further interpretation of the measured data.

Viscoelasticity is a material property that exhibit characteristics that are both viscous and elastic when undergoing deformation [43]. The material response is usually a time-dependent response to a strain that behaves sinusoidal.

Most materials have viscous properties as well as elastic characteristics. Elastic behaviour is described in section 3.7.3. This means that they are viscoelastic by nature, and one example is biopolymer solutions [44]. Most fluids used in oil-field applications tend to exhibit properties that are viscoelastic to some degree. Determining the viscoelastic properties of a drilling fluid may help evaluate characteristics such as the gel structure, gel strength, barite sag and solid suspension phenomenon.

The most common way to quantify the viscoelastic properties is by measuring the elastic modulus (G') and the viscous modulus (G''). These may also be referred to as the storage modulus and loss modulus respectively. This due to the elastic energy is stored while the viscous energy is lost [44].

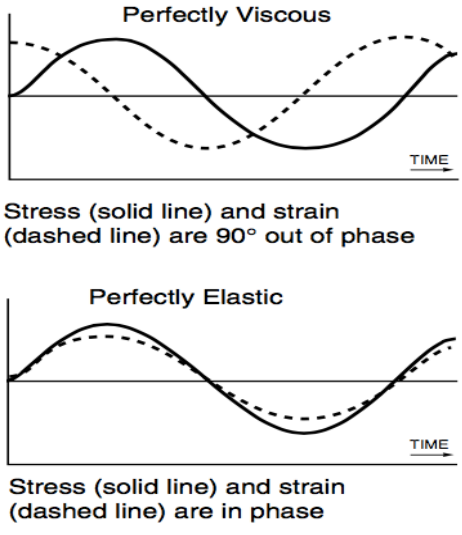

Figure 3.11: Illustration of a viscous and elastic material's behaviour over time [44]

3.6.1 Viscoelastic Theory

The sinusoidal deformation and the stress response of the drilling fluid is measured during the viscoelastic experiments. In terms of stain, the shear stress may be expressed as the following function of time [43]:

$$\tau(t) = \tau_o[\sin(\omega t)\, cos\delta + \cos(\omega t)\, sin\delta] \tag{3.21}$$

$$\tau(t) = \gamma_0 \left[\left(\frac{\tau_o}{\gamma_0} cos\delta\right) \sin(\omega t) + \left(\frac{\tau_o}{\gamma_0} sin\delta\right) \cos(\omega t)\right] \tag{3.22}$$

$$\tau(t) = \gamma_0[G' \sin(\omega t) + G'' \cos(\omega t)] \tag{3.23}$$

$$G' = \left(\frac{\tau_o}{\gamma_0} cos\delta\right) \tag{3.24}$$

$$G'' = \left(\frac{\tau_o}{\gamma_0} sin\delta\right) \tag{3.25}$$

$$tan\delta = \left(\frac{G''}{G'}\right) \text{ or } tan^{-1}\left(\frac{G''}{G'}\right) = \delta \tag{3.26}$$

δ represents the phase angle for the fluid. If the fluid is purely viscous, it will experience a phase angle equal to 90. The fluid will experience a phase angle equal to 0 for a purely elastic material. When the shear modulus and storage modulus are equal, the material will be in the transitioning phase and the phase angle will equal 45. This may bee seen from Equation 3.26.

Phase angle	$0 < \delta < 45$	$\delta = 45$	$45 < \delta < 90$
Behaviour	Elastic	Transitional	Viscous
G' and G''	G' > G''	G' = G''	G' < G''

Table 3.10: Viscoelastic parameters

3.6.2 Viscoelastic Measurements

One type of viscoelastic test will be performed on selected fluids in this thesis. That is the oscillatory amplitude sweep test. The viscoelastic region (LVER) may be determined from the test, and further used to determine the stability of the fluid systems. The length of the LVER of the elastic modulus will describe the degree of sample dispersion as well as the stability [45].

3.6.2.1 Oscillatory Amplitude Sweep Test

For this viscoelasticity test, the amplitude of the oscillation for the shear stress is varied while the frequency is held constant. For lower shear rates, the storage and loss modules are constant, and the structure of the fluid is not disturbed. The linear horizontal region before disruption is linear viscoelastic. With increasing shear rates, the sample structure will deform irreversibly, hence the fluid response will go from linear viscoelastic to nonlinear viscoelastic [43]. This is illustrated in Figure 3.12.

The yield point may be derived from this test, and is explained as the point at where the storage modulus deviates from the horizontal linear viscoelastic region. In the intersection point of the G' and G'' lines, one may derive the flow point. This is the point where the system becomes equally viscous and equally elastic. The phase angle will be 45 degrees in this point. The fluid will become more viscous dominated after the intersection point.

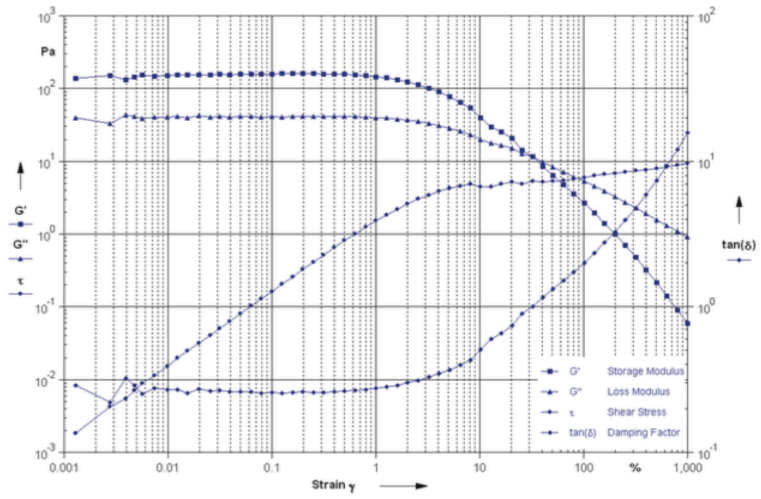

Figure 3.12: Example of Oscillatory Amplitude Sweep Test figure [43]

3.6 Tribology and Friction

Tribology is known as the study of interacting surfaces in relative motion from a macroscopic perspective [46]. This term was first coined in the 1960's but has been pursued for centuries. Amontons, a French military engineer published the classical friction laws in the 17th century, where he stated that [46]:

- Shear resistance between two bodies is independent of the apparent area of contact.
- The shear resistance is proportional to the normal load.

A third rule is often added to these rules and states that [46]:

- Dynamic friction is independent of sliding velocity.

Antoine Parent introduced Amontons work to mechanics by the following equation [47]:

$$tan\theta = \frac{F}{N} \tag{3.27}$$

Where θ is the inclination of the plane, F is the tangential force and N is the normal force. Later on, Euler proved that the coefficient of friction might be described as [47]:

$$\mu_f = tan\theta \tag{3.28}$$

For use today, the friction coefficient is the relation between the friction force and a normal load applies to objects that is in contact, and defined as [47]:

$$\mu_i = \frac{F_i}{N} \tag{3.29}$$

Where i describes the friction as either kinetic or static, F is the frictional force, N the normal force and μ is the coefficient of friction.

The friction coefficient may be influenced by the load applied, humidity, surface roughness, temperature, viscosity and speed [47].

The friction may be characterized as either dynamic (kinetic) or static, where the static friction is the force counteracting the applied force when two objects are not moving relative to one another. The dynamic friction is described as the force counteracting the pulling force when the objects in contact are moving relative to each other. Typical behaviour of these two types of friction is illustrated in Figure 3.13 [47].

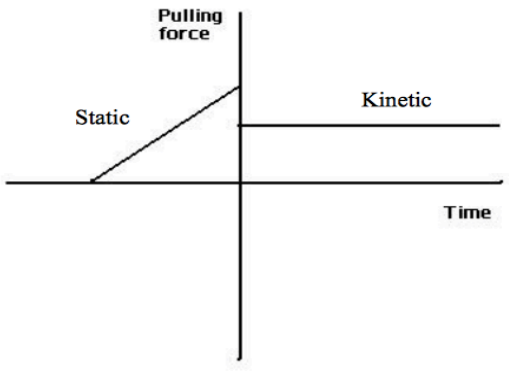

Figure 3.13: Typical behaviour of static and dynamic friction as a function of time [47].

3.6.1 Wear Mechanics

Adhesive wear is one of the wear modes generated under plastic contact. The plastic contact interface between similar materials has adhesive bonding strength. If the contact interface between two surfaces are inclined or curved and interlocked, the plastic deformation will take place in a sliding form. A certain volume of the surface material is removed due to ploughing, and an abrasive groove is formed on the weaker surface [48]. Abrasive wear is the main wear function during tribometer testing. The tribometer function and setup is explained in the experimental study.

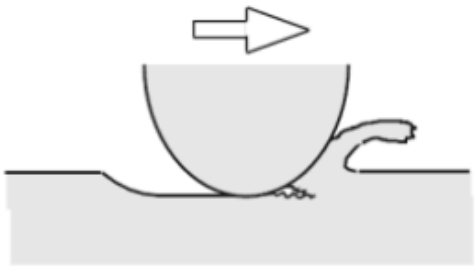

Figure 3.14: Illustration of Abrasive wear mechanisms [48]

3.7 Torque and drag

This section will provide general information about the torque and drag theory relevant for further simulation studies. The designed well for simulation studies were curved, hence information regarding curved wells were included.

An illustration of a drill-string for any curved well is presented in Figure 3.15 [49]. The drill-string is divided into segments along the length of the pipe. The segments are loaded both at the top and at the bottom with compressive (-) or tensile (+) loads. These loads are created by thermal, hydrostatic and fluid flow shear forces and are responsible for the length variation of the drill-pipe.

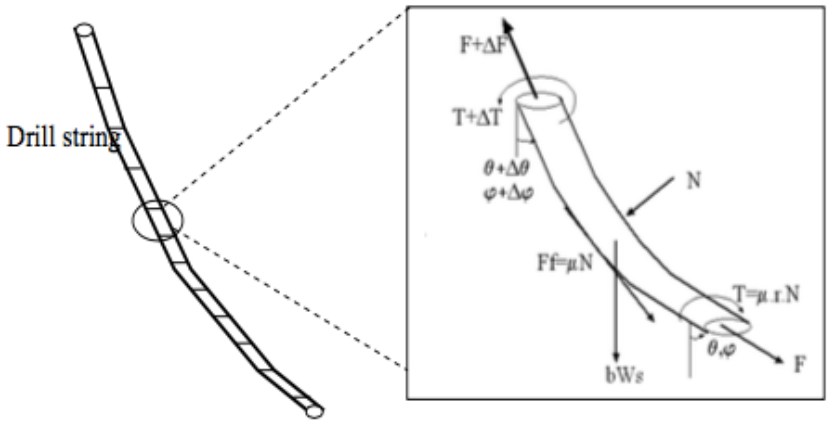

Figure 3.15: Segmented drill-string with a presented load distribution [49]

A smooth wellbore is desired, but are rarely a reality. There are often a continuous change in both inclination (θ) and azimuth (φ). Johansick presented a first differential force equation, balancing between the net force and the vector sum of the axial weight components (w) and the friction force (μ_f) [10]:

$$\frac{dF}{ds} = \pm\mu_f \left(\sqrt{\left(\beta w_s \, sin\theta + F\frac{d\theta}{ds}\right)^2 + \left(Fsin\theta \frac{d\varphi}{ds}\right)^2} \right) + \beta w_s \, cos\theta \qquad (3.30)$$

Where β describes the buoyance factor, the + sign describes tension (pulling the string) and the – sign describes compression (lowering the string). The square root term in Equation 3.30 is represented as the normal force per length unit for any curved well geometry. The normal force for each string segment may be calculated by the following equation [49]:

$$N_i = \sqrt{\left(\beta w_i \sin\left(\frac{\theta_{i+1}+\theta_i}{2}\right) + F_i\left(\frac{\theta_{i+1}+\theta_i}{S_{i+1}-S_i}\right)\right)^2 + \left(F \sin\left(\frac{\theta_{i+1}+\theta_i}{2}\right)\left(\frac{\varphi_{i+1}-\varphi_i}{S_{i+1}-S_i}\right)\right)^2} \qquad (3.31)$$

Were S represents the string segments.

3.7.1 Drag

The drag load is described as the required force to pull and run the pipe within the hole [49]. Great drag and torque forces are often experienced at the same time. The drag force is paralleled to the load and is compared to the free rotating drill string weight. However, it does not account for reciprocating. This weight is usually positive when pulling out of hole (POOH) and negative while running into hole (RIH) due to movement direction of the pipe. In the upward direction, the friction will add to the weight [49]. Excessive tensional loads may lead to a stretched drill-pipe, which decreases the pipe integrity and may lead to fracture. Excessive compressive loads may lead to drill-string buckling. The contact drag force is given by the following equation [49]:

$$F_{i+1} = F_i + \sum_{i=1}^{n}\left[\beta w_i \cos\left(\frac{\theta_{i+1}+\theta_i}{2}\right) \pm \mu_i N_i\right](S_{i+1} - S_i) \qquad (3.32)$$

The negative and positive sign of the equation allows the equation to be suitable for the pipe movement, either POOH or RIH. The plus sign lets friction add to the axial load when pulling out of hole, whilst subtract the friction when running in hole. F_i is the bottom weight when integrating from the bottom to the top of the string.

The material needs to withstand both the torsional movement and drag movement when exposed to torsional loads and axial loads. Torque and drag may become excessive due to various reasons such as tight hole conditions, differential sticking, sliding wellbore friction and cuttings bedding. But in wells with overall good hole conditions, the primary source of excessive torque and drag seems to be the sliding friction [50]. Two factors that affect the sliding wellbore friction are the normal contact force and the friction coefficient between the contact surfaces.

3.7.2 Torque

Torque is described as a moment where the force applied is multiplied with the radius or distance in arm. For drilling operations, the torque is the moment required to rotate the drill-pipe. Torque is essential to break the formation, hence essential to be able to drill in depths [49].

The torque needs to overcome the rotational friction force at the bit and in the well. Moment is applied at the top of the drill-string, and usually less of the rotational torque is available at the bit due to losses along the string. The torque loss in vertical wells is ideally set to zero, except for small losses due to the viscous forces in the drilling fluid. The torque loss for deviated and horizontal wells may be significant, especially in complex and long extended reach wells where the well friction will increase [51]. This is a significantly limiting factor as the drilled measured depth of the well may decrease with the torque loss.

Torque is dependent on the rotation radius, the coefficient of friction and the normal force over pipe. The increment of torque may be calculated by the following equation [49]:

$$\Delta T = \mu_f N_i r \Delta S \tag{3.33}$$

Where ΔT is the torque addition, μ_f is the coefficient of friction, r is the rotating radius and ΔS is the change of length. It is also possible to calculate the torque loss per length unit for both a buckled and non-buckled drill-string and the equation is expressed as the following [49]:

$$T_{i+1} = T_i + \sum_{i=1}^{n} \mu r_i N_i (S_{i+1} - S_i) \tag{3.34}$$

Where the equation to calculate the contact force N_i is given in Equation 3.31.

3.7.3 Torsional and tensile limit

It is critical if a material used during drilling operations is exposed to stress exceeding the lower yield strength, as it may deform the material plastic and impact the materials integrity. The experienced loads during a drilling operation must therefore be inside the safe operational window to avoid problems occurring due to permanent deformation.

The torsional limit is defined as the ability of a material to withstand a twisting load [52]. It is the ultimate material strength when subjected to a torsional load, and it is the maximum torsional stress that a material is able to sustain before it may rupture. This is also called the shear strength. If exceeding this limit, the material will fail. The tensile limit is defined as the pipe strength reaching the maximum yield point [51]. The tensile limit needs to be within the elastic deformation area, as a plastic deformation of the pipe is not desired. If exceeding the tensile limit, the material will fail.

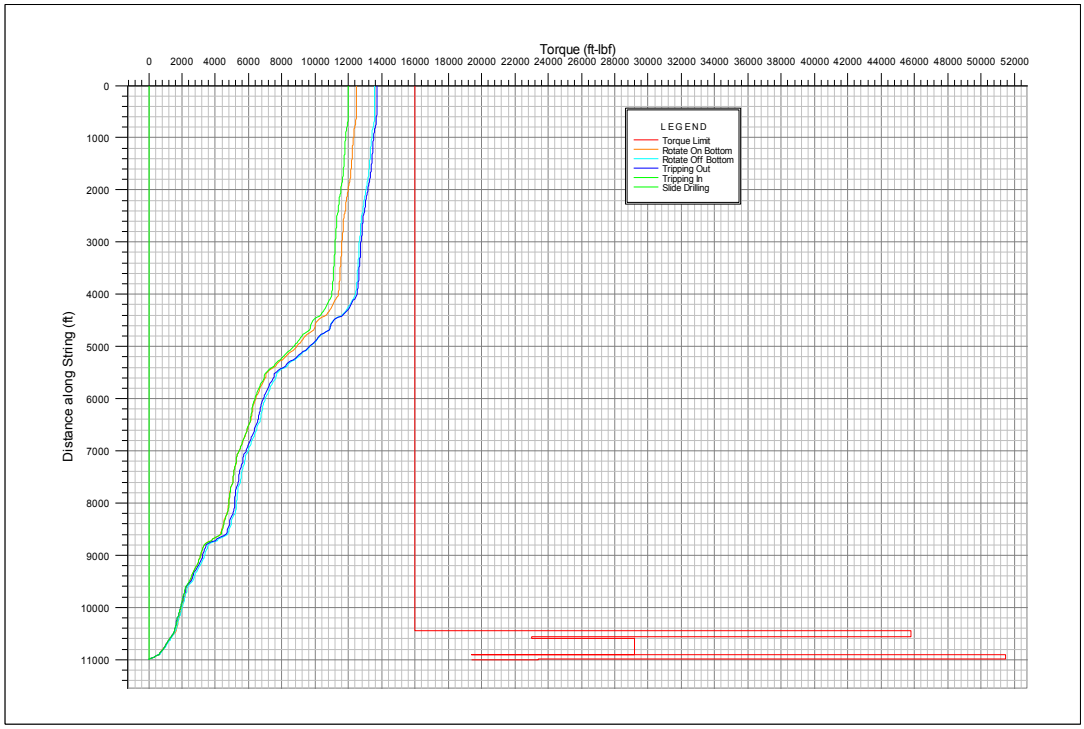

Figure 3.16: Torsional limit example where the loads does not exceed the tensile limit [51]

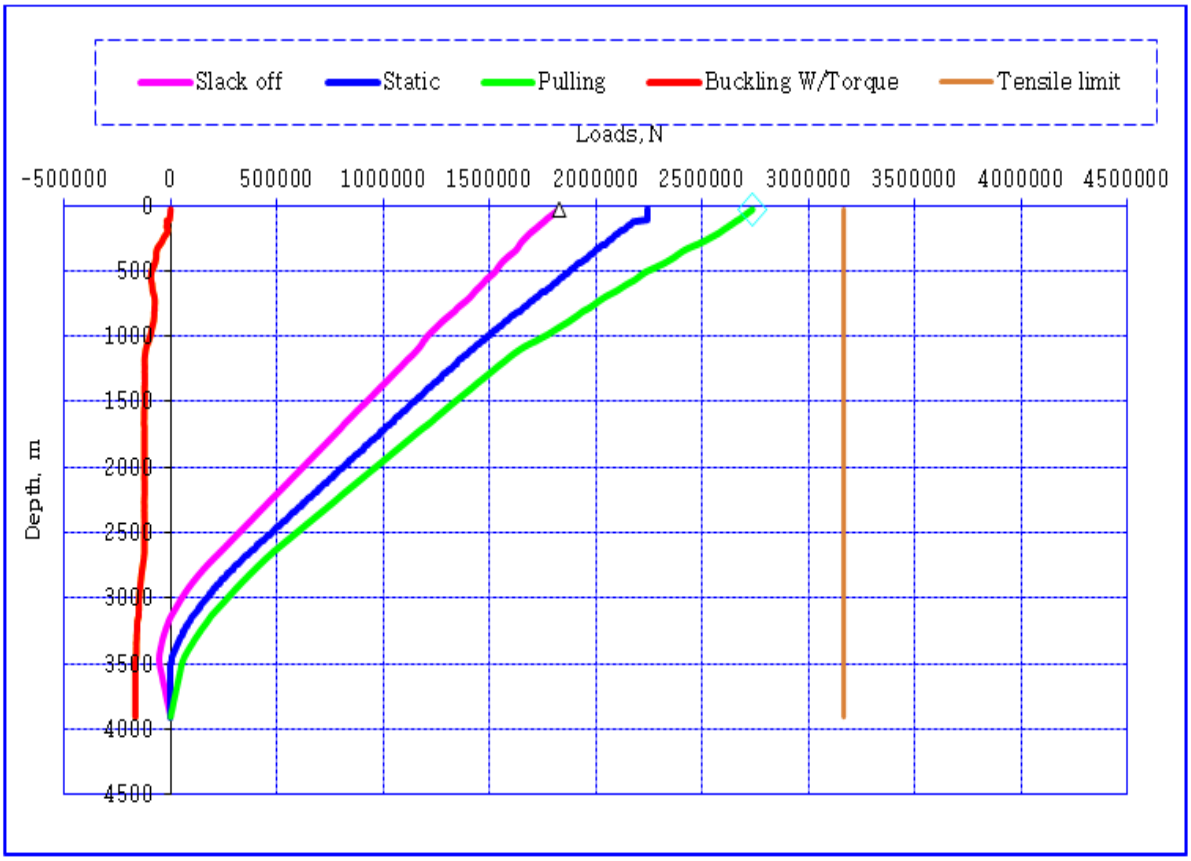

Figure 3.18: Tensile limit example where the loads does not exceed the tensile limit [51]

3.8 Hydraulics

For engineers, fluid mechanics is a branch of science that studies all of the aspects of fluid behaviour. A subsection for the science of fluid mechanics is called hydraulics. This subsection focuses mainly on the behaviour and movement of liquids [53]. This includes matters such as the friction in the surface equipment, pipe, through the bit nozzles and in the annulus.

Drilling fluid flows through a circulation system, where it is pumped from the surface equipment, down the pipe, through the nozzles into the annulus and back to surface through the return line. When the fluid is circulated through this system, pressure will be lost due to parameters like friction. It is therefore important that the rig pump will overcome all of the pressure losses. The pressure loss will act the opposite way of the flow direction. The pressure losses are:

- Pressure loss through parts like swivels and pipes in the surface equipment, ΔP_{surf}.
- Flow through the drill-string and drill-collar, $\Delta P_{drillstring}$ and $\Delta P_{drillcollar}$.
- Flow through the drill-bit and nozzles, ΔP_{bit}.
- Flow through the annulus, $\Delta P_{annulus}$.
- Flow in the annular space between the drill-string and riser, $\Delta P_{dsannulus}$.

The total pressure loss in the well is the sum of the stated pressure drops and may be described through the following equation:

$$\Delta P_{total} = \Delta P_{surf} + \Delta P_{drillstring} + \Delta P_{drillcollar} + \Delta P_{bit} + \Delta P_{annulus} + \Delta P_{dsannulus} \quad (3.35)$$

A typical drilling circulation system is illustrated in Figure 3.19. The surface equipment is not represented in this figure.

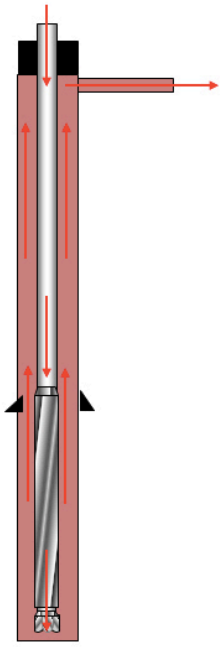

Figure 3.19: Typical drilling circulation system (forward circulation) [54]

The pressure determining gradient in the well system is called equivalent circulation density. The ECD takes friction loss in the annulus when pumping into account and is expressed by the following formula [55]:

$$ECD = \left(\frac{\Delta P_{annulus}}{0.052 \cdot D_{TVD}}\right) + MW \quad (3.36)$$

Where ECD [ppg] is the equivalent circulation density, $\Delta P_{annulus}$ [psi] is the annulus frictional pressure loss, D_{TVD} [ft] is the total vertical depth and MW [ppg] is the mud-weight. The equation presented is solely applicable for field units as it contains the conversion factor of 0.052. The equation would be different if stated for metric units.

3.8.1 Hydraulic performance

The hydraulic performance of the drilling fluids will be presented by simulation later in this thesis. To analyse the hydraulic performance of selected formulated fluids, the Unified model was solely considered.

The results for the rheological modelling of the fluids showed that for solely the nano-enhanced fluids, the unified model was the best model for three out of six fluids. The main reason was due to a literature study of hydraulic performance, executed in section 2.10.

Based on the reviewed information the unified model was chosen. A summary of the Unified hydraulic model equations used for simulation is presented in Table 3.11 [56].

Unified model	
Pipe Flow	Annular flow
$\mu_p = R_{600} - R_{300}, [cP] \quad \tau_y = R_{300} - \mu_p, [lbf/100ft^2] \quad \tau_0 = 1.066 \cdot (2 \cdot R_3 - R_6)$	
$n_p = 3.32 \cdot log\left(\frac{2 \cdot \mu_p + \tau_y}{\mu_p + \tau_y}\right)$ $k_p = 1.066\left(\frac{\mu_p + \tau_y}{511^{n_p}}\right)$	$n_a = 3.32 \cdot log\left(\frac{2 \cdot \mu_p + \tau_{y-\tau_y}}{\mu_p + \tau_{y-\tau_y}}\right)$ $k_a = 1.066\left(\frac{\mu_p + \tau_y - \tau_0}{511^{n_a}}\right)$ $k = [lbf \cdot sec^n/100ft^2]$
$G = \left(\frac{(3-\alpha)n+1}{(4-\alpha)n}\right) \cdot \left(1 + \frac{\alpha}{2}\right)$ $\alpha = 1\ for\ pipe \qquad \alpha = 1\ for\ annuli$	
$v_p = \frac{24.51 \cdot q}{D_P^2}$	$v_a = \frac{24.51 \cdot q}{D_2^2 - D_1^2}$ $v = [ft/min]$
$\gamma_w = \frac{1.6 \cdot G \cdot v}{D_R} = [sec^{-1}]$	
$\tau_w = \left[\left(\frac{4-\alpha}{3-\alpha}\right)^n \tau_0 + (k \cdot \gamma_w^n)\right] = [lbf/100ft^2]$	
$N_{Re} = \frac{\rho \cdot v_p^2}{19.36 \cdot \tau_w}$	$N_{Re} = \frac{\rho \cdot v_a^2}{19.36 \cdot \tau_w}$
$f_{laminar} = \frac{16}{N_{Re}}$ $f_{transient} = \frac{16 \cdot N_{Re}}{(3470 - 1370 \cdot n_p)^2}$ $f_{turbulent} = \frac{a}{N_{Re}^b}$ $a = \frac{\log(n) + 3.93}{50} \qquad b = \frac{1.75 - \log(n)}{7}$	$f_{laminar} = \frac{24}{N_{Re}}$ $f_{transient} = \frac{16 \cdot N_{Re}}{(3470 - 1370 \cdot n_a)^2}$ $f_{turbulent} = \frac{a}{N_{Re}^b}$ $a = \frac{\log(n) + 3.93}{50} \qquad b = \frac{1.75 - \log(n)}{7}$
$f_{partial} = (f_{transient}^{-8} + f_{turbulent}^{-8})^{-1/8}$	
$f_p = (f_{partial}^{12} + f_{laminar}^{12})^{1/12}$	$f_a = (f_{partial}^{12} + f_{laminar}^{12})^{1/12}$
$\left(\frac{dp}{dL}\right) = 1.076 \cdot \frac{f_p \cdot v_p^2 \cdot \rho}{10^5 \cdot D_p} = [psi/ft]$ $\Delta p = \left(\frac{dp}{dL}\right) \cdot \Delta L = [\text{psi}]$	$\left(\frac{dp}{dL}\right) = 1.076 \cdot \frac{f_a \cdot v_a^2 \cdot \rho}{10^5 \cdot (D_2 - D_1)} = [psi/ft]$ $\Delta p = \left(\frac{dp}{dL}\right) \cdot \Delta L = [\text{psi}]$
$\Delta p_{Nozzles} = \frac{156 \cdot \rho \cdot q^2}{\left(D_{N1}^2 - D_{N2}^2 - D_{N3}^2\right)^2} = [psi]$	

Table 3.11: Parameters and equations for the Unified model used in hydraulic simulation

4 Experimental Evaluations of Nano Treated Drilling Fluids

Several batches of nano treated drilling fluids were formulated and designed to investigate the effect of nano in bentonite treated WBM systems, mainly how the particles influence the rheology and friction of the system. The fluids are going to be characterized through their rheological properties, the filtrate loss, pH, coefficient of friction and the viscoelastic properties.

4.1 Fluid Formulation and Mixing

The added commercial nanoparticles of the fluid systems were selected due to their lubricating abilities and use in other industries. The fluids were designed realistic to get a picture of how the polymers, salt and nano affect each other in the formulated system. However, weight material for density was not used. Salt was added for inhibitive properties, polymer for viscous and filtrate loss purposes and bentonite for viscous and shear thinning abilities. The fluids were formulated in-situ and in the following order:

1. Water. 2. Salt. 3. Nano. 4. Polymer. 5. Bentonite.

The fluids were mixed with a Hamilton beach mixer until the fluid system was free of lumps and smooth. The polymers were added with uttermost care as they tend to cluster and form lumps if not added to water carefully. The fluid aged for 48 hours before further testing to ensure bentonite swelling. The mixing and ageing process was applied for all the drilling fluid formulations. Water from the tap was used for the drilling fluid formulations prepared in this thesis. The tap water chemistry is not available, but bentonite swelled using the tap water with no other additives. For the nano-fluid formulations, the following reference systems were used.

Drilling fluid reference systems	
System 1	500ml H_20 + 2.5g KCl + 0.5g XG + 25g Bentonite
System 2	500ml H_20 + 2.5g KCl + 0.5g CMC + 25g Bentonite

Table 4.1: Presentation of the drilling fluid reference systems

4.2 Rheological Tests

This section will present the investigation set up, description of formulated drilling fluid systems and the results of the rheological tests executed. This includes the nano drilling fluids and their reference system. Bingham and power law values were calculated to investigate if the nanoparticles had any significant impact on the particle association of the drilling fluids.

4.2.1 Set Up for Investigation

Before the rheological tests, the drilling fluid was mixed for 2 minutes to ensure particle dispersion. The rheology was measured with a Fann-35 viscometer, with a rotational cylinder that is possible to set at shear rates of 600, 300, 200, 100, 60, 30, 6 and 3. Measurements were taken for all the shear rates at room temperature. The filtrate loss was measured for 7.5 minutes with an API Filter press. This is a static, pressurised cell that is fitted with a filter medium. The API Filter press is a LPLT device. A graph presenting the viscometer data was generated, and Bingham and Power law parameters were calculated and evaluated. This set up was executed for all the formulated fluid systems.

Figure 4.1 Fann-35 Viscometer used for readings

Figure 4.2: Filtrate loss measurement with an API Filter press

4.2.2 Rheological Tests for the TiN Fluids

Nano-sized TiN was added to a water based drilling fluid system to investigate how it will affect the system's rheological properties, and if it affects the friction coefficient and viscoelasticity of the mud system.

4.2.2.1 Description of the Formulated Fluid Systems

The TiN drilling fluids were formulated with various concentrations of TiN added to the selected water based reference system. At first, low concentrations of the nano-additive were implemented in the reference system to investigate the influence on the viscometer readings and the filtrate loss. A new batch with higher concentrations were made later for comparison. Table 4.2 and Table 4.3 describes the formulated drilling fluids.

Low concentration TiN drilling fluids					
	Ref	Ref + 0.05	Ref + 0.10	Ref + 0.15	Ref + 0.20
Water	500 ml	500 ml	500 ml	500 ml	500 ml
Bentonite	25 g	25 g	25 g	25 g	25 g
KCl	2.5 g	2.5 g	2.5 g	2.5 g	2.5 g
XG	0.5 g	0.5 g	0.5 g	0.5 g	0.5 g
Tin	0 g	0.05 g	0.1 g	0.15 g	0.2 g

Table 4.2: Low concentration TiN drilling fluids

High concentration TiN drilling fluids					
	Ref	Ref + 0.5	Ref + 1.25	Ref + 2.5	Ref + 3.75
Water	500 ml	500 ml	500 ml	500 ml	500 ml
Bentonite	25 g	25 g	25 g	25 g	25 g
KCl	2.5 g	2.5 g	2.5 g	2.5 g	2.5 g
XG	0.5 g	0.5 g	0.5 g	0.5 g	0.5 g
Tin	0g	0.5g	1.25g	2.5g	3.75g

Table 4.3: High concentration TiN drilling fluids

4.2.2.2 Results and Analysis of the Low Concentration TiN Fluids

Figure 4.3 shows the viscometer data, of the low TiN concentration drilling fluids.

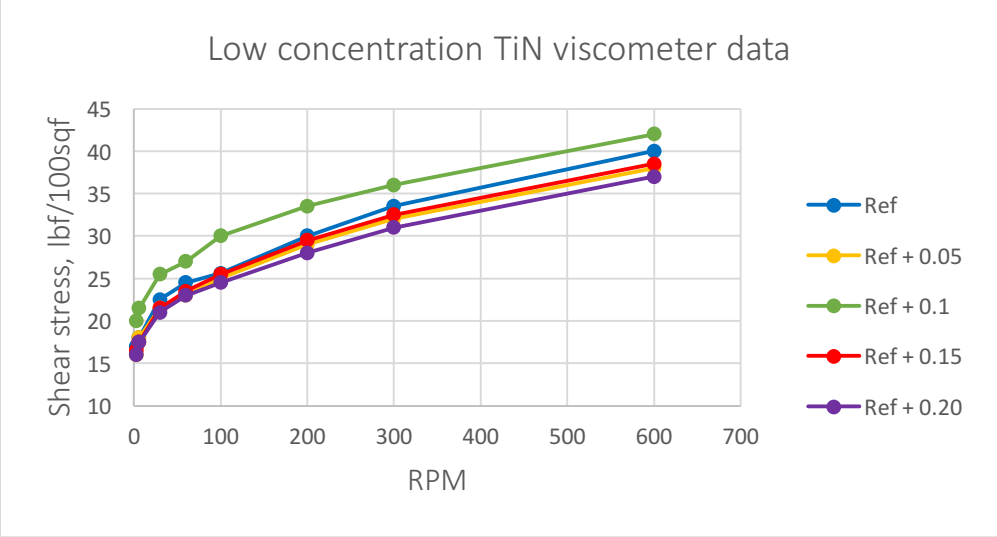

Figure 4.3: Low concentration TiN viscometer data

The viscometer data revealed that some changes to the viscometer readings were experienced with low concentration TiN as an additive. The shear stress increased solely for the Ref + 0.1 fluid compared to the reference system. The shear stress curves were lower or equalling the reference curve. From the shear stress measurements, both Bingham and Power Law parameters were calculated and is presented in Figure 4.4 and Figure 4.5.

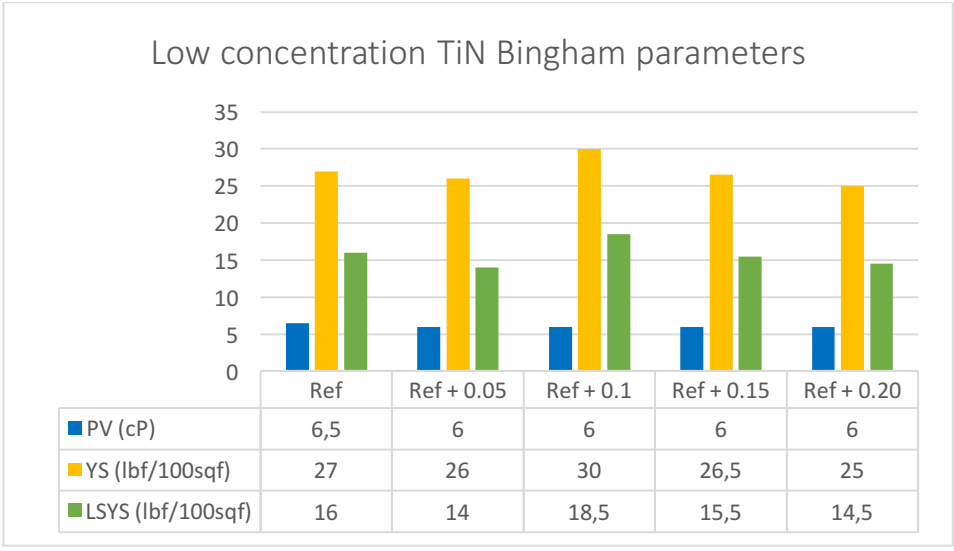

	Ref	Ref + 0.05	Ref + 0.1	Ref + 0.15	Ref + 0.20
PV (cP)	6,5	6	6	6	6
YS (lbf/100sqf)	27	26	30	26,5	25
LSYS (lbf/100sqf)	16	14	18,5	15,5	14,5

Figure 4.4: Bingham parameters for the low concentration TiN fluids

The Bingham parameters report the following:

- The PV decreased slightly with 8.3% for all the fluids.
- The YS increased the Ref + 0.1 fluid, while it decreased slightly for all the other fluids compared to the Reference system. The YS of the Ref + 0.1 fluid increased by 11% compared to the reference fluid. An increased YS value indicates a greater electrostatic force between the particles in the mud system.

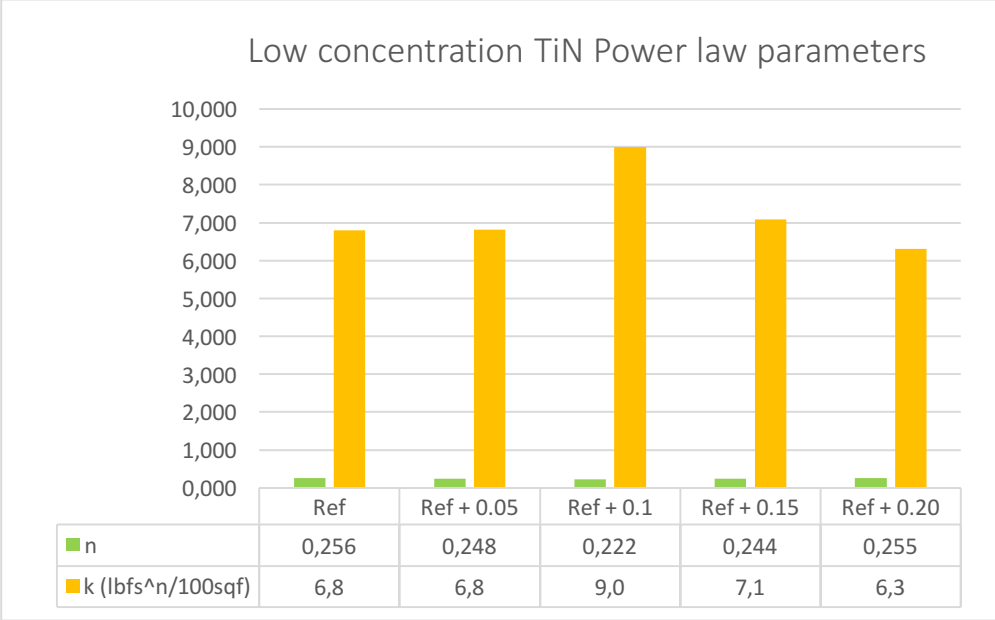

	Ref	Ref + 0.05	Ref + 0.1	Ref + 0.15	Ref + 0.20
n	0,256	0,248	0,222	0,244	0,255
k (lbfs^n/100sqf)	6,8	6,8	9,0	7,1	6,3

Figure 4.5: Power law parameters for the low concentration TiN fluids

The power law parameters report the following:

- The fluids with TiN added to the reference system showed a decrease in the exponent law index with a maximum decrease of 13.3% for the Ref + 0.1 system. All of the flow index values were below 1, which indicates that the formulated fluids exhibit pseudo plastic behaviour. The lowest n value was obtained for the Ref + 0.1 system.
- Most of the consistency index values increased compared to the reference system with the highest value for the Ref + 0.1 system. The increase for this system was of 32.4%. The K value decreased for the Ref + 0.20 system. The decrease was of 7.4%.

Table 4.4 report a filtrate decrease for the Ref + 0.05 and Ref + 0.1 fluids of 9.4%. With the Ref + 0.15 and Ref + 0.20 fluids the filtrate loss increased to a value equal and higher than the reference system (0.0% and 6.3% respectively).

	Filtrate changes for low concentration TiN				
System	Ref	Ref + 0.05	Ref + 0.1	Ref + 0.15	Ref + 0.20
Changes in %		-9.4	-9.4	0.0	6.3

Table 4.4: Filtrate changes for low concentration TiN

Table 4.5 report a pH decrease for all the fluid systems containing nano additives compared to the reference system. The decrease varies from 0.6% to 1.1%.

	pH changes for low concentration TiN				
System	Ref	Ref + 0.05	Ref + 0.1	Ref + 0.15	Ref + 0.20
Changes in %		-0.6	-1.1	-1.1	-1.1

Table 4.5: pH changes for low concentration TiN

4.2.2.3 Results and Analysis of the High Concentration TiN Fluids

Figure 4.6 shows the viscometer data of the high TiN concentration drilling fluids.

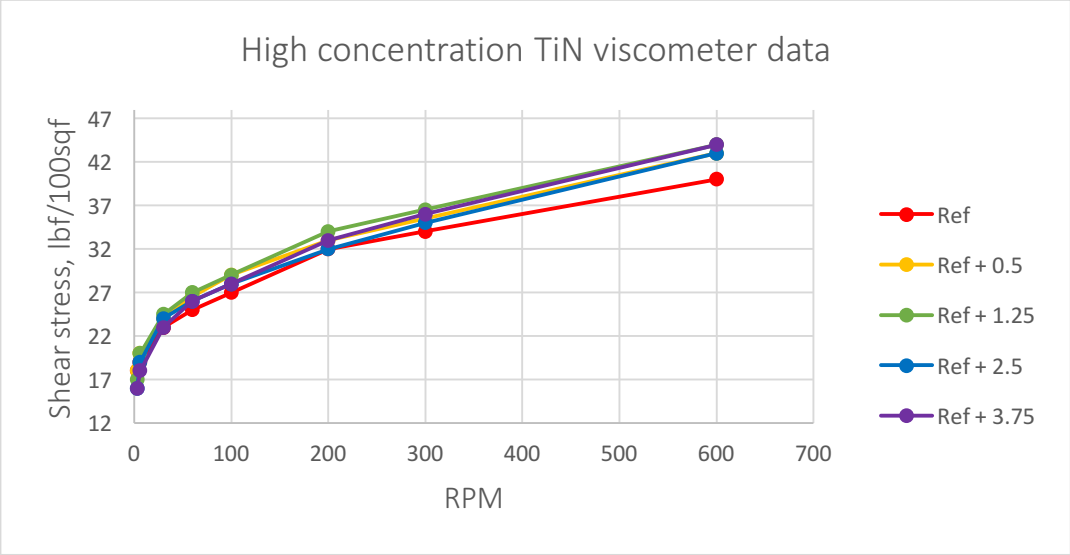

Figure 4.6: High concentration TiN Viscometer data

The viscometer data revealed that the curves equalled or contained values that are greater then the values of the reference system. The additives did not have any significant impact on the fluid systems viscometer readings, but some changes were seen, especially for the readings at 300 and 600 RPM. Bingham parameters and Power law parameters were calculated for further investigation and are presented in Figure 4.7 and Figure 4.8.

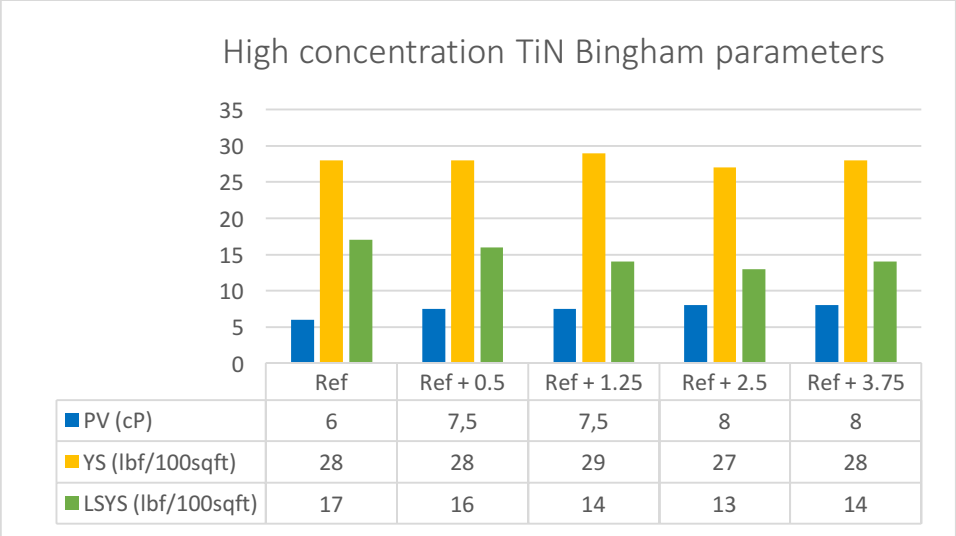

	Ref	Ref + 0.5	Ref + 1.25	Ref + 2.5	Ref + 3.75
PV (cP)	6	7,5	7,5	8	8
YS (lbf/100sqft)	28	28	29	27	28
LSYS (lbf/100sqft)	17	16	14	13	14

Figure 4.7: Bingham parameters for the high concentration TiN drilling fluids

The Bingham parameters reported the following:

- The PV of the fluids increased for all the systems with high concentration TiN as an additive. The greatest increase was of 33% for the Ref + 2.5 and Ref + 3.75 fluids compared to the reference system.
- The YS of the fluids either decreased or increased by 3.6% compared to the reference system.

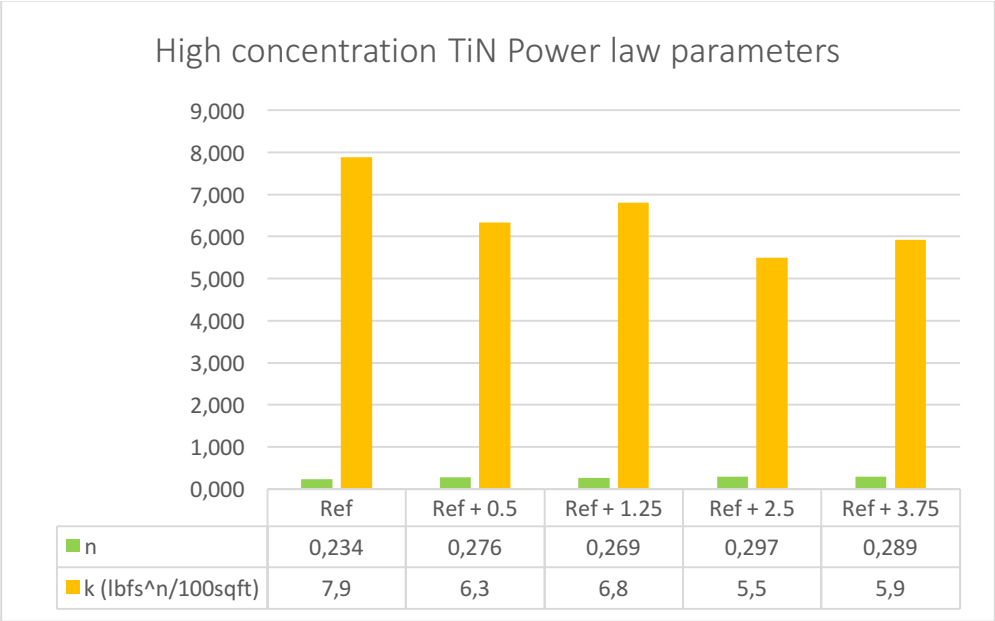

	Ref	Ref + 0.5	Ref + 1.25	Ref + 2.5	Ref + 3.75
n	0,234	0,276	0,269	0,297	0,289
k (lbfs^n/100sqft)	7,9	6,3	6,8	5,5	5,9

Figure 4.8: Power law parameters for the high concentration TiN fluids

The Power law parameters reported the following:

- The exponent law index increased for all the high concentration systems compared to the index for the reference system. The increase varied from 15.0% to 26.9%, where the largest increase was recorded for the Ref + 2.5 system. The fluids do still exhibit pseudo-plastic behaviour, but the increase may indicate that very high concentrations of nano TiN in the system can effect this behaviour.
- The consistency index decreased for all the systems. The largest decrease was of 30.4% for the Ref + 2.5 fluid.

Table 4.6 reports the filtrate change in % for the high concentration TiN fluids. With higher concentrations of TiN present in the fluids, the filtrate loss increased compared to the reference system with the lowest increase for the Ref + 0.5 fluid of 3.6% and the highest increase for the Ref + 2.5 system of 17.9%.

	Filtrate changes for high concentration TiN				
System	Ref	Ref + 0.5	Ref + 1.25	Ref + 2.5	Ref + 3.75
Changes in %		3.6	7.1	17.9	17.3

Table 4.6: Filtrate changes for high concentration TiN

Table 4.7 reports the changes in pH of the high concentration fluid systems. The pH values decreased for the fluids with TiN as an additive, with the largest decrease of 2.3% for the Ref + 3.75 fluid system.

	pH changes for high concentration TiN				
System	Ref	Ref + 0.5	Ref + 1.25	Ref + 2.5	Ref + 3.75
Changes in %		-0.6	-1.1	-1.1	-2.3

Table 4.7: pH changes for low concentration TiN

4.2.3 Rheological Tests for the MoS_2 Fluids

Nano-sized MoS_2 was added to a water based drilling fluid system to investigate the effect of MoS_2 on the rheology, friction and viscoelasticity of the system.

4.2.3.1 Description of the Formulated Fluid Systems

The MoS_2 fluids were formulated with a wide spectrum of MoS_2 concentrations to a selected water based reference system. Both high and low concentrations were added to the fluids to investigate the influence on the viscometer readings and filtrate loss. Table 4.8 describes the formulated drilling fluids.

Low and high concentration MoS_2 drilling fluids							
	Ref	Ref + 0.2	Ref + 0.5	Ref + 0.8	Ref + 1.25	Ref + 2.5	Ref + 3.75
Water	500 ml	500 ml	500 ml	500 ml	500 ml	500 ml	500 ml
KCl	2.5 g	2.5 g	2.5 g	2.5 g	2.5 g	2.5 g	2.5 g
XG	0.5 g	0.5 g	0.5 g	0.5 g	0.5 g	0.5 g	0.5 g
MoS_2	0 g	0.2 g	0.5 g	0.8 g	1.25 g	2.5 g	3.75 g

Table 4.8: Low and high concentration MoS_2 drilling fluids

4.2.2.2 Results and Analysis of the MoS_2 Fluids

Figure 4.9 shows the viscometer data of the prepared MoS_2 drilling fluids.

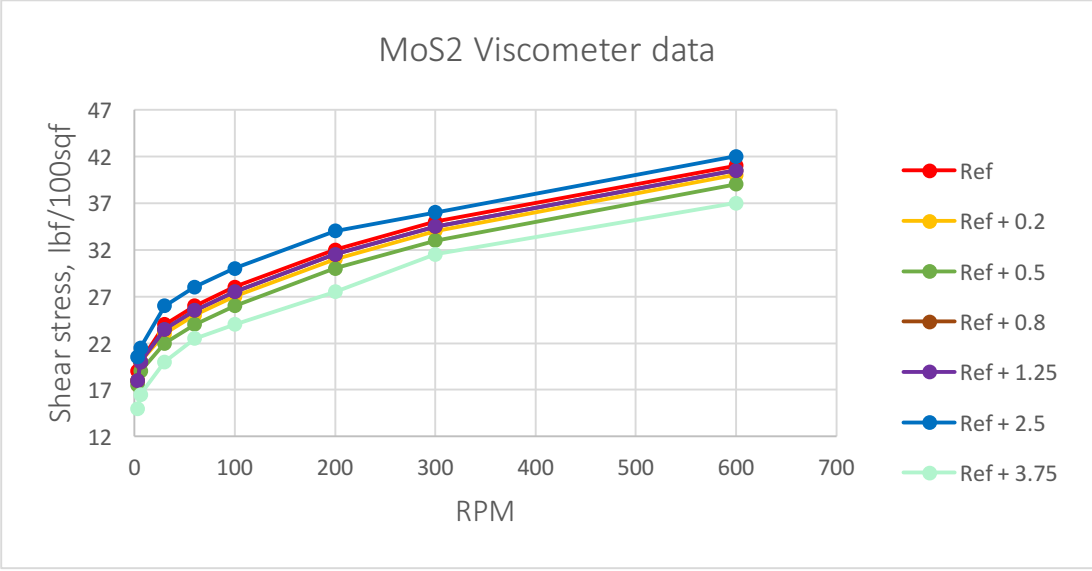

Figure 4.9: MoS_2 Viscometer data

The viscometer data revealed small changes to the nano-fluid systems compared to the reference system. There was solely an increase for the Ref + 2.5 fluid and a more significant decrease for the Ref + 3.75 fluid according to Figure 4.9. Bingham parameters and Power law parameters were calculated for further investigation and are presented in Figure 4.10 and Figure 4.11.

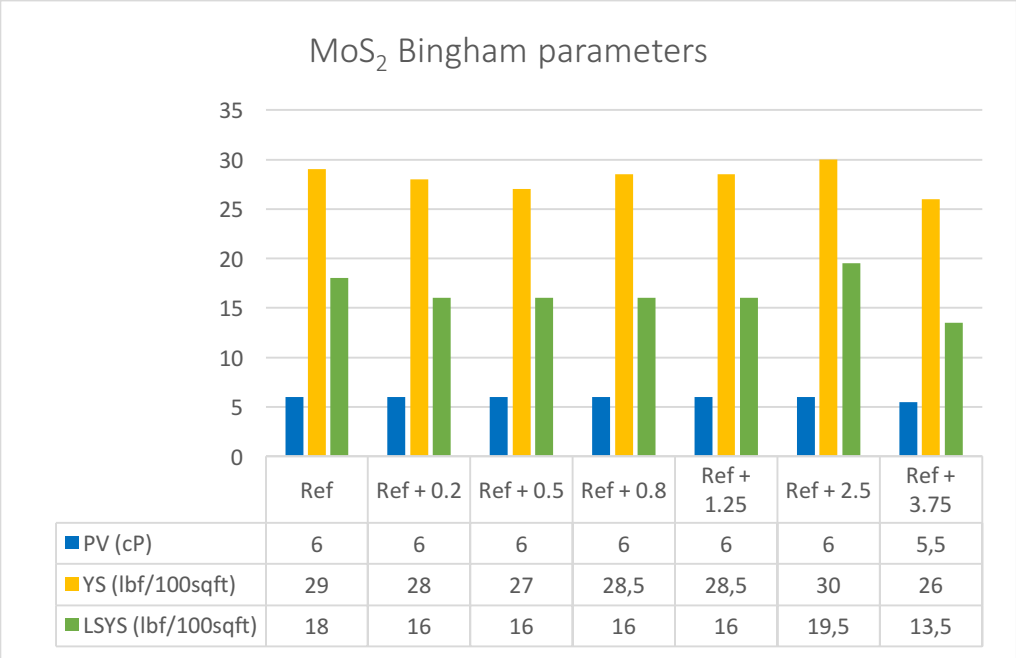

	Ref	Ref + 0.2	Ref + 0.5	Ref + 0.8	Ref + 1.25	Ref + 2.5	Ref + 3.75
PV (cP)	6	6	6	6	6	6	5,5
YS (lbf/100sqft)	29	28	27	28,5	28,5	30	26
LSYS (lbf/100sqft)	18	16	16	16	16	19,5	13,5

Figure 4.10: Bingham parameters for the MoS_2 drilling fluids

The Bingham parameters reported the following:

- The PV of the fluids were constant for all the fluids except for the Ref + 3.75 fluid where the readings revealed a reduction of 8.3%.
- The YS of the fluids either decreased with a maximum percentage of 10.3% for the Ref + 3.75 fluid or increased with a maximum percentage of 3.5% for the Ref + 2.5 fluid.
- There was no consistency in the changing YS values with increasing concentrations of nano in the fluids.

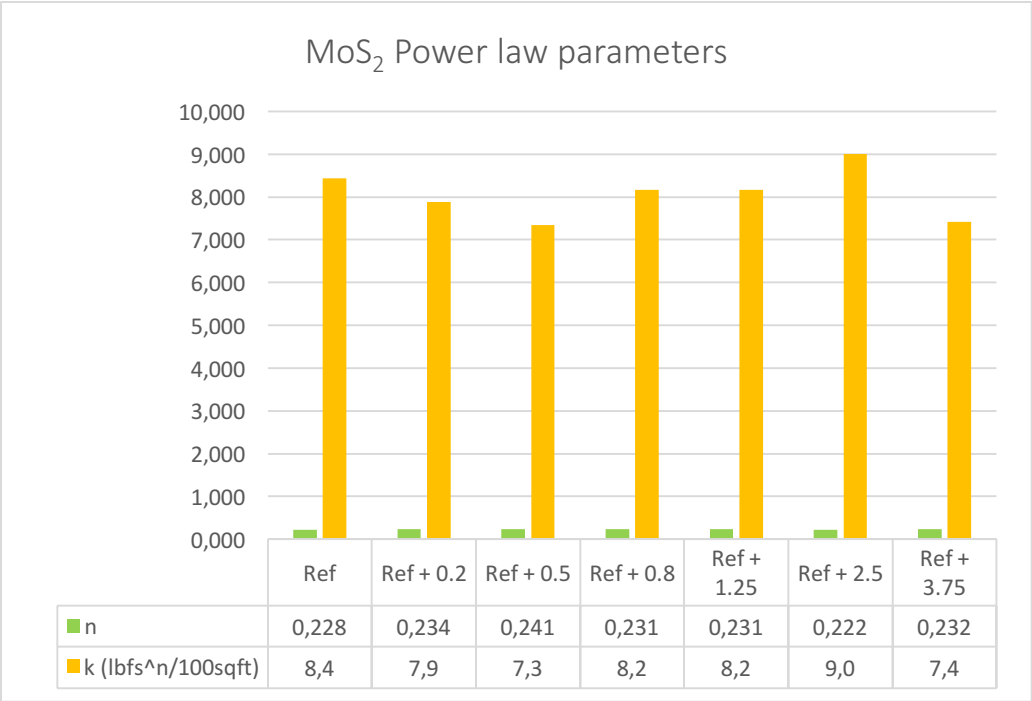

Figure 4.11: Power law parameters for the MoS_2 fluids

The Power law parameters reported the following:

- The exponent law index increased for five of the fluids with a percentage interval of 1.3% to 5.4%. The index increased for the Ref + 2.5 fluid with a percentage of 2.63%. The low n value indicates pseudo-plastic behaviour.
- The consistency index decreased for all the systems except for the Ref + 2.5 fluid where the increase was of 7.14%.

Table 4.9 reports the filtrate change in % for the MoS_2 fluids. The filtrate loss decreased for the Ref + 0.2 and Ref + 0.5 fluids with 10.7% and 3.6% respectively. Further, the filtrate loss values for the reference system and Ref + 0.8 system were equal while the filtrate loss increased with 7.1% for the remaining Ref + 1.25, Ref + 2.5 and Ref + 3.75 fluids.

	Filtrate changes for MoS_2 fluids						
System	Ref	Ref + 0.2	Ref + 0.5	Ref + 0.8	Ref + 1.25	Ref + 2.5	Ref + 3.75
Changes in %		-10.7	-3.6	0.0	7.1	7.1	7.1

Table 4.9: Filtrate changes for the MoS_2 fluids

Table 4.10 reports the pH changes for the MoS_2 fluids. The pH values increased with 1.1% for the lower concentration fluids, while the changes were set to 0,0% for the Ref + 1.25 fluid. The pH decreased for the Ref + 2.5 and Ref + 3.75 fluid with 0.6% and 2.3% respectively.

	pH changes for MoS_2 fluids						
System	Ref	Ref + 0.2	Ref + 0.5	Ref + 0.8	Ref + 1.25	Ref + 2.5	Ref + 3.75
Changes in %		1.1	1.1	1.1	0.0	-0.6	-2.3

Table 4.10: pH changes for the MoS_2 fluids

4.2.4 Rheological tests for the Graphene fluids

Nano-sized Graphene was added to a water based drilling fluid system to investigate how it will affect the system's rheological properties and if it affects the friction of the mud system.

4.2.4.1 Description of the Formulated Fluid Systems

The Graphene fluids were formulated with various concentrations of Graphene added to a selected wate -based reference system. Both high and very low concentrations of the substance were added to the reference fluids to investigate the viscometer readings and filtrate loss. Table 4.11 describes the formulated drilling fluids.

Low and high concentration Graphene fluids					
	Ref	Ref + 0.05	Ref + 0.1	Ref + 0.2	Ref + 0.4
Water	500 ml	500 ml	500 ml	500 ml	500 ml
Bentonite	25 g	25 g	25 g	25 g	25 g
KCl	2.5 g	2.5 g	2.5 g	2.5 g	2.5 g
CMC	0.5 g	0.5 g	0.5 g	0.5 g	0.5 g
Graphene	0 g	0.05 g	0.1 g	0.2 g	0.4 g
	Ref + 0.6	Ref + 0.8	Ref + 1.25	Ref + 2.5	Ref + 3.75
Water	500 ml	500 ml	500 ml	500 ml	500 ml
Bentonite	25 g	25 g	25 g	25 g	25 g
KCl	2.5 g	2.5 g	2.5 g	2.5 g	2.5 g
CMC	0.5 g	0.5 g	0.5 g	0.5 g	0.5 g
Graphene	0.6 g	0.8 g	1.25 g	2.5 g	3.75 g

Table 4.11: Low and high concentration Graphene fluids

4.2.4.2 Result and Analysis of the Graphene Fluids

Figure 4.12 shows the viscometer data of the prepared Graphene drilling fluids.

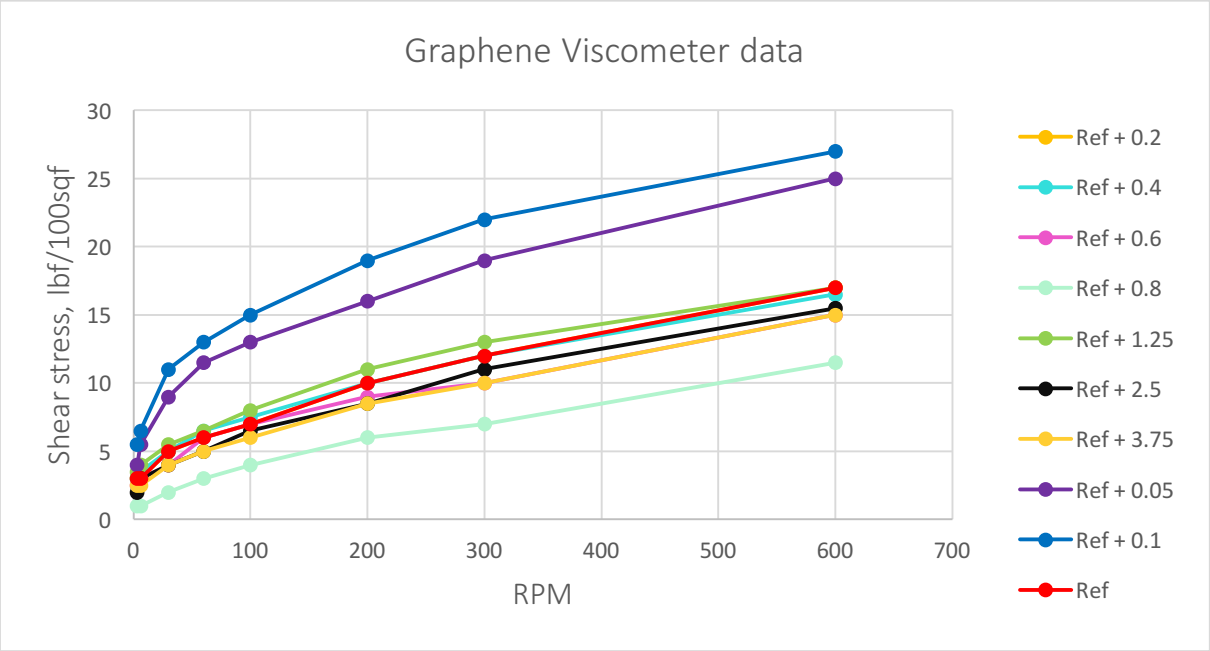

Figure 4.12: Graphene Viscometer data

The viscometer data revealed that with 0.05g and 0.1g of nano-sized Graphene to the reference system, the shear stress increased significantly. The shear stress also decreased slightly for the Ref + 0.8 fluid. For further investigation of the viscometer data, Bingham parameters and Power law parameters were calculated. The values are presented in Figure 4.13 and Figure 4.14.

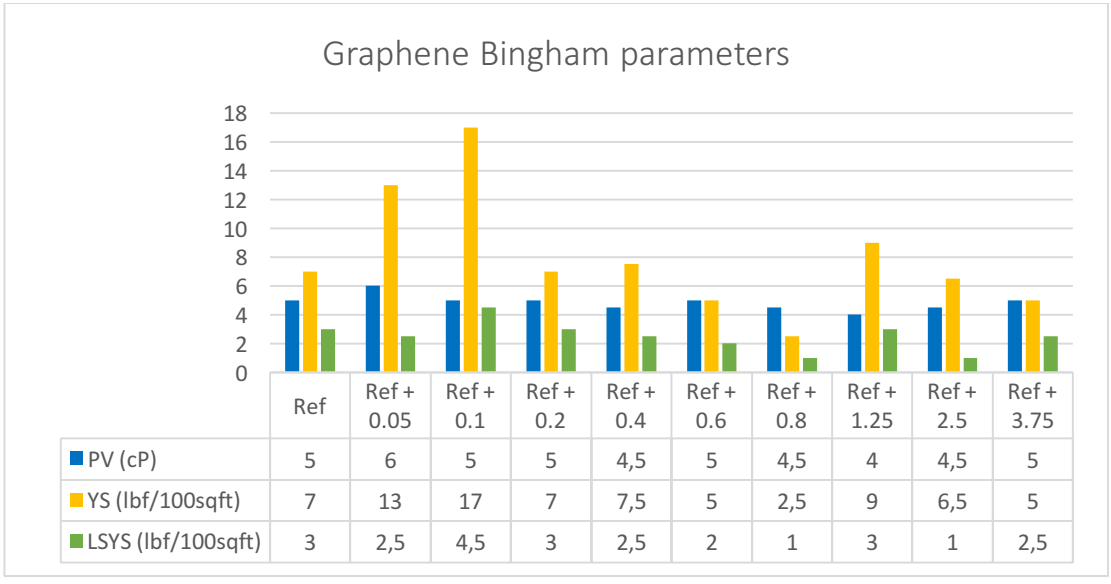

	Ref	Ref + 0.05	Ref + 0.1	Ref + 0.2	Ref + 0.4	Ref + 0.6	Ref + 0.8	Ref + 1.25	Ref + 2.5	Ref + 3.75
PV (cP)	5	6	5	5	4,5	5	4,5	4	4,5	5
YS (lbf/100sqft)	7	13	17	7	7,5	5	2,5	9	6,5	5
LSYS (lbf/100sqft)	3	2,5	4,5	3	2,5	2	1	3	1	2,5

Figure 4.13: Bingham parameters for the Graphene drilling fluids

The Bingham parameters reported the following:

- The PV of the Ref + 0.05 fluid increased compared to the reference system with 20%. The PV remained constant for the other fluids except for the Ref + 0.5, Ref + 0.8 and Ref + 1.25 fluids, where the PV decreased with 10%.
- The YS of the fluids showed significantly greater values compared to the reference fluid for the Ref + 0.05 and Ref + 0.1 fluids with an increase of 85.7% and 142.9% respectively. The lowest YS value was reported for the Ref + 0.8 system, with a decrease of 64.3%.

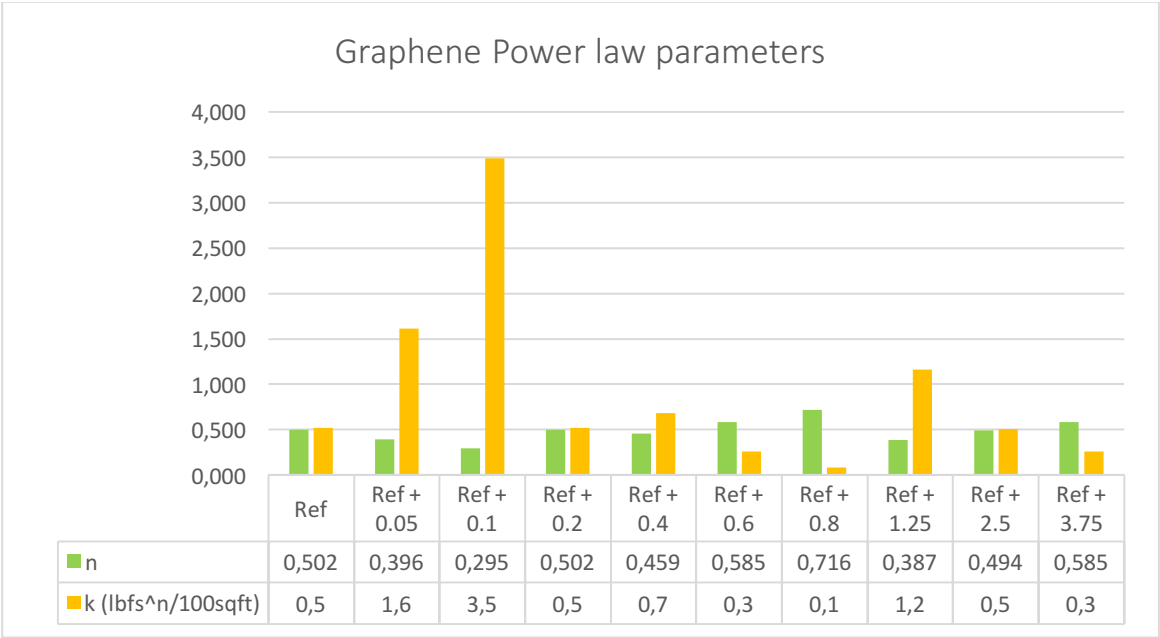

	Ref	Ref + 0.05	Ref + 0.1	Ref + 0.2	Ref + 0.4	Ref + 0.6	Ref + 0.8	Ref + 1.25	Ref + 2.5	Ref + 3.75
n	0,502	0,396	0,295	0,502	0,459	0,585	0,716	0,387	0,494	0,585
k (lbfs^n/100sqft)	0,5	1,6	3,5	0,5	0,7	0,3	0,1	1,2	0,5	0,3

Figure 4.14: Power law parameters for the Graphene drilling fluids

The power law parameters reported the following:

- The exponent law index value was reduced with 41.2% for the Ref + 0.1 fluid compared to the reference. The largest increase of the index was for the Ref + 0.8 fluid with 42.6%. All of the fluids exhibited flow index values greater than the systems formulated with XG. The values still indicate that the behaviour is pseudo-plastic.
- The consistency index increased the most for the Ref + 0.1 fluid system with a growth of 600%, while the consistency index for the Ref + 0.8 fluid decreased the most with a reduction of 40%.

Table 4.12 reports the filtrate changes in % for the Graphene fluids. The filtrate loss increased for all the fluids with Graphene as an additive. The largest increase was for the Ref + 0.1 fluid with 19.2%.

Filtrate changes for the Graphene fluids					
System	Ref	Ref + 0.05	Ref + 0.1	Ref + 0.2	Ref + 0.4
Changes in %		7.7	19.2	3.8	15.4
System	Ref + 0.6	Ref + 0.8	Ref + 1.25	Ref + 2.5	Ref + 3.75
Changes in %	3.8	3.8	3.8	7.7	18.5

Table 4.12: Filtrate changes for the Graphene fluids

Table 4.13 reports the pH changes in % for the Graphene fluids. The pH was not influenced by the nano-additive.

pH changes for the Graphene fluids					
System	Ref	Ref + 0.05	Ref + 0.1	Ref + 0.2	Ref + 0.4
Changes in %		0.0	0.0	0.0	0.0
System	Ref + 0.6	Ref + 0.8	Ref + 1.25	Ref + 2.5	Ref + 3.75
Changes in %	0.0	0.0	0.0	0.0	0.0

Table 4.13: pH changes for the Graphene fluids

4.2.4.3 Fluid observations

For the drilling fluid systems made with CMC, the water and particle phase separated after some hours. This disappeared after mixing before the rheological tests, but did occur after some time again. This did not occur for the systems formulated with XG. This may be an indication that Graphene as an additive is in an aggregated, and not dispersed state.

4.3 Friction Tests

This section will present the investigation set up, the calibration method, and the results of the frictional tests that were executed. This includes the nano drilling fluids and their reference system. The friction tests were executed at various temperatures. The investigation results were plotted, and a temperature depended equation of the friction coefficient of each fluid were modelled to investigate the effect of temperature and nano.

4.3.1 Set Up for Investigation

The instrument used for the experiments was a Tribometer from CMI instruments located at the University of Stavanger. The Tribometer is based on a “ball on disc” technology, and it is computer controlled. An associated heating element, or heating spiral was used to heat up the sample and used for measurements taken above room temperature. The heating spiral is fixed to the Tribometer apparatus and inserted into the sample cup. The Tribometer containing a fluid sample is illustrated in Figure 4.15.

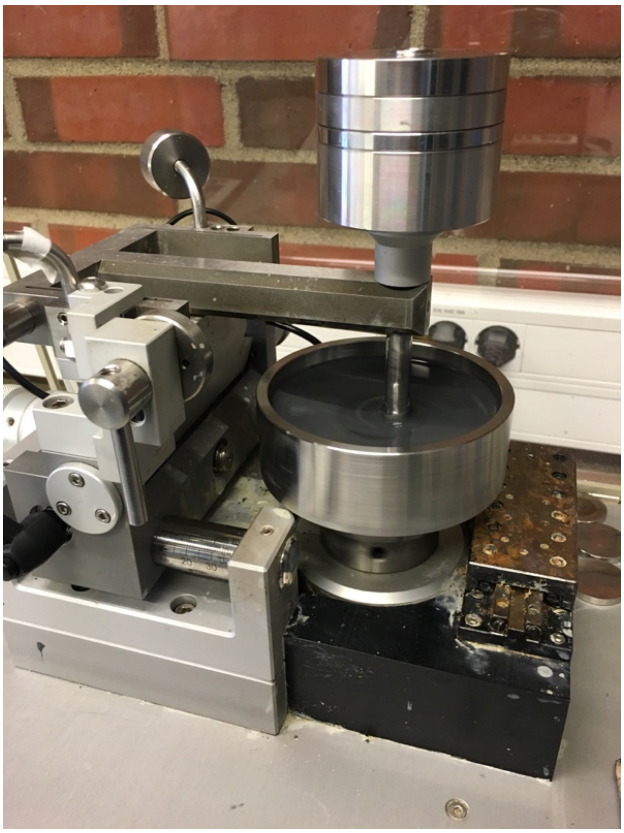

Figure 4.15: CMI Tribometer measurement

There is a disk mounted to the bottom of the sample cup, where the pin containing the test ball is in contact. The pin is fixed at a chosen radius, whereas the cup is rotating. There is a load placed on the top of the pin to ensure wanted contact with the disk. The load was set to 10N for all the measurements. All parts of the sample cup and pin, including screws and disk were cleaned properly before, in between and after the measurements to ensure no contamination from other samples.

The samples were tested at radiuses from 3mm to 7mm and run for times varying from 2 to 9 minutes. The test temperatures were set to 22°C, 50°C and 70°C for each fluid sample. It was observed that when heating the sample to a temperature of approximately 70°C the sample dehydrated, and the test was executed quickly for this temperature as the lubricating abilities may be affected by the dehydration. The results were recorded and noted from an accommodating software program where the wanted parameters were inserted.

4.3.2 Method of calibration

The apparatus software described the following calibration method:

- Insert fluid in test cup
- Choose wanted parameters (set temperature if wanted and connect the oven)
- Rotation calibration of the cup with the Tribometer arm up
- Lower the arm with load and press start
-

However, with the given calibration method, it was experienced a deviation from zero of friction coefficient values up to 0.3. Theoretically this is incorrect as the friction coefficient with the arm down without load on top should equal zero (no contact), a new calibration method was executed:

- Insert fluid in test cup
- Choose wanted parameters (set temperature if wanted and connect the oven)
- Rotation calibration of the cup with the Tribometer arm down
- Press start and put on load

This proved to be efficient as the minimum friction coefficient was set to a value equalling 0 when the load was lifted. To ensure that the obtained values could relate to documented friction coefficient of the WBM's, a literature study of friction coefficients in drilling fluids were executed and presented in section 2.8.

4.3.3 Sources of error

There are several possible sources of error for the tribology tests. These are presented as:

- As the tribology tests were time demanding, they were executed over several days. A possible source of error may be the changing room temperature (22°C) and humidity as they may vary from day to day. The room temperature may not be influenced.
- As several tests were executed for the same sample, the rheology might change due to waiting time and the fluid not being put in motion.
- When the samples were heated for the tests, some water from the sample may have evaporated, changed the rheology and influenced the lubricity of the samples.
- Possibly imperfect cleaning if not executed properly.

4.3.4 Friction tests for the reference systems with different polymers

To investigate the lubricating effect of the formulated reference systems, several tests with the Tribometer were executed at stated temperatures. The averaged mean values of the several tests are presented in Table 4.14 and Figure 4.16.

Degrees C	Reference system with XG	Reference system with CMC
22	0.245	0.441
50	0.244	0.565
70	0.319	0.529

Table 4.14: Averaged mean values of the reference systems

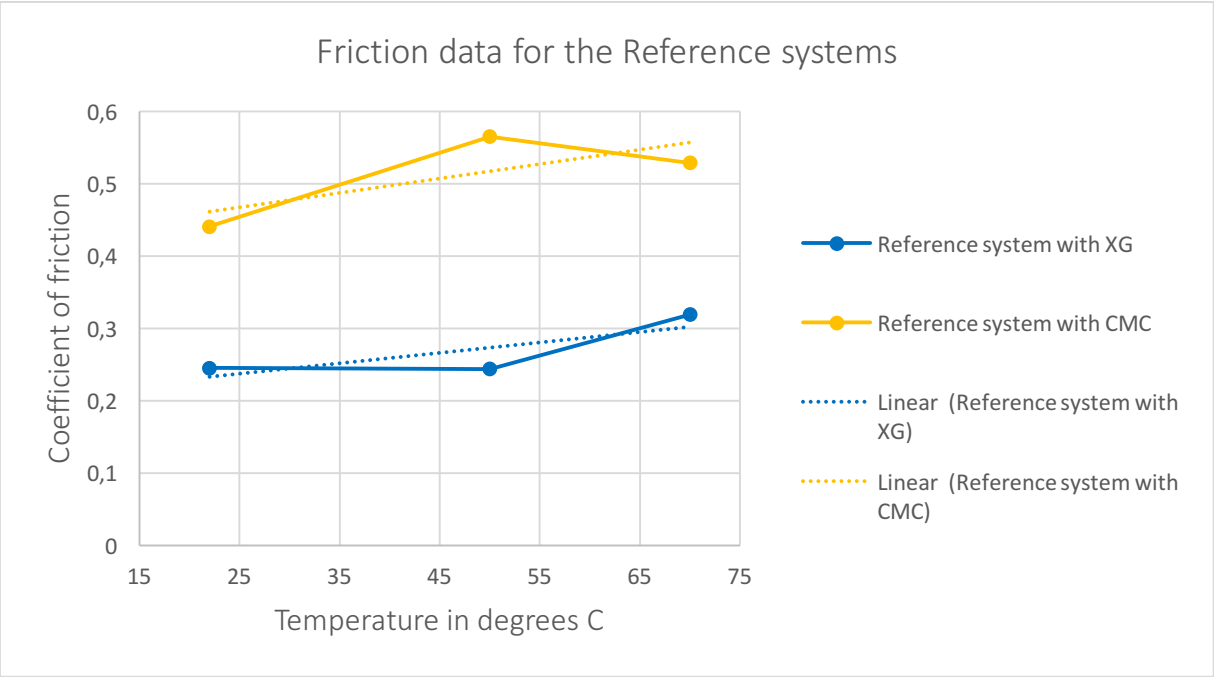

Figure 4.16: Plotted values of the reference systems with accommodating trend-lines

As there are sources of error to the tests, trend lines were calculated to form a better picture of how the coefficient of friction varies with temperature. It is also possible to see that the system is more viscous with XG as the added polymer, and has a lower average coefficient of friction compared to the reference system containing CMC. However, this was not further investigated. All tests were executed with the same calibration method. From the trend-lines, it seems like the coefficient of friction increases with increasing temperatures.

4.3.5 Friction tests for the TiN drilling fluids

To investigate the lubricating effect of the formulated TiN drilling fluids, selected high and low concentrations of the fluids were tested with the Tribometer. The tested fluids were selected due to the following reasons:

- Ref + 0.1: Selected due to the increase in YS and decrease in filtrate loss. The Ref + 0.15 and Ref + 0.2 fluids were selected to test if there was any significant change with small increasing concentrations. Ref + 2.5 fluid was selected to investigate if there was any significant change with great increasing concentrations.

4.3.5.1 Results and Analysis

Several tests were executed with every fluid sample to obtain the closest possible average mean, and to ensure as correct data as possible. The results are presented in Figure 4.17 with accommodating trend-lines in 4.16.

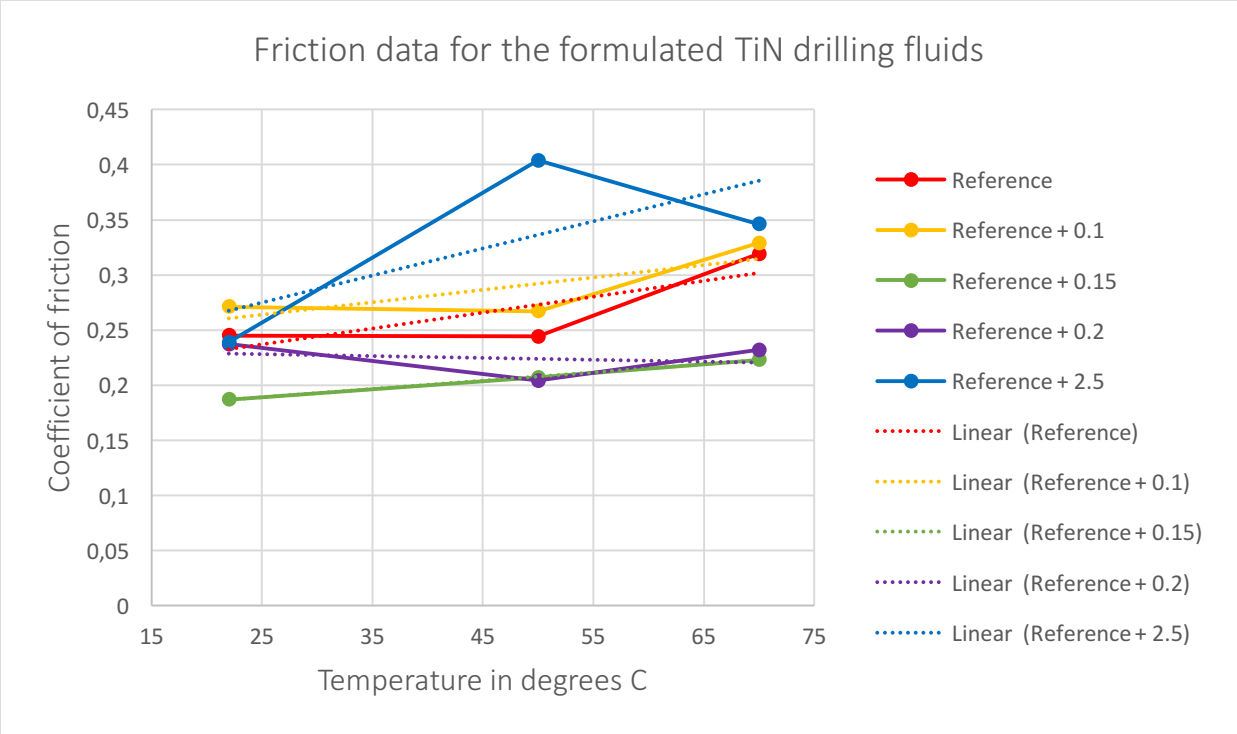

Figure 4.17: Plotted values of the TiN drilling fluids with accommodating trend-lines

The friction reduction percentage is illustrated in Table 4.15.

Friction coefficient changes for the TiN drilling fluids					
Degrees C	Reference	Ref + 0.1	Ref + 0.15	Ref + 0.2	Ref + 2.5
22		10.6	-23.7	-3.3	-2.4
50		9.4	-15.2	-16.4	65.6
70		3.1	-30.1	-27.3	8.5

Table 4.15: Friction coefficient changes for the TiN fluids in percent

The coefficient of friction for the formulated fluids was modelled according to the trend-lines. The results of the modelling are presented in Table 4.16, where T is the temperature and μ is the coefficient of friction.

Coefficient of friction modelling for the TiN drilling fluids		
Fluid	Model	R^2
Reference	$\mu_f = 0.00014T + 0.2012$	0.652
Ref + 0.1	$\mu_f = 0.011T + 0.2359$	0.607
Ref + 0.15	$\mu_f = 0.0007T + 0.1703$	0.999
Ref + 0.2	$\mu_f = -0.002T + 0.2353$	0.055
Ref + 2.5	$\mu_f = 0.0025T + 0.213$	0.504

Table 4.16: Coefficient of friction modelling for the TiN drilling fluids

The obtained data gave the following results:

- All of the modelled coefficient of friction equations exhibits positive slopes, except for the Ref + 0.2 fluid. This is not expected from literature studies.
- The friction data for the Ref + 0.1 system is of greater value compared to the reference system. The added nano concentration is possibly too low for any significant change.
- The best system measurements were registered for the Ref + 0.15 system as the percentage reduction was of greatest value.
- The Ref + 0.2 system has a negative slope, possibly due to source errors. However, the Ref + 0.2 system gave decreasing values of the friction coefficient and positive results with a reduction in percentage.
- The Ref + 2.5 system gave friction coefficient values of a great number, possibly due to over saturation of nanoparticles.

4.3.6 Friction tests for the MoS_2 drilling fluids

To investigate the lubricating effect of the formulated MoS_2 drilling fluids, selected high and low concentrations of the fluids were tested with the Tribometer. The tested fluids were selected due to the following reasons:

- The filtrate loss values decreased for the Ref + 0.2 system, while it did not change for the Ref + 0.8 system. The filtrate loss increased for the higher concentration fluids, and positive results were not obtained during the testing of the high concentration TiN fluids.
- There was not any significant change in the YS values for the Ref + 0.2 and Ref + 0.8 fluids

4.3.6.1 Results and Analysis

Several tests were executed with every fluid sample to obtain the closest possible average mean, and to ensure as correct data as possible. The results are presented in Figure 4.18 with accommodating trend-lines in Table 4.18.

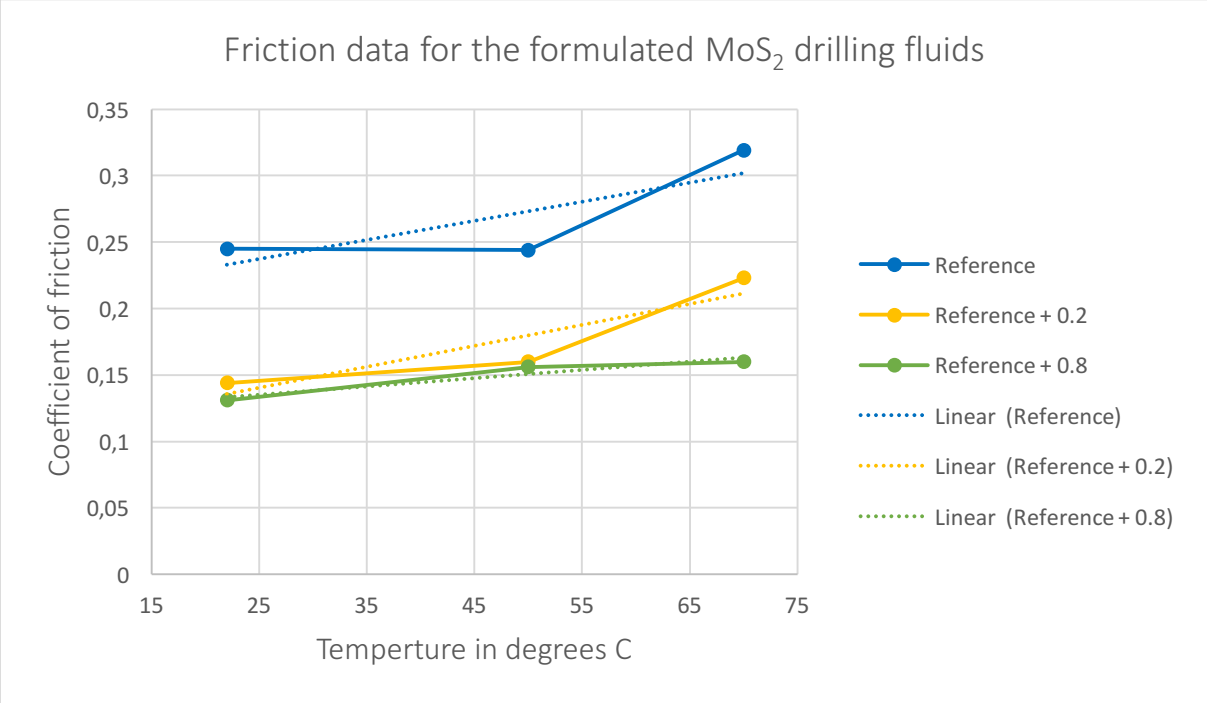

Figure 4.18: Plotted values of the MoS_2 drilling fluids with accommodating trend-lines

The friction reduction percentage is illustrated in Table 4.17.

Friction coefficient changes for the MoS_2 drilling fluids			
Degrees C	Ref	Ref + 0.2	Ref + 0.8
22		-41.2	-46.5
50		-34.4	-36.1
70		-30.1	-49.8

Table 4.17: Friction coefficient changes for the MoS_2 fluids in percent

The coefficient of friction for the formulated fluids was modelled according to the trend-lines. The results of the modelling are presented in Table 4.18, where T is the temperature and μ is the coefficient of friction.

Coefficient of friction modelling for the MoS_2 drilling fluids		
Fluid	Model	R^2
Reference	$\mu_f = 0.00014T + 0.2012$	0.652
Ref + 0.2	$\mu_f = 0.0016T + 0.101$	0.829
Ref + 0.8	$\mu_f = 0.0006T + 0.1995$	0.913

Table 4.18: Coefficient of friction modelling for the MoS_2 drilling fluids

The obtained data gave the following results:

- The coefficient of friction equations has a positive slope as expected from the literature study. The slope was of the lowest value for the Ref + 0.8 fluid.
- The best measurements were given for the Ref + 0.8 fluid with the greatest overall percentage reduction for the friction coefficient. The largest was for the Ref + 0.8 fluid for 70 degrees with a 49.8% reduction.
- Great measurements were also given for the Ref + 0.2 fluid where the maximum reduction was seen at 22 degrees with a percentage value of 41.2.

4.3.7 Friction tests for the Graphene drilling fluids

To investigate the lubricating effect of the formulated Graphene drilling fluids, selected high and low concentrations of the fluids were tested with the Tribometer. The tested fluids were selected due to the following reasons:

- The Ref + 0.2 fluid and Ref + 1.25 fluid was selected due to the low increase in filtrate loss, as all of the formulated fluids filtrate loss increased when adding nano.
- The Ref + 0.05 and Ref + 0.1 fluid was selected to determine the effect of very low concentration on friction, and because of the increased values of YS.

4.3.7.1 Results and Analysis

Several tests were executed with every fluid sample to obtain the closest possible average mean, and to ensure as correct data as possible. The results are presented in Figure 4.19 with accommodating trend lines in Table 4.20.

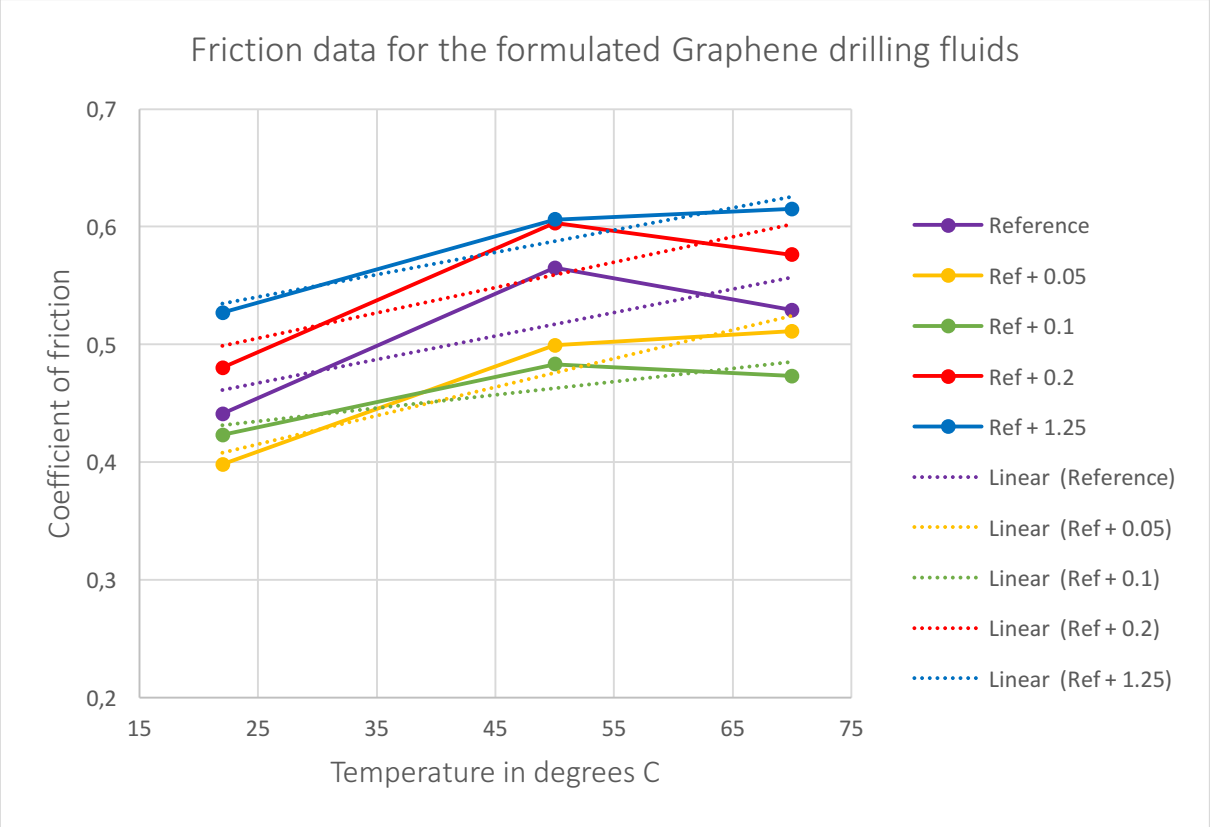

Figure 4.19: Plotted values of the Graphene drilling fluids with accommodating trend-lines

The percentage reduction is illustrated in table 4.19.

Friction coefficient changes for the Graphene drilling fluids					
Degrees C	Ref	Ref + 0.05	Ref + 0.1	Ref + 0.2	Ref + 1.25
22		-9.8	-4.1	8.8	19.5
50		-11.7	-14.5	6.7	7.3
70		-3.4	-10.6	8.9	16.3

Table 4.19: Friction coefficient changes for the Graphene fluids in percent

The coefficient of friction for the formulated fluids was modelled according to the trend-lines. The results of the modelling are presented in Table 4.20, where T is the temperature and μ is the coefficient of friction.

Coefficient of friction modelling for the Graphene drilling fluids		
Fluid	Model	R^2
Reference	$\mu_f = 0.002T + 0.417$	0.571
Ref + 0.05	$\mu_f = 0.0024T + 3541$	0.895
Ref + 0.1	$\mu_f = 0.0011T + 0.407$	0.696
Ref + 0.2	$\mu_f = 0.0022T + 0.4511$	0.645
Ref + 1.25	$\mu_f = 0.0019T + 0.4929$	0.892

Table 4.20: Coefficient of friction modelling for the Graphene drilling fluids

The obtained data gave the following results:

- All the modelled coefficient of friction equations had a positive slope, which showed an increase of the friction coefficient with increasing temperature. This is expected from the literature study.
- The Ref + 0.05 and Ref + 0.1 showed a reduction of the friction coefficient at all temperatures, while the Ref + 0.2 and Ref + 1.25 fluids showed an increase at all temperatures.
- The maximum percentage reduction for both the Ref + 0.05 fluid and Ref + 0.1 fluid was seen at a temperature of 50 degrees with a reduction of 11,7% and 14,5% respectively.

4.4 Viscoelasticity Measurements

This section will evaluate the effect of nano-additives on the viscoelasticity of a selected set of drilling fluids. An Anton Paar MCR 302 rheometer was used to characterise the viscoelastic properties of a set of selected drilling fluids. The selected drilling fluids are presented in Table 4.21, and are based on the results of the friction measurements.

Fluids selected for viscoelasticity measurements	
Polymer	System
XG	Reference system with XG
XG	Reference + 0.15g TiN
XG	Reference + 0.20g TiN
XG	Reference + 0.20g MoS2
XG	Reference + 0.80g MoS2
CMC	Reference system with CMC
CMC	Reference + 0.05g Graphene
CMC	Reference + 0.10g Graphene

Table 4.21: Matrix of the viscoelasticity measured fluids

4.4.1 Measurement Set Up

For this thesis, an oscillatory amplitude sweep test was performed on all the fluids mentioned above. This test determines the LVE. It also detects structural stability, strength and the dynamic yield point of the drilling fluids. The tests were performed at 22.3°C in a parallel plate, with a constant frequency (ω) of 10 rad/s. The strain was varied from 0.0005 to 100%. The results were used to plot the storage and loss modulus against the strain, as well as to calculate the damping angle and plot it against the shear stress. This made one able to retrieve information about the flow point (where the storage modulus and the loss modulus are equal) and yield point of the tested fluids.

4.4.2 Oscillatory Amplitude Sweep Test Results for the TiN Drilling Fluids

The storage and loss modulus were plotted for the TiN drilling fluids.

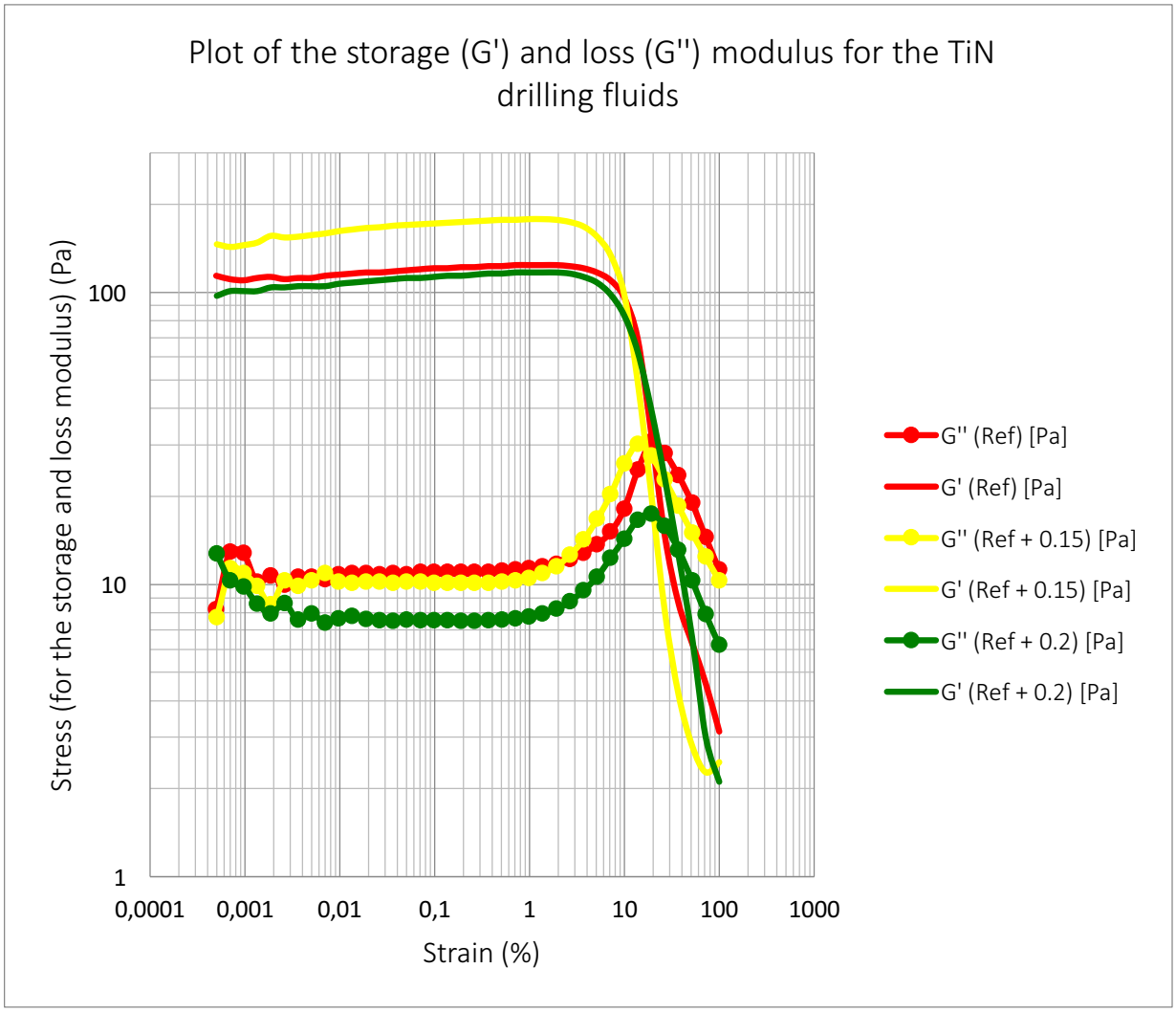

Figure 4.20: Plot of the storage and loss modulus for the TiN drilling fluids

The figure indicates storage modules of greater values than the corresponding loss modulus. This verifies gel like behaviour of the drilling fluid. Since G' is greater than G'' for the entire LVER, the elastic behaviour is dominant. As this portion is dominant, there is certain stability in the low shear range. The figure indicates a limit for the LVER at approximately 1% strain for the reference and TiN drilling fluids, hence this strain value will be used to determine the yield point for the formulated fluids.

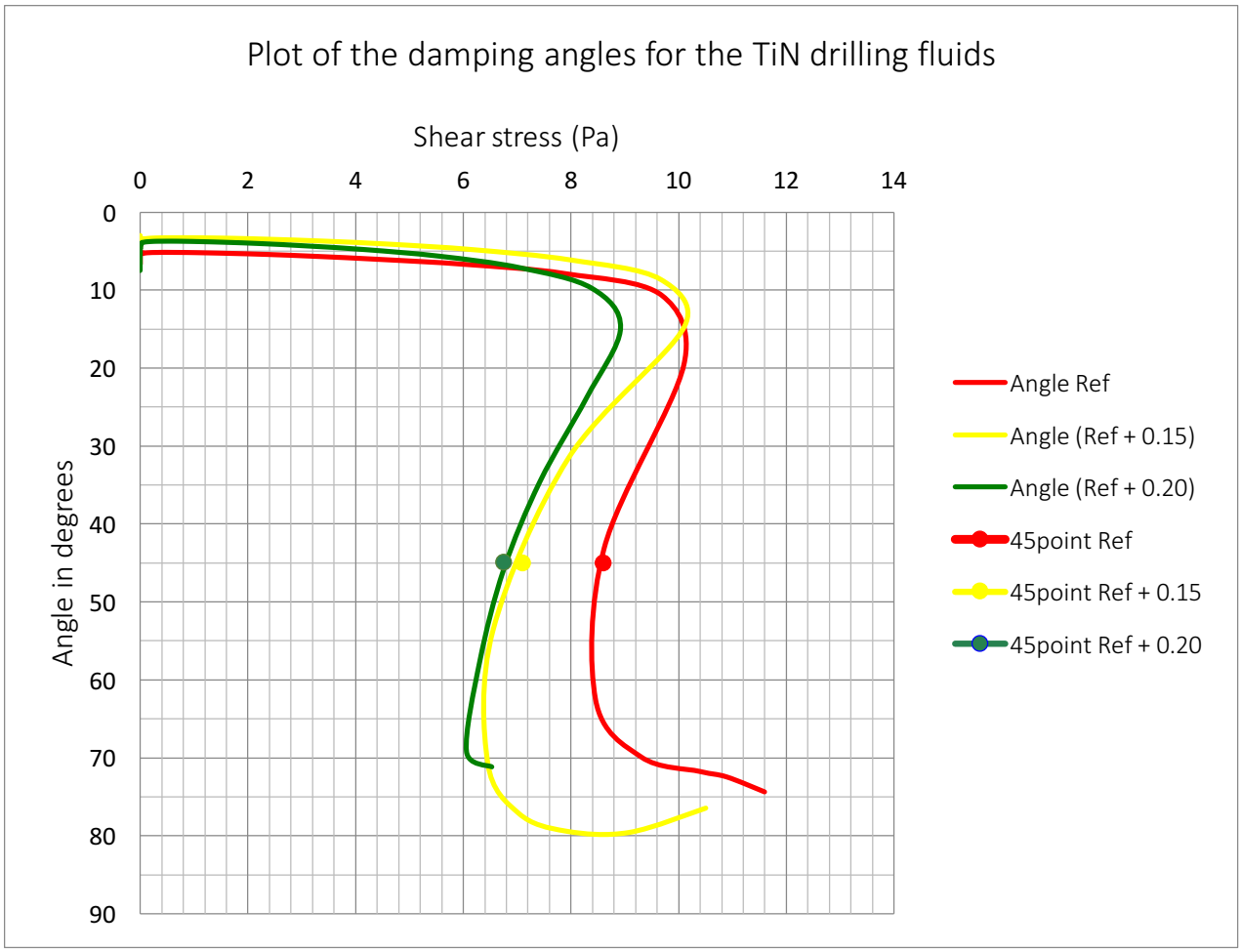

Figure 4.21: Plot of the damping angles for the TiN drilling fluids

The 45° point represents the flow points. The flow points of the nano-treated systems are of lower values than the reference system, according to the graph. This means that the nano-treated fluids experience viscoelastic behaviours for lower shear stress values than the reference system. The fluids exhibit a decrease in flow point as the concentration of nano increases.

4.4.2.1 Flow Points and Yield Points of the Formulated TiN Drilling Fluids

The flow points from the oscillatory amplitude sweep tests are calculated using interpolation. The results are presented in the chart below.

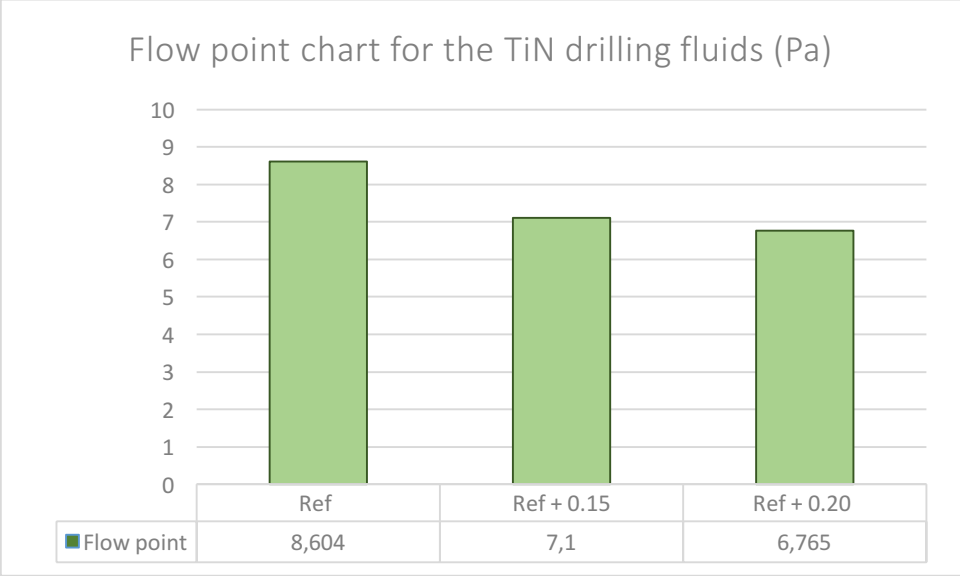

Figure 4.22: Flow point chart for the TiN drilling fluids (Pa)

The yield points from the oscillatory amplitude sweep tests are read from the loss modulus graph at the strain value of 1%.

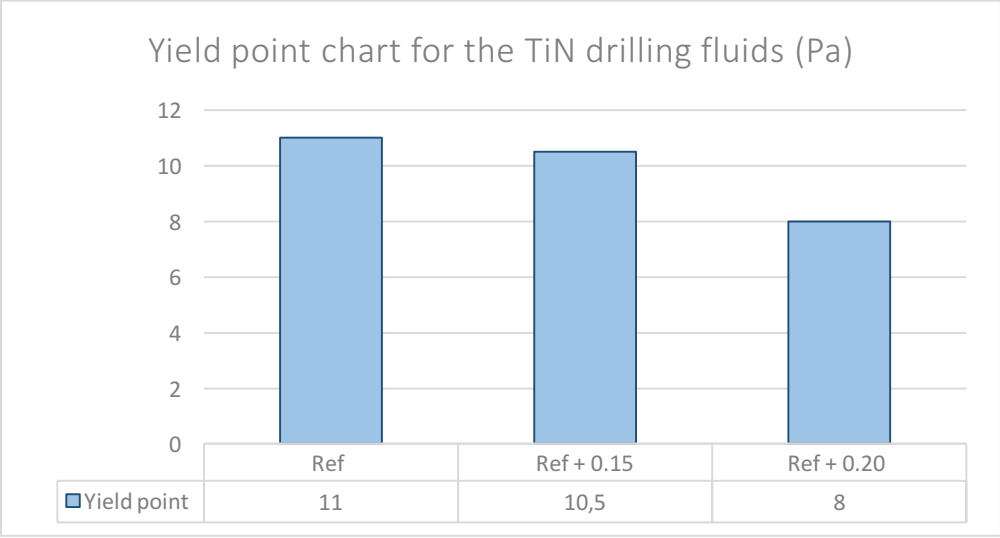

Figure 4.23: Yield point chart for the TiN drilling fluids (Pa)

4.4.3 Oscillatory Amplitude Sweep Test Results for the MoS_2 Drilling Fluids

The storage and loss modulus were plotted for the MoS_2 drilling fluids.

Figure 4.24: Plot of the storage and loss modulus for the MoS_2 drilling fluids

Similar to the chart presented for the TiN drilling fluids, the figure indicates storage modules of greater values than the corresponding loss modulus for the LVER. This also verifies gel like behaviour for the MoS_2 drilling fluids. There is also certain stability in the low shear range. The figure indicated a LVER limit of approximately 1% strain for all the presented fluids. This strain value will be used to determine the yield point of the fluids.

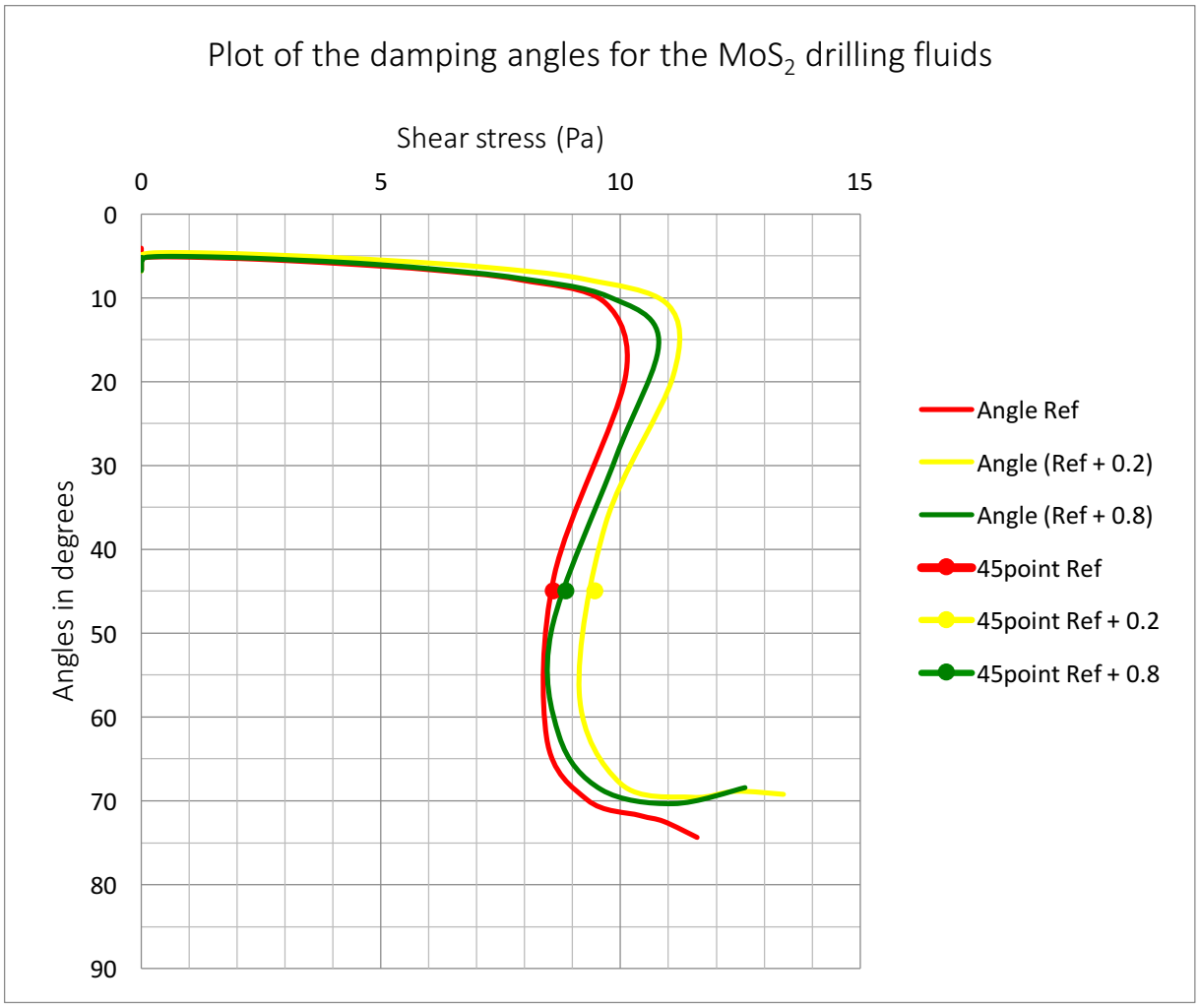

Figure 4.25: Plot of the damping angles for the MoS_2 drilling fluids

The 45° point represents the flow points. The flow points of the nano treated systems unlike for the TiN drilling fluids of higher values than the reference system. This means that the nano-treated fluids experience viscoelastic behaviours for higher shear stress values than the reference system. The fluid containing the greatest weight% of nano seems to exhibit a lower flow point than that of the Ref + 0.2 system.

4.4.3.1 Flow Points and Yield Points of the Formulated MoS_2 Drilling Fluids

The flow points from the oscillatory amplitude sweep tests are calculated using interpolation. The results are presented in the chart below.

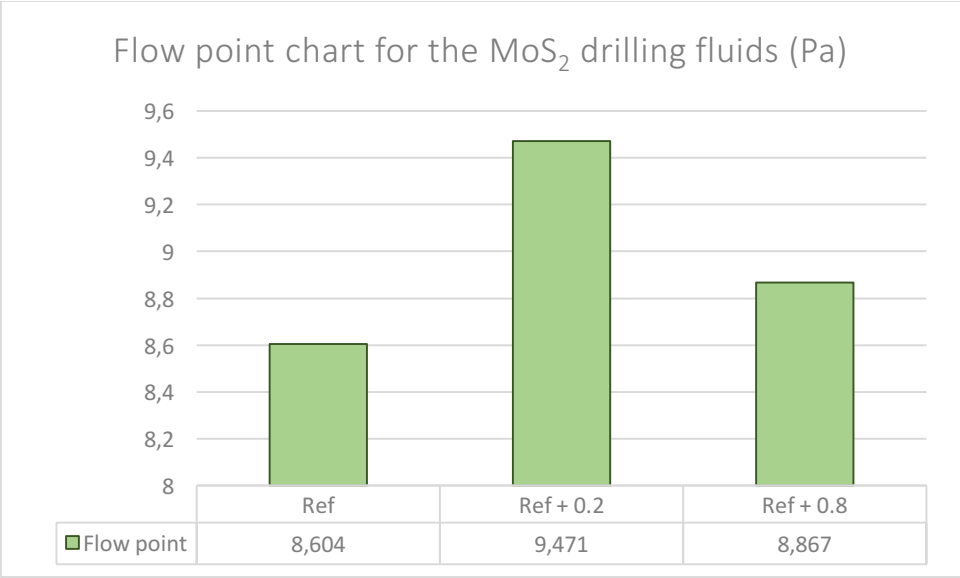

Figure 4.26: Flow point chart for the MoS2 drilling fluids (Pa)

The yield points from the oscillatory amplitude sweep tests are read from the loss modulus graph at the strain value of 1%.

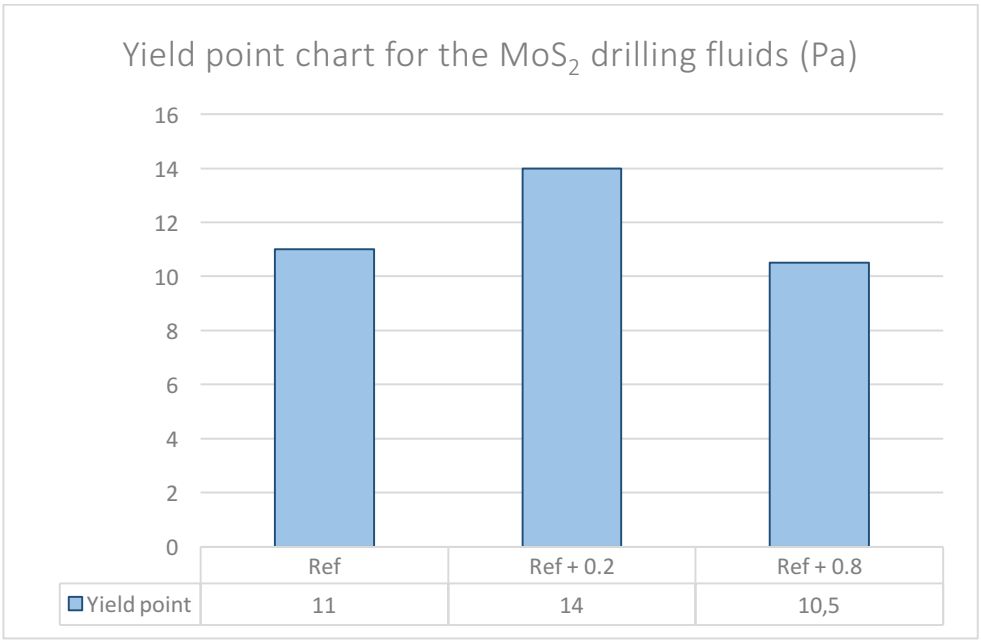

Figure 4.27: Yield point chart for the MoS2 drilling fluids (Pa)

4.4.4 Oscillatory Amplitude Sweep Test Results for the Graphene Drilling Fluids

The storage and loss modulus were plotted for the Graphene drilling fluids.

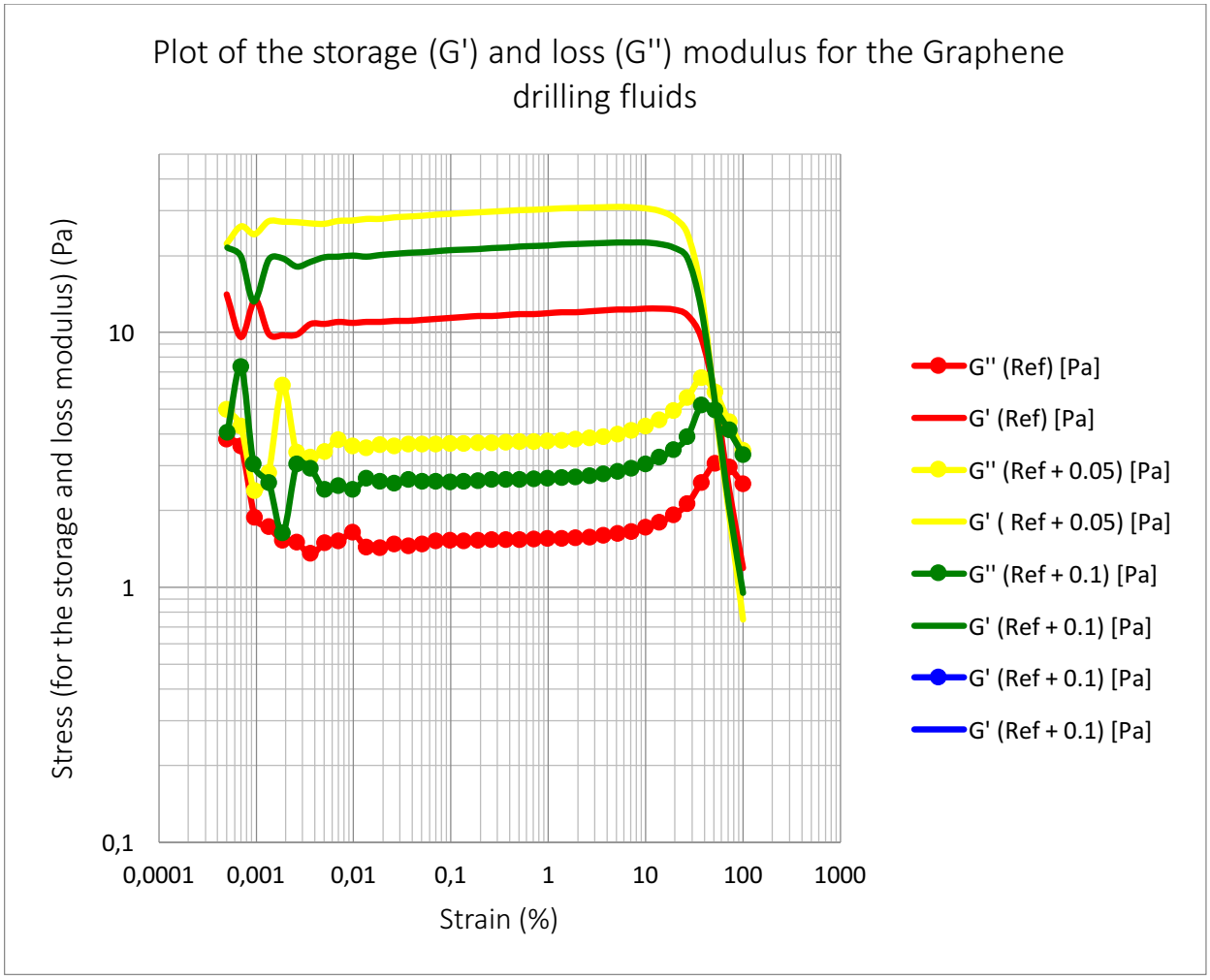

Figure 4.28: Plot of the storage and loss modulus for the Graphene drilling fluids

The plot exhibits storage values greater than the corresponding loss modulus values, similar to the other fluids. The LVER is dominated by elastic behaviour, and verifies both a gel like structure and certain stability in the low shear range. An observation is that the graph lines are located further apart from each other compared to the two other presented drilling fluid batches. The LVER limit seems to be located around 6% of strain value, and the yield points will be retrieved using this value.

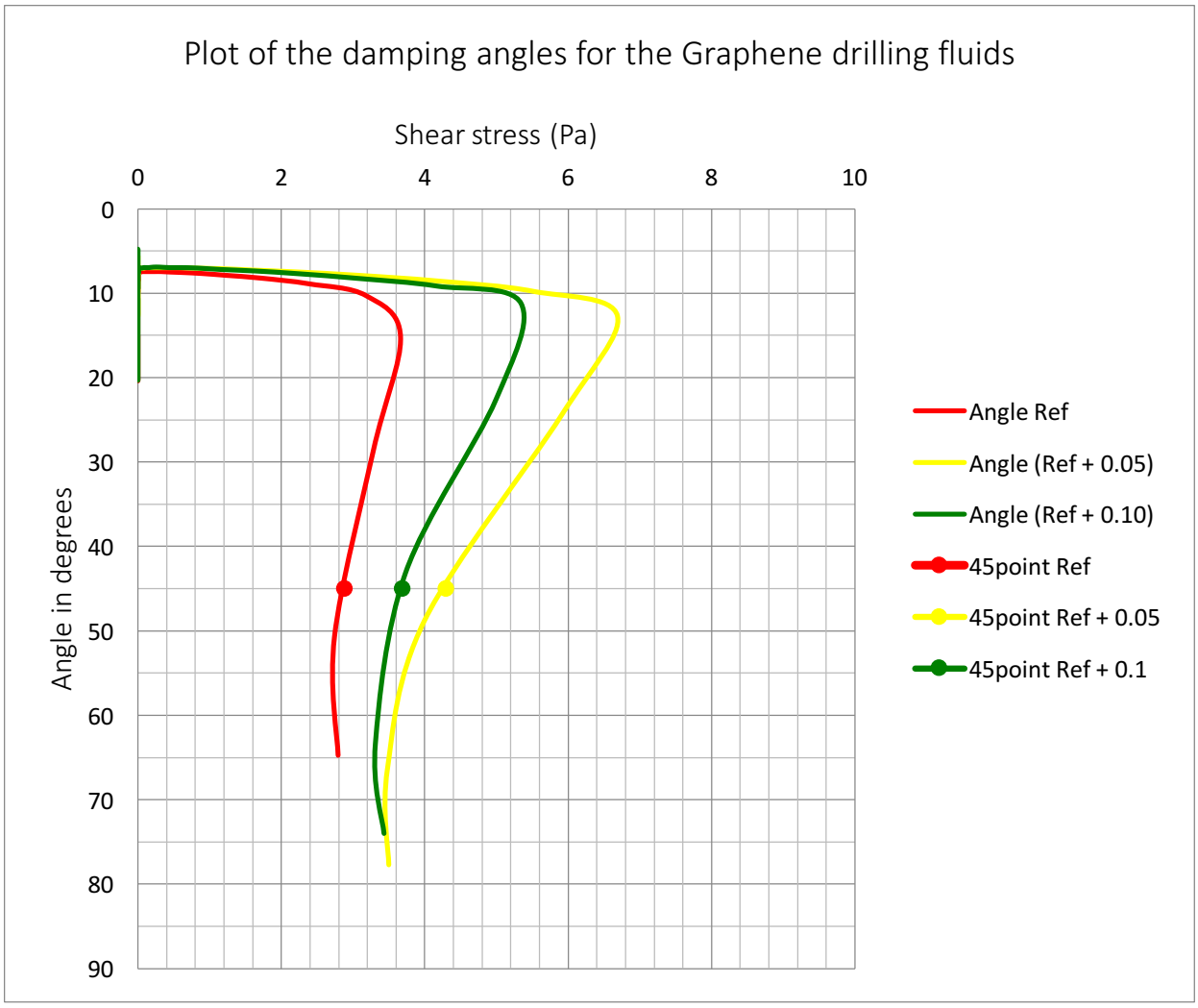

Figure 4.29: Plot of the damping angles for the Graphene drilling fluids

The 45° point represents the flow points. The flow points of the nano treated systems, similar to the MoS_2 drilling fluid values exhibit higher values than the reference system. This means that the nano-treated fluids experience viscoelastic behaviours for higher shear stress values than the reference system. The fluid containing the greatest weight% of nano seems to exhibit a lower flow point than that of the Ref + 0.1 system.

4.4.4.1 Flow Points and Yield Points of the Formulated MoS_2 Drilling Fluids

The flow points from the oscillatory amplitude sweep tests are calculated using interpolation. The results are presented in the chart below.

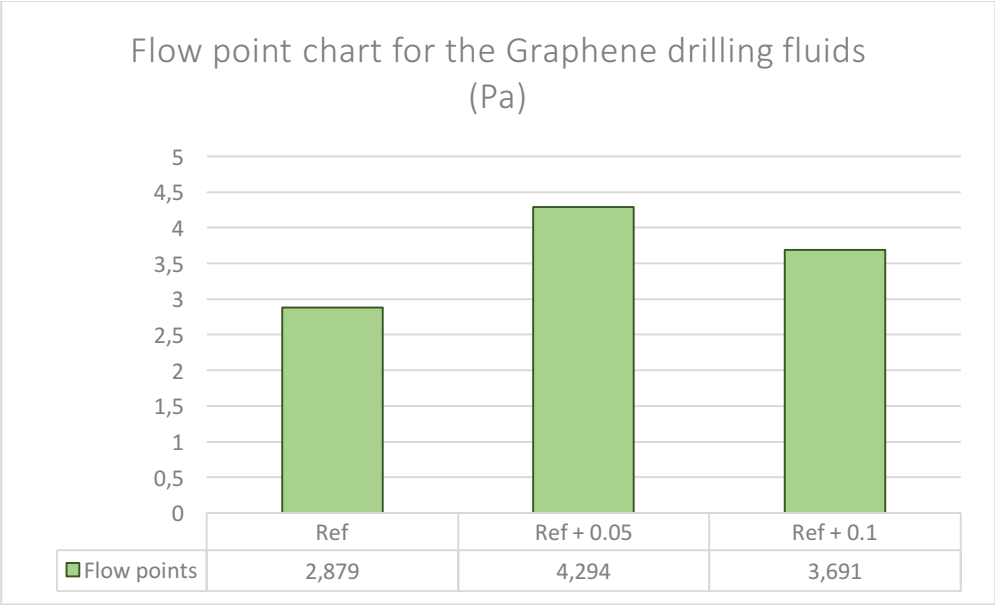

Figure 4.30: Flow point chart for the Graphene drilling fluids (Pa)

The yield points from the oscillatory amplitude sweep tests are read from the storage modulus graph at the strain value of 6%.

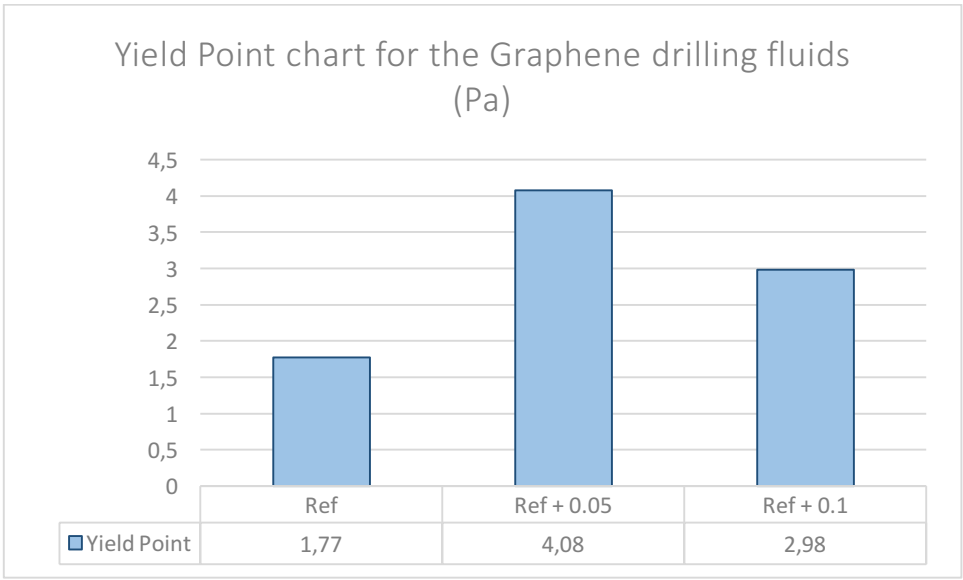

Figure 4.31: Yield point chart for the Graphene drilling fluids (Pa)

5 Simulation Study of Nano Treated Drilling Fluids

The fluids with the best rheological and frictional results from the experimental study were analysed with a study of simulation. This study addresses rheological modelling, torque, drag and hydraulic performance simulation.

5.1 Rheological modelling

This section will present the results of rheological modelling, where the focus was to obtain the rheological model that best describes the selected, formulated drilling fluids. A calculator was created in excel, where parameters were calculated according to the following rheological models:

- Newtonian model.
- Bingham Plastic model.
- Power law model.
- Herschel Bulkley model.
- Unified model.
- Robertson stiff model.

A trend-line was calculated with an accommodating percentage deviation according to the obtained original measurements. The formula of the trend line represents the best model formula, and other parameters were calculated in Excel according to the formulas presented in section 3.5. The plastic viscosity in cP was also calculated for all the Newtonian and Bingham models. Equations were stated for all the models according to calculated parameters. An example of a calculated trend line according to the Power Law theory is illustrated in Figure 4.32, where the deviation is set to 3.77%.

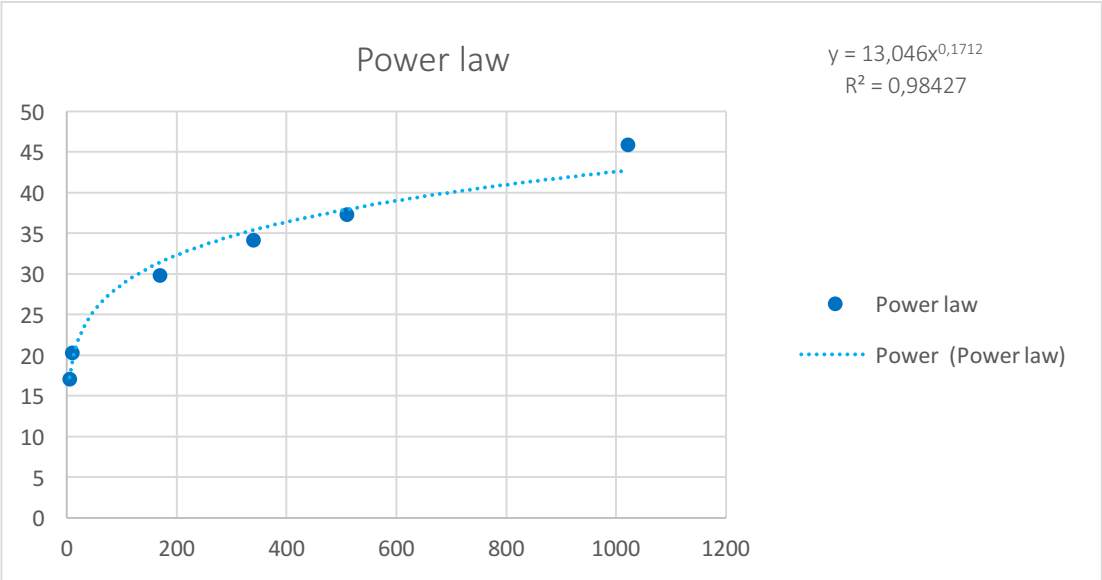

Figure 5.1: Example of a Power law trend-line according to measured data

5.1.1 Rheological Modelling of the TiN Drilling Fluids

This section will present the obtained models for a selected set of TiN drilling fluid systems with accommodating parameters and a presentation of the best model. Based on the experimental study, the selected fluids for the rheological modelling presentations are the Reference, Ref + 0.15 and Ref + 0.20 fluids. Modelling for the Ref + 2.5 fluid system was also executed and is presented in the Appendix C.1.

5.1.1.1 TiN Reference System

The trend-lines for all the rheology models are plotted in Figure 5.2 with accommodating equations and parameters in Table 5.1.

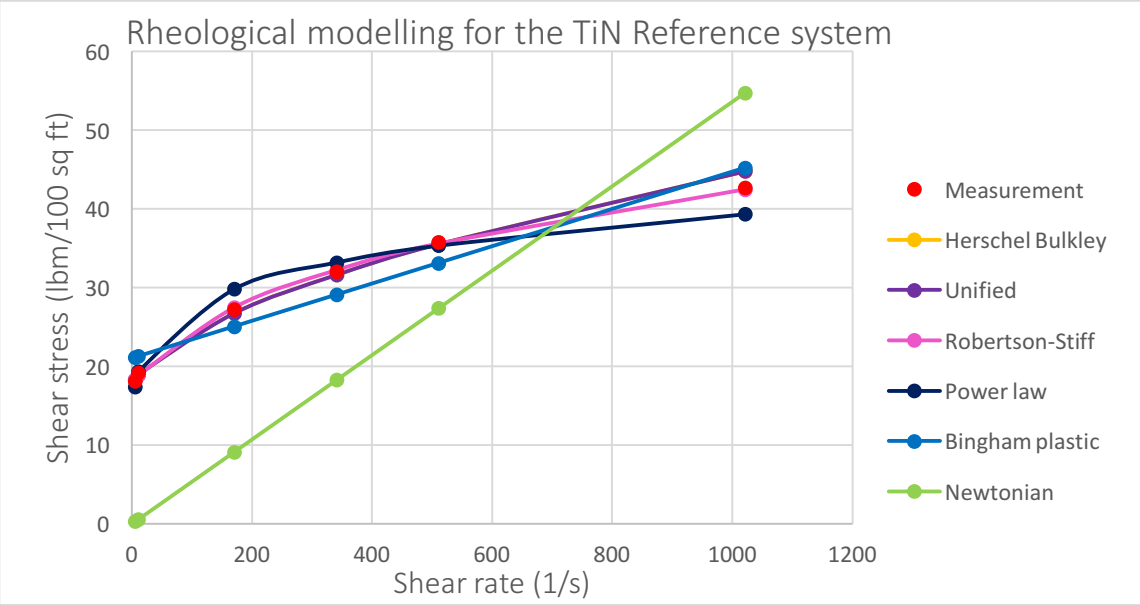

Figure 5.2: Modelled trend-lines for the TiN Reference system

		Parameters					
Model	Equation	τo,τy, A	k, C	n, B	μp, μ	Error	cP
Herschel Bulkley	$17.067 + 0.4755\gamma^{0.5868}$	17.067	0.4755	0.5868		1.80	
Unified	$17.072 + 0.4731\gamma^{0.5875}$	17.072	0.4731	0.5875		1.81	
Power Law	$13.508\gamma^{0.1543}$		13.508	0.1543		4.54	
Bingham	$0.0237\gamma+21.021$	21.021			0.0237	9.60	11.348
Newtonian	0.0536γ				0.0536	59.46	25.664
Robertson and Stiff	$6.4611(42.5075+\gamma)^{0.2701}$	6.4611	42.5075	0.2701		0.93	

Table 5.1: Modelled equations for the TiN Reference system

Error deviation in % is also presented in Table 5.1. The largest deviation is set for the Newtonian model, with a deviation of 59.46%. All of the other models deviate with values above 1.80% except for the Robertson and Stiff model, where the deviation is set to 0.93%. This results in the Robertson and Stiff being the most suitable model for the Reference system and its shear stress values. A comparison of the Robertson and stiff model and the shear rates are presented in Appendix C.5.

5.1.1.2 TiN Ref + 0.15 System

The trend-lines for all the rheology models are plotted in Figure 5.3 with accommodating equations and parameters in Table 5.2.

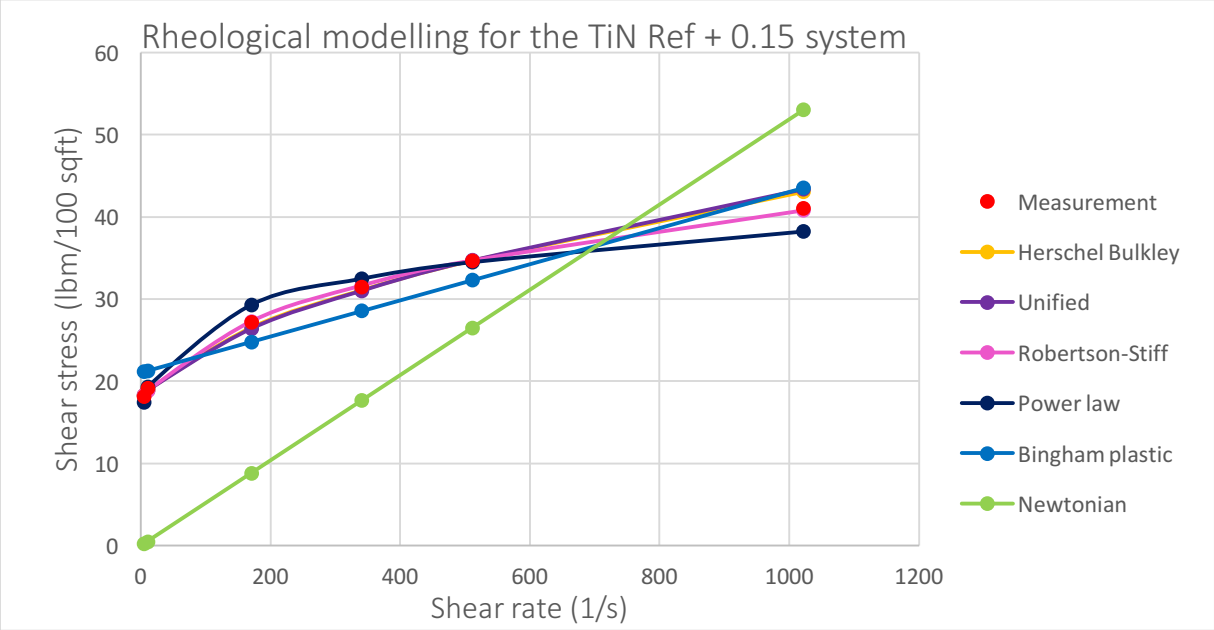

Figure 5.3: Modelled trend-lines for the TiN Ref + 0.15 system

		Parameters					
Model	Equation	τo,τy, A	k, C	n, B	μp, μ	Error	cP
Herschel Bulkley	$16.949 + 0.5466\gamma^{0.5580}$	16.949	0.5466	0.5580		1.79	
Unified	$17.072 + 0.4866\gamma^{0.5759}$	17.072	0.4866	0.5759		2.06	
Power Law	$13.722\gamma^{0.1479}$		13.722	0.1479		3.82	
Bingham	$0.022\gamma + 21.071$	21.071			0.022	9.76	10.534
Newtonian	0.0519γ				0.0519	59.96	24.850
Robertson and Stiff	$7.3789(35.7224 + \gamma)^{0.2456}$	7.3789	35.7224	0.2456		0.75	

Table 5.2: Modelled equations for the TiN Ref + 0.15 system

The largest error deviation is set for the Newtonian model, with a deviation of 59.96 %. All of the other models deviate with values above 1.79%, except for the Robertson and Stiff model, where the deviation is set to 0.75%. The Robertson and Stiff model is therefore most suitable for the Ref + 0.15g TiN system, and a comparison of the two models are presented in Appendix C.5.

5.1.1.3 TiN Ref + 0.2 System

The trend-lines for all the rheology models are plotted in Figure 5.4 with accommodating equations and parameters in Table 5.3.

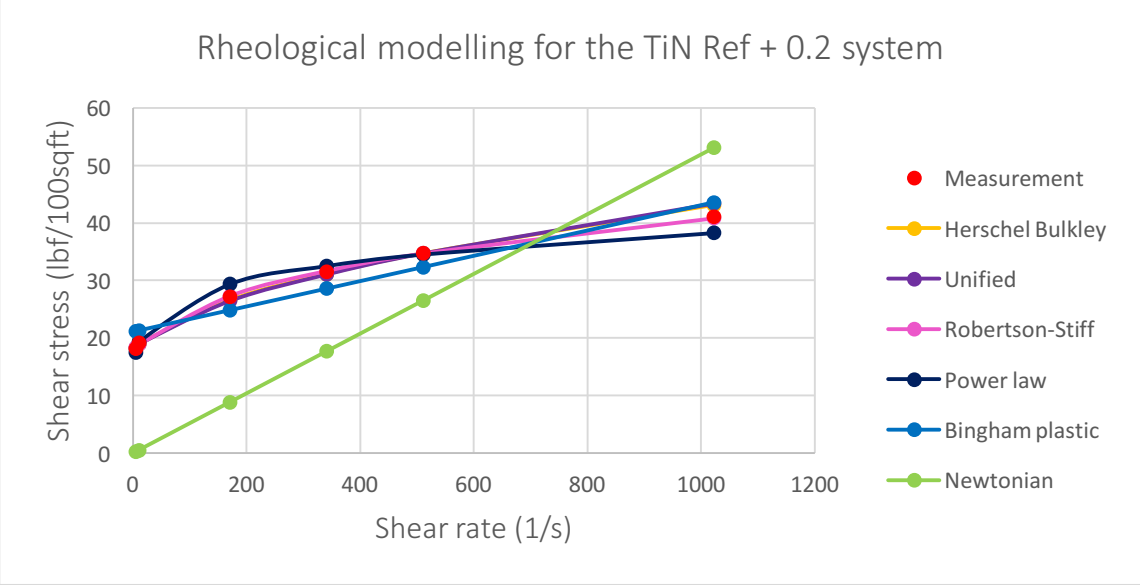

Figure 5.4: Modelled trend-lines for the TiN Ref + 0.20 system

		Parameters					
Model	Equation	τo,τy, A	k, C	n, B	μp, μ	Error	cP
Herschel Bulkley	$15.566 + 0.8064\dot{\gamma}^{0.49450}$	15.566	0.8064	0.4945		1.50	
Unified	$15.572 + 0.8598\dot{\gamma}^{0.485}$	15.472	0.8598	0.4850		1.40	
Power Law	$13.096\dot{\gamma}^{0.1483}$		13.096	0.1483		3.70	
Bingham	$0.0212\dot{\gamma} + 20.115$	20.115			0.0212	9.56	10.151
Newtonian	$0.0497\dot{\gamma}$				0.0497	59.77	23.796
Robertson and Stiff	$7.3513(32.3912 + \dot{\gamma})^{0.2394}$	7.3513	32.3912	0.2394		1.59	

Table 5.3: Modelled equations for the TiN Ref + 0.20 system

As the Newtonian model is a linear model that does not account for the fluids YS, this model deviates once again the most from the original measurements, in this case with 59.77%. The Bingham model accounts for the YS, but is linear and deviates with 9.56%. The other models deviate with more than 1%, with the Power Law model giving the closest approximation with a deviation value of 1.40%. The Unified model is therefore the most suitable model for the Ref + 0.20 fluid system. A comparison of the measurements and the Unified model is illustrated in Appendix C.5.

5.1.1.4 Summary of Rheological Modelling for the TiN Drilling Fluids

The best suited rheological model for the three presented fluids are summarised in Table 5.4.

Summary of the rheological modelling for the TiN drilling fluids		
Fluid	Model	Equation
Reference	Robertson and Stiff model	$\tau = 6.4611(42.5075+\gamma)^{0.2701}$
Reference + 0.15	Robertson and Stiff model	$\tau = 7.3789(35.7224 + \gamma)^{0.2456}$
Reference + 0.20	Unified model	$\tau = 15.572 + 0.8598\gamma^{0.485}$

Table 5.4: Table of summary for the rheological modelling of TiN drilling fluids

The percentage of error versus the different models were summarised for all the fluids in the following chart.

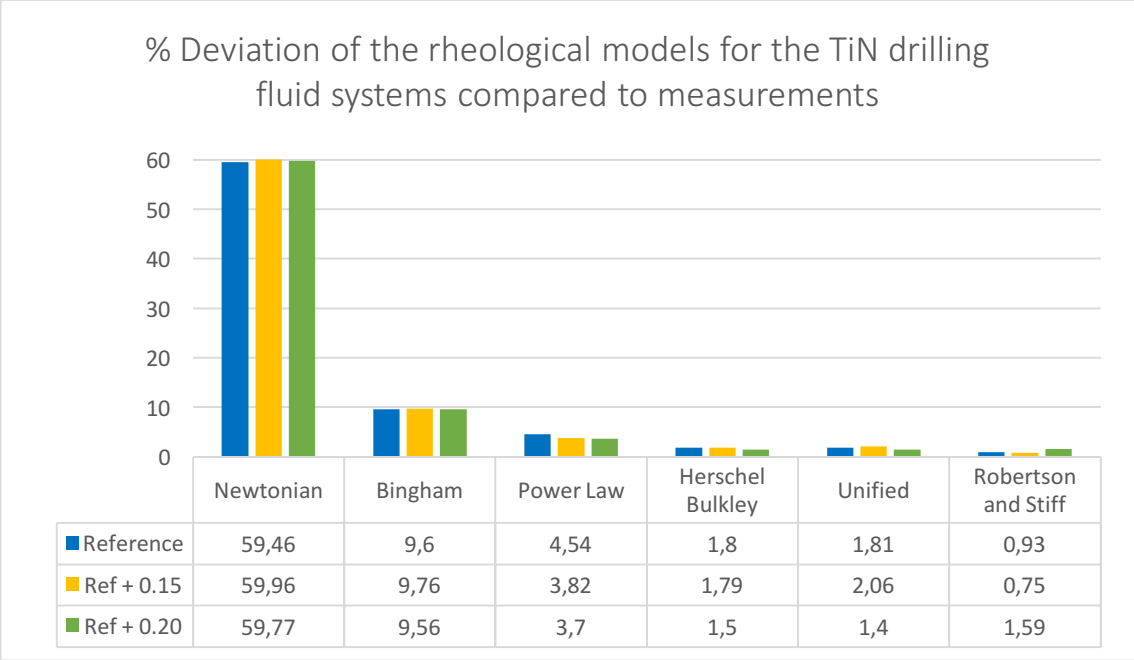

Figure 5.5: % Deviation of the rheological models for the TiN drilling fluid systems compared to measurements

As illustrated, the largest deviation occurs with the Newtonian model and the Bingham model for all the TiN fluids tested. The Robertson and Stiff model is the most reliable model for the Reference and Ref + 0.15 systems, while the Unified model is the most reliable for the Ref + 0.20 fluid.

5.1.2 Rheological modelling of the MoS_2 drilling fluids

This section will present the obtained models for a selected set of the MoS_2 drilling fluid systems with accommodating parameters and a presentation of the best model. Based on the experimental friction study, the selected fluids for the rheological modelling presentations are the Reference, Ref + 0.2 and Ref + 0.8 fluids. Modelling for the Ref + 0.5 fluid system was also executed, but presented in the Appendix C.2.

5.1.2.1 MoS_2 Reference System

The trend-lines for all the rheology models are plotted in Figure 5.6 with accommodating equations and parameters in Table 5.5.

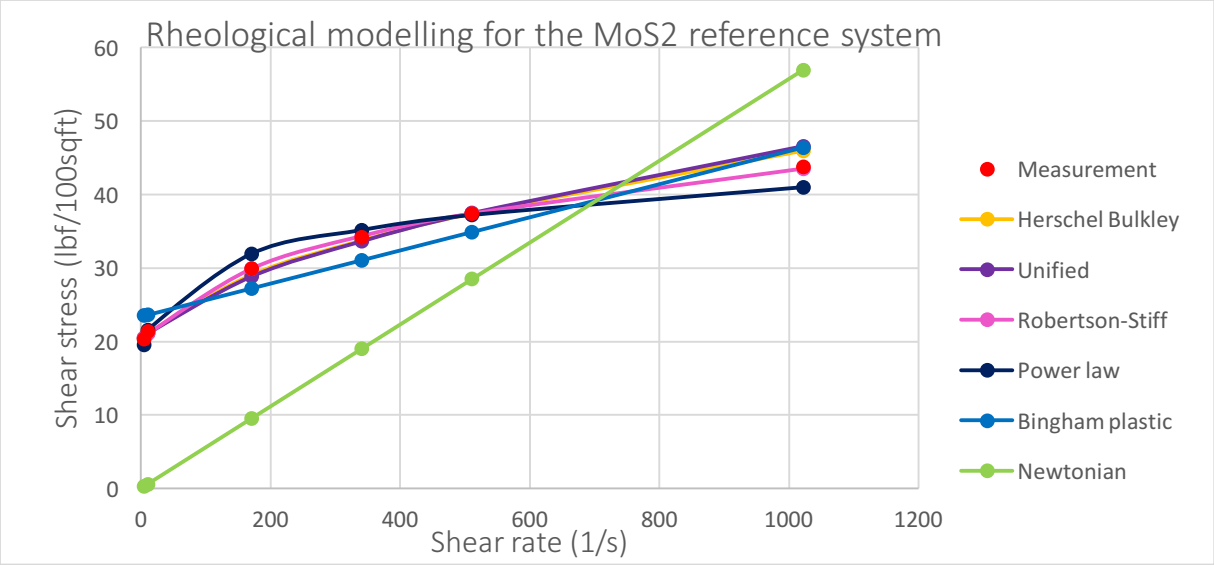

Figure 5.6: Modelled trend-lines for the MoS_2 Reference system

		Parameters					
Model	Equation	τo,τy, A	k, C	n, B	μp, μ	Error	cP
Herschel Bulkley	$18.973 + 0.5968\gamma^{0.55}$	18.973	0.5968	0.5500		1.85	
Unified	$19.206 + 0.4825\gamma^{0.5826}$	19.206	0.4825	0.5826		2.31	
Power Law	$15.569\gamma^{0.1397}$		15.569	0.1397		3.49	
Bingham	$0.0225\gamma + 23.395$	23.395			0.0225	9.53	10.773
Newtonian	0.0557γ				0.0557	60.42	26.669
Robertson and Stiff	$8.8966(33.5930 + \gamma)^{0.228}$	8.8966	33.593	0.2280		0.62	

Table 5.5: Modelled equations for the MoS_2 Reference system

The error deviation presented in the Table 5.5 illustrates the largest error deviation for the Newtonian model, with the Robertson and Stiff model only deviating with 0.62%. Excluding the Robertson and Stiff model, all the other models deviate with values equal or greater than 1.85%, hence the best suited model for the MoS_2 Reference system is set to be the Robertson and Stiff model. A comparison of solely the measurements and the Robertson and Stiff model for the Reference system is illustrated in Appendix C.5.

5.1.2.2 MoS_2 Ref + 0.2 System

The trend-lines for all the rheology models are plotted in Figure 5.7 with accommodating equations and parameters in Table 5.6.

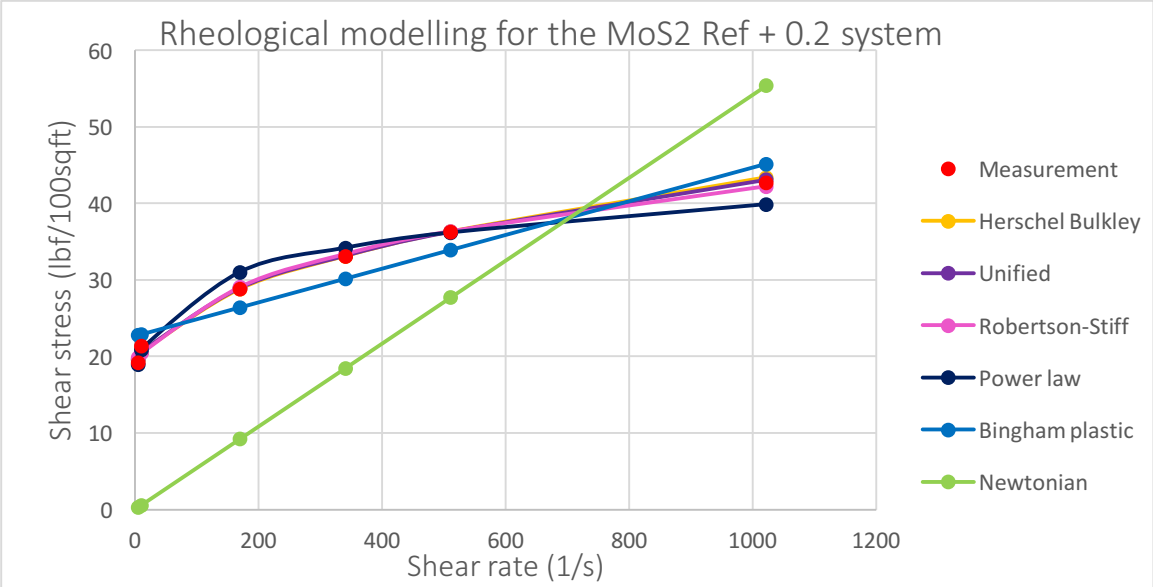

Figure 5.7: Modelled trend-lines for the MoS_2 Ref + 0.2 system

		Parameters					
Model	Equation	τo,τy, A	k, C	n, B	μp, μ	Error	cP
Herschel Bulkley	$17.322 + 1.0956\gamma^{0.4573}$	17.322	1.0965	0.4573		1.34	
Unified	$17.072 + 1.2479\gamma^{0.4384}$	17.072	1.2479	0.4384		1.28	
Power Law	$15.086\gamma^{0.1402}$		15.086	0.1402		3.53	
Bingham	$0.022\gamma + 22.670$	22.670			0.0220	9.22	10.534
Newtonian	0.0542γ				0.0542	60.26	25.951
Robertson and Stiff	$8.7507(32.4143 + \gamma)^{0.2261}$	8.7507	32.4143	0.2261		1.79	

Table 5.6: Modelled equations for the MoS_2 Ref + 0.2 system

The trend-lines illustrate an error percentage deviation of more or equal than 1.28% for all the rheological models. The best model for the Ref + 0.2 system is the Unified model, with a deviation error of 1.28%, whilst the most deviating model is the Newtonian model. A comparison of the modelled Unified model and the measurements are illustrated in Appendix C.5.

5.1.2.3 MoS_2 Ref + 0.8 System

The trend-lines for all the rheology models are plotted in Figure 5.8 with accommodating equations and parameters in Table 5.7.

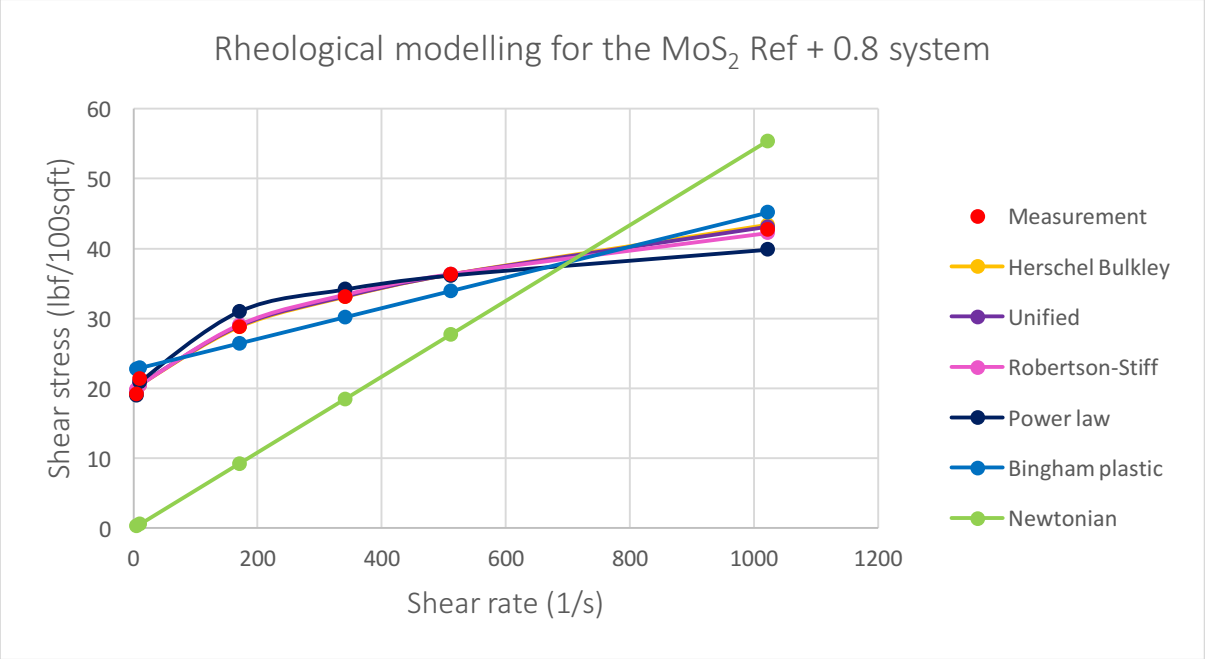

Figure 5.8: Modelled trend-lines for the MoS_2 Ref + 0.8 system

		Parameters					
Model	Equation	τo,τy, A	k, C	n, B	μp, μ	Error	cP
Herschel Bulkley	$17.182 + 1.1717\gamma^{0.4526}$	17.182	1.1717	0.4526		1.51	
Unified	$17.072 + 1.238\gamma^{0.4446}$	17.072	1.238	0.4446		1.40	
Power Law	$15.012\gamma^{0.1434}$		15.012	0.1434		3.24	
Bingham	$0.0225\gamma + 22.860$	22.860			0.0225	9.80	10.773
Newtonian	0.055γ				0.055	60.33	26.334
Robertson and Stiff	$9.0404(28.6308 + \gamma)^{0.2236}$	9.0404	28.6308	0.2236		1.66	

Table 5.7: Modelled equations for the MoS_2 Ref + 0.8 system

All the models deviated with more or equal to 1.40%. The least deviating models where the Robertson and Stiff model, Herschel Bulkley model and the Unified model with 1.66%, 1.51% and 1.40% respectively. Hence, the best suited model for the MoS_2 Ref + 0.8 fluid is the Unified model. A comparison between the Unified model and the measurements is illustrated in Appendix C.5.

5.1.2.4 Summary of Rheological Modelling for the MoS_2 Drilling Fluids

The best suited rheological models for the three presented fluids are summarised in Table 5.8.

Summary of the rheological modelling for the MoS_2 drilling fluids		
Fluid	Model	Equation
Reference	Robertson and Stiff model	$\tau = 8.8966(33.5930 + \gamma)^{0.228}$
Reference + 0.20	Unified model	$\tau = 17.072 + 1.2479\gamma^{0.4384}$
Reference + 0.80	Unified model	$\tau = 17.072 + 1.238\gamma^{0.4446}$

Table 5.8: Table of summary for the rheological modelling of MoS_2 drilling fluids

The percentage of error versus the different models were summarised for all the fluids in the following chart.

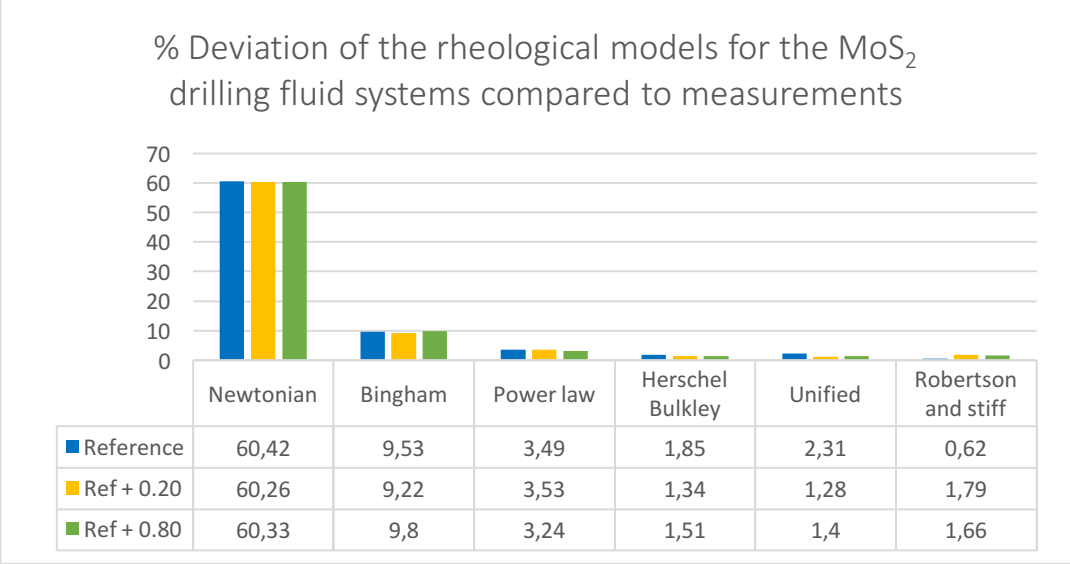

Figure 5.9: % Deviation of the rheological models for the MoS_2 drilling fluid systems compared to measurements

The chart illustrates that the most reliable model for the Reference fluid is the Robertson and Stiff model, whilst the most reliable model for the Ref + 0.2 and Ref + 0.8 fluid is the Unified model. The other models deviated at a greater extent, hence they were not suitable. Once again the Newtonian model deviated by far the most, with percentages above 60.

5.1.3 Rheological Modelling of the Graphene Drilling Fluids

This section will present the obtained models for a selected set of the Graphene drilling fluid systems with accommodating parameters and a presentation of the best model. Based on the experimental friction study, the selected fluids for the rheological modelling presentations are the Reference, Ref + 0.05 and Ref + 0.1 fluids. Modelling for the Ref + 0.2 and Ref + 1.25 fluid systems were also executed, but presented in the Appendix C.3 and C.4 respectively.

5.1.3.1 Graphene Reference System

The trend-lines for all the rheology models are plotted in Figure 5.10 with accommodating equations and parameters in Table 5.9.

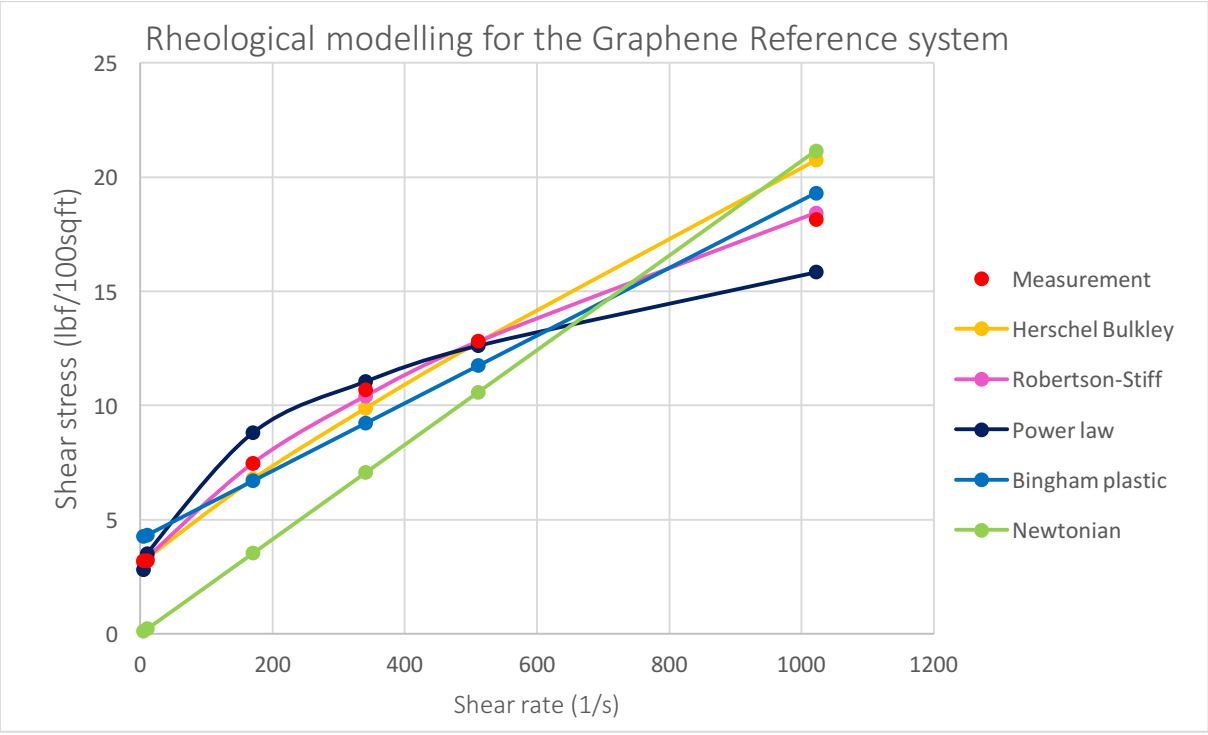

Figure 5.10: Modelled trend-lines for the Graphene Reference system

		Parameters					
Model	Equation	τo,τy, A	k, C	n, B	μp, μ	Error	cP
Herschel Bulkley	$2.966 + 0.0458\gamma^{0.8603}$	2.966	0.0458	0.8603		6.04	
Unified	Not definable						
Power Law	$1.6329\gamma^{0.3279}$		1.6329	0.3279		9.62	
Bingham	$00148\gamma + 4.176$	4.176			0.0148	17.78	7.086
Newtonian	0.0207γ				0.0207	51.80	9.911
Robertson and Stiff	$0.3846(38.1363 + \gamma)^{0.5555}$	0.3846	38.1363	0.5555		1.74	

Table 5.9: Modelled equations for the Graphene Reference system

In the process of modelling, it was not possible to define a trend-line for the Unified model. Therefore, the equation was not defined. Most of the models deviated with values greater or equal to 6.04%, which is significantly higher than for the previous fluids. There was only one model where the deviation percentage was of 1.74%, and that was for the Robertson and Stiff model. This means that the Robertson and Stiff model is the most reliable for the Graphene Reference system. A comparison of solely the Robertson and Stiff model compared to the measurements are illustrated in Appendix C.5.

5.1.3.2 Graphene Ref + 0.05 System

The trend-lines for all the rheology models are plotted in Figure 5.11 with accommodating equations and parameters in Table 5.10.

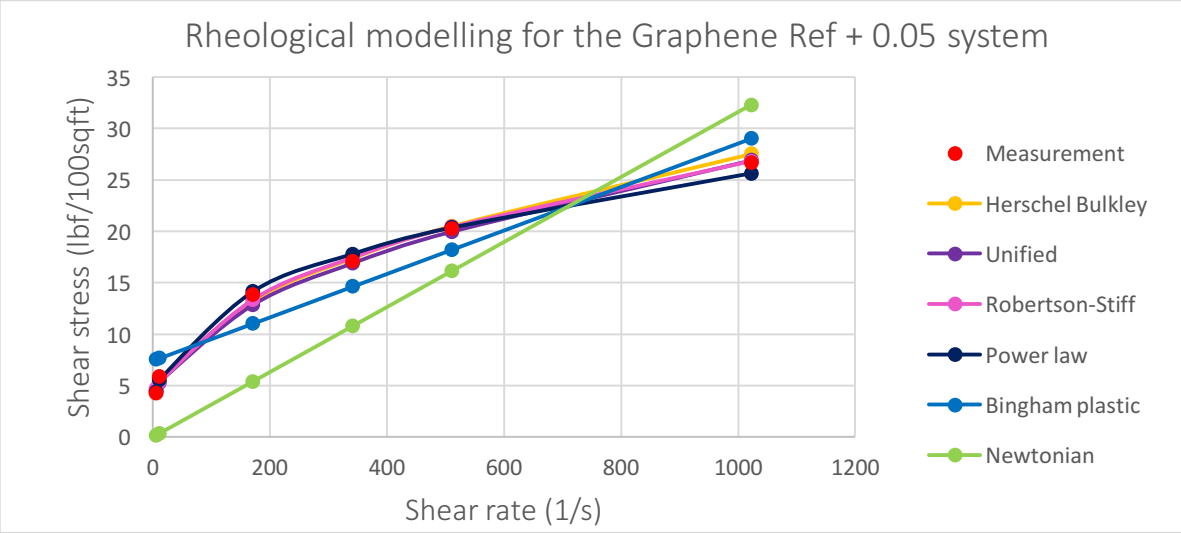

Figure 5.11: Modelled trend-lines for the Graphene Ref + 0.05 system

		Parameters					
Model	Equation	τo,τy, A	k, C	n, B	μp, μ	Error	cP
Herschel Bulkley	$2.568 + 0.9198\gamma^{0.47640}$	2.568	0.9198	0.4764		4.46	
Unified	$2.668 + 0.836\gamma^{0.4895}$	2.668	0.836	0.4859		4.55	
Power Law	$2.5666\gamma^{0.332}$		2.5666	0.332		3.19	
Bingham	$0.0211\gamma + 7.443$	7.443			0.0211	26.83	10.103
Newtonian	0.0316γ				0.0316	55.05	15.130
Robertson and Stiff	$1.7161(7.4564 + \gamma)^{0.3963}$	1.7161	7.4564	0.3963		4.25	

Table 5.10: Modelled equations for the Graphene Ref + 0.05 system

All of the models experienced a large deviation compared to the original measurements. However, the least deviating model was the Power law model with a deviation percentage of 3.19%. The other models deviated with more or equal to 4.25%. A comparison of solely the Power law model and the measurements for the Ref + 0.05 system is illustrated in Appendix C.5.

5.1.3.3 Graphene Ref + 0.10 System

The trend-lines for all the rheology models are plotted in Figure 5.12 with accommodating equations and parameters in Table 5.11.

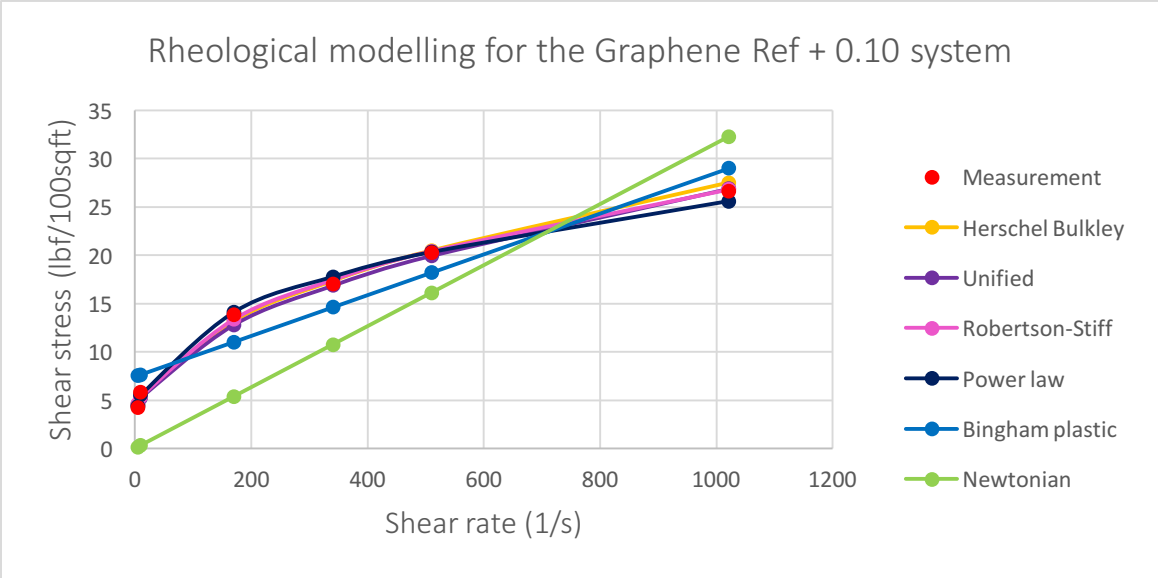

Figure 5.12: Modelled trend-lines for the Graphene Ref + 0.10 system

		Parameters					
Model	Equation	τo,τy, A	k, C	n, B	μp, μ	Error	cP
Herschel Bulkley	$4.345 + 0.7135\gamma^{0.5851}$	4.345	0.7135	0.5851		24.47	
Unified	$4.802 + 0.4843\gamma^{0.5851}$	4.802	0.4843	0.5851		5.57	
Power Law	$3.4935\gamma^{0.3026}$		3.4935	0.3026		1.87	
Bingham	$0.022\gamma + 9.337$	9.337			0.022	26.15	10.534
Newtonian	0.0353γ				0.0353	57.21	16.902
Robertson and Stiff	$2.1224(10.7787 + \gamma)^{0.3821}$	2.1224	10.7787	0.3821		2.80	

Table 5.11: Modelled equations for the Graphene Ref + 0.10 system

The deviation for all of the system is set in the interval from 1.87% to 57.21% where the smallest deviation occurs for the Power Law model, hence it is the best suited system to describe the Graphene Ref + 0.10 system. The deviation values are still of a great amount for the other models, where three of the models deviate with values above or equal to 24.47%. A comparison of the Power law model and the measurements are exhibited in Appendix C.5.

5.1.3.4 Summary of Rheological Modelling for the Graphene Drilling Fluids

The best suited rheological models for the three presented fluids are summarised in Table 5.12.

Summary of the rheological modelling for the Graphene drilling fluids		
Fluid	Model	Equation
Reference	Robertson and Stiff model	$\tau = 0.3846(38.1363 + \gamma)^{0.5555}$
Reference + 0.05	Power Law model	$\tau = 2.5666\gamma^{0.332}$
Reference + 0.10	Power Law model	$\tau = 3.4935\gamma^{0.3026}$

Table 5.12: Table of summary for the rheological modelling of Graphene drilling fluids

The percentage of error versus the different models were summarised for all the fluids in the following chart.

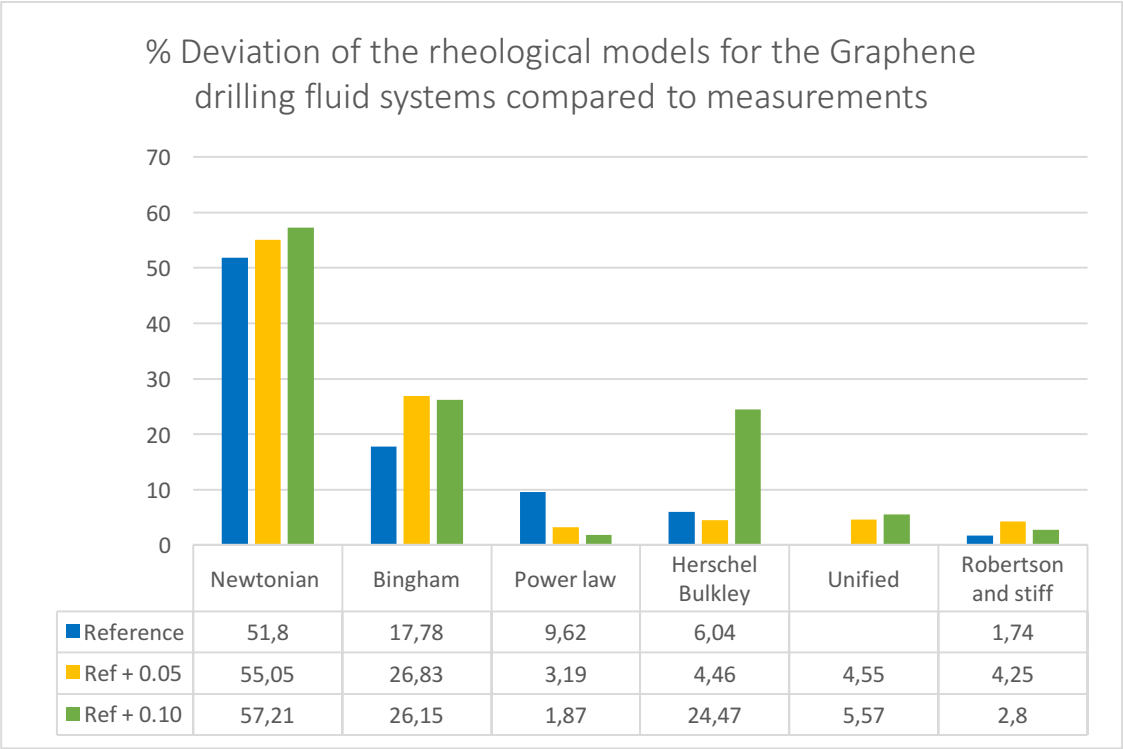

	Newtonian	Bingham	Power law	Herschel Bulkley	Unified	Robertson and stiff
Reference	51,8	17,78	9,62	6,04		1,74
Ref + 0.05	55,05	26,83	3,19	4,46	4,55	4,25
Ref + 0.10	57,21	26,15	1,87	24,47	5,57	2,8

Figure 5.13: % Deviation of the rheological models for the Graphene drilling fluid systems compared to measurements

As seen from Figure 5.13, the Robertson and Stiff model is the best suited model for the Reference system, whilst the Power Law is the best choice for the Ref + 0.05 and Ref + 0.10 systems. The most deviating model is as expected the Newtonian model. The Unified model could not be defined for the Reference system, and compared to the two other nano treated fluid batches where Robertson and Stiff and the Unified model deviated the least, the Power law model seemed to be the best suited for the Graphene and CMC treated fluids.

5.1.4 Rheological Modelling Summary and Comparison for the TiN Drilling Fluids

Table 5.13: Rheological modelling summary of the TiN drilling fluids. % Deviation of parameters compared to the reference system

Model		Ref	Ref + 0.15	Ref + 0.20
Herschel Bulkley	τo	17.067	16.949	15.566
	% deviation		-0.691	-8.79
	k	0.4755	0.5466	0.8064
	% deviation		14.95	69.59
	n	0.5868	0.5580	0.4945
	% deviation		-4.91	-15.73
Unified	τy	17.072	17.072	15.472
	% deviation		0.00	-9.37
	k	0.4731	0.4866	0.8598
	% deviation		2.85	81.74
	n	0.5875	0.5759	0.4850
	% deviation		-1.97	-17.45
Power Law	k	13.508	13.722	13.096
	% deviation		1.95	-3.05
	n	0.1543	0.1479	0.1483
	% deviation		-4.15	-3.89
Bingham	τy	21.021	21.071	20.115
	% deviation		0.239	-4.31
	μp	0.0237	0.022	0.0212
	% deviation		-7.17	-10.55
Newtonian	μ	0.0536	0.0519	0.0497
	% deviation		3.28	-4.24
Robertson and Stiff	A	6.4611	7.3789	7.3513
	% deviation		14.21	13.78
	C	42.5075	35.7224	32.3912
	% deviation		-15.96	-23.80
	B	0.2701	0.2456	0.2394
	% deviation		-9.07	-11.36

The observations from Table 5.13 exhibits that:

- Herschel Bulkley model: The yield stress (τo) decreased for the Ref + 0.15 and Ref + 0.20 fluids with 0.691% and 8.79% respectively. This indicates that there is less of a flow resistance in the fluids containing TiN, and less pressure needs to be applied to initiate flow. The consistency index increased while the flow behaviour index decreased with 4.91% and 15.73% for the Ref + 0.15 and Ref + 0.20 fluids respectively. This indicates that the fluids are moving towards a more pseudo-plastic state.
- The Unified model: The low shear yield stress (τy) stayed constant for the Ref + 0.15 fluid while it decreased for the Ref + 0.20 fluid. The decrease was of 9.37%. The consistency index increased for all fluids, while the flow behaviour index decreased for the Ref + 0.15 and Ref + 0.20 fluid with 1.97% and 17.45% respectively. The n value exhibited that the TiN nano-enhanced fluids behave pseudo-plastic.
- Power Law model: The consistency index value increased for the Ref + 0.15 fluid with 1.95% while it decreased for the Ref + 0.20 fluid with 3.05%. The flow behaviour index decreased for the Ref + 0.15 fluid with 4.15% and decreased for the Ref + 0.20 fluid with 3.05%. The n values were low compared to the Herschel Bulkley model and the Unified model.
- Bingham model: The yield stress (τy) for the measurements according to the Bingham model, exhibited an increase for the Ref + 0.15 fluid and a decrease for the Ref + 0.20 fluid of 0.239% and 4.31% respectively. This model indicates that more pressure needs to be applied to initiate flow for the Ref + 0.15 fluid, and less pressure for the Ref + 0.20 fluid. The plastic viscosity for both the fluids decreased which indicates a less steep slope of the Bingham model graph.
- Newtonian model: The viscosity for the Newtonian model decreased with 4.24% for the Ref + 0.20 fluid and increased for the Ref + 0.15 fluid. Using this model indicates that the shear rate at 600RPM will be lower for the Ref + 0.20 fluid and higher for the Ref + 0.15 fluid compared to the reference system.
- Robertson and Stiff model: The A parameter (corresponding to k) increased for both the fluids while the B parameter (corresponding to n) decreased for both the fluids. This exhibits that the fluids act more pseudo plastic according to this model. The shear rate correction factor decreased for both the TiN nano-enhanced fluids.

5.1.5 Rheological Modelling Summary and Comparison for the MoS_2 Drilling Fluids

Table 5.14: Rheological modelling summary of the MoS_2 drilling fluids. % Deviation of parameters compared to the reference system

Model		Ref	Ref + 0.20	Ref + 0.80
Herschel Bulkley	τo	18.973	17.322	17.182
	% deviation		-8.70	-9.44
	k	0.5968	1.0965	1.1717
	% deviation		83.73	96.33
	n	0.5826	0.4573	0.4526
	% deviation		-21.51	-22.31
Unified	τy	19.206	17.072	17.072
	% deviation		-11.11	-11.11
	k	0.4825	1.2479	1.238
	% deviation		158.6	156.7
	n	0.5826	0.4384	0.4446
	% deviation		-24.75	-23.68
Power Law	k	15.569	15.086	15.012
	% deviation		-3.10	-3.58
	n	0.1397	0.1402	0.1434
	% deviation		0.358	2.65
Bingham	τy	23.395	22.670	22.860
	% deviation		-3.10	-2.29
	μp	0.0225	0.022	0.0225
	% deviation		-2.22	0.00
Newtonian	μ	0.0557	0.0542	0.055
	% deviation		-2.69	-1.26
Robertson and Stiff	A	8.8966	8.7507	9.0404
	% deviation		-1.64	1.62
	C	33.593	32.4143	28.6308
	% deviation		-3.51	-14.77
	B	0.2280	0.2261	0.2236
	% deviation		-0.833	-1.93

The observations from Table 5.14 exhibits that:

- Herschel Bulkley model: The yield stress (τo) decreased for both the MoS_2 systems compared to the conventional fluid system. The decrease was of 8.70% and 9.44% for the Ref + 0.20 and Ref + 0.80 fluids respectively. This indicates that less pressure needs to be applied to initiate flow with the nano-enhanced fluids. The k values increased while the n values decreased with 21.51% and 22.31% for the Ref + 0.20 and Ref + 0.80 fluids respectively, exhibiting pseudo plastic behaviour.
- The Unified model: The low shear yield stress (τy) decreased for both the fluids with 11.11%. The k values increased while the n values decreased with 24.75% and 23.68% for the Ref + 0.20 and Ref + 0.80 fluids respectively, exhibiting pseudo-plastic behaviour.
- Power Law model: The n values for the Power Law modelling exhibited a decrease in k value for both the nano-enhanced fluids. The n values increased with 0.358% and 2.65% for the Ref + 0.20 fluid and Ref + 0.80 fluid respectively. This model indicates that the fluids are moving away from a pseudo-plastic state when adding MoS_2 to the conventional fluid system.
- Bingham model: The yield stress (τy) for the Bingham model indicated that the less pressure needs to be applied to initiate flow for the MoS_2 enhanced drilling fluids compared to the conventional system. The plastic viscosity stayed constant for the Ref + 0.80 fluid which means that the graph slope is of the same value. The plastic viscosity decreased for the Ref + 0.20 fluid indicating a less steep slope compared to the conventional system.
- Newtonian model: The viscosity decreased for both the Ref + 0.20 and Ref + 0.80 fluids with 2.69% and 1.26% respectively. This indicates lower shear stress values for all shear rates for both the nano-enhanced fluids.
- Robertson and Stiff model: The A parameter (corresponding to k) decreased for the Ref + 0.20 fluid with 1.64% and increased for the Ref + 0.80 fluid with 1.62%. The B parameter (corresponding to n) decreased for both the Ref + 0.20 and Ref + 0.80 fluids with 0.833% and 1.93% respectively. This exhibits a more pseudo-plastic behaviour with nano added to the conventional system. The shear rate correction factor decreased for both of the fluids.

5.1.6 Rheological Modelling Summary and Comparison for the Graphene Drilling Fluids

Table 5.15: Rheological modelling summary of the Graphene drilling fluids. % Deviation of parameters compared to the reference system

Model		Ref	Ref + 0.05	Ref + 0.10
Herschel Bulkley	τo	2.966	2.568	4.345
	% deviation		-13.42	46.49
	k	0.0458	0.9198	0.7135
	% deviation		1908	1458
	n	0.8603	0.4764	0.4843
	% deviation		-40.92	-39.94
Unified	τy	Not definable	2.668	4.802
Bin	% deviation			
	k	Not definable	0.836	0.4843
	% deviation			
	n	Not definable	0.4859	0.5851
	% deviation			
Power Law	k	1.6329	2.5666	3.4935
	% deviation		57.18	113.9
	n	0.3279	0.332	0.3026
	% deviation		1.25	-7.72
Bingham	τy	4.176	7.443	9.337
	% deviation		78.23	123.6
	μp	0.0148	0.0211	0.022
	% deviation		42.57	48.65
Newtonian	μ	0.0207	0.0316	0.0353
	% deviation		52.66	70.53
Robertson and Stiff	A	0.3846	1.7161	2.1224
	% deviation		346.2	451.8
	C	38.1363	7.4564	10.7787
	% deviation		-80.44	-71.73
	B	0.5555	0.3963	0.3821
	% deviation		-28.66	-31.22

The observations from Table 5.13 exhibits that:

- Herschel Bulkley model: The yield point (τo) values according to this model decreased by 13.42% for the Ref + 0.05 fluid and increased by 46.49% for the Ref + 0.10 fluid compared to the conventional system. This indicates that less pressure is needed to initiate flow for the Ref + 0.05 fluid while more pressure is needed to initiate flow for the Ref + 0.10 fluid. The k values decreased for both the fluids, whilst the n values decreased with 40.92% and 39.94% for the Ref + 0.05 anf Ref + 0.10 fluids respectively. This indicates a strong movement to a more pseudo-plastic behaviour for both the fluids.
- The Unified model: As the Unified model parameters could not be definable for the reference system according to the rheological modelling calculator, a comparison evaluation could not be conducted. However, the parameters exhibit that more pressure is needed to initiate flow for the Ref + 0.10 system compared to the Ref + 0.05 system, and that both fluids are pseudo-plastic in behaviour as their n value is below one. This is according to the unified model
- Power Law model: The power law model exhibited an increase in k values for both the Graphene enhanced fluids. The flow behaviour index increased with 1.25% for the Ref + 0.05 fluid system, while it decreased with 7.72% for the Ref + 0.10 system. This indicates that this model interprets the Ref + 0.10 fluid as more pseudo-plastic and the Ref + 0.05 system as less pseudo-plastic than the conventional system.
- Bingham model: The yield stress (τy) according to the Bingham model increased for both fluids, which indicates that more pressure needs to be applied to initiate flow. The plastic viscosity also increased with 42.57% and 48.65% for the Ref + 0.05 and Ref + 0.10 fluids respectively, indicating a steeper graph slope for the enhanced fluids.
- Newtonian model: The Newtonian model exhibited a large increase in viscosity of 52.66% and 70.53% for the Ref + 0.05 and Ref + 0.10 fluids compared to the conventional system. This means that the shear stress values for the graphene system will be of greater values at all shear rates.
- Robertson and Stiff model: The A parameter increased, while the B parameter decreased with 28.66% and 31.22% for the Ref + 0.05 and Ref + 0.10 system respectively. This indicates more pseudo-plastic behaviour. The correction factor decreased for both the enhanced fluids.

5.2 Torque and drag simulation

As explained in the theory part, the torque and drag may be critical parameters for extended reach drilling, as values exceeding the torque limit and the tensile limit may lead to drill-pipe failure in the well. The torque and drag values are most critical in inclined wells. A better lubricating fluid with a lower coefficient of friction may increase the measured depth (MD) of drilling. From the literature study, it is clear that OBM is more lubricating than WBM, but it is also costlier and less environmentally friendly due to the treatment and disposal of mud returns.

The experimental study showed that adding nanoparticles to WBM might decrease the coefficient of friction, hence lubricate the bit and drill-string, and reduce the torque and drag values. This may reduce the cost and environmental impact of using OBM, and lead to an extended reach of the well path with WBM.

This section will present a torque and drag simulation study that illustrates the obtainable extended reach for a stated well with the formulated nano fluids, showing a decrease in fluid friction.

5.2.1 Simulation arrangement

The torque and drag simulation was executed in WellPlan^{TM} 5000.1, a part of the Landmark Software. This software is created by Halliburton, and was provided by the University in Stavanger when executing the simulations.

The torque and drag performance study for the formulated drilling fluids were simulated in a deviated well with a measured depth (MD) of 9923 ft for the Graphene drilling fluids and 13123 ft for the TiN and MoS_2 drilling fluids. The well consisted of a 13 3/8” casing and of a deviated 12.615” open hole section. A 5” OD and 4.86” ID drilling pipe was used for the simulation study. The tripping in and tripping out speed was set to 60ft/min, while the RPM was set to 100.

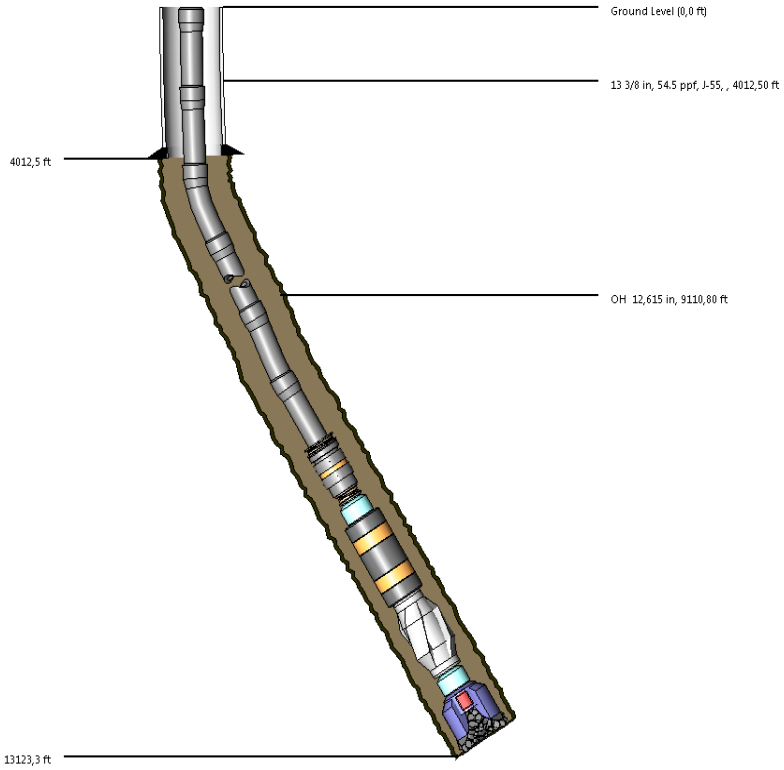

Figure 5.14: The deviated well setup used for the TiN and MoS_2 reference systems

The friction coefficient was registered in WellPlan^{TM}, and used to conduct the experiments for the different fluids. The friction was set to be the average of all values for the different temperatures. These values are represented in the Table 5.16.

Table of friction coefficients used to execute the torque and drag simulation	
Fluid	Coefficient of friction
Reference with XG	0.269
Reference with CMC	0.512
TiN Ref + 0.15	0.206
TiN Ref + 0.20	0.224
MoS_2 Ref + 0.2	0.178
MoS_2 Ref + 0.8	0.149
Graphene Ref + 0.05	0.469
Graphene Ref + 0.10	0.460

Table 5.16: Table of friction coefficients used to execute the torque and drag simulation

5.2.2 Torque and Drag for the TiN and MoS_2 Reference System

Drag and torque charts for the TiN and MoS_2 reference system are presented in Figure 5.15 and Figure 5.16.

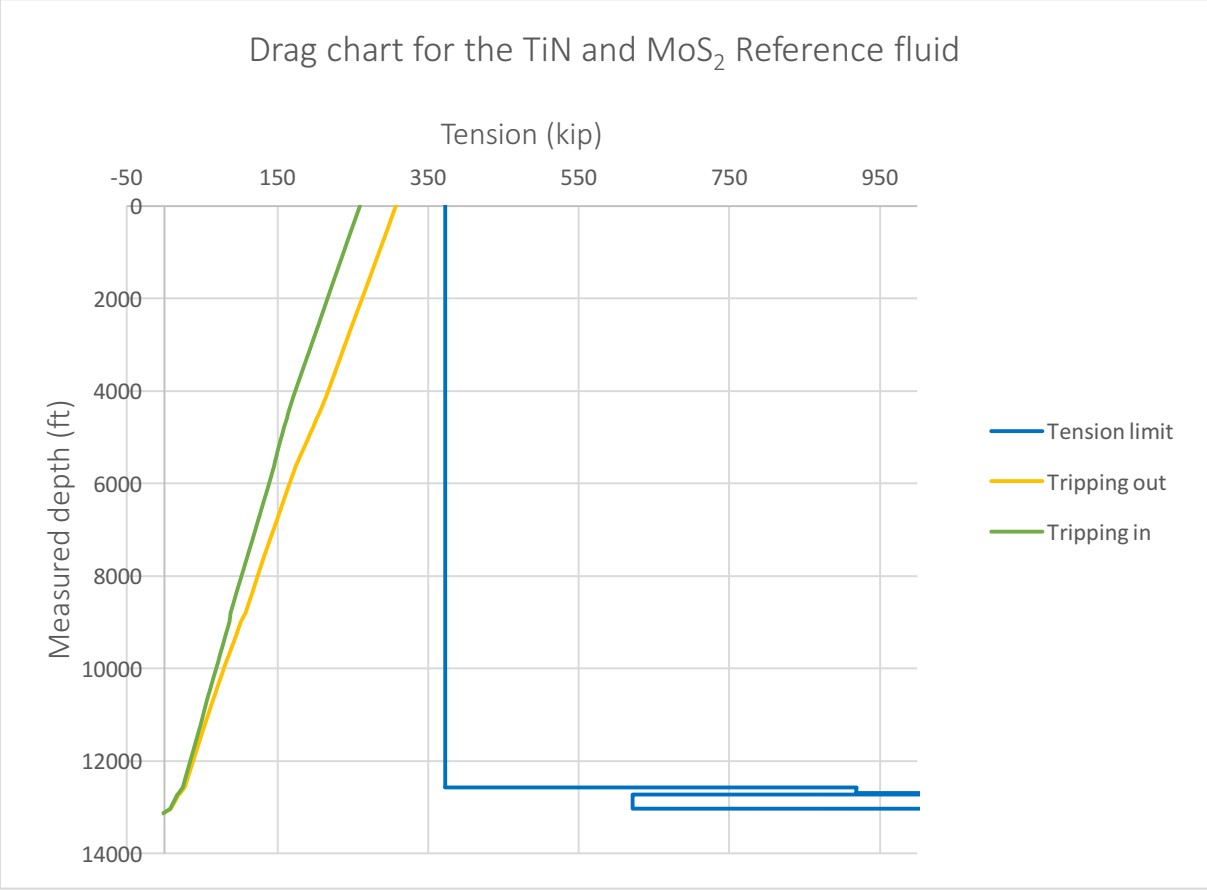

Figure 5.15: Drag chart for the TiN and MoS_2 Reference fluid

It is possible to see that with a friction coefficient equalling 0.269, tripping out and tripping in operations will be safe at the depth of 13123ft and with given speed and RPM, as the curves do not cross the tension limit.

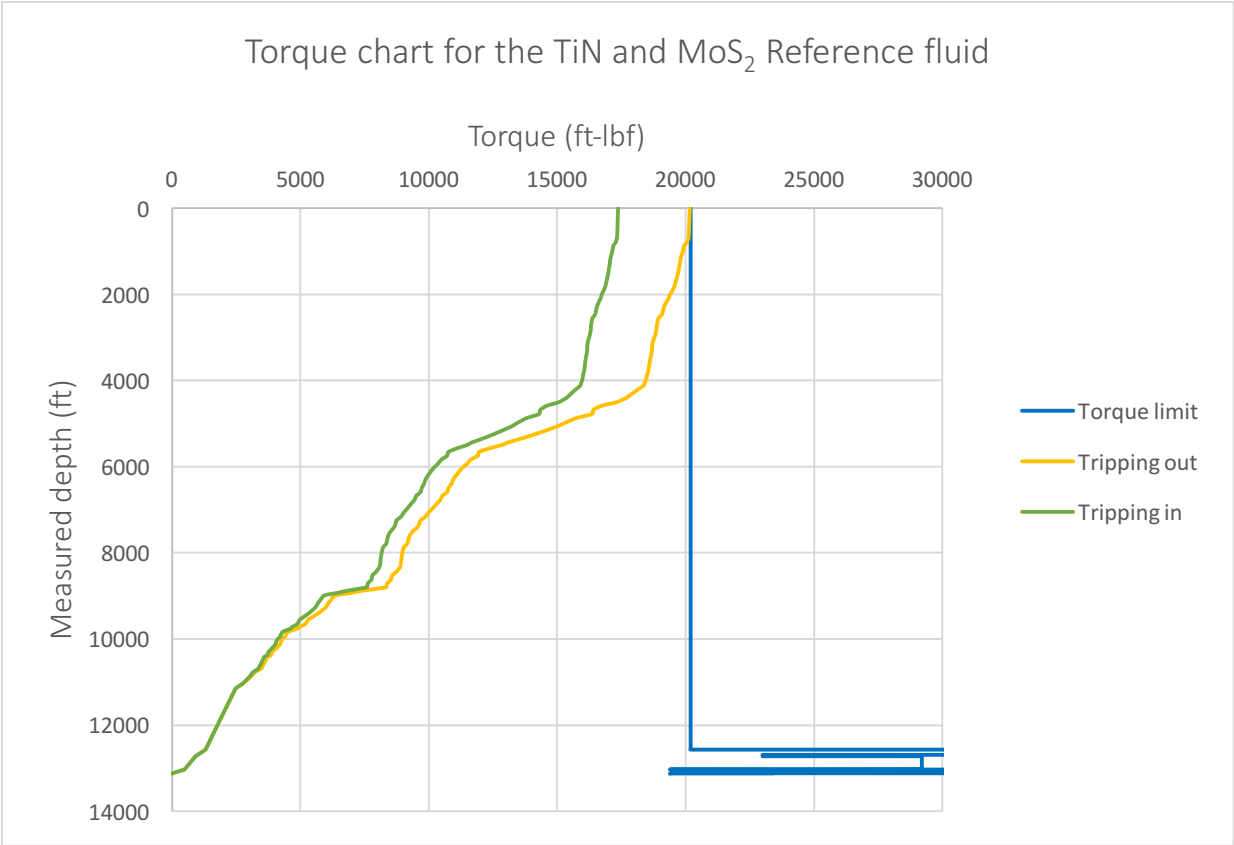

Figure 5.16: Torque chart for the TiN Reference fluid

With a friction coefficient of 0.269, tripping out and tripping in operations are barely safe at the depth of 13123ft and with given speed and RPM, as the tripping out curve is equalling the torque limit. It would not be possible to drill the well any further as a tripping out operation to e.g. change a worn out bit would have led to drill-pipe failure due to excessive torque values.

5.2.3 Torque and Drag Simulation for the TiN Drilling Fluids

A presentation of the torque and drag simulations for the TiN drilling fluids will be presented. The start MD for the reference fluid was set to 13123ft and increased according to the drag and torque values as the coefficient of friction value was set to lower values. A comparison of the simulations will be presented, with charts describing the torque and drag values for all the fluids at 13123ft.

5.2.3.1 Torque and Drag for the TiN Ref + 0.15 System

Drag and torque charts for the TiN Ref + 0.15 system are presented Figure 5.17 and Figure 5.18. During simulation, the measured depth of the well was changed to the value of 15020ft as this was the longest possible MD of drilling before any of the chart curves exceeded the tension or torque limit.

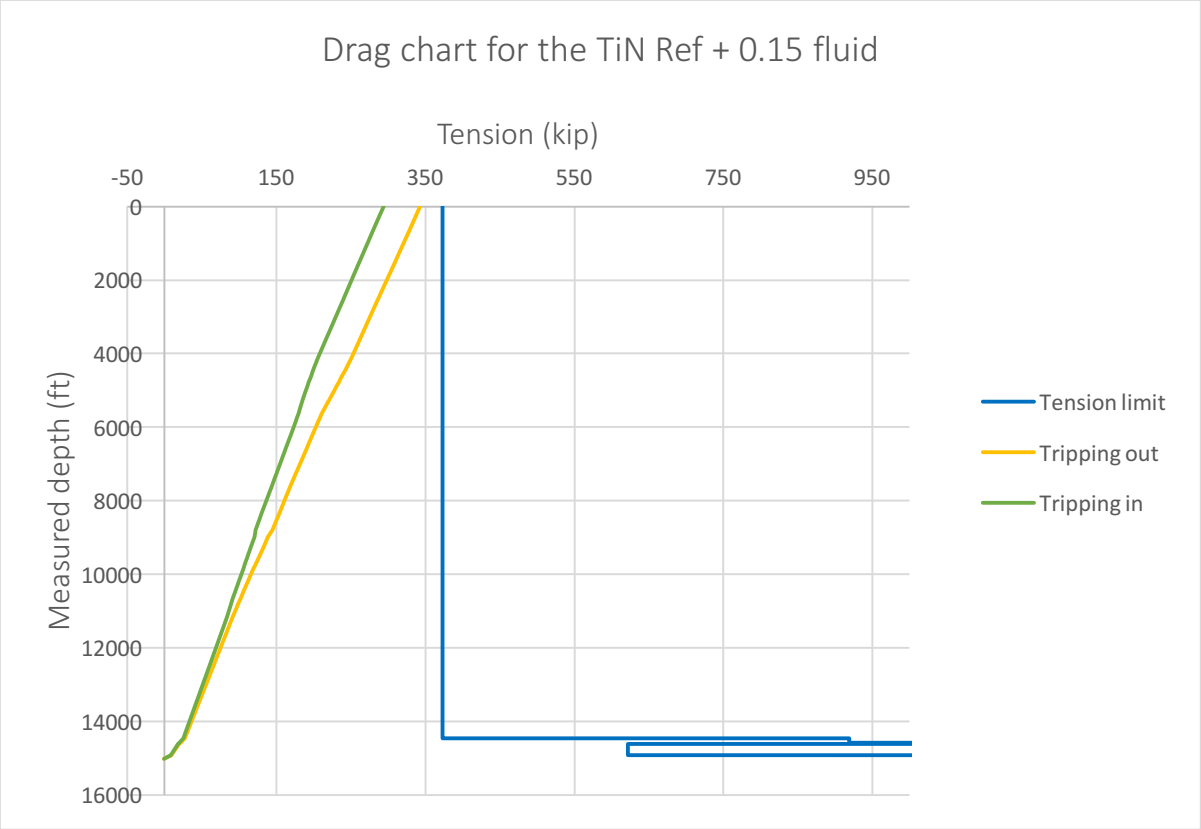

Figure 5.17: Drag chart for the TiN Ref + 0.15 fluid

The drag chart shows a tripping out curve that is close to the tension limit. Any further drilling of the well would be difficult as a tripping out operation from a deeper well as the drill-pipe material would experience a plastic elongation deformation due to excessive axial tension.

The percentage of decrease in the tripping out value is set to 2.1% compared to the reference system as the reference value is set to 307.5 kip, while the Ref + 0.15 system has a tripping out drag value of 301 kip.

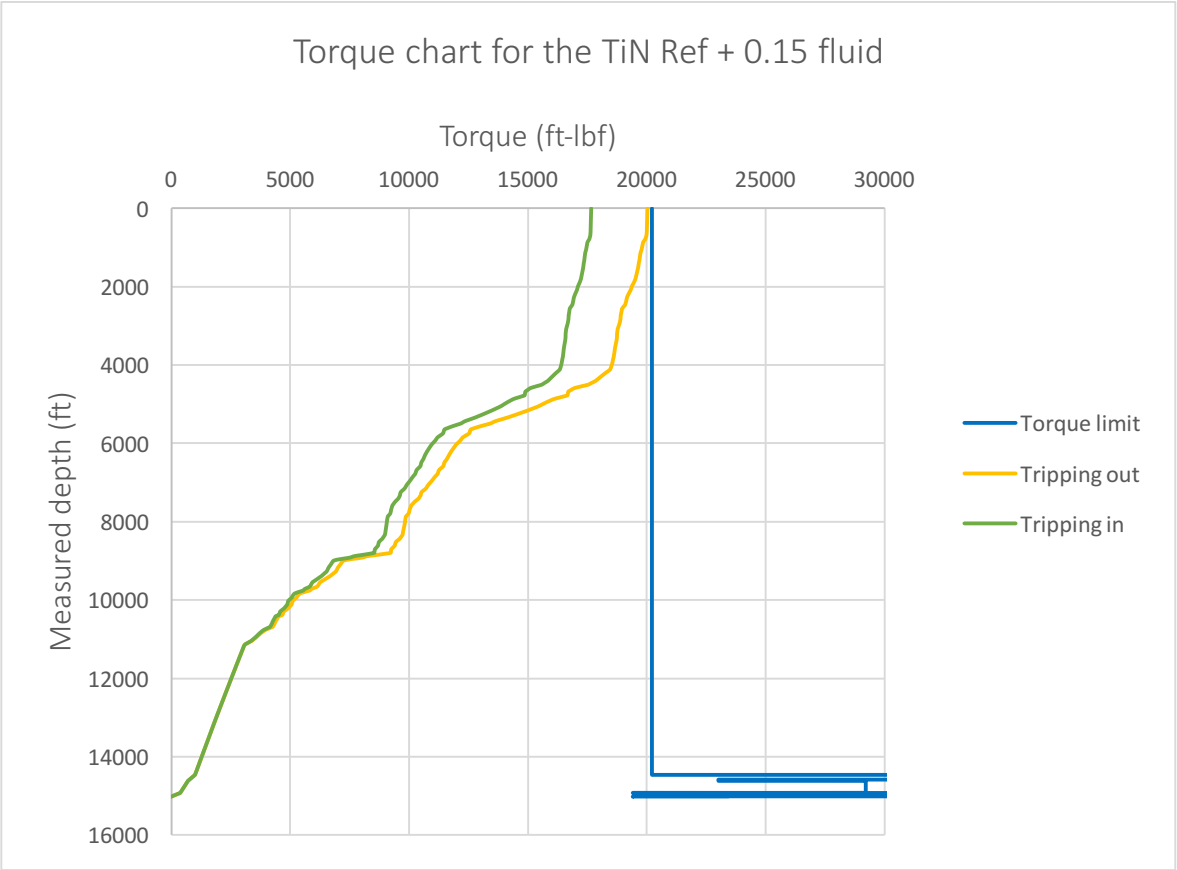

Figure 5.18: Torque chart for the TiN Ref + 0.15 fluid

The tripping out curve for the torque charts shows critical values for the tripping out curve. It would not have been possible to drill any further than 15020ft with the stated coefficient of friction without experiencing torque issues while tripping out.

However, the tripping out torque value has decreased significantly with the enhanced fluid system, with a reduction from 20242.3 ft-lb to 15162.3 ft-lb. This equals a decrease of 25.1% compared to the reference system.

5.2.3.2 Torque and Drag for the TiN Ref + 0.20 System

Drag and torque charts for the TiN Ref + 0.20 system are presented in Figure 5.19 and Figure 5.20. During simulation, the measured depth of the well was changed to the value of 14423ft as this was the longest possible MD of drilling before any of the chart curves exceeded the tension or torque limit.

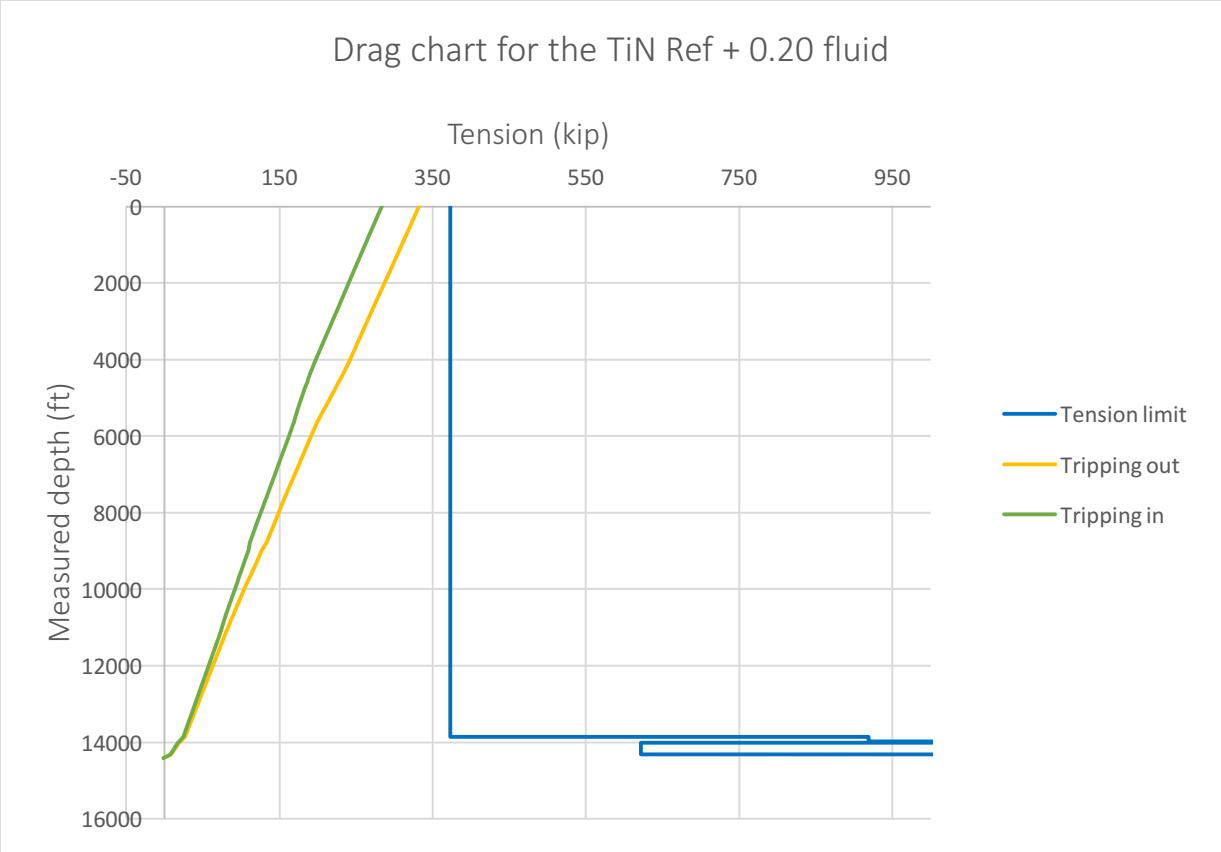

Figure 5.19: Drag chart for the TiN Ref + 0.20 fluid

The chart illustrated that it is not possible to drill much further than 14423ft before the tripping out curve would have exceeded the tension limit of the equipment. The stated coefficient of friction for this enhanced drilling fluid is of higher value than the Ref + 0.15 system.

The tripping out value with this fluid has decreased with 1.5%, from 307.5 kip to 302.8 kip.

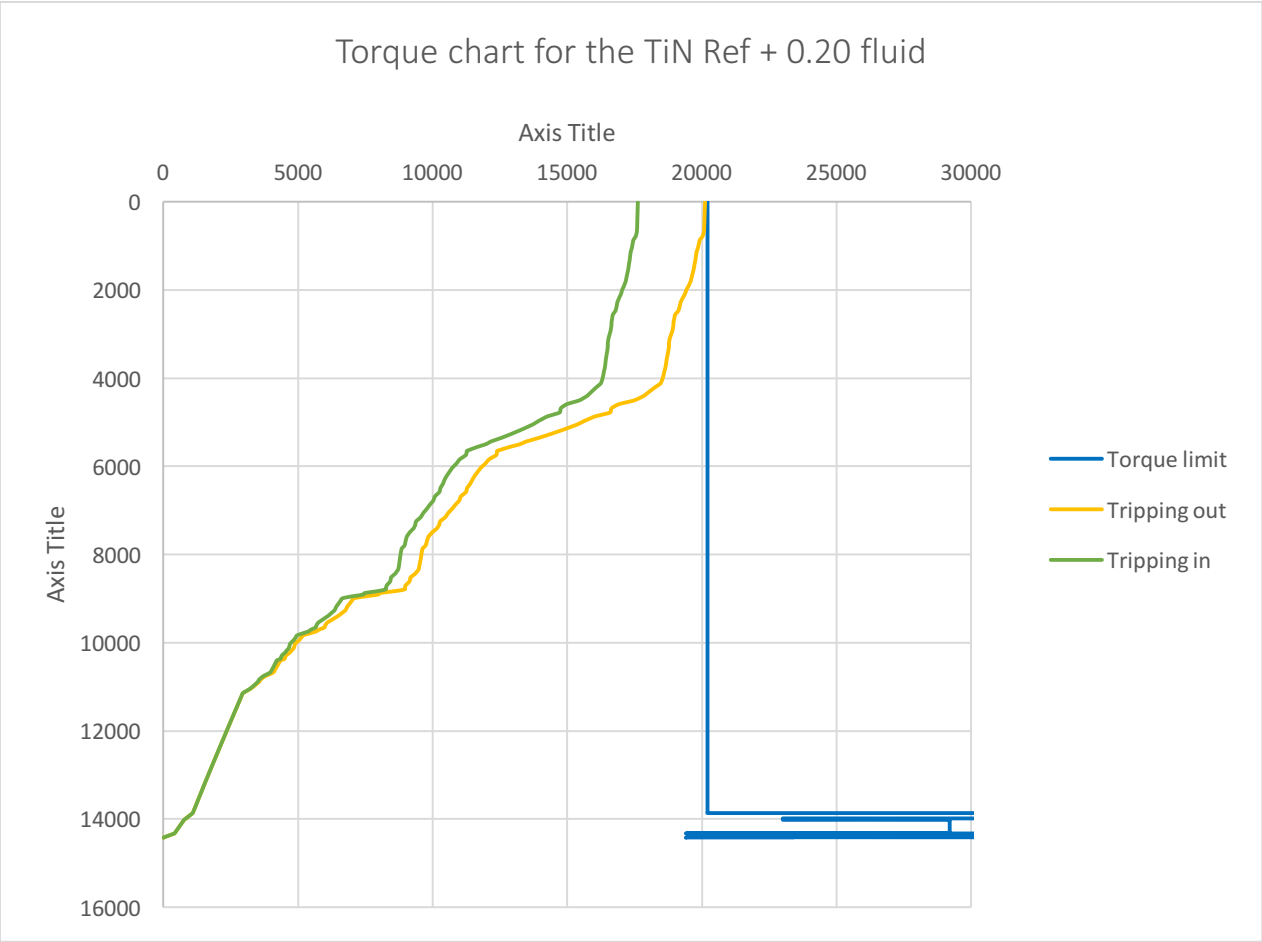

Figure 5.20: Torque chart for the TiN Ref + 0.20 fluid

This chart illustrates that a MD of 14423 in the given well is the absolute maximum it is possible to drill without experiencing any torque issues while tripping out of the well. The tripping out curve is equalling the torque limit and the value is critical.

The tripping out torque value of this fluid has experienced a reduction of 23.1 % compared to the reference fluid. The value is set to 15572.4 ft-lb.

5.2.3.3 Comparison of the Torque and Drag Simulation Study for the TiN Drilling Fluids

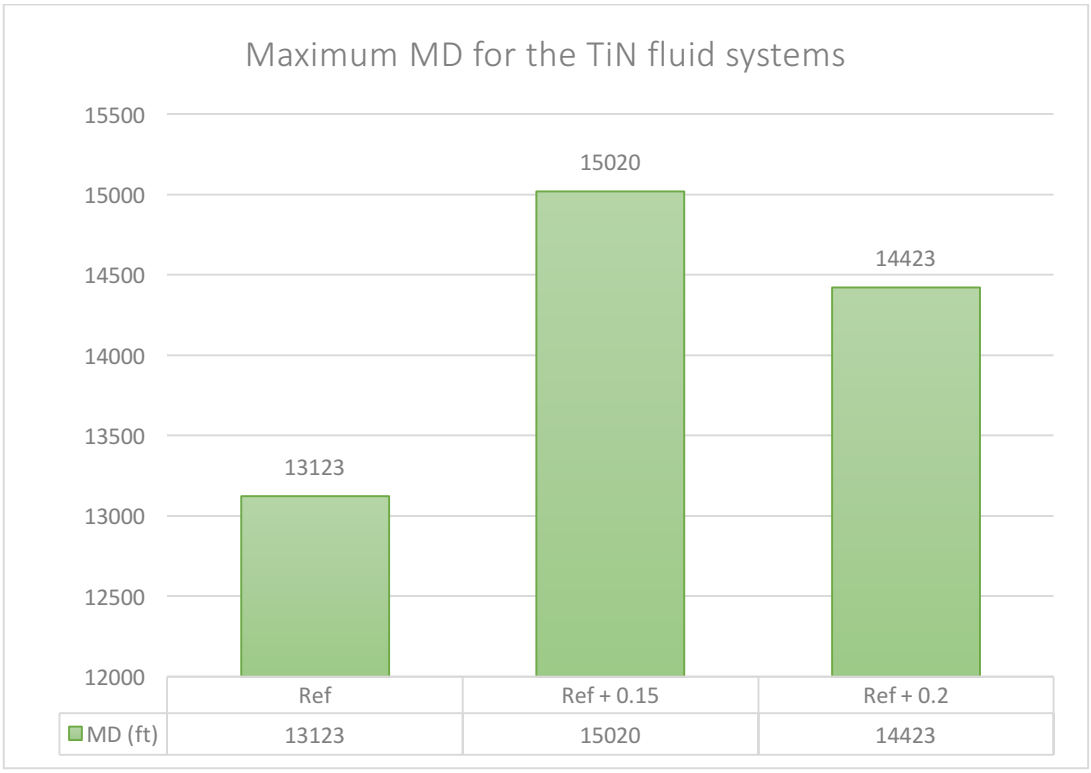

Figure 5.21: Maximum measured drilling depth for the formulated TiN fluid systems

The chart in figure 5.21 illustrates the different MD reaches for the formulated TiN drilling fluid. It is possible to drill the furthest with the Ref + 0.15 fluid as the maximum depth varies from 13123ft for the reference system to 15020ft for the stated fluid. This is a length change of 1897ft and an increase of 14.5%. It is possible to extend the reach for the Ref + 0.2 system in the given well with 9.9% compared to the reference system (1300ft).

The torque and drag values for all the fluids in the given well with a MD of 13123ft are plotted in Figure 5.22 and Figure 5.23 for comparison. From the charts it is possible to see that the most significant change for the fluids enhanced with nano occurs in the torque values, as the drag curves are equalling and harder to separate by eye.

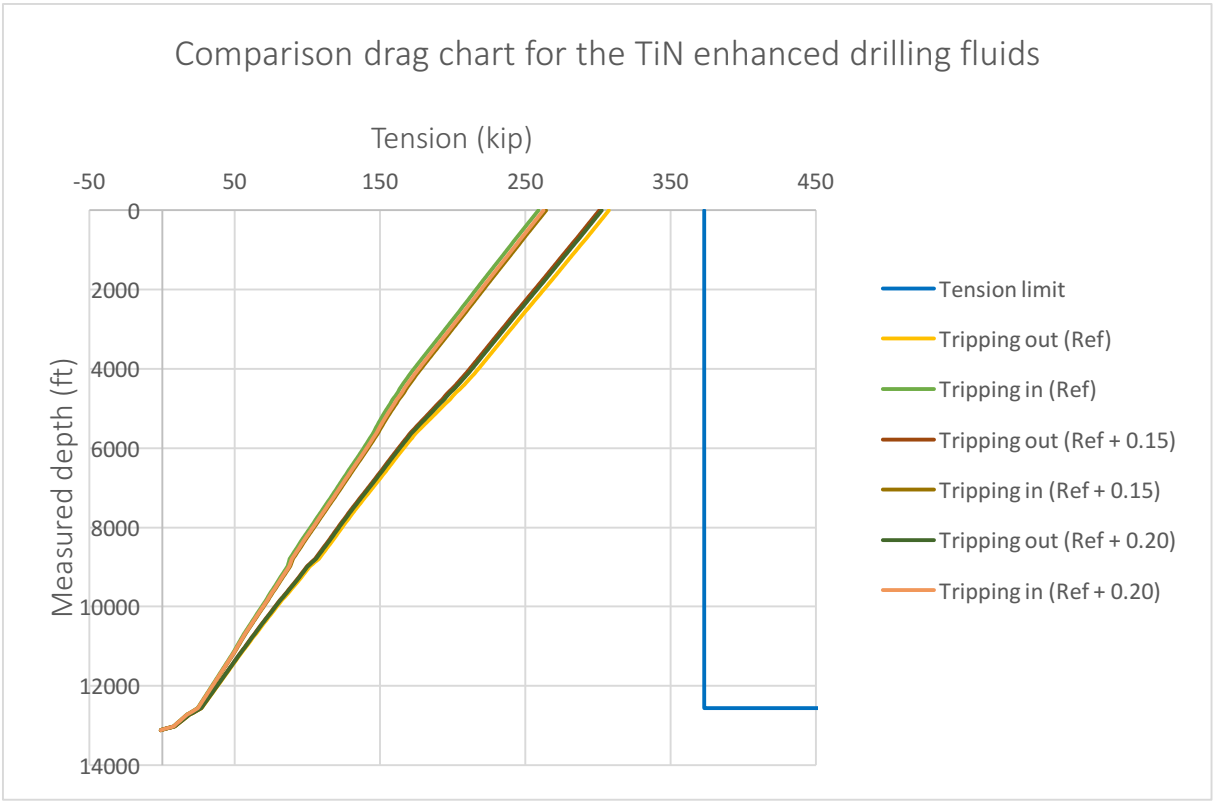

Figure 5.22: Comparison drag chart for the TiN enhanced drilling fluids

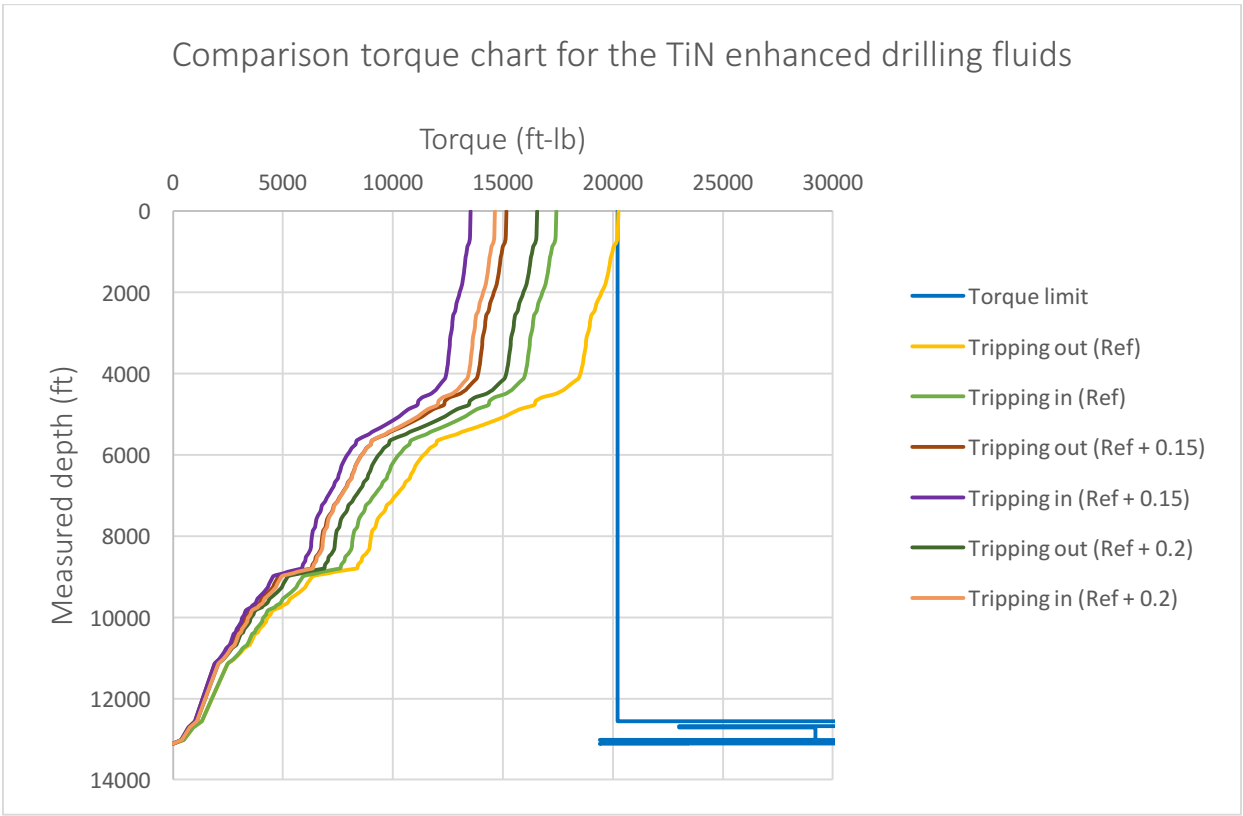

Figure 5.23: Comparison torque chart for the TiN enhanced drilling fluids

5.2.4 Torque and Drag Simulation for the MoS_2 Drilling Fluids

A presentation of the torque and drag simulations for the MoS_2 drilling fluids will be presented. The start MD for the reference fluid was set to 13123ft and increased according to the drag and torque values as the coefficient of friction value was set to lower values. A comparison of the simulations will be presented, with charts describing the torque and drag values for all the fluids at 13123ft.

5.2.4.1 Torque and Drag for the MoS_2 Ref + 0.20 System

Drag and torque charts for the MoS_2 Ref + 0.20 system are presented in Figure 5.24 and Figure 5.25. During simulation, the measured depth of the well was changed to the value of 15123ft as this was almost the longest possible MD of drilling before any of the chart curves exceeded the tension or torque limit.

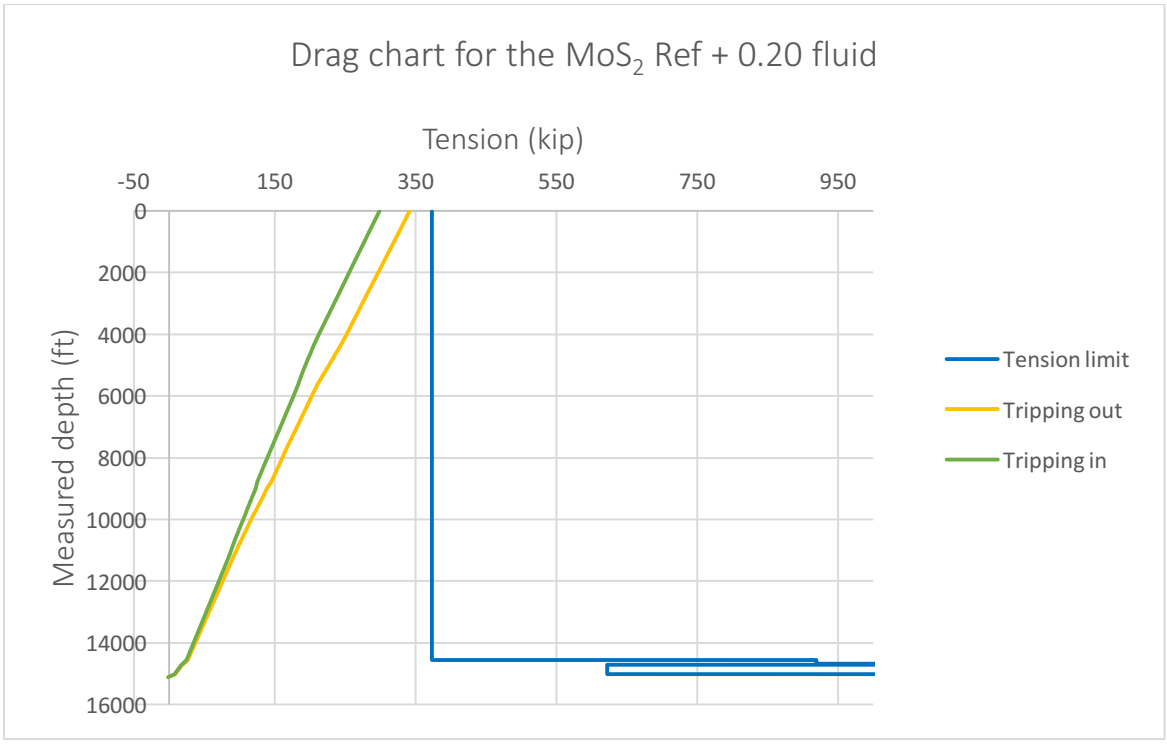

Figure 5.24: Drag chart for the MoS_2 Ref + 0.20 fluid

From the figure it is possible to see that any further drilling than 15123ft may possibly result in excessive drag loads while tripping out of the well. However, with the MoS_2 enhanced drilling fluid, the tripping out value has decreased with 3.1% compared to the reference system.

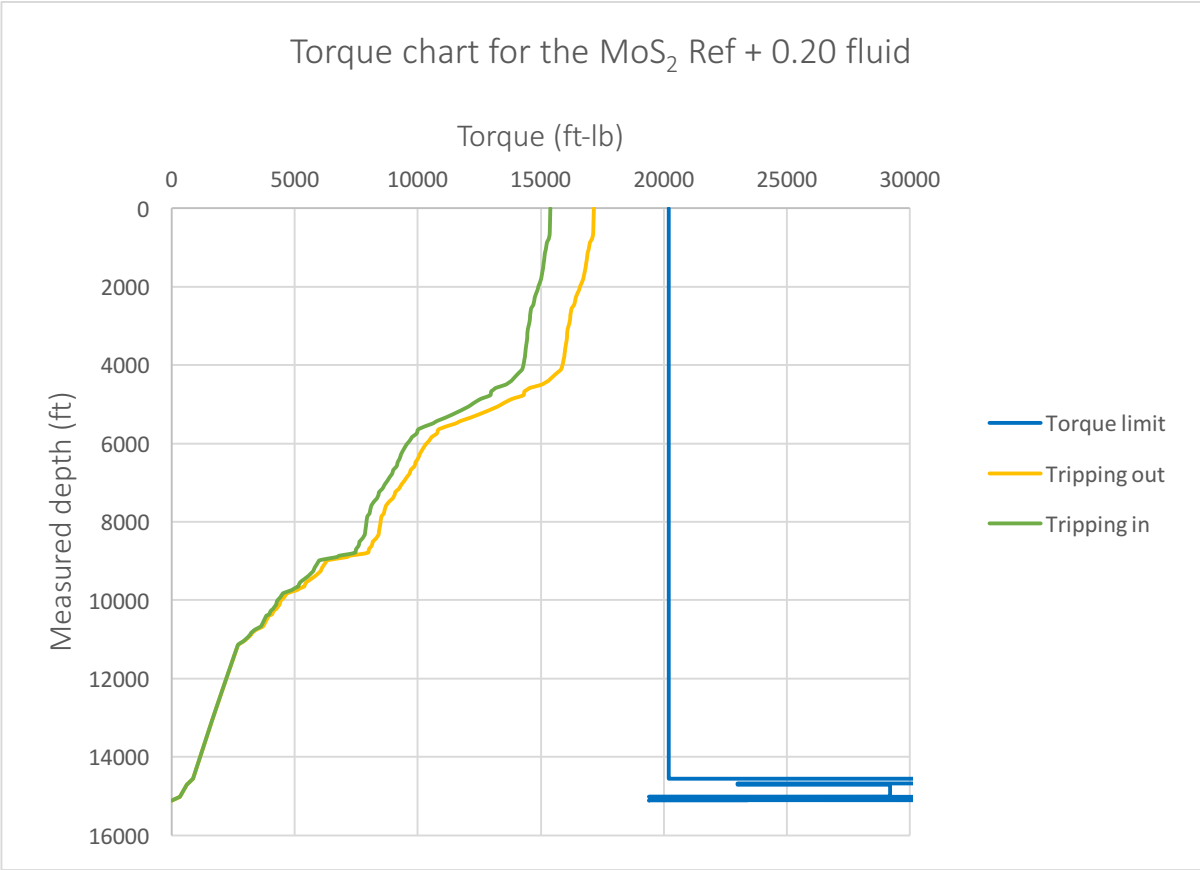

Figure 5.25: Torque chart for the MoS_2 Ref + 0.20 fluid

From the torque chart it is possible to see that both the tripping in and tripping out curves are well inside the safe window. It would have been possible to drill further with solely the torque loads in mind, but not in reality as the drag loads are critical. Using a material grading with a greater yield strength value may have increased the well reach to greater depths, but also may have increased the costs.

The tripping out torque load for the Ref + 0.20 fluid system has decreased with 36.3% compared to the reference system, with a value of 12843.6 ft-lb.

5.2.4.2 Torque and Drag for the MoS_2 Ref + 0.80 System

Drag and torque charts for the MoS_2 Ref + 0.80 system are presented in Figure 5.26 and Figure 5.27. During simulation, the measured depth of the well was changed to the value of 16523ft as this was the longest possible MD of drilling before any of the chart curves exceeded the tension or torque limit.

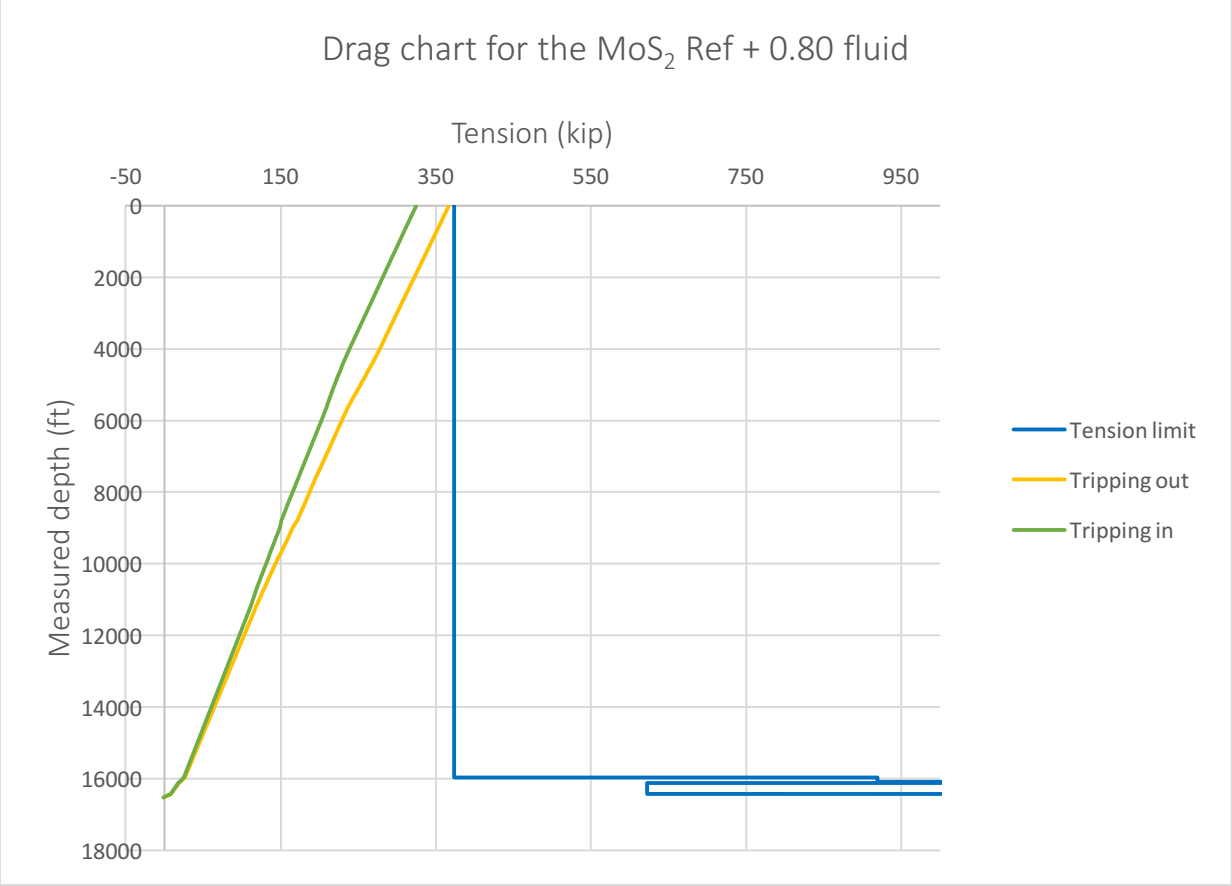

Figure 5.26: Drag chart for the MoS_2 Ref + 0.80 fluid

Both the tripping out and tripping in drag loads are critical as they are close to or equalling the tension limit curve. A MD of 16523ft is the absolute reach in the stated well for this fluid with a friction coefficient value of 0.149.

The tripping out drag value has decreased with 3.9% compared to the reference system, and the load value has decreased to 295.4 kip.

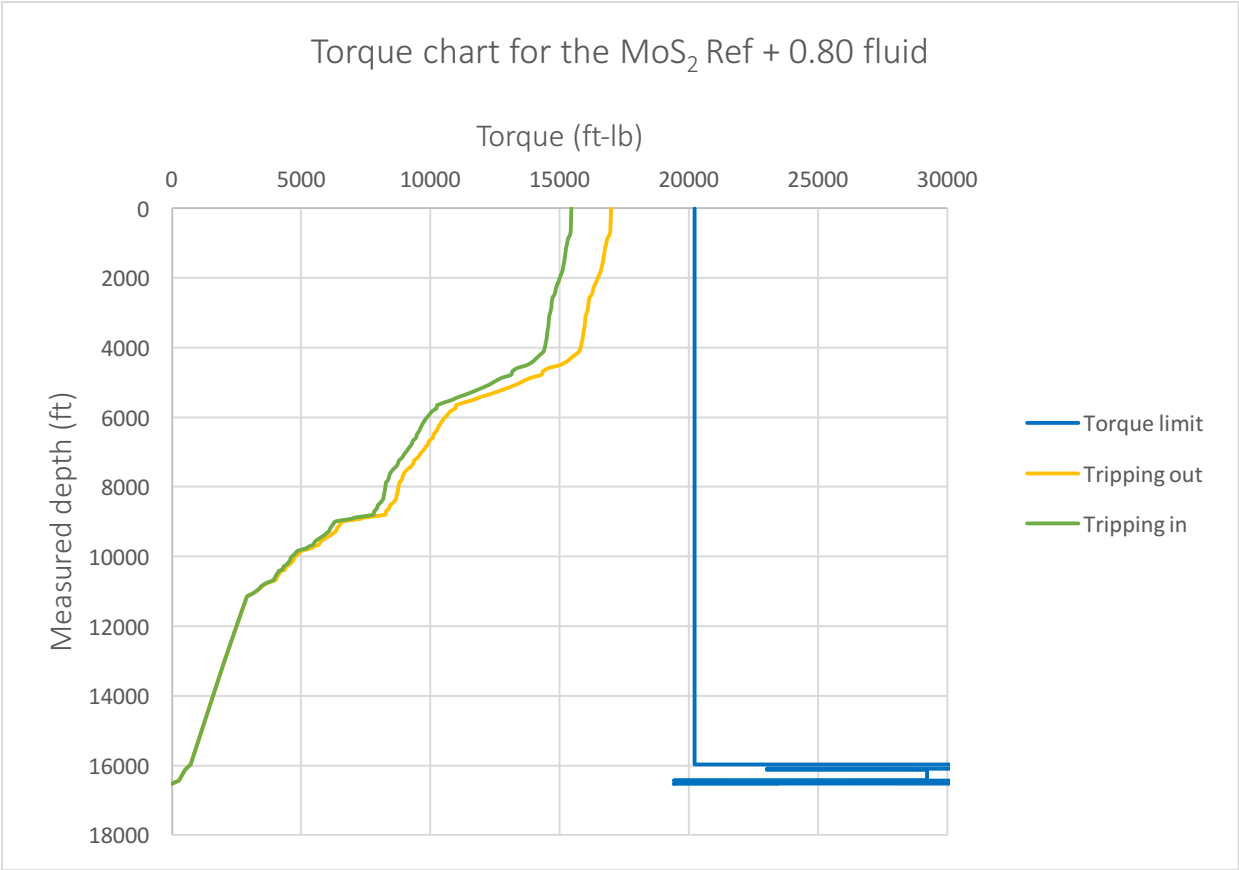

Figure 5.27: Torque chart for the MoS_2 Ref + 0.80 fluid

The torque chart for the MoS_2 Ref + 0.80 fluid system shows similar results as the chart for the Ref + 0.2 system. The torque curves are well inside the safe window, and it would have been possible to drill even further than accomplished with the friction-reduced fluid if the pipe material strength was increased.

The tripping out torque load has decreased with as much as 46.5%, nearly half the value compared to the reference system. The value decreased from 20161.5 ft-lb for the reference system to 10790.2 ft-lb for the measured fluid.

5.2.4.3 Comparison of the Torque and Drag Simulation Study for the MoS_2 Drilling Fluids

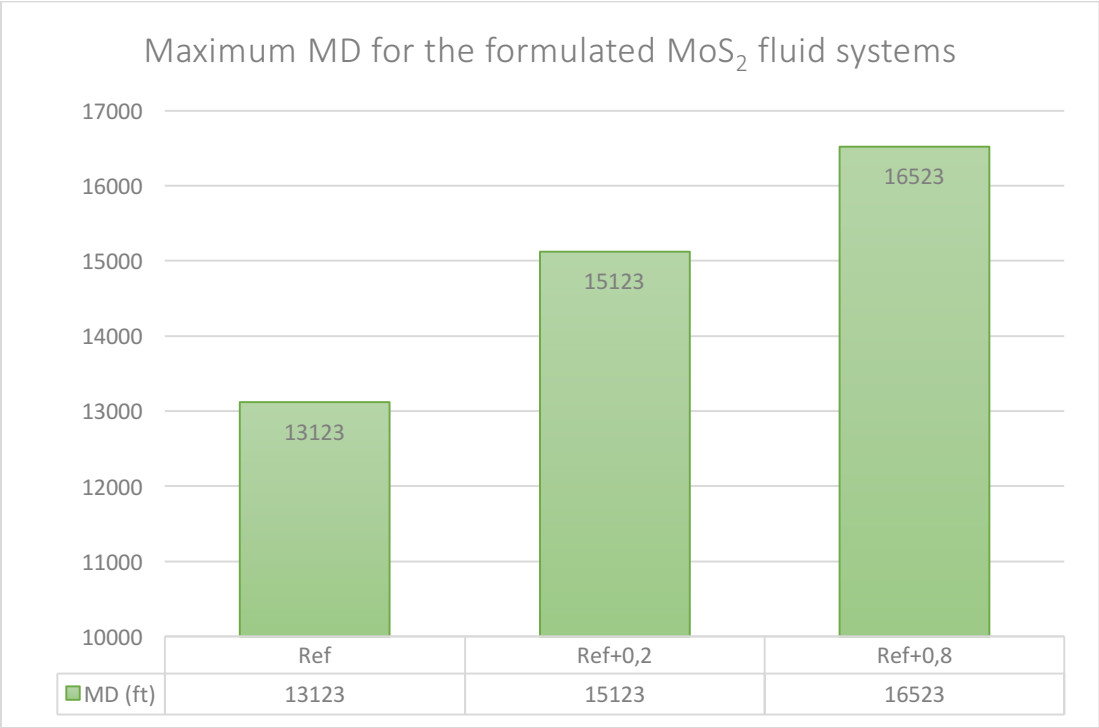

Figure 5.28: Maximum MD for the formulated MoS_2 fluid systems

The chart in Figure 5.28 illustrates the different MD reaches for the formulated MoS_2 drilling fluids. It is possible to drill the furthest with the Ref + 0.80 fluid as the maximum depth varies from 13123ft for the reference system to 16523ft for the stated fluid. This is a length change of 3400ft and an increase of 25.9%. It is possible to extend the reach for the Ref + 0.20 system in the given well with 15.2% compared to the reference system (200ft).

The torque and drag values for all the fluids in the given well with a MD of 13123ft are plotted in Figure 5.29 and Figure 5.30 for comparison. From these charts it is also possible to see that the most significant change for the fluids enhanced with nano occurs in the torque values, as the drag curves are equalling and harder to separate by eye. This is similar to the results of the TiN simulations.

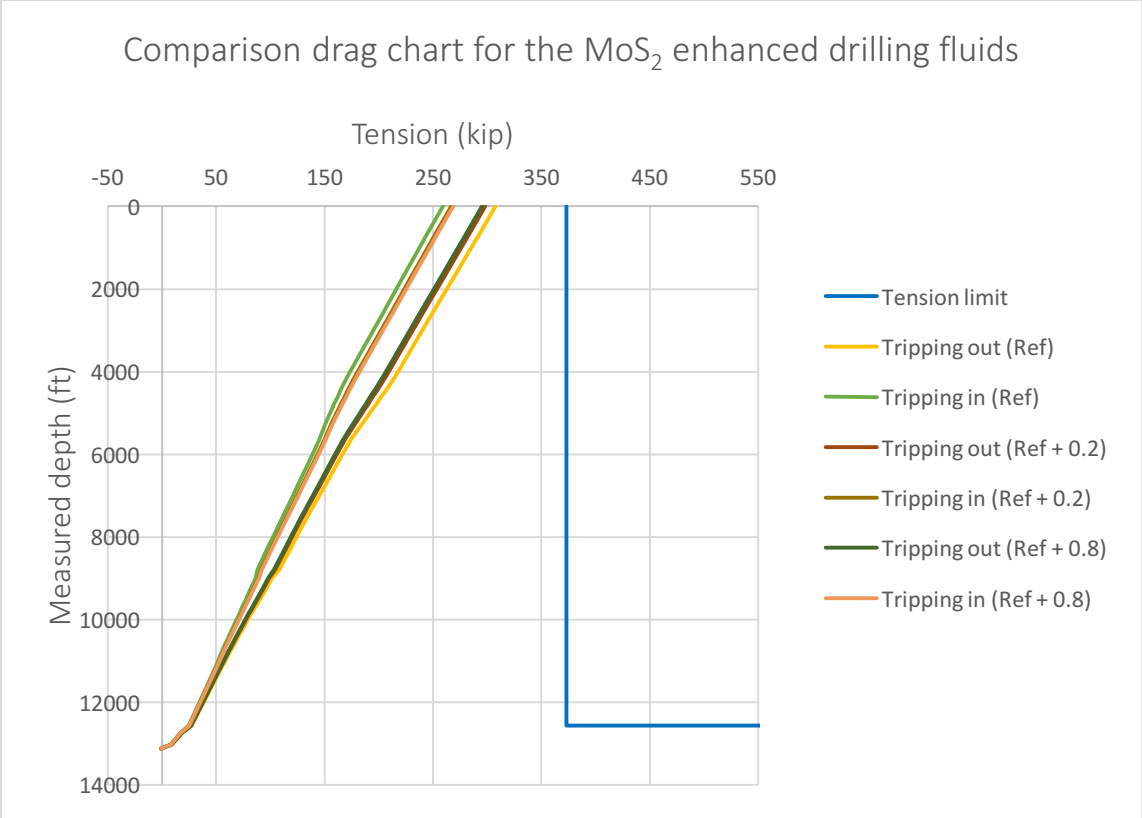

Figure 5.29: Comparison drag chart for the MoS_2 enhanced drilling fluids

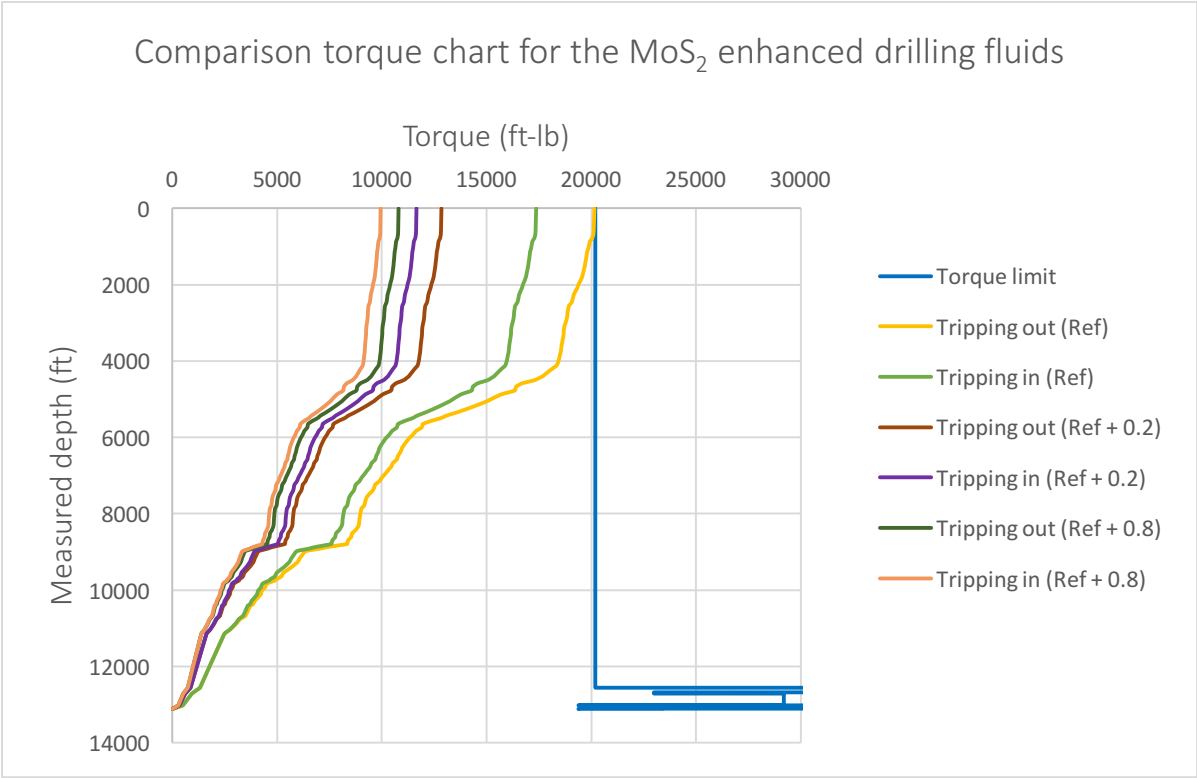

Figure 5.30: Comparison torque chart for the MoS_2 enhanced drilling fluid

5.2.5 Torque and Drag for the Graphene Reference System

Drag and torque charts for the Graphene reference system is presented below.

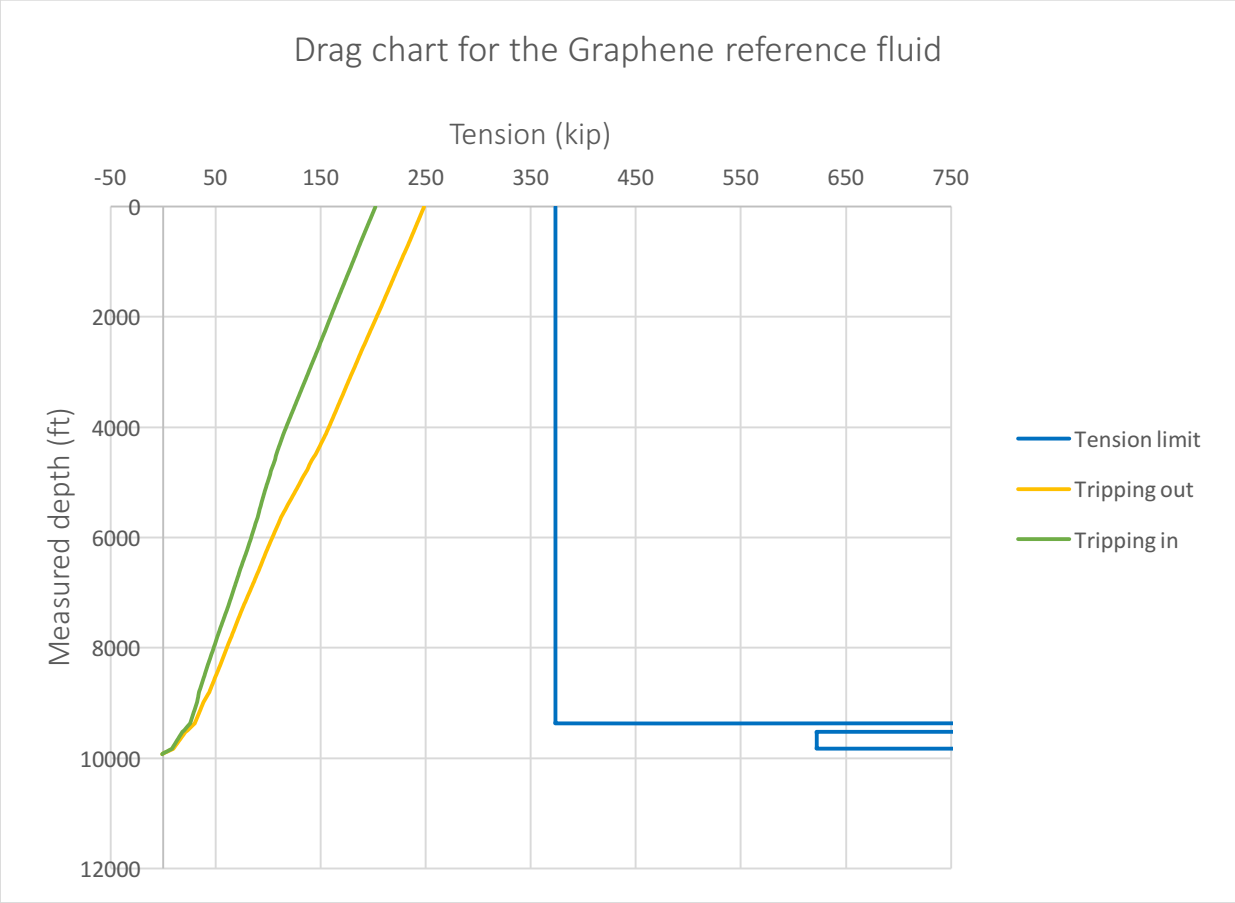

Figure 5.31: Drag chart for the Graphene reference fluid

It is possible to see that with a friction coefficient equalling 0.512, tripping out and tripping in operations will be safe at the depth of 9923ft with the given speed and RPM, as the curves do not cross the tension limit.

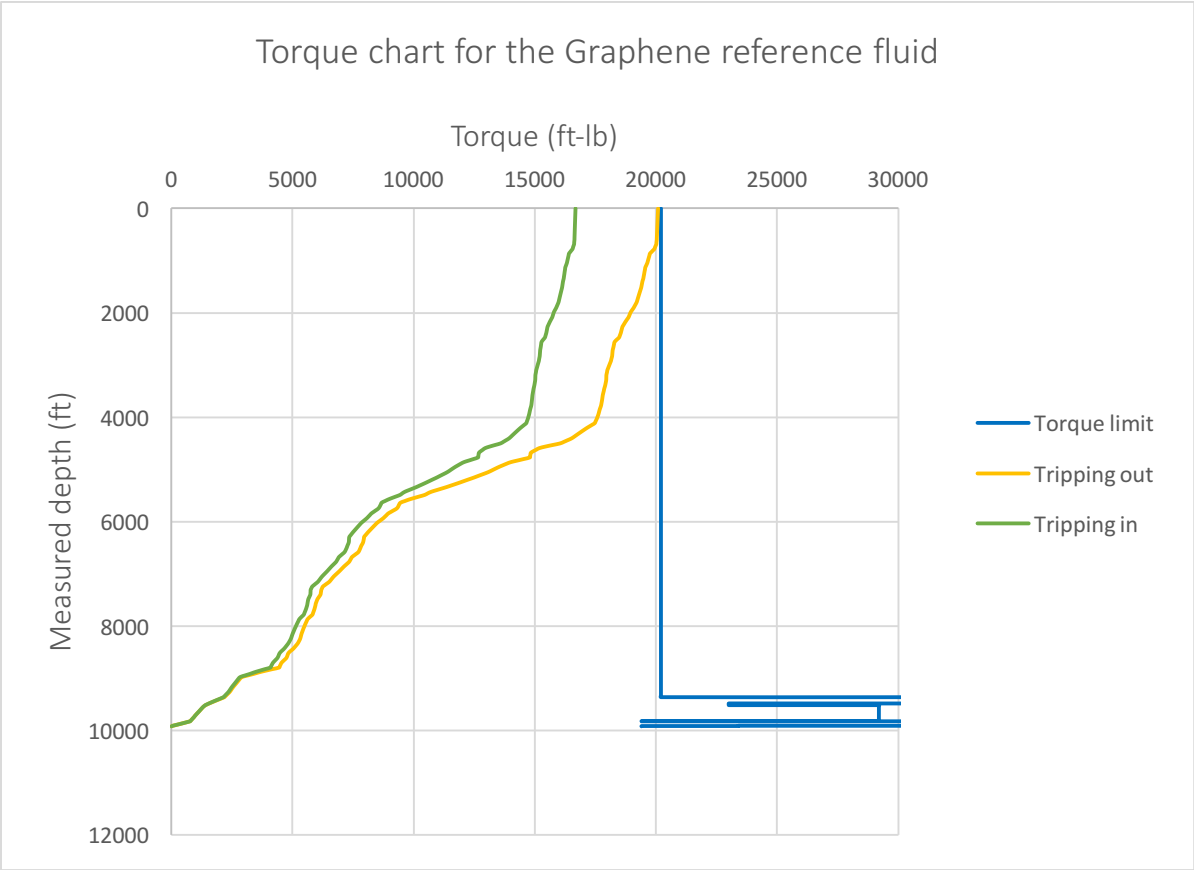

Figure 5.32: Torque chart for the Graphene reference fluid

It is possible to see that with a friction coefficient equalling 0.512, tripping out and tripping in operations are barely safe at the depth of 9923ft with the given speed and RPM, as the tripping out curve is equalling the torque limit. It would not be possible to drill the well any further as a tripping out operation to e.g. change a worn out bit would have led to drill-pipe failure due to excessive torque values.

5.2.6 Torque and Drag simulation for the Graphene Drilling Fluids

A presentation of the torque and drag simulations for the Graphene drilling fluids will be presented. The start MD for the reference fluid was set to 9923ft and increased according to the drag and torque values as the coefficient of friction value was set to lower values. A comparison of the simulations will be presented, with charts describing the torque and drag values for all the fluids at 9923ft.

5.2.6.1 Torque and Drag for the Graphene Ref + 0.05 System

Drag and torque charts for the Graphene Ref + 0.05 system are presented in Figure 5.33 and Figure 5.34. During simulation, the measured depth of the well was changed to the value of 10323ft as this was the longest possible MD of drilling before any of the chart curves exceeded the tension or torque limit.

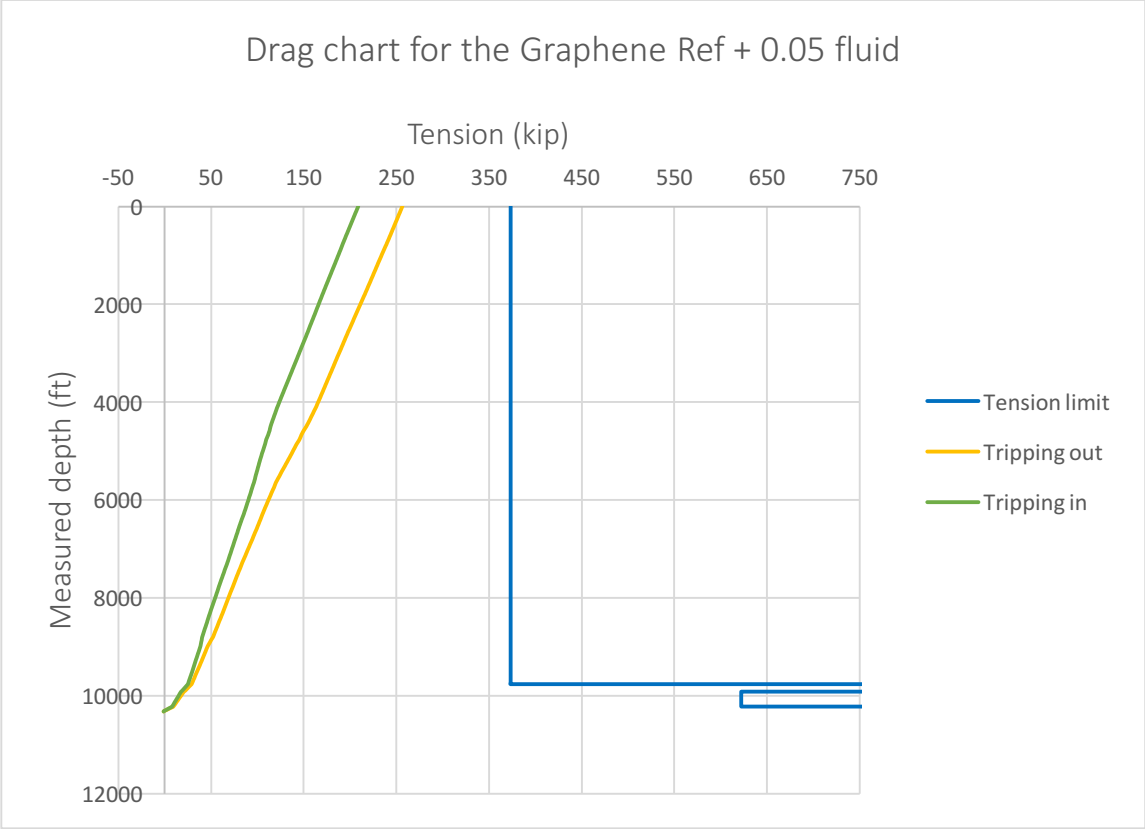

Figure 5.33: Drag chart for the Graphene Ref + 0.05 fluid

The figure illustrates that the tripping in and tripping out values for the Graphene Ref + 0.05 system are within the safe window. Solely considering the tension, it would have been possible to drill a bit further with this enhanced nano system.

The tripping out drag values experienced a small change, with a 0.9% decrease compared to the reference system. The tripping out value for this system is set to 246.1 kip as the reference system is set to 248.4 kip.

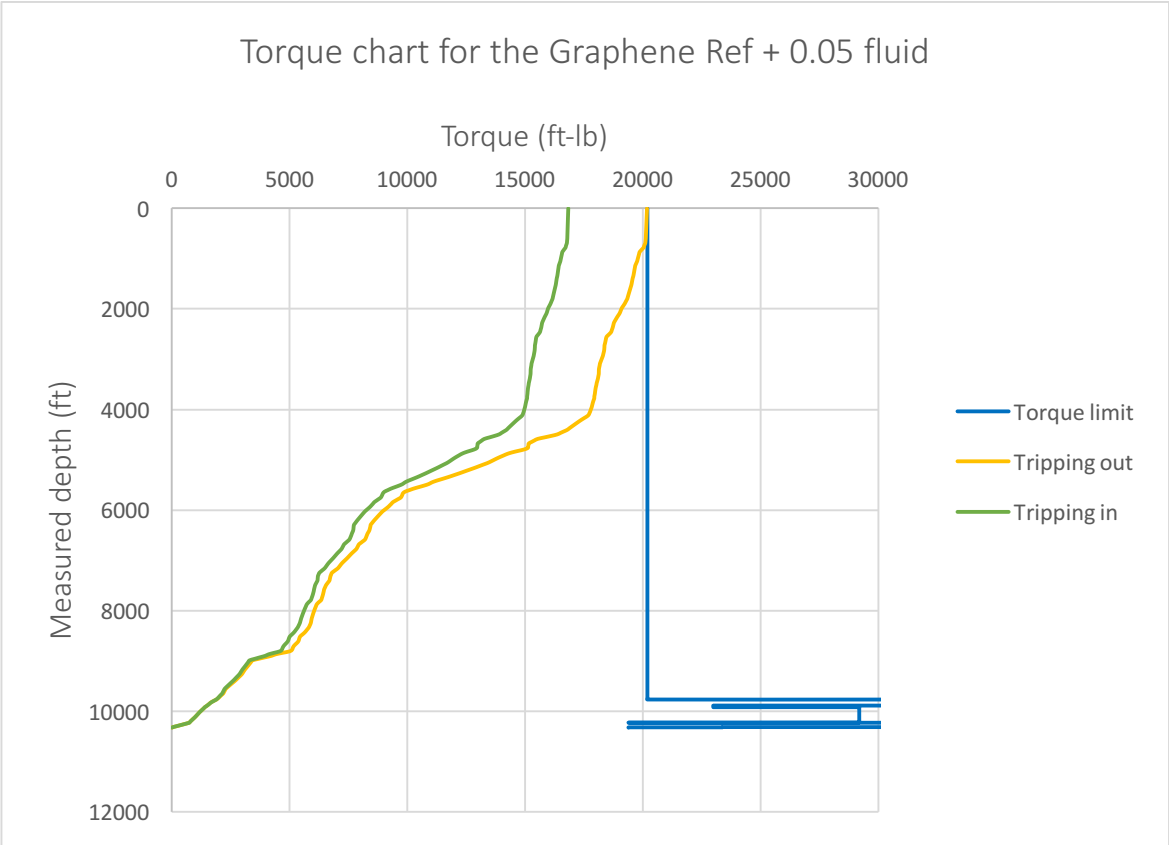

Figure 5.34: Torque chart for the Graphene Ref + 0.05 fluid

It is clear from the chart that the tripping out torque load is of a critical value regarding the drill-pipe integrity, and further drilling could not be executed. The tripping in load of the Graphene Ref + 0.05 system is in the safe window.

The tripping out drag values for the Ref + 0.05 system were reduced with 8.9% compared to the reference system. The load values were set to 20079.3 ft-lb and 18286 ft-lb respectively.

5.2.6.2 Torque and Drag for the Graphene Ref + 0.10 System

Drag and torque charts for the Graphene Ref + 0.10 system are in Figure 5.35 and Figure 5.36. During simulation, the measured depth of the well was changed to the value of 10393ft as this was the longest possible MD of drilling before any of the chart curves exceeded the tension or torque limit.

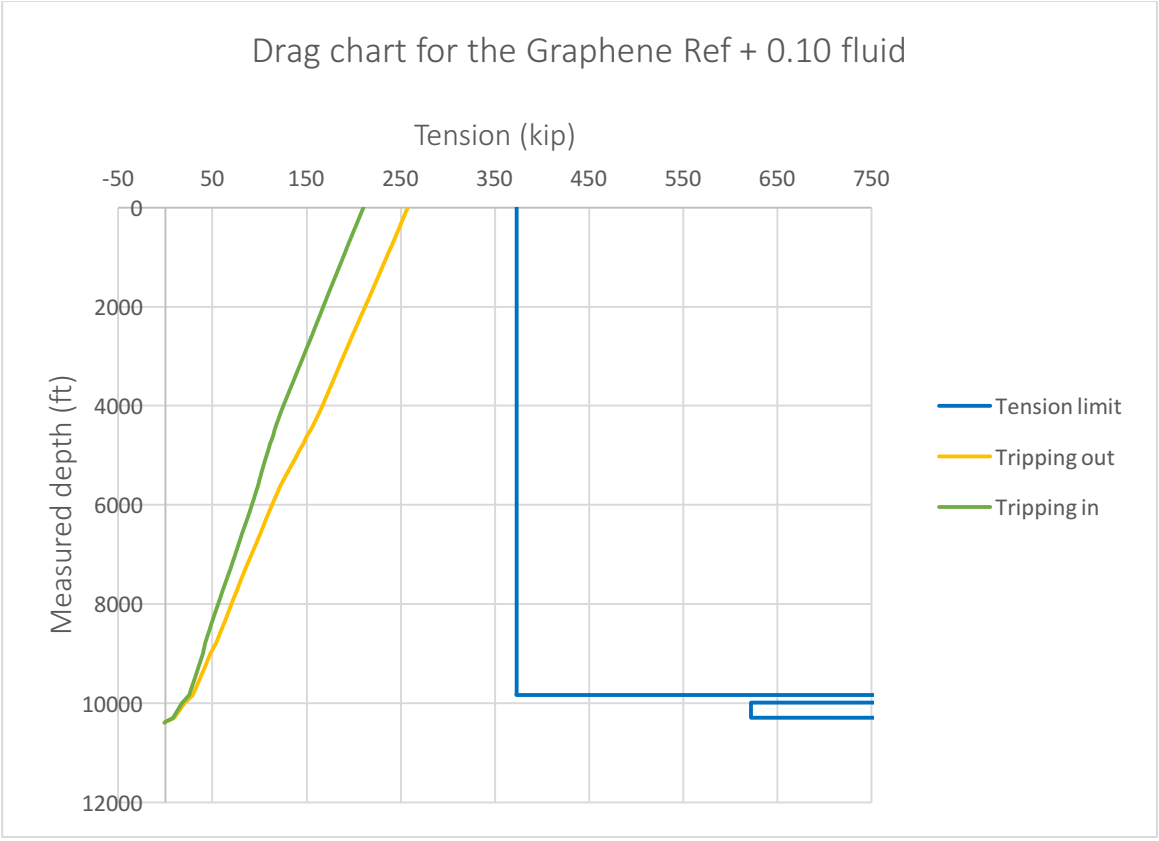

Figure 5.35: Drag chart for the Graphene Ref + 0.10 fluid

The tripping in and tripping out values for the Graphene Ref + 0.10 system are also within the safe window. Solely considering the tension, it would have been possible to drill a bit further with this enhanced nano system.

The tripping out drag values experienced a small change, with a 1.1% decrease compared to the reference system. The tripping out value for this system is set to 245.6 kip as the reference system is set to 248.4 kip.

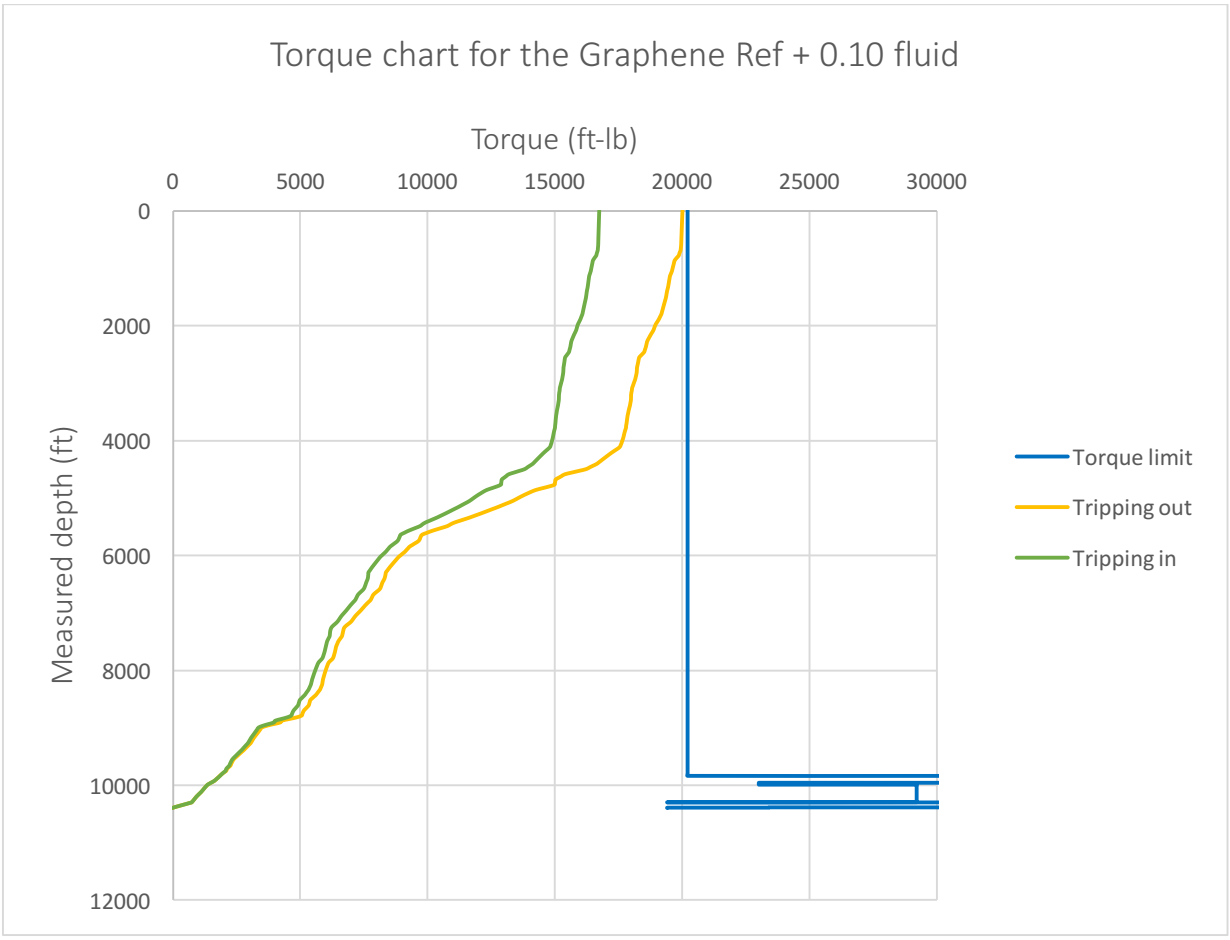

Figure 5.36: Torque chart for the Graphene Ref + 0.10 fluid

The figures illustrate a critical tripping out torque value, and the well could not have been extended, drilling with the Graphene Ref + 0.10 fluid without the drill-pipe experiencing torque related integrity issues.

The tripping out torque was reduced with 11% with this fluid compared to the reference fluid. The tripping out torque value was set to 17863.1 ft-lb for the Ref + 0.10 system where as the value was set to 20079 ft-lb for the reference system.

5.2.6.3 Comparison of the Torque and Drag Simulation Study for the Graphene Drilling Fluids

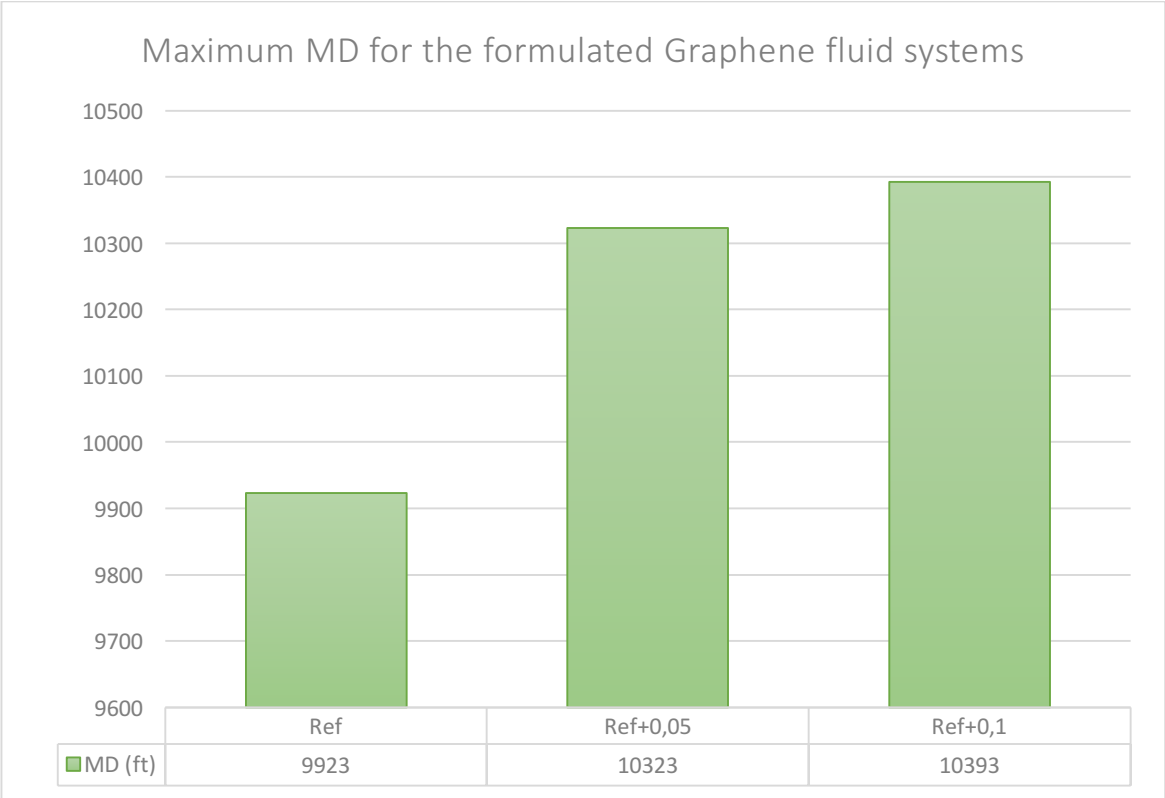

Figure 5.37: Maximum MD for the formulated Graphene fluid systems

The chart in Figure 5.37 illustrates the different MD reaches for the formulated Graphene drilling fluids. It is possible to drill the furthest with the Ref + 0.10 fluid as the maximum depth varies from 9923ft for the reference system to 10393ft for the stated fluid. This is a length change of 470ft and an increase of 4.7%. It is possible to extend the reach for the Ref + 0.05 system in the given well with 4.0% compared to the reference system (400ft).

The torque and drag values for all the fluids in the given well with a MD of 9923ft are plotted in Figure 5.38 and Figure 5.39 for comparison. From these charts it is also possible to see that the most significant change for the fluids enhanced with nano occurs in the torque values, as the drag curves are equalling and harder to separate by eye. This is similar to the results of the TiN simulations.

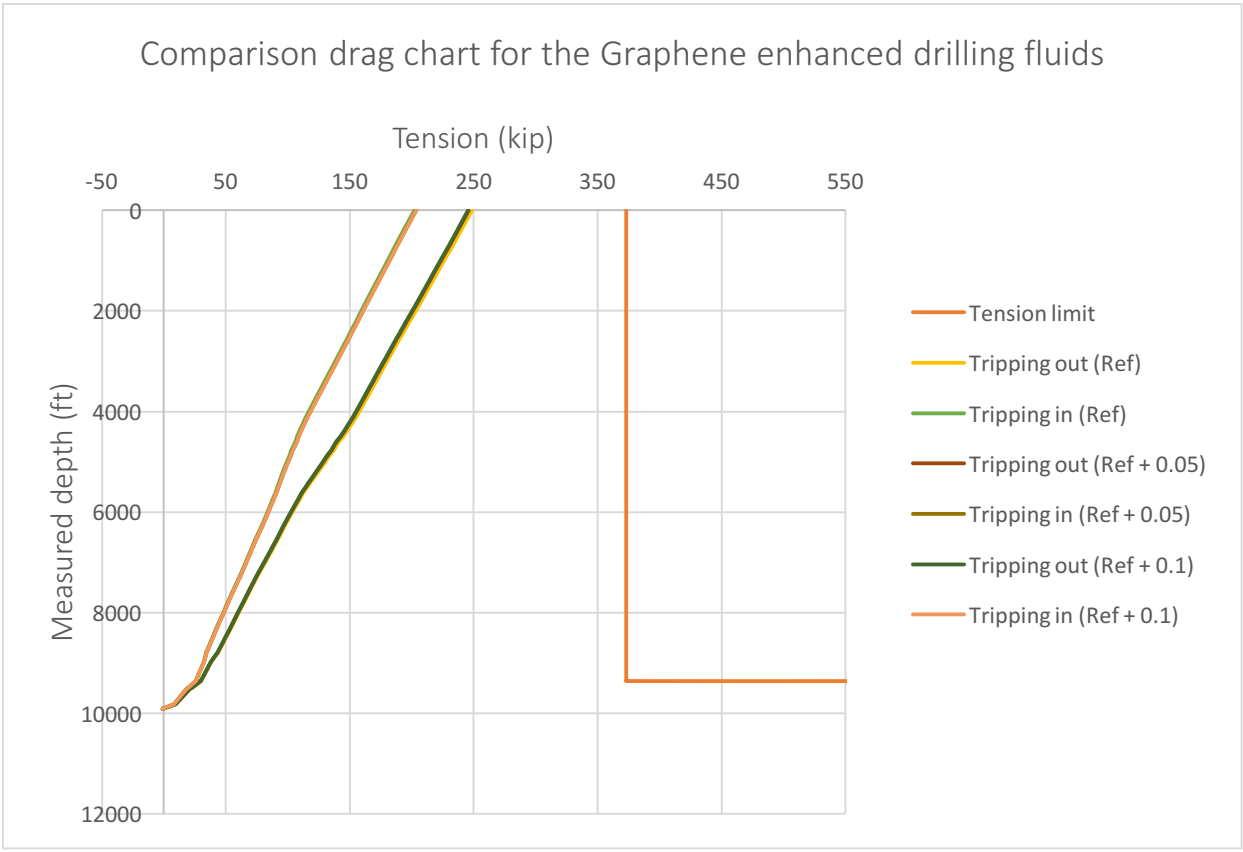

Figure 5.38: Comparison drag chart for the Graphene enhanced drilling fluids

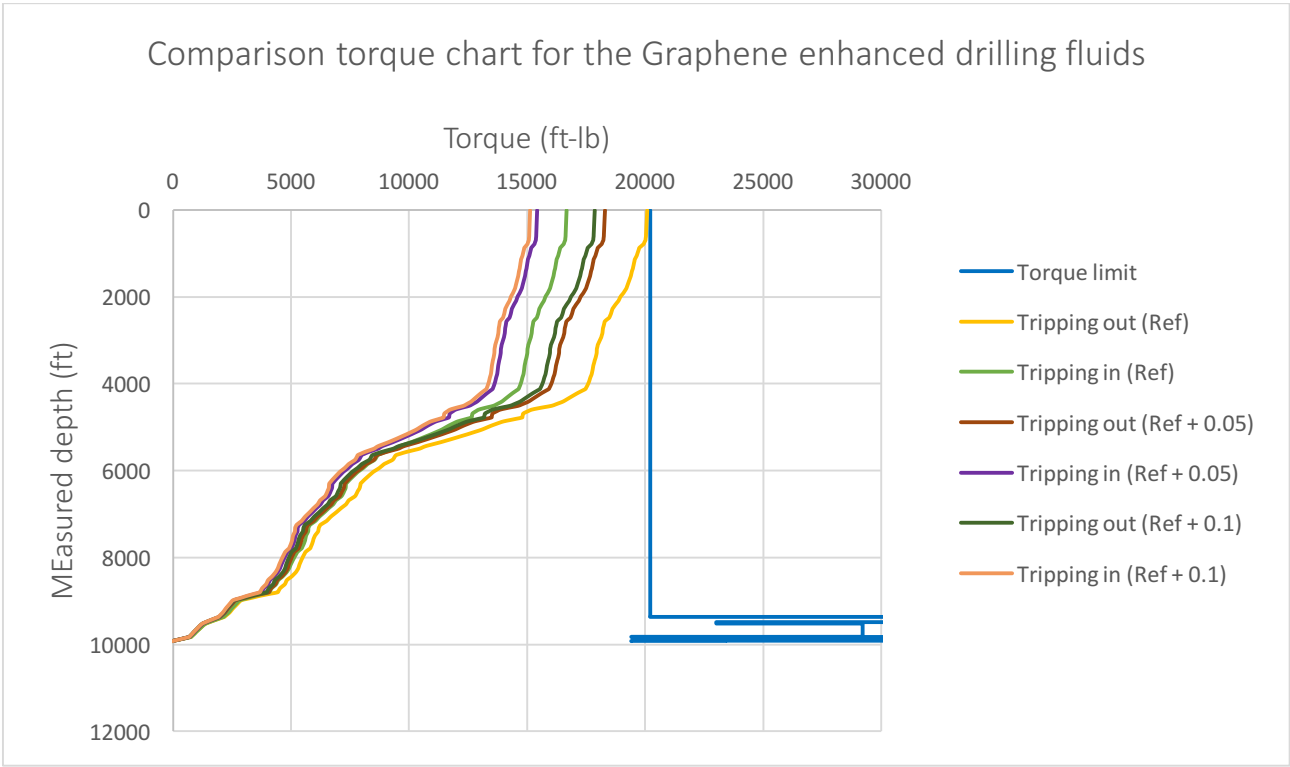

Figure 5.39: Comparison torque chart for the Graphene enhanced drilling fluids

5.3 Hydraulic Performance Simulation

This section will present the hydraulic performance of the selected formulated nano-enhanced drilling fluids. ECD is an important parameter in the drilling industry, and well stability and stress in the drill-string are both functions of the ECD. The ECD is the sum of the static mud weight as well as the annular friction loss. These parameters are determined by hydraulic models. Based on the literature study and on the rheological modelling, the Unified model was selected for calculations as described in previous sections.

5.3.1 Simulation arrangement

The hydraulic calculations were executed for a fictional, vertical well with a total depth of 10000ft. The well was cased with an 8.5” pipe, and the drill-pipe had the following dimensions, 5” OD x 4,8” ID. The surface pressure was set to zero, and the drill-bit had three nozzles at 28” size.

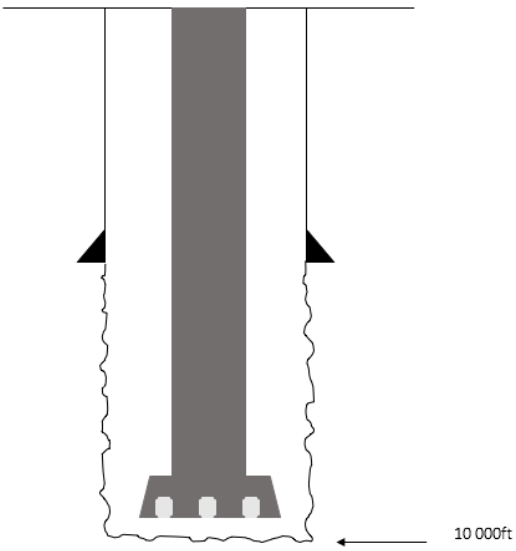

Figure 5.40: Well setup for the hydraulic performance simulation

During the simulation, the flowrate was varied from 1 to 600gpm. The simulation was performed using the rheology data obtained from the experimental study. The density of the fluids was set to 1.025sg or 8.539ppg as they are not weighted. The ECD and total pressure loss (pump pressure required to circulate the fluids back to surface) was analysed.

5.3.2 Simulation Result for the TiN Drilling Fluids

The hydraulic performance simulation was executed for the Ref, Ref + 0.15, Ref + 0.20 and Ref + 2.50 TiN fluids. The fluids were selected based on the frictional study, as well as to investigate the influence of both high and low concentrations. The viscometer data is presented in the experimental study, but as they are relevant for further simulation they are again presented in Table 5.17.

Viscometer data for the TiN fluids used for hydraulic simulation				
RPM	Ref	Ref + 0.15	Ref + 0.20	Ref + 2.50
600	40	38.5	37	43
300	33.5	32.5	31	35
200	30	29.5	28	32
100	25.5	25.5	24.5	28
6	18	17.5	17.5	19
3	17	16.5	16	16

Table 5.17: Viscometer data for the TiN fluids used for hydraulic simulation

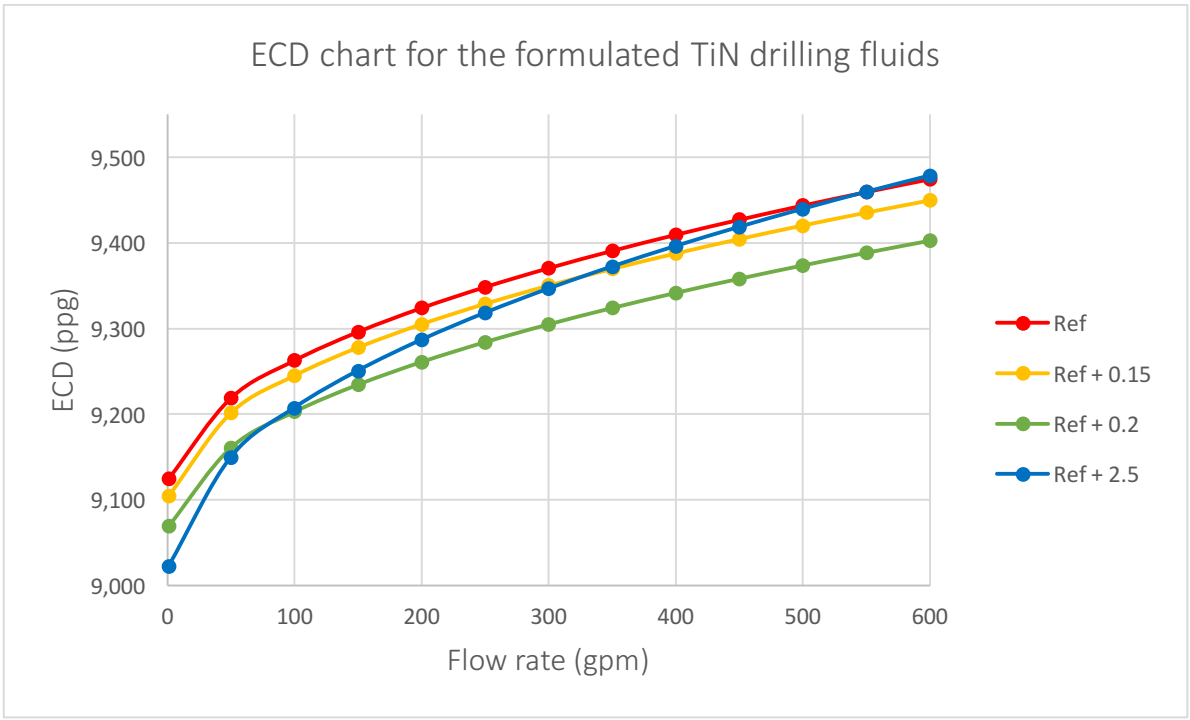

Figure 5.41: ECD chart for the formulated TiN drilling fluids

The obtained ECD results showed that the simulation results gave the lowest ECD value for the Ref + 0.2 fluid from flowrates above 100gpm. The Ref + 2.5 fluid curve exhibit the lowest ECD value from flowrates up until 100, before it exhibits the highest ECD value at rate 600. All the fluids that tested positive for friction reduction exhibit lower ECD values than the reference system. Since the Ref + 2.5 system was of higher ECD values at 600, it indicated that 2.5g of TiN as an additive in the system is not adequate.

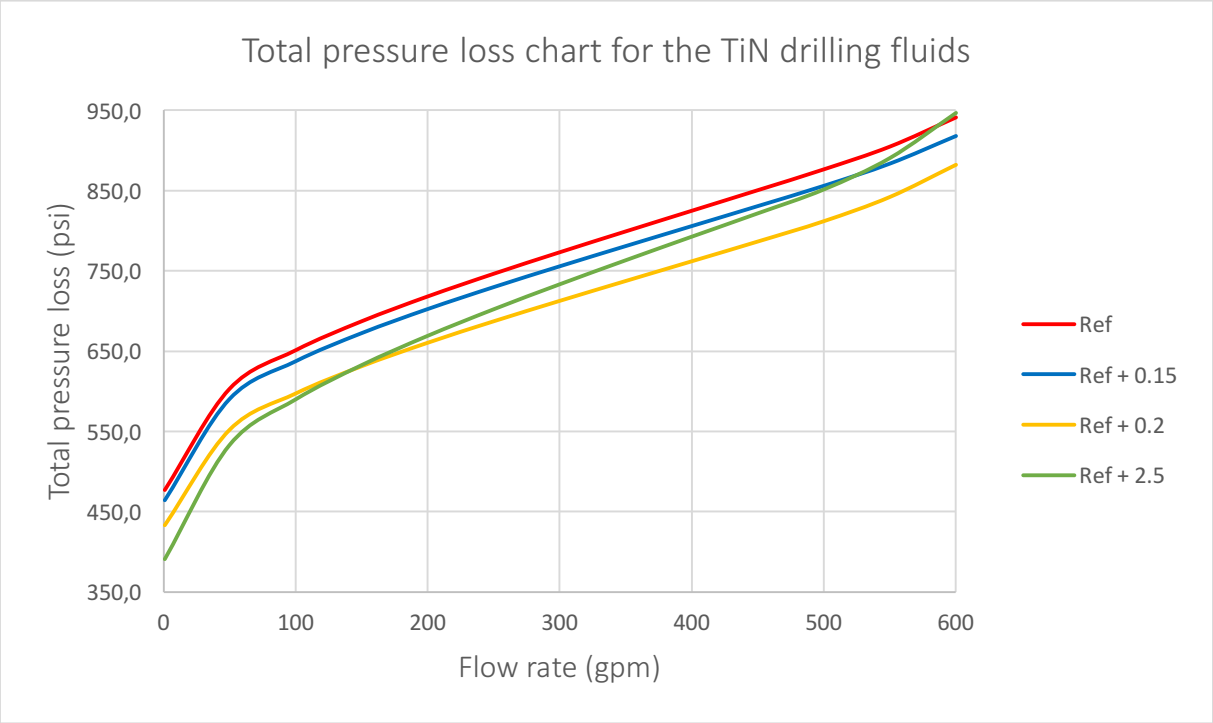

Figure 5.42: Total pressure loss chart for the TiN drilling fluids

The total pressure loss is experienced as the lowest for the Ref + 0.2 fluid for flowrates between 120 to 150gpm. Before flowrates of approximately 120, the Ref + 2.5 exhibited the lowest pressure loss. Both the Ref + 0.15 and Ref + 0.20 fluids experienced lower pressure loss values, where the Ref + 0.2 fluid performed the best. As the Ref + 2.5 fluid exceeded the pressure loss of the reference system at 600gpm, the fluid is not adequate. Both the Ref + 0.15 fluid and Ref + 0.2 fluid are adequate.

5.3.3 Simulation Result for the MoS_2 Drilling Fluids

The hydraulic performance simulation was executed for the Ref, Ref + 0.20, Ref + 0.50 and Ref + 0.80 MoS_2 fluids. The fluids were selected based on the frictional study, as well as to investigate the influence of both high and low concentrations. The viscometer data is presented in the experimental study, but as they are relevant for further simulation they are again presented in Table 5.18.

Viscometer data for the MoS_2 fluids used for hydraulic simulation				
RPM	Ref	Ref + 0.20	Ref + 0.50	Ref + 0.80
600	41	40	39	40.5
300	35	34	33	34.5
200	32	31	30	31.5
100	28	27	26	27.5
6	20	20	19	20
3	19	18	17.5	18

Table 5.18: Viscometer data for the MoS_2 fluids used for hydraulic simulation

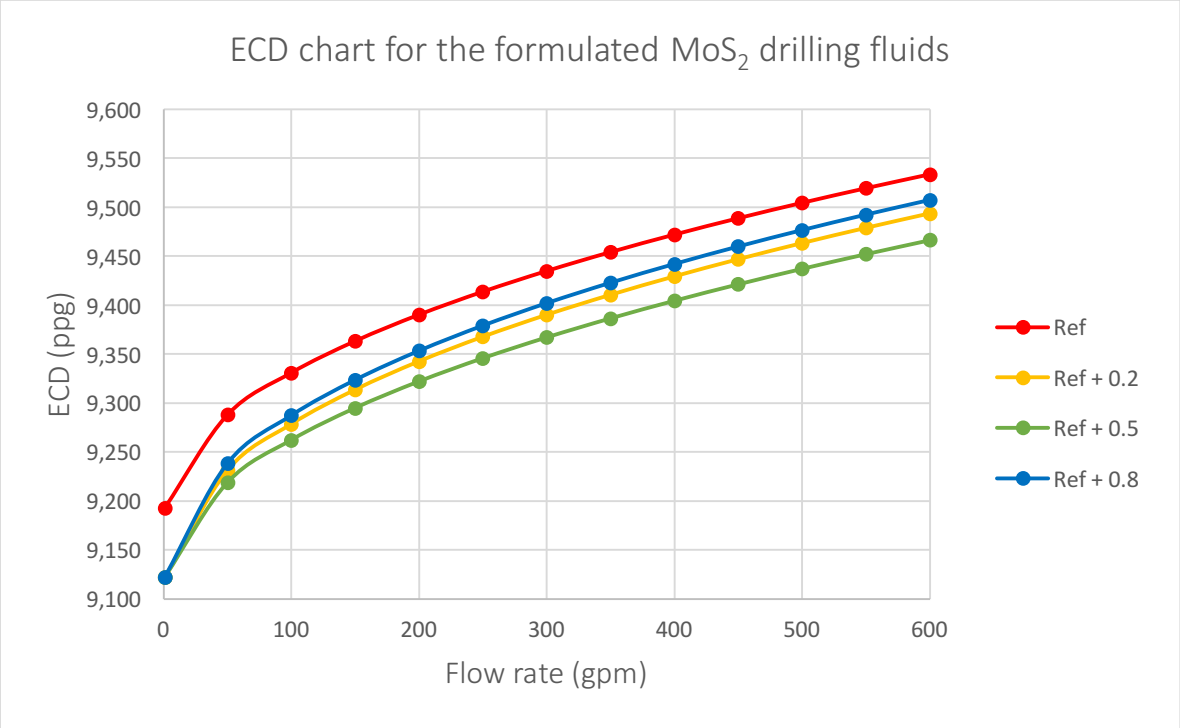

Figure 5.43: ECD chart for the formulated MoS_2 drilling fluids

It is clear from Figure 5.43 that all of the MoS_2 enhanced drilling fluids exhibited lower ECD values for all the tested flowrates compared to the reference system. The best result was given for the Ref + 0.5 system, although the other systems performed well. This shows that all the added MoS_2 concentrations are of adequate values considering hydraulic performance.

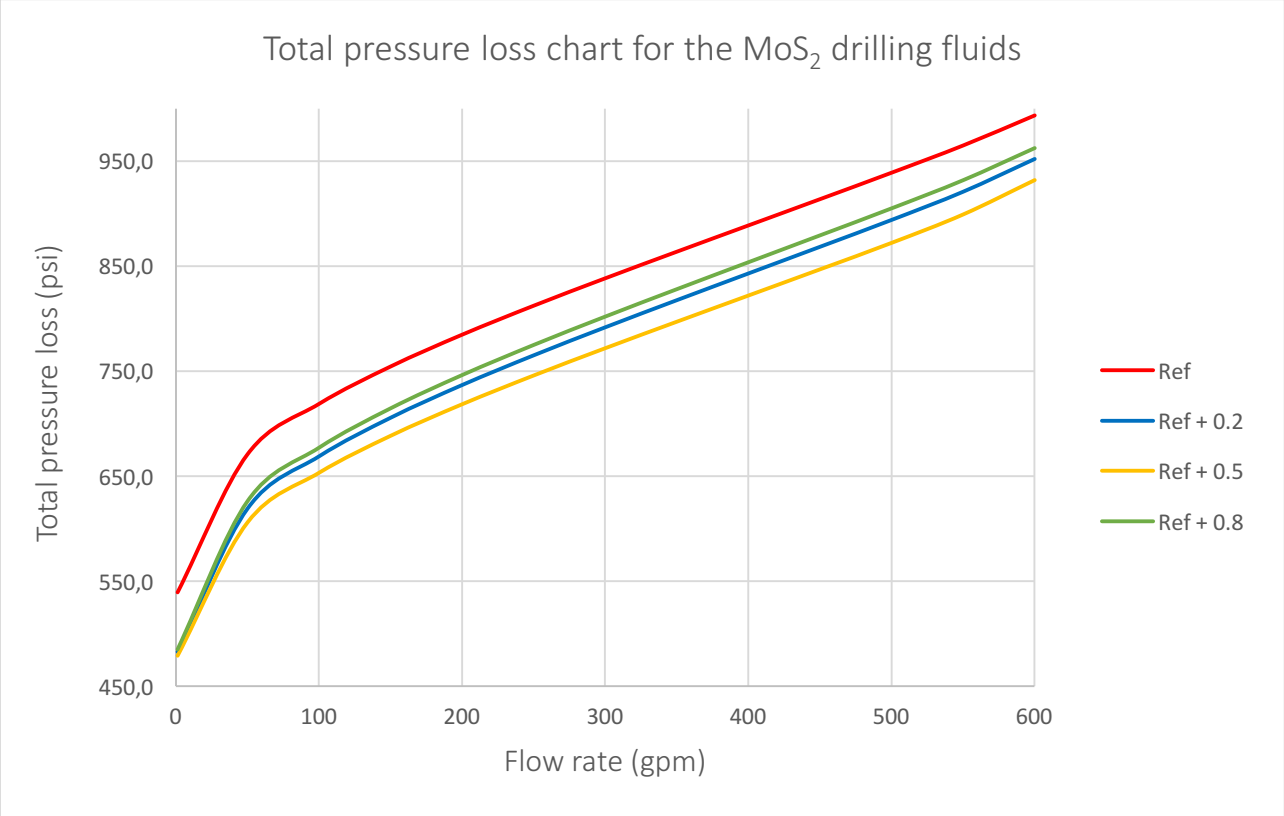

Figure 5.44: Total pressure loss chart for the MoS_2 drilling fluids

All of the nano enhanced fluids exhibited lower total pressure loss values compared to the reference system for all flow rates. This means that less pump pressure is required to transport the enhanced fluids back to surface.

5.3.4 Simulation Result for the Graphene Drilling Fluids

The hydraulic performance simulation was executed for the Ref, Ref + 0.05, Ref + 0.10, Ref + 0.20 and Ref + 1.25 Graphene fluids. The fluids were selected based on the frictional study, as well as to investigate the influence of both high and low concentrations. The viscometer data is presented in the experimental study, but as they are relevant for further simulation they are again presented in Table 5.19.

Viscometer data for the Graphene fluids used for hydraulic simulation					
RPM	Ref	Ref + 0.05	Ref + 0.10	Ref + 0.20	Ref + 1.25
600	17	25	17	17	17
300	12	19	12	12	13
200	10	16	10	10	11
100	7	13	7	7	8
6	3	5.5	3	3	4
3	3	4	3	3	3.5

Table 5.19: Viscometer data for the Graphene fluids used for hydraulic simulation

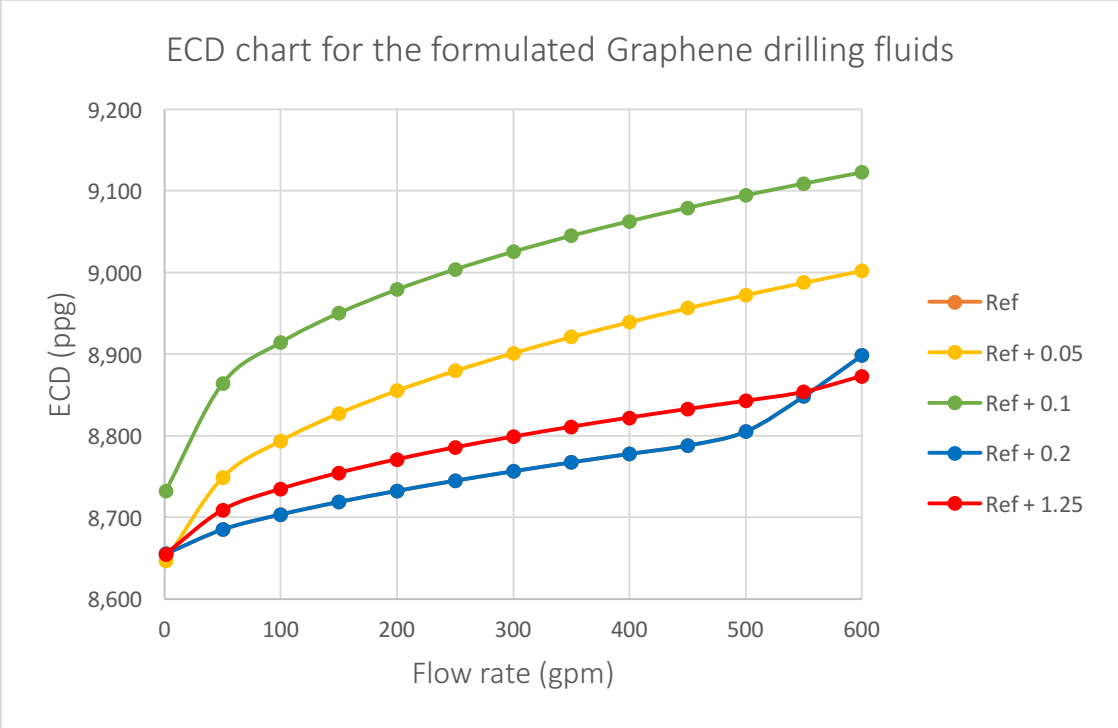

Figure 5.45: ECD chart for the formulated graphene fluids

Since the viscometer data for the reference fluid and the Ref + 0.2 fluid is identical, it is not possible to spot the Ref curve in the chart. However, it is possible to see that all the fluid curves show higher ECD values compared to the reference system. The exception is for the Ref + 1.25 fluid at flowrates exceeding approximately 550-560gpm. In terms of ECD increase, none of the Graphene concentrations are adequate.

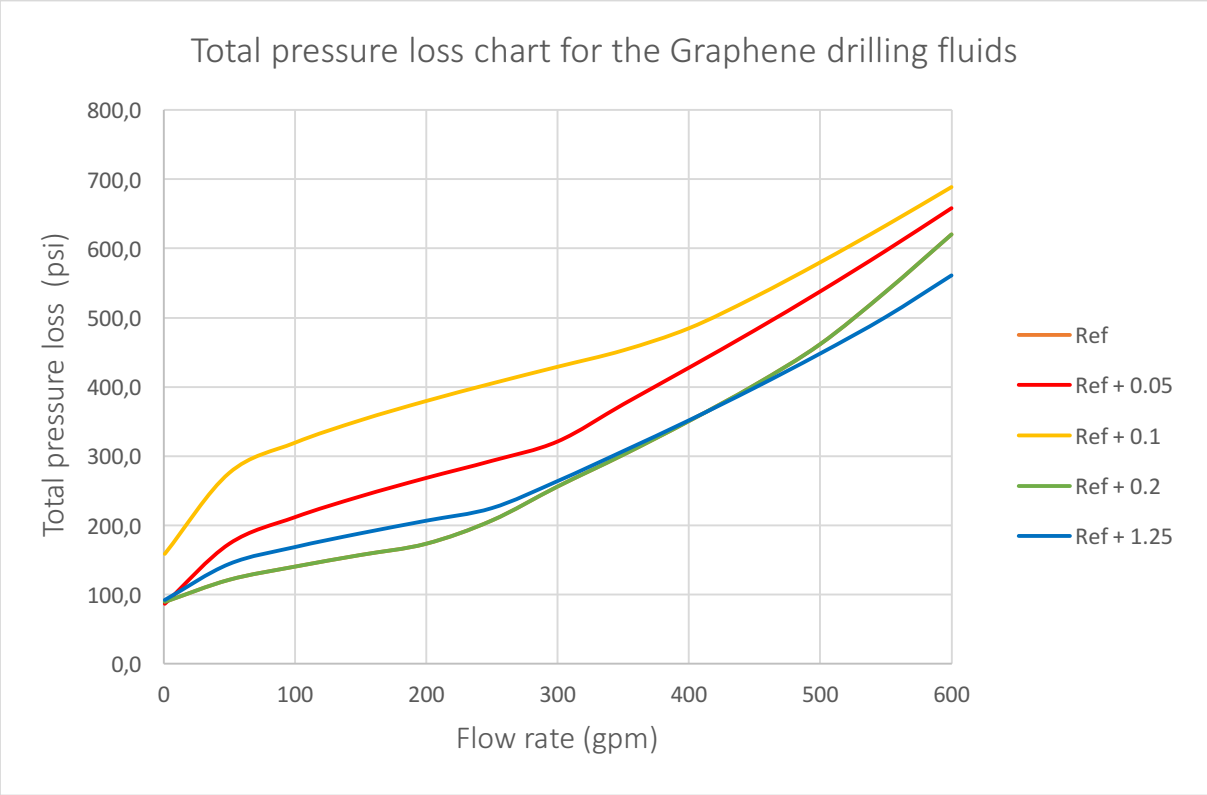

Figure 5.46: Total pressure loss chart for the Graphene drilling fluids

In terms of the viscometer data, the same information as given in the ECD section apply, and the Ref curve does not appear in the total pressure loss chart. It is possible to see that the total pressure loss increases when the fluid is enhanced with nano Graphene. This means that higher values of the pump pressure is required to transport the fluids to surface. Solely the Ref + 1.25 fluid shows pressure losses lower than the Ref curve after approximately 450 gpm. This after equalling the Ref curve for about 100gpm.

6 Result Summary and Discussion

This section will present the summary and discussion part of the overall experimental and simulation study. The purpose of the experimental part of this thesis was to investigate the effect nano-additives in WBM had on the rheology, friction and viscoelasticity. Three different nano-sized materials were added to a WBM system in different concentrations. From literature, these additives were proven to act lubricating or protecting in other fields of science. The formulated fluids were tested for rheological effects as well as frictional effects. The fluids with the best frictional results were tested for viscoelastic properties. Further a simulation study was executed, where the main purpose was to investigate the enhanced fluids impact on torque and drag, as well as to investigate the hydraulic performance of the fluids. Rheological modelling of all the formulated fluids and a literature study was executed to determine which rheological model was best suitable for the hydraulic simulation.

6.1 Rheological Effects of the Nano-Enhanced Fluids

In this part of the experimental study, several test matrixes were designed to investigate the rheological effects of the presented nanoparticles as additives. The fluid behaviours were characterized by the viscometer data, Bingham parameters, Power Law parameters, filtrate loss and pH values. The experimental design and results are presented in chapter 4, with attachments such as the viscometer data in table and filtrate + pH charts in Appendix A. All of the drilling fluids were formulated with 500ml H_20, 25g Bentonite, 2.5g KCl and 0.5g of either XG or CMC. Effect of nano additives in the Bentonite fluids will be summarized in the following sections. The nano additives are TiN, MoS_2 and Graphene.

6.1.1 Rheological Effects of TiN as a Nano-Additive

Drilling fluids containing both high and low concentrations of TiN were formulated and tested for rheological effects. The fluids are presented in chapter 4.2.2, and the weight percentage of TiN as additive is presented in Appendix A.1.

During the analysis of the low concentration TiN fluids, the shear stress increased solely for the low concentration Ref + 0.1 fluid, while an increase was experienced for all of the high concentration TiN fluids compared to the reference system. The results show that TiN as a nano-additive had some impact on the viscometer readings, PV and YS of the fluid systems. The YS increased for solely the Ref + 0.1 and Ref + 1.25 fluids. PV readings stayed more or less constant for the low concentration fluids, but increased for all the high concentration fluids. All the formulated fluids were pseudo-plastic as the Power law n values were less than 1.

Filtrate losses for all the fluids both decreased and increased. The largest decrease was experienced for the Ref + 0.05 system and Ref + 0.10 system with 9.4%. The filtrate loss stayed constant or increased for concentrations of greater values, where the maximum increase was of 17.9% experienced for the Ref + 2.5 fluid. This indicates that higher concentrations of TiN as an additive increase the filtrate loss of the fluids. This may be critical during drilling, as it may result in the drill-pipe being exposed to pressure sticking. The filtrate loss evaluation indicates that lower concentrations of TiN keep the system dispersed and flocculated.

The pH values decreased for all the fluids, in the range of 0.6% to 2.3%. A low pH value may expose the downhole material such as drill-pipes and casing to a sour environment, hence induce corrosion. However, the pH values for all the formulated fluids stayed over the neutral value of 7. This indicates that the tested weight percentages of TiN as an additive will not create any sour downhole environment.

In the end, the results indicated that lower weight percentages of TiN as an additive in drilling fluids is most desirable as the filtrate loss decreased or stayed constant. Thee viscometer data did reveal that TiN had some effect on the particle associations of the reference system, and the pH decrease was of the least value. All the fluids remained pseudo-plastic.

6.1.2 Rheological Effects of MoS_2 as a Nano-Additive

Drilling fluids containing both high and low concentrations of MoS_2 were formulated and tested for rheological effects. The fluids are presented in chapter 4.2.3 and the weight percentage of MoS_2 as an additive is presented in Appendix A.2.

When performing rheological tests of the MoS_2 drilling fluid, the viscometer data revealed small changes for the fluids. There was solely a value increase for the Ref + 2.5 system, and a more significant decrease for the Ref + 3.75 fluid. The PV of the fluids stayed more or less constant, while the YS varied with both an increase and decrease in value. This reveals that the additives to the reference fluid had very little impact on the particle associations of the system. All of the power law n values were below 1, and nano had no impact on the pseudo-plastic behaviour of the fluid.

A filtrate decrease was experienced for the Ref + 0.2 and Ref + 0.5 fluid, with 10.7% and 3.6% respectively. There was not experienced any changes of filtrate loss for the Ref + 0.8 fluid, whilst the higher concentration fluids all experienced a filtrate loss increase of 7.1%. Like for the TiN drilling fluids, the filtrate loss decreased when lower concentrations were added, while it increased with higher concentrations. Again, this indicates that lower concentrations of MoS_2 added may keep the system dispersed and flocculated.

The pH value for the Ref + 0.2, Ref + 0.5 and Ref + 0.8 fluids increased with 1.1% which is desirable as an alkaline environment is necessary to prevent corrosion. The value stayed constant for the Ref + 1.25 fluid compared to the reference, while it decreased with 0.6% and 2.3% for the Ref + 2.5 and Ref + 3.75 fluids respectively. All the measurements stayed above the neutral pH value of 7.

The results exhibited the best properties for the drilling fluids formulated with MoS_2 additives below the value of 1g. The filtrate loss decreased or stayed constant, the pH value increased and there was no significant change in the viscometer readings. Observations of the Reference system for both TiN and MoS_2 revealed that XG acts more as a viscosifier than CMC, as the viscometer readings were of much greater values than the CMC Reference.

6.1.3 Rheological Effects of Graphene as a Nano-Additive

Drilling fluids containing both high and low concentrations of Graphene were formulated and tested for rheological effects. The fluids are presented in chapter 4.2.4 and the weight percentage of Graphene as an additive is presented in Appendix A.3.

The impact of Graphene on the viscometer data was of much more significant compared to the two other nano-additives. While the Ref + 0.2 and Reference fluid experienced identical viscometer data, the Ref + 0.05 and Ref + 0.1 fluids experienced a large reading increase at 600RPM, 47.1% and 58.8% respectively. This indicates that small concentrations of Graphene may be an adequate additive for viscosifying properties. The YS of the Ref + 0.05 and Ref + 0.1 system increased with 87.7% and 142.9% respectively. This indicates a much greater electrostatic force between the particles compared to the reference system and that the system is moving from an aggregated state to an aggregated and flocculated state. The n value decreased significantly for the Ref + 0.05 and Ref + 0.1 system, which indicates more stable pseudo-plastic fluid behaviour.

The filtrate loss increased for all the Graphene fluids, in the range of 3.8% to 23%. This indicates poor filtrate loss control for the additive, but may be corrected with a different polymer. However, the effect of Graphene combined with another polymer was not investigated. A variation of the filtrate loss for the Graphene fluids were experienced, and there seems to be no relationship between increasing additive concentrations and increasing filtrate loss values. This evaluation builds on the theory of the systems being in an aggregated state.

The pH values for all the fluids stayed constant during rheological testing, with a value of 8.95. Even higher concentrations had no impact on the pH value, which indicates that Graphene does not affect the pH of the reference system. The pH stayed at an alkaline level.

The obtained results exhibits that lower concentrations of Graphene as an additive in the formulated reference system is of interest due to the viscosifying properties with the low level of addition. The filtrate loss increased for all the fluids. This indicates that the system is not in a dispersed and flocculated state, but it may be corrected with fluid additives or with a different

salt system. The additive showed no effect on pH and the pseudo-plastic behaviour of the fluid systems.

6.2 Frictional Effects of the Nano-Enhanced Fluids

Some drilling fluids in the rheology experiment were chosen to investigate the frictional effects of the nanoparticle additives. The fluids were tested using a CMI Tribometer and were exposed to temperatures of 22°C, 50°C and 70°C, and the behaviour was characterized by the obtained software results. The experimental design and results are presented in chapter 4 with attachments in Appendix B. Not all of the drilling fluids were tested, but several were selected based on the rheology experiments. The effect of nano additives on the coefficient of friction will be summarized in the following sections.

6.2.1 Frictional Effects of the Reference Systems

The lubricating effect of the reference fluids was investigated. The results are presented in 4.3.5 and in Appendix B.1

The Reference system with XG exhibited significant lower friction values, which may indicate experiment errors. At 22°C, the percentage of difference for the two reference fluids was calculated to be 80%. However, tests were executed several times for the given system, to ensure consistency. The lower values of the Reference system with XG compared to the Reference system with CMC may indicate that the polymer selection influences the coefficient of friction, as this was the only additive difference of the two fluids. This is just an indication as polymer influence was not further investigated.

The test values were averaged and plotted with modelled trend lines. The trend lines represented a temperature depended function of the friction coefficient, and exhibited that the coefficient of friction increased with increasing temperatures. This is consistent with the presented information from the literature study.

6.2.2 Frictional Effects of TiN as a Nano-Additive

To investigate the lubricating effect of TiN in drilling fluids, a set of high and low concentration drilling fluids were selected based on the rheological experiments. The selected fluids are presented in section 4.3.6 and Appendix B.2.

The results showed a friction increase for the Ref + 0.1 fluid and Ref + 2.5 fluid. This increase may be due to both under saturation and over saturation of nanoparticles. The coefficient of friction increased for all temperatures when testing both the Ref + 0.15 and Ref + 0.20 fluids. The overall largest increase was experienced for the Ref + 0.15 fluid with 23.7% at 22°C and 30.1% at 70°C. The weight percentage additive of this fluid is 0.03%, hence a very small concentration. Such positive results with that amount of additive is cost efficient in the sense of particle cost and disposal cost compared to OBM.

In the end, the results showed promising parameters with low concentration of TiN as an additive. The only good results were obtained from the lower concentration of TiN fluids. As the friction values are lower than predicted considering this is WBM, a literature study was conducted and presented in section 2.8. Regardless, the enhanced fluids friction decreased with consistent measurements. The best results for the TiN fluids are presented in Figure 6.1.

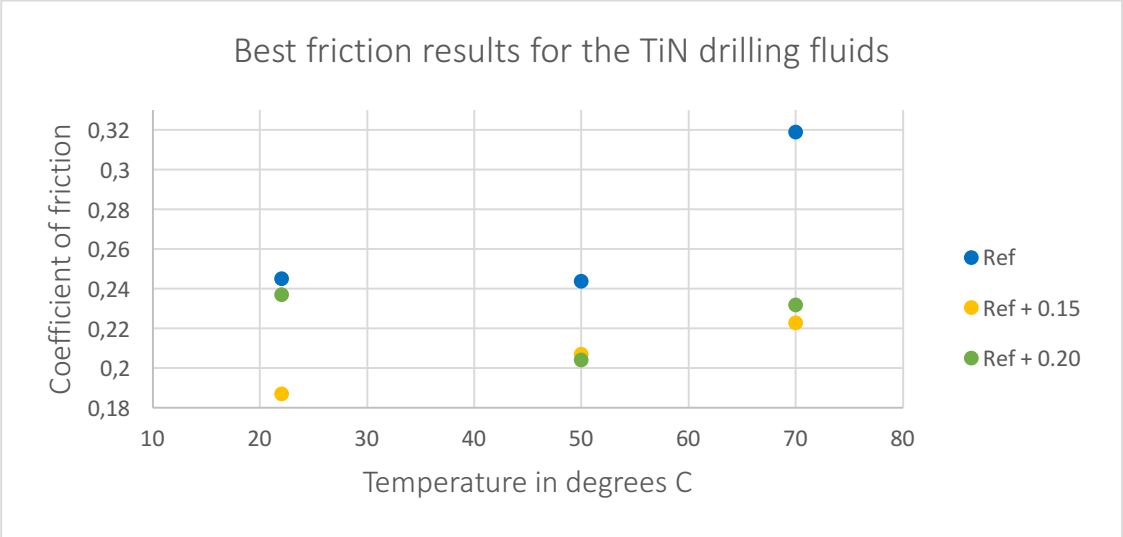

Figure 6.1: Best friction results for the TiN drilling fluids

6.2.3 Frictional Effects of MoS_2 as a Nano-Additive

To investigate the lubricating effect of MoS_2 in drilling fluids, a set of high and low concentration drilling fluids were selected based on the rheological experiments. The selected fluids are presented in section 4.3.7 and Appendix B.3.

The results showed a significant decrease for both the MoS_2 fluids that were tested. The Ref + 0.2 and Ref + 0.8 fluids exhibited similar results at 22°C and 50 °C but with a large deviation at 70°C. The coefficient of friction was decreased with as much as 41.2% and 46.5% for the Ref + 0.2 and Ref + 0.8 fluids respectively. This with weight percentages of only 0.04% and 0.16%. This is extremely good results as small concentrations of the additive is cheaper, but still provide a desirable friction coefficient. The results show that WBM enhanced with MoS_2 may be a competitive alternative to less environmentally friendly lubrication additives in drilling fluids.

The results showed promising parameters with both low concentrations of MoS_2 samples. Regardless of the significant low values, the decrease of friction was consistent during the measurements. The results are presented in section 4.3.7.1, but are summarised and presented in Figure 6.2.

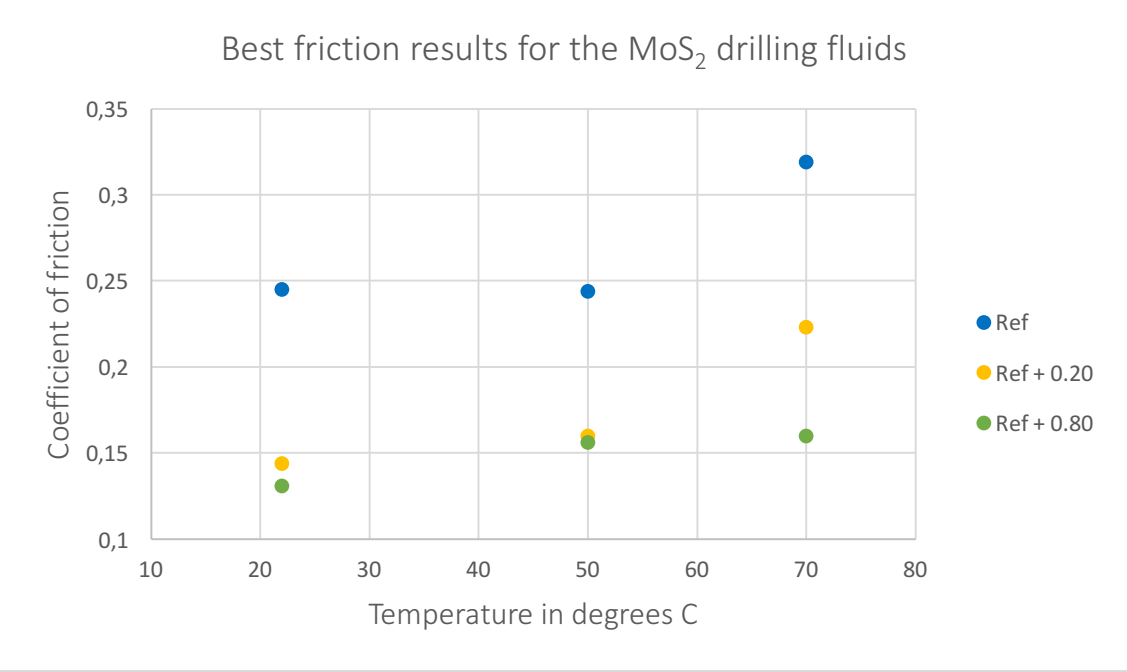

Figure 6.2: Best friction results for the MoS_2 drilling fluids

6.2.4 Frictional Effects of Graphene as a Nano-Additive

To investigate the lubricating effect of Graphene in drilling fluids, a set of high and low concentration drilling fluids were selected, based on the rheological experiment. The selected fluids are presented in section 4.3.8 and Appendix B.4.

The results showed a friction reduction for the fluids enhanced with the lowest concentration of Graphene. The Ref + 0.05 and Ref + 0.10 fluids with a weight percentage of 0.01% and 0.02% respectively showed the greatest decrease with a maximum at 22°C of 9.8% for the Ref + 0.05 fluid. The Ref + 0.1 fluid decreased the most at 50°C and 70°C with 14.5% and 10.6% respectively. There is a decrease present, but it is not as significant as experienced with the two other additives. However, this fluid was formulated with another reference system. A possibility is that the particles does not work as effectively combined with CMC as the polymer present.

In the end, the result again showed promising parameters for the fluids formulated with smaller concentrations of Graphene. The decrease of friction was consistent during measurements. The results are presented in section 4.3.8.1 but a summarisation of the best results is presented in Figure 6.3.

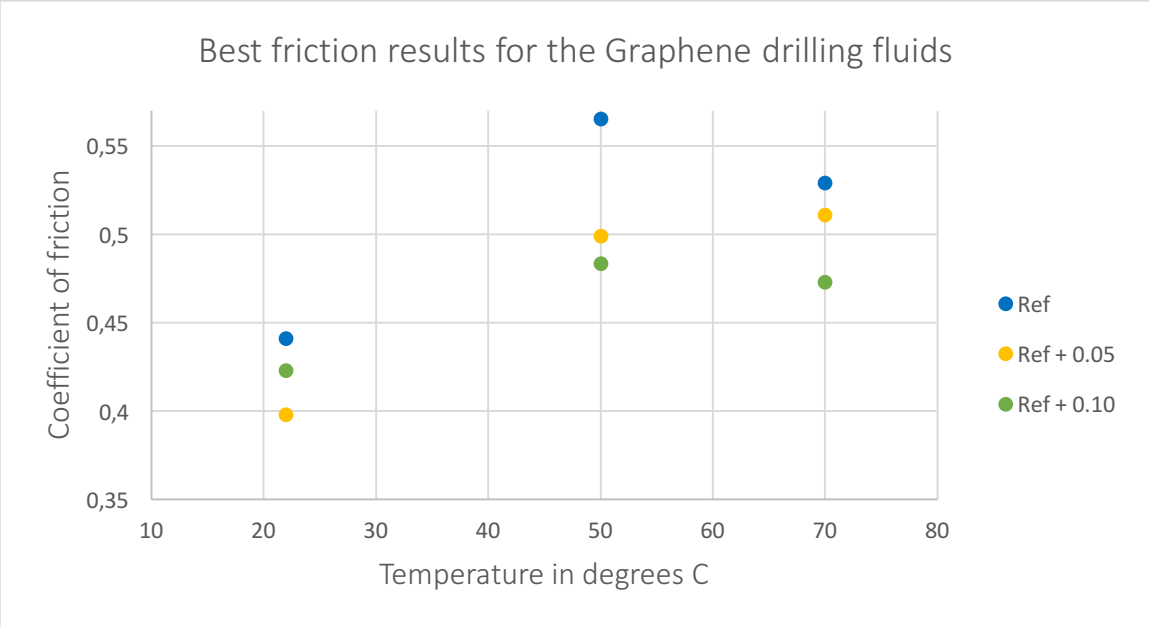

Figure 6.3: Best friction results for the Graphene drilling fluids

6.3 Viscoelastic Effects of the Nano-Enhanced Fluids

In order to keep particles and cuttings in suspension, it is essential that a good drilling fluid should create gel structure quickly when at rest. The gel structure and stability of the enhanced nano-fluids were studied using the Anton Paar Rheometer. Selection of the fluids were based on the best results from the friction experiments. The reference systems were also measured for comparison reasons.

The viscoelastic measurement performed was the oscillatory amplitude test. The LVER of the fluids were found out to be at 1% strain for the TiN and MoS_2 drilling fluids, while it was set to 6% strain for the Graphene drilling fluids. The flow point and yield stress were determined for the test.

A clear observation from all of the tests is that in the elastic dominated zone (before the intersection point), the storage modulus is exhibiting greater values than the loss modulus. This is an indication that all of the fluid systems obtains a stable gel structure.

The YPs from the Anton Paar Rheometer is compared to the YP calculated from the Bingham model for the XG fluids in Table 6.1.

YS comparison between the Bingham method and Anton Paar method for the XG fluids					
YS [Pa]	Ref	Ref + 0.15 TiN	Ref + 0.20 TiN	Ref + 0.20 MoS_2	Ref + 0.80 MoS_2
Anton Paar	11	10.5	8	14	10.5
Bingham	27	26.5	25	28	28.5
Difference	16	16	17	14	18
Difference %	59.3%	60.4%	68%	50%	63.2%

Table 6.1: YS comparison between the Bingham method and Anton Paar method for the XG fluids

The table exhibits that there is a big difference of the measured YPs between the Bingham parameters and Anton Paar parameters. The greatest difference was exhibited for the Ref + 0.20 TiN fluid with 68%. The decrease of YS for the Ref system was of 59.3%. The same analysis was conducted for the CMC fluids, and the analysis is illustrated in Table 6.2.

YS comparison between the Bingham method and Anton Paar method for the CMC fluids			
YS [Pa]	Ref	Ref + 0.05	Ref + 0.10
Anton Paar	1.77	4.08	2.98
Bingham	7	13	17
Difference	5.23	8.92	14.02
Difference %	74.7%	68.6%	82.5%

Table 6.2: YS comparison between the Bingham method and Anton Paar method for the CMC fluids

This table exhibits a greater difference of the measured YPs between the Bingham parameters and Anton Paar parameters than observed with the XG fluids. In this case, the greatest difference was exhibited for the Ref + 0.10 system with 82.5% while the reference system decreased with 74.7%.

During analysis, the damping angles were plotted against the fluids shear stresses. The flow point is presented at 45° as G'=G'' at this angle. The chart for the TiN fluids illustrated that the flow points of the nano-enhanced fluids were obtained at lower shear stress values than the reference system. This means that the enhanced fluids experience viscoelastic properties for lower shear stress values than the reference system. The opposite was experienced for the MoS_2 and Graphene drilling fluids, which means that they experience viscoelastic properties for higher shear stress values than the reference system. There is no consistency in terms of polymers as the MoS_2 fluids and Graphene fluids were formulated with different types of polymers. This means that the flow point is most likely influenced by the nanoparticles.

When the intersection point is located at lower frequencies than the reference system, it may indicate a more unstable gel structure. This is the case for the Graphene and TiN drilling fluids. The MoS_2 fluids all intersect at the same frequency, so the formulated fluids are most likely stable in terms of gel structure.

6.4 Rheological Modelling of the Nano-Enhanced Fluids

Rheological models are used to describe a drilling fluid the best possible way. To investigate which model that is the most dominating, as well as which model to use for hydraulic performance, rheological modelling was executed. Rheological modelling was executed for the fluids with the best result during frictional testing. A trend-line was created according to the measurements, and the best model is represented by the trend-line that deviates the least. The results from the analysis is presented in Table 6.3.

Results of the rheological modelling for all the selected fluids			
Fluid	Model	Equation	Deviation in %
Ref for TiN	Robertson and Stiff	$\tau = 6.4611(42.5075+\gamma)^{0.2701}$	0.93%
Ref + 0.15 TiN	Robertson and Stiff	$\tau = 7.3789(35.7224 + \gamma)^{0.2456}$	0.75%
Ref + 0.20 TiN	Unified	$\tau = 15.572 + 0.8598\gamma^{0.485}$	1.40%
Ref for MoS_2	Robertson and Stiff	$\tau = 8.8966(33.5930 + \gamma)^{0.228}$	0.62%
Ref + 0.20 MoS_2	Unified	$\tau = 17.072 + 1.2479\gamma^{0.4384}$	1.28%
Ref + 0.80 MoS_2	Unified	$\tau = 17.072 + 1.238\gamma^{0.4446}$	1.40%
Ref for Graphene	Robertson and Stiff	$\tau = 0.3846(38.1363 + \gamma)^{0.5555}$	1.74%
Ref + 0.05 Graphene	Power Law	$\tau = 2.5666\gamma^{0.332}$	3.19%
Ref + 0.10 Graphene	Power Law	$\tau = 3.4935\gamma^{0.3026}$	1.87%

Table 6.3: Results of the rheological modelling for all the selected fluids

The results exhibited that the Robertson and Stiff model is the most repeating model describing the fluids best, as it deviates the least for 44.4% of all the fluids. In second place, the Unified model is the best fitting model for 33.3% of the fluids. However, considering solely the nano-enhanced fluids, the Unified model works best for 50% of the fluids, where as the Power Law comes in second place with 33.3%.

The main objective of the simulation study is to evaluate the performance of the nano-enhanced fluids. In the end, from both the literature study perspective and the rheological modelling results considering solely the enhanced fluids, the Unified model was selected for further hydraulic simulation studies.

6.5 Torque and Drag Effects of the Nano-Enhanced Fluids

As the frictional experiment was conducted with positive results, it was decided to perform a torque and drag simulation of the fluids exhibiting lubricating abilities. The simulation was conducted using the WellPlan^{TM} 5000.1 simulation program, provided by the University of Stavanger. As the muds friction coefficient is critical in deviated wells, a fictional, inclined well was set up for simulation arrangements. The obtained coefficients of friction were used as data in the simulation. The measured depth of the well was increased as the decreased friction coefficients were used until critical torque or drag values were obtained. By this, the extended reach of the well obtained by using the enhanced drilling fluids were illustrated.

Using the Reference for the TiN drilling fluids and the MoS_2 drilling fluids showed that the furthest possible MD before obtaining critical levels of torque and drag was 13123ft. The most critical parameter was the tripping out torque, as the curve equalled the material torque limit. Implementing the coefficient of friction for the TiN Ref + 0.15 and Ref + 0.20 fluids, it was possible to obtain a MD increase of 1897ft and 1300ft respectively. The critical parameter that restricted further drilling for the TiN Ref + 0.15 fluid was the tripping out torque. The same applied for the TiN Ref + 0.20 fluid. For the MoS_2 drilling fluids, it was possible to drill 2000ft longer for the Ref + 0.20 fluid and 3400ft for the Ref + 0.80 fluid. Unlike for the TiN drilling fluids, the critical parameter for the MoS_2 fluids were the tripping out drag value, as it was equalling the tension limit in both cases. The torque loads could have been of greater values before experiencing criticality.

Using the Reference for the Graphene drilling fluids showed that the furthest possible MD before obtaining critical levels of torque and drag was 9923ft. The most critical parameter for this fluid was again the tripping out torque as it equalled the torque limit. When implementing the Graphene Ref + 0.05 and Ref + 0.10 fluids, it was possible to drill 400ft and 470ft longer respectively. The critical parameter for both the Graphene enhanced fluids were the tripping out torque value, as it equalled the torque limit.

The best results for the XG fluids were achieved by the MoS_2 fluids, where it was possible to drill more than 1km further compared to the Reference system. This is a total of 25.9% of length increase. With the great reduction in friction, this is ground breaking as it would save money on mud replacement and possibly OBM disposal costs. As the concentration of MoS_2 added was of such a low weight percentage, the cost could be limited as well. The Graphene fluids exhibited a much lower length increase percentage of solely 4.0% and 4.7%. This is due to the low friction decrease of the fluids.

The study also illustrated that the significant parameter influencing the MD in the investigation well was the torque load. The drag values only influenced the MD when using the MoS_2 fluids. The drag values deviated less compared to the torque values, and this is illustrated in the comparison sections in chapter 5.2. The comparison torque chart for the MoS_2 enhanced drilling fluids are again presented for illustration purposes.

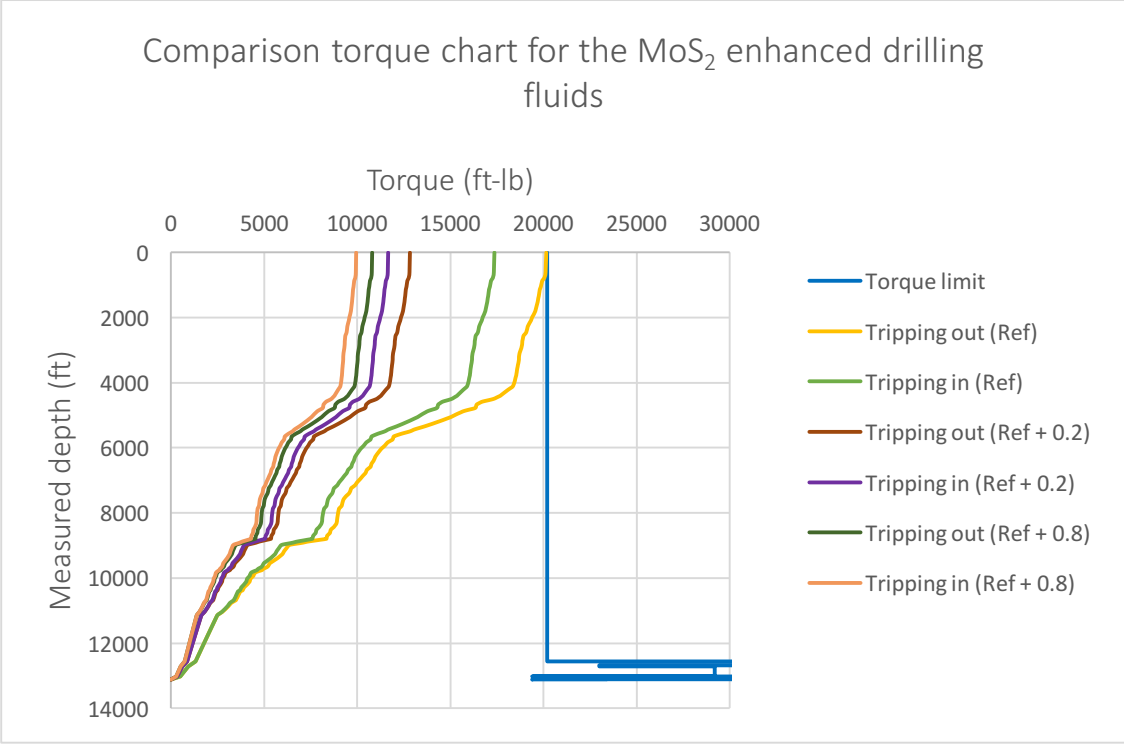

Figure 6.4: Comparison torque chart for the MoS_2 enhanced drilling fluid

In the end, the best torque and drag simulation performance was obtained using the MoS_2 enhanced drilling fluids.

6.6 Hydraulic Performance Effects of the Nano-Enhanced Fluids

Again, the nano-fluids were selected based on the frictional experiments and fluids of higher concentrations were also selected as it was desirable to investigate the effect of the higher concentration fluid. The fluids were analysed in terms of their ECD and the required pump pressure in a 10000ft vertical well. The Unified model was selected for the analysis, and the reason is justified in previous sections. The main drilling fluid controlling parameters for the ECD/pump pressure are the rheology and the density of the drilling fluid.

The ECD of the enhanced TiN fluids all decreased compared to the reference system. All of the fluids that tested positive for friction reduction illustrated constant lower ECD values compared to the reference system. The pump pressure also exhibited lower values compared to the reference system. This means that the frictional pressure loss while circulating the mud in well decreased for the nano-enhanced TiN fluids, except for the Ref + 1.25 fluid, where the curve equalled the reference system for flowrates of greater velocity. This may indicate that the use of low concentration TiN in the drilling fluids is positive in terms of well stability. The optimal amount was 0.20g, as this fluid exhibited the lowest ECD and pump pressure values.

The ECD for the enhanced MoS_2 fluids all decreased compared to the reference system. All of the fluids that tested positive for friction reduction exhibited constant lower ECD values. The pump pressure provided the same results, with the most significant reduction for the Ref + 0.50 fluid. However, the Ref + 0.20 fluid decreased the more than the Ref + 0.80 fluid compared to the reference system. This is also positive in the terms of well stability. The optimal concentration was set to 0.20g in terms of pump pressure, ECD and friction.

The ECD for the Graphene drilling fluid deviated more than the TiN and MoS_2 fluids. However, the ECD increased for all of the Graphene enhanced systems. The Ref + 0.20 system curve equals the Reference curve. The Ref + 1.25 fluid was the only fluid that at some point experienced a decrease in ECD, but for greater flowrates. The same applied for the pump pressure. This may indicate that the formulated fluid system exhibits bad well stability. Well stability is critical during drilling, in terms of drilling problems.

6.7 Summary Matrix

Table 6.4: Summary matrix of fluids conducted experiment and simulation on

Fluid	Filtrate	Friction	Viscoelasticity	Modelling	T & D	Hydraulic
TiN fluids						
Ref + 0.05	Decrease	X	X	X	X	X
Ref + 0.10	Decrease	Increase	X	X	X	X
Ref + 0.15	No change	Decrease	Executed	Executed	Executed	Executed
Ref + 0.20	Increase	Decrease	Executed	Executed	Executed	Executed
Ref + 0.50	Increase	X	X	X	X	X
Ref + 1.25	Increase	X	X	X	X	X
Ref + 2.50	Increase	Increase	X	Executed	X	Executed
Ref + 3.75	Increase	X	X	X	X	X
MoS_2 fluids						
Ref + 0.20	Decrease	Decrease	Executed	Executed	Executed	Executed
Ref + 0.50	Decrease	X	X	Executed	X	Executed
Ref + 0.80	No change	Decrease	Executed	Executed	Executed	Executed
Ref + 1.25	Increase	X	X	X	X	X
Ref + 2.50	Increase	X	X	X	X	X
Ref + 3.75	Increase	X	X	X	X	X
Graphene fluids						
Ref + 0.05	Increase	Decrease	Executed	Executed	Executed	Executed
Ref + 0.10	Increase	Decrease	Executed	Executed	Executed	Executed
Ref + 0.20	Increase	Increase	X	Executed	X	Executed
Ref + 0.40	Increase	X	X	X	X	X
Ref + 0.60	Increase	X	X	X	X	X
Ref + 0.80	Increase	X	X	X	X	X
Ref + 1.25	Increase	Increase	X	Executed	X	Executed
Ref + 2.50	Increase	X	X	X	X	X
Ref + 3.75	Increase	X	X	X	X	X
X= *Not tested* Executed = *Performed, but detailed results is documented in the main report*						

6.8 Final Discussion

Experimenting with nanoparticles in drilling fluids have shown both positive and negative results during testing. The most fascinating result was that low concentration of nano had the most positive effect on both the rheology and friction. This is great in terms of cost and environmental impact. A weak side to the tests were the very low coefficient of friction obtained for the systems containing XG as the polymer. This may be an effect of the polymer, as it is more viscous and literature studies in section 2.8 have shown that the more of a viscous system, the more reduction in friction. However, this may also be due to measurement errors. But since the tests were executed in a short span of time and in the same way, it should still be reliable in terms of the reduction percentage and prove that the nanoparticles reduced the friction for some concentrations. Greater concentrations of nano additives increased the filtrate loss and friction coefficient.

Lee S. et al. (2015) [19] has previously developed a product that were enhanced with nano-sized Graphene, which was successfully applied in field trial. When the base mud was enhanced with Graphene, the rheology readings showed an increase of about 40-60%. The same applies for the viscometer readings of the Ref + 0.05 and Ref + 0.10 fluids, where an increase was experienced with 47% and 58.8% respectively. However, the torque reduction was set to 50-60%, while for the Ref + 0.05 and Ref + 0.10 Graphene fluids, the tripping out torque was only reduced with 8.9% and 11% respectively. This may indicate that the fluid system containing Graphene was not optimal. However, the systems containing MoS_2 and TiN had a torque reduction from 36-47% and 23-25% respectively. Further testing of these additives should be executed to investigate if they obtain superior lubricating abilities compared to Graphene.

The XG systems containing a low nano concentration exhibited superior results for all the tests and simulations conducted.

7 Conclusion

The objective of this thesis was to formulate a nano treated WBM system that would improve the frictional behaviour and rheology of a conventional system. Several reference and nano-enhanced systems were designed and tested. The mud systems were evaluated with various concentrations of TiN, MoS_2 and Graphene. These nano-additives were mixed with 25g of bentonite, 0.5g of polymer (either CMC or XG), 2.5g of KCl and 500g of H_2O. The effect of adding the nanoparticles to the conventional fluid systems were investigated by comparing the obtained results to the conventional system. Observations showed that the formulated Graphene systems might have been in a deflocculated and aggregated state. However, the best systems were further investigated to obtain information about the lubricating effects of Graphene.

Based on the experimental part and the simulation study, the following conclusions can be drawn:

- Observations from the Reference systems containing CMC and XG revealed that XG is a better viscosifier, as the shear readings were of significant higher values compared to the CMC system.
- The rheological effects of TiN as a nano-additive in XG based bentonite drilling fluid exhibited that small concentrations of TiN kept the fluid system dispersed and flocculated with decreasing filtrate losses. For greater concentrations, the system seemed to move towards a more aggregated state. Some change of the PV and YS of the systems were experienced. The optimum systems were the fluids containing 0.05g, 0.10g and 0.15g of TiN. Very low concentrations of TiN gave the best effect.
- The rheological effects of MoS_2 as a nano-additive in XG based bentonite drilling fluid exhibited a decrease of filtrate loss for the Ref + 0.20 and Ref + 0.50 fluid. This may indicate that the additive keeps the system dispersed and flocculated. For greater concentrations of MoS_2 added, the system seemed to move towards a more aggregated state. The optimum systems were the fluids containing 0.20g, 0.50g and 0.80g of MoS_2. Low concentrations of MoS_2 gave the best effect.

- The rheological effects of Graphene revealed that the formulated reference and nano-enhanced system were not optimal as the system seemed to be aggregated. However, the readings revealed that for the Ref + 0.05 and Ref + 0.10 system, a significant increase of YS was experienced. This indicates that the system with these additives seems to move towards a flocculated and aggregated system. The filtrate loss amount was inconsistent with increasing concentration, and increased for all the fluid compared to the reference. Very low concentrations of graphene gave the best effect.
- All of the fluids exhibited pseudo-plastic behaviour as the flow index values were below 1. The Graphene fluids exhibited greater n values than the formulated XG systems. This means that the fluids are less shear thinning when containing CMC and Graphene compared to the TiN and MoS_2 systems.
- The friction tests of the TiN drilling fluid revealed an increase for the Ref + 0.1 fluid and Ref + 2.5 fluid, possibly due to under and over saturation of nanoparticles. Positive results were obtained for the very low concentrations fluids Ref + 0.15 and Ref + 0.20. The mean friction was reduced with 23.6% and 16.7% respectively.
- The friction tests of the MoS_2 drilling fluids revealed very good results for the lower concentration fluids, with a mean decrease for all the temperatures of 44.7% for the Ref + 0.8 fluid and 34.8% for the Ref + 0.2 fluid.
- The friction tests of the Graphene drilling fluids revealed positive results for the Ref + 0.05 and Ref + 0.10 fluids. The mean friction for all temperatures was reduced with 8.3% and 10.1% respectively. Greater concentrations (Ref + 0.20 and Ref + 1.25) exhibited an increase in friction.
- The amplitude sweep test revealed that the storage modulus exhibited greater values than the loss modulus in the LVER. This indicated that all of the fluids had a stable gel structure. However, the nano-enhanced fluids with an intersection point at the same frequency as the reference was the MoS_2 fluids. This indicates that these fluids are the most certain in terms of a stable gel structure.
- The damping angle analysis revealed that with the addition of TiN and MoS_2, the fluids would experience viscoelastic properties at higher shear stress values than the reference system. The opposite effect was experienced for the Graphene drilling fluids.

- Rheological modelling and a literature study were executed. The obtained information indicated that the best suitable rheological model for the hydraulic performance simulation was the Unified model.
- All the enhanced TiN and MoS_2 fluids that provided positive results in the friction tests also exhibited lower ECD values and pump pressure values during hydraulic simulation. This means that the frictional pressure loss during circulation decreased for these fluids, and that they may work well in terms of well stability. The opposite was experienced for the Graphene drilling fluids.
- Torque and drag evaluation revealed that the optimum nano-enhanced fluid systems were the fluid enhanced with MoS_2 as it is possible to drill as much as 3400ft longer with the Ref + 0.8 system. The critical parameter was the tripping out drag values while the opposite was experienced for all the other Graphene and TiN fluids.

The objective of this thesis was to investigate if it was possible to improve the rheology and the lubricating effect of conventional water based mud by adding nanoparticles to the fluid system. Finally, this thesis comes to the conclusion that nanoparticles as an additive in drilling fluids has shown both positive and negative results. The negative filtrate results may be improved by polymer treatment. Positive effects of nano shows that it may not alter the rheology of the fluid to a great extent, but still exhibit superior friction reducing abilities. All of the tested fluids exhibited the best friction reduction with low concentrations of nano. This is great in terms of cost, as higher concentrations added for results would be expensive. The results have also illustrated that further investigation of implementing nanoparticles in drilling mud may lead to WBM being able to possibly replace the use of OBM in challenging environments with the addition of nano, which is positive in terms of potential environmental effects as well. The best results were definitely obtained with low concentration MoS_2 as a nano-additive in a XG reference system, both in terms of rheology, friction, viscoelasticity and hydraulic/torque and drag performance.

8 Future Work

This thesis has illustrated that implementing nanoparticles in the conventional drilling fluid system makes way for more lubricating water based systems. It has also shown that there is possibly some lubricating effect from the addition of polymers.

The best results were obtained by using MoS_2 in a XG based system. During research, no particular papers describing the implementation of nano-sized MoS_2 or nano-sized TiN in drilling fluids were found. Some papers of the implementation of Graphene was found, and it has already been tested in the field. The results make way for a big research field, that may address issues such as:

- Friction and rheology evaluation of MoS_2 and TiN in water based drilling fluid systems with other Polymer additives. Will it still act as lubricating, affect the rheology, or will it be more enhanced?
- Friction and rheology evaluation of MoS_2 and TiN in water based drilling fluid systems with other salt and multi-salt systems. Whill this affect the rheology and lubricating abilities?
- Friction and rheology evaluation of MoS_2 and TiN in water based drilling fluid systems with weighting material present. Will weigh clay like Barite influence the lubricating effects?
- Friction and rheology evaluation of Graphene in a water based drilling fluid system containing XG. Will nano Graphene work more lubricating in this system?
- Investigate the friction behaviour of different nano's combined with different polymers. Is there a particularly good composition of nano and type of polymer? Do some nanoparticles work better with some polymers?
- Investigate the effect of nano for fluids exposed to temperature over a long time. How will this affect the properties of the enhanced fluid systems?

Another future work prospect of this research could be to possibly try and implement nano-particles in a water based drilling fluid system containing environmentally friendly and natural oils. It would be interesting to see if implementing nano in such a system would not alter the rheology to a very great extent, but still act as lubricating as an oil based system.

9 References

1 Zheng, X. 2010. *Drilling fluids.* Beijing: School of Engineering and Technology China University of Geosciences.

2 Skjeggestad, O. (1989) *Boreslamteknologi: Teori og Praksis,* Bergen: Alma Mater Forlag

3 Azar J.J. (2006) Drilling Problems and Solutions. In *Petroleum Engineering Handbook,* Vol. 2, ed. L.W. Lake and R.F. Mitchell, Chap. 10, 433-454. University of Tulsa. (ISBN: 978-1-55563-114-7).

4 West G., Hall J., Seaton S. (2006) Drilling Fluids. In *Petroleum Engineering Handbook,* Vol. 2, ed. L.W. Lake and R.F. Mitchell, Chap. 2, 89-118.Halliburton Fluid Systems Div., Baroid Fluid Services. (ISBN: 978-1-55563-114-7).

5 Strand S. (2014) *Øvinger i Bore og Brønnvæsker*, Compendium in the BIP 200 class, University of Stavanger, Stavanger, Rogaland (January 2014).

6 Caenn R., Gray G.R., Darley H.C.H (2011) Clay Mineralogy and the Colloid Chemistry of Drilling Fluids. In *Composition and properties of drilling and completion fluids,* Vol. 6, Chap. 4, 138-175. Oxford: Elseveier Inc. (ISBN: 978-0-12-383858-2).

7 Ali S.A., Austin G.S., Barker J.M. et al. (2006) Part Two: Commodities. In *Industrial Minerals and Rocks,* Vol. 7, ed. J.E. Kogel, N.C. Trivedi, S.T. Krukowski. et al. Chap. 2, 357. Colorado: Society for Mining, Metallurgy, and Exploration, Inc. (ISBN-13: 978-0-87335-223-8).

8 Sobota I. et al. (2012) *Bentonite Processing Oplemenjivanje Bentonita,* Rud.-geol.-naft. zb., Vol. 24, Zagreb: University of Zagreb

9 Slb, Thixotropic, *Oilfield Glossary,* (accessed 13 February 2016) http://www.glossary.oilfield.slb.com/Terms/t/thixotropic.aspx

10 MISwaco Manual. (1998) Polymer chemistry and applications. In *Drilling Fluids Engineering Manual.* Chap. 6, 6.9-6.19.

11 Khaled B., Abdelbaki B. (2012) Rheological and Electrokinetic Properties of Carboxymethylcellulose-Water Dispersions in the Presence of Salts. *International Journal of Physical Science,* Vol. **7**(11): 1790-1798. DOI: 10.5897/IJPS11.1779**.** http://www.academicjournals.org/IJPS

12 Skjeggestad, O. (1989) *Boreslamteknologi: Teori og Praksis,* Bergen: Alma Mater Forlag

13 O'Brien D.E., Chenevert, M.E. (1973) Stabilizing Sensitive Shales with Inhibited, Potassium-Based Drilling Fluids. In *Journal of Petroleum Technology.* 1089-1100. SPE-4232-PA. DOI: http://dx.doi.org.ezproxy.uis.no/10.2118/4232-PA

14 El-Diasty A.I., Ragab A.M.S. (2013) Applications of Nanotechnology in the Oil & Gas Industry: Latest Trends Worldwide & Future Challenges in Egypt. North Africa Technical Conference & Exhibition, Cairo, 15-17 April. SPE-164716-MS. DOI: http://dx.doi.org.ezproxy.uis.no/10.2118/164716-MS

15 Perillo P.M. (2006) Corrosion Behaviour of Coatings of Titanium Nitride and Titanium-Titanium Nitride on Steel Substrates. In *Corrosion* 62 (2): 182-185. NACE-06020182.

16 OSHA HCS. (2013) Safety Data Sheet. *Vwr,* 23 January 2014, (accessed 12 May 2016) https://ca.vwr.com/assetsvc/asset/en_CA/id/16152439/contents

17 Lansdown A.R. (1999) *Tribology Series, 35: Molybdenum Disulphide Lubrication,* first edition. Amsterdam: Elsevier Science B.V. (ISBN: 0-4444-50032-4)

18 Katsnelson M.I. (2012) *Graphene Carbon in two dimensions,* first edition. New York: Cambridge University Press. (ISBN: 978-0-521-19540-9 Hardback)

19 Taha N.M., Lee S. (2015) Nano Graphene Application Improving Drilling Fluids Performance. International Petroleum Technology Conference, Doha, 6-9 December. IPTC-18539-MS. DOI: http://dx.doi.org.ezproxy.uis.no/10.2523/IPTC-18539-MS

20 Li L., Xu X., Sun J. et al. (2012) Vital Role of Nanomaterials in Drilling Fluid and Reservoir Protection Applications. Abu Dhabi International Petroleum Conference and Exhibition, Abu Dhabi, 11-14 November. SPE-160940-MS. DOI: http://dx.doi.org.ezproxy.uis.no/10.2118/160940-MS

21 Abdo J., Haneef M.D. (2013) Clay Nanoparticles Modified Drilling Fluids for Drilling of Deep Hydrocarbon Wells. In *Applied Clay Science,* ed. F. Bergaya, B. Percival, V. Rives. et al. Vol. 86, 76-82. (ISSN: 0169-1317).

22 William J.K.M, Ponami S., Samuel R. et al. (2014) Effect of CuO and ZnO nanofluids in Xanthan Gum on Thermal, Electrical and High Pressure Rheology of WB Drilling Fluids. In *Journal of Petroleum Science and Engineering,* 117: 15-27. DOI: 10.1016/j.petrol.2014.03.005

23 Barry M.M., Jung Y., Chyu M.K. et al. (2015) Fluid Filtration and Rheological Properties of Nanoparticle Additive and Intercalated Clay Hybrid Bentonite Drilling Fluids. In *Journal of Petroleum Science and Engineering,* **127**: 338-346. DOI: 10.1016/j.petrol.2015.01.012

24 Nwaoji C.O., Hareland G., Husein M. (2013) Wellbore Strengthening – Nano-Particle Drilling Fluid Experimental Design Using Hydraulic Fracture Apparatus. SPE/IADC Drilling Conference, Amsterdam, 5-7 March. SPE-163434-MS. DOI: http://dx.doi.org.ezproxy.uis.no/10.2118/163434-MS

25 Amanullah M.D., AlArfaj M.K., Al-abdullatif A. (2011) Preliminary Test Results of Nano-Based Drilling Fluids for Oil and Gas Field Application. SPE/IADC Drilling Conference and Exhibition, Amsterdam, 1-3 March. SPE-139534-MS. DOI: http://dx.doi.org.ezproxy.uis.no/10.2118/139534-MS

26 Sadeghalvaad M., Sabbaghi S. (2014) The Effect of the TiO_2/Polycrylamide Nanocomposite on Water-Based Drilling Fluid Properties. In *Powder Technology,* **272**: 113-119. DOI: 10.1016/j.powtec.2014.11.032

27 Taha N.M., Lee S. (2015) Nano Graphene Application Improving Drilling Fluids Performance. International Petroleum Technology Conference, Doha, 6-9 December. IPTC-18539-MS. DOI: http://dx.doi.org.ezproxy.uis.no/10.2523/IPTC-18539-MS

28 Deng Z., Livanec P.W., Derville J.P. (2015) Novel Water-Based Fluids for Oil-Sands Drilling. SPE Canada Heavy Oil Technical Conference, Calgary, 9-11 June. SPE-174420-MS. DOI: http://dx.doi.org.ezproxy.uis.no/10.2118/174420-MS

29 Robello S. (2010) Friction Factors: What are They for Torque, Drag, Vibration, Drill Ahead and Transient Surge/Swab Analysis. IADC/SPE Drilling Conference and Exhibition, New Orleans, 2-4 February. SPE-128059-MS. DOI: http://dx.doi.org.ezproxy.uis.no/10.2118/128059-MS

30 Xu L., Xu M.B., Zhao L. et al. (2014) Experimental Investigations into the Performance of a Flat-Rheology Water-Based Drilling Fluid. *SPE Journal* **19** (01): 69-77. SPE-163107-PA. DOI: http://dx.doi.org.ezproxy.uis.no/10.2118/163107-PA

31 Vos B.E., Rieber F. (2000) The Benefits of Monitoring Torque & Drag in Real Time. IACD/SPE Asia Pacific Drilling Technology, Kuala Lumpur, 11-13 September. SPE-62784-MS. DOI: http://dx.doi.org.ezproxy.uis.no/10.2118/62784-MS

32 Seireg A.A. (1998) *Friction and Lubrication in Mechanical Design,* first edition. New York, NY: Marcel Dekker, Inc. (ISBN: 0-8247-9974-7).

33 Payne M.L., Abbassian F. (1997) Advanced Torque and Drag Considerations in Extended-Reach Wells. *SPE Drilling & Completion* **12** (01): 55-62. SPE-35102-PA. DOI: http://dx.doi.org.ezproxy.uis.no/10.2118/35102-PA

34 McCormick J.E., Evans C.D., Le J. et al. (2011) The Practice and Evolution of Torque and Drag Reduction: Theory and Field Results. International Petroleum Technology Conference, Bangkok, 15-17 November. IPTC-14862-MS. DOI: http://dx.doi.org.ezproxy.uis.no/10.2523/IPTC-14863-MS

35 Champ J.H., Estes B.L., Keller S.R. (2006) Torque Reduction Techniques in ERD Wells. IACD/SPE Drilling Conference, Miami, 21-23 February. SPE-98969-MS. DOI: http://dx.doi.org.ezproxy.uis.no/10.2118/98969-MS

36 Kaarstad E., Aadnoy B.S., Fjelde T. (2009) A Study of Temperature Dependent Friction in Wellbore Fluids. SPE/IADC Drilling Conference and Exhibition, Amsterdam, 17-19 March. SPE-119768-MS. DOI: http://dx.doi.org.ezproxy.uis.no/10.2118/119768-MS

37 Sadigov J. (2013) *Comparisons of Rheology and Hydraulics Prediction of Mud Systems in Concentric and Eccentric Well Geometry*. MSc Thesis, University of Stavanger, Stavanger, Rogaland (June 2013)

38 Ochoa M.V. (2006) *Analysis of Drilling Fluid Rheology and Tool Joint Effect to Reduce Errors in Hydraulics Calculations.* PhD Dissertation, Texas A&M University, College Station, Texas (August 2006)

39 American Petroleum Institute (2009). API Recommended Practice 13D – Rheology and Hydraulics of Oil-Well Drilling Fluids. *Api,* 5 October 2009, (accessed 24 April 2016) http://ballots.api.org/ecs/sc13/ballots/docs/apirp13de6.pdf

40 Saasen A., Bui B., Maxey J. et al (2012) Viscoelastic Properties of Oil-Based Drilling Fluids. In *Annular Transactions of the Nordic Rheology Society,* **20**: 33-47. (ISSN 1601-4057)

41 Oil&Gas Journal (1993) Yield-Power Law Model More Accurately Predicts Mud Rheology. *Oil&Gas Journal*, 23 August 1993, (accessed 24 April 2016) http://www.ogj.com/articles/print/volume-91/issue-34/in-this-issue/drilling/yield-power-law-model-more-accurately-predicts-mud-rheology.html

42 Zamora M., Power D. (2002) Making A Case for AADE Hydraulics and the Unified Rheological Model. AADE 2002 Technology Conference "Drilling & Completion Fluids and Waste Management", Texas, 2-3 April. AADE-02-DFWM-HO-13

43 Saasen A., Bui B., Maxey J. et al (2012) Viscoelastic Properties of Oil-Based Drilling Fluids. In *Annular Transactions of the Nordic Rheology Society,* 20: 33-47. (ISSN 1601-4057)

44 Kelco Oil Field Group Technical Bulletin (2006) Rheology. In *Technical Bulletin*.

45 Mezger T.G. (2014) *The Rheology Handbook,* 4th edition. Hanover, Germany: BWH GmbH. (ISBN: 3-86630-842-6)

46 Reitsma M.G., Cain R.G., Smith D. et al. (2000) Lateral Force Microscopy: A Tool for Tribology. ISRM International Symposium, Melbourne, 19-24 November. ISRM-IS-2000-189.

47 Kaarstad E., Aadnoy B.S., Fjelde T. (2009) A Study of Temperature Dependent Friction in Wellbore Fluids. SPE/IADC Drilling Conference and Exhibition, Amsterdam, 17-19 March. SPE-119768-MS. DOI: http://dx.doi.org.ezproxy.uis.no/10.2118/119768-MS

48 Kato K., Adachi K. (2001) Wear Mechanisms. In *Modern Tribology Handbook, Volume one Principles of Tribology*, first edition, ed. B. Bhushan, Chap. 7, 273-299. Danvers, MA: CRC Press LCC. (ISBN: 0-8493-8403-6)

49 Taboada J.V., Belayneh M. (2014) *Well Engineering Simulation (WellPlan™) Challenges and Uncertainties in Drilling Engineering*. Compendium in the PET525 class, University of Stavanger, Stavanger, Rogaland (May 2014).

50 Pegasus Vertex, Inc. (2015) Prediction Technique. *Pvisoftware,* 24 February 2015, (accessed 29 April 2016) http://www.pvisoftware.com/blog/tag/drillstring-drag/

51 Belayneh M. (2014) *Drill String Mechanics with a Special Focus on Buckling*. Compendium in the PET252 class, University of Stavanger, Stavanger, Rogaland (2014)

52 Instron, Torsional Strength, *Instron,* (accessed 2 May 2016) http://www.instron.us/en-us/our-company/library/glossary/t/torsional-strength

53 Chadwick A., Morfett J., Borthwick M. (2004) *Hydraulics in civil and environmental engineering*, fourth edition. London: Spon Press. (ISBN: 0-415-30609-4)

54 Drilling Formulas, Effect of Frictional Pressure on ECD while Forward Circulation, *drilling formulas,* (accessed 7 May 2016) http://www.drillingformulas.com/effect-of-frictional-pressure-on-ecd-while-forward-circulation/

55 Lyons W.C., Carter T., Lapeyrouse N.J. (2016) *Formulas and Calculations for Drilling, Production and Workover: All the Formulas You Feed to Solve Drilling and Production Problems*, fourth edition. Waltham, MA: Gulf Professional Publishing. (ISBN: 978-0-12-803417-0)

56 Zamora, M., Roy, S. and Slater, K. (2005) Comparing a Basic Set of Drilling Fluid Pressure-Loss Relationships to Flow-Loop and Field Data. AADE National Technical Conference and Exhibition, Houston, 5-7 April. AADE-05-NTCE-27.

57 Kodja M., Khodja-Saber M., Canselier J.P. et al. (2010) Drilling Fluid Technology: Performances and Environmental Considerations. In *Products and Services; from R&D to Final Solutions,* ed. I. Fuerstner, Chap. 13, 227-256. Published online: Sciyo (InTech). (ISBN: 978-953-307-211-1).

58 Axon Energy Products (2015) Navigating Narrow Drilling Margins, *axonep,* (accessed 29 May 2016) http://www.axonep.com/navigating-narrow-drilling-margins

10 Appendix

Appendix A – Rheological Tests

A.1 – Rheological Tests of TiN

Low concentration TiN viscometer data repetition					
RPM	Ref	Ref + 0.05	Ref + 0.10	Ref + 0.15	Ref + 0.20
600	40	38	42	38.5	37
300	33.5	32	36	32.5	31
200	30	29	33.5	29.5	28
100	25.6	25	30	25.5	24.5
60	24.5	23	27	23.5	23
30	22.5	21.5	25.5	21.5	21
6	18	18	21.5	17.5	17.5
3	17	16	20	16,5	16
pH	8.95	8.9	8.85	8.85	8.85
Filtrate (ml)	8	7.25	7.25	8	8.5

Table A.1: Viscometer data, pH data and filtrate data of the low concentration TiN drilling fluids

High concentration Tin viscometer data					
RPM	Ref	Ref + 0.50	Ref + 1.25	Ref + 2.50	Ref + 3.75
600	40	43	44	43	44
300	34	35.5	36.5	35	36
200	32	33	34	32	33
100	27	29	29	28	28
60	25	26.5	27	26	26
30	23	24	24.5	24	23
6	19	20	20	19	18
3	18	18	17	16	16
pH	8.85	8.8	8.75	8.75	8.65
Filtrate (ml)	7	7.25	7.5	8.25	9.25

Table A.2: Viscometer data, pH data and filtrate data of the high concentration TiN drilling fluids

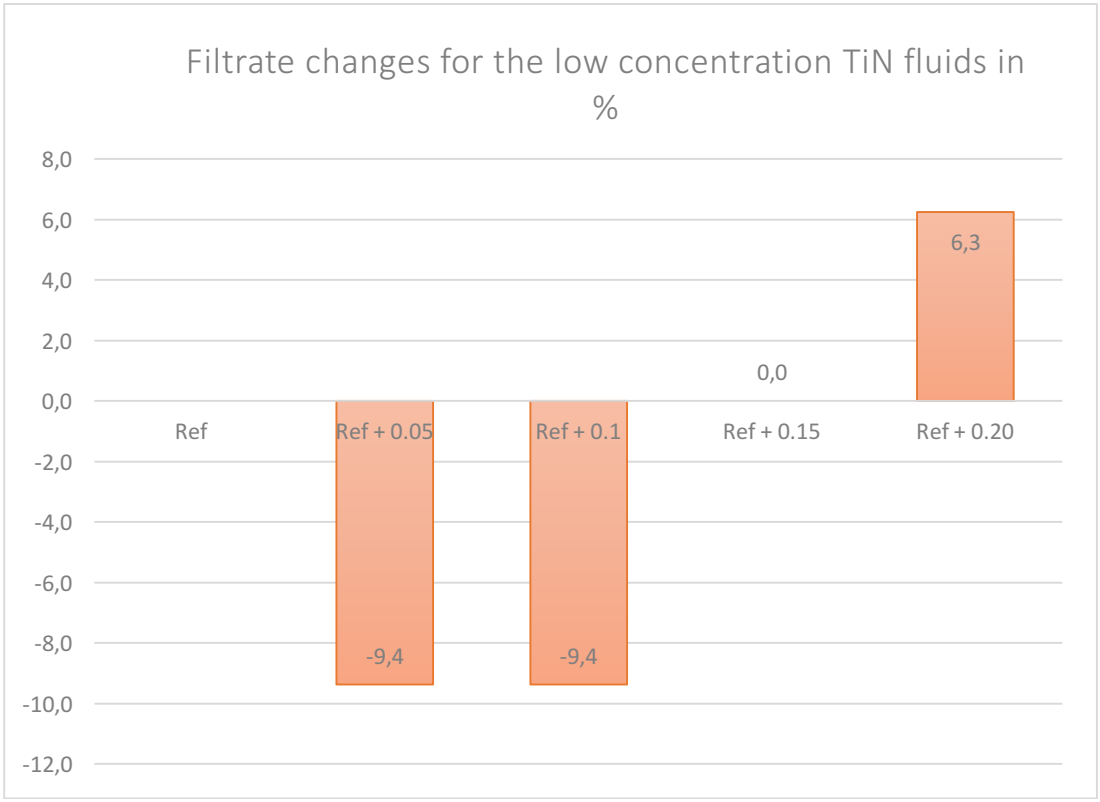

Figure A.1: Filtrate changes for the low concentration TiN fluids in %

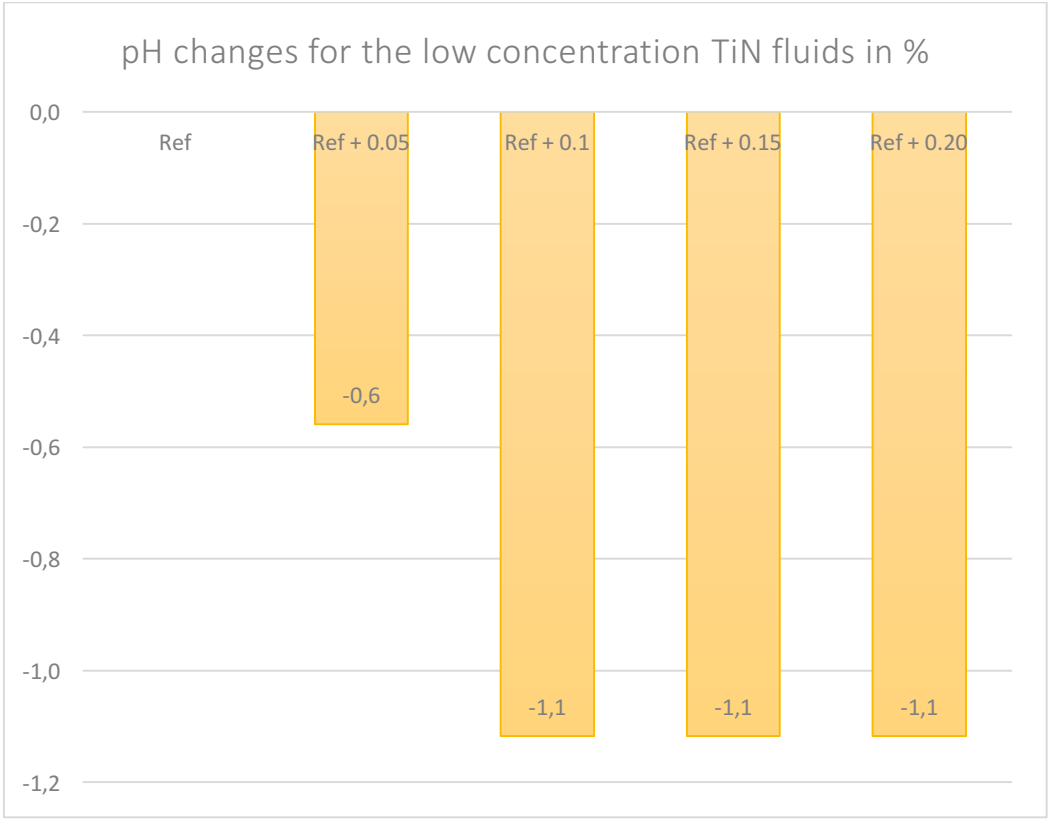

Figure A.2: pH changes for the low concentration TiN fluids in %

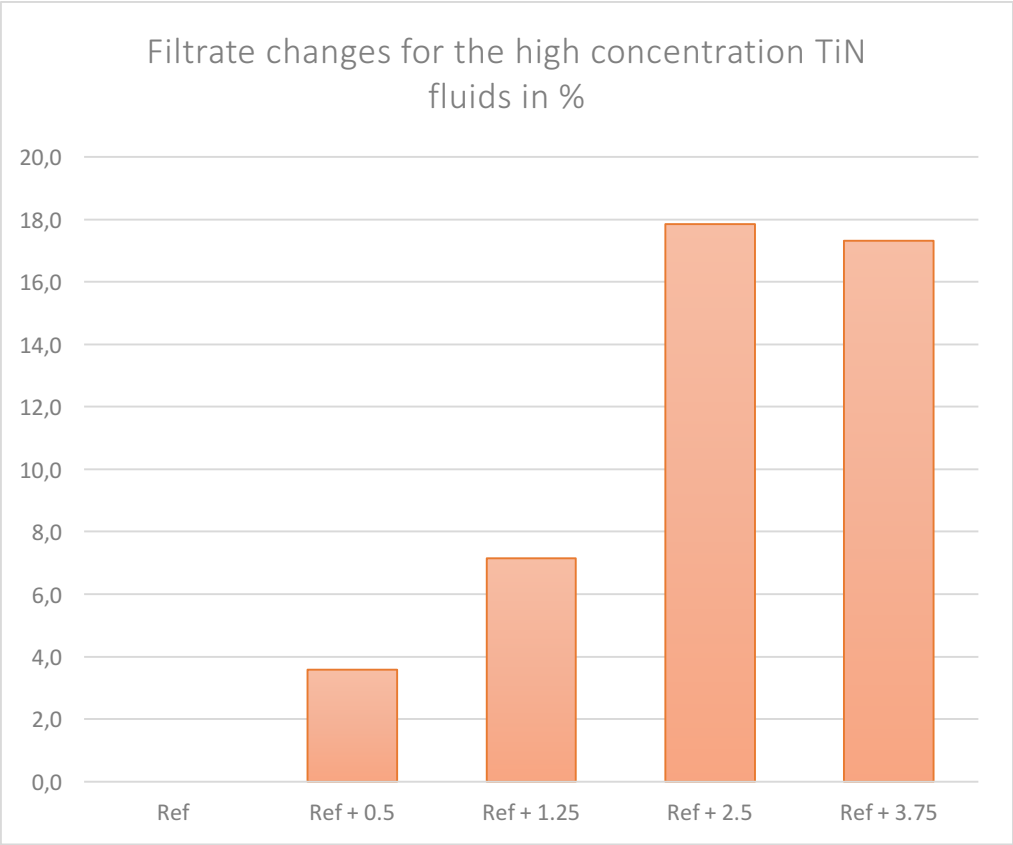

Figure A.3: Filtrate changes for the high concentration TiN fluids in %

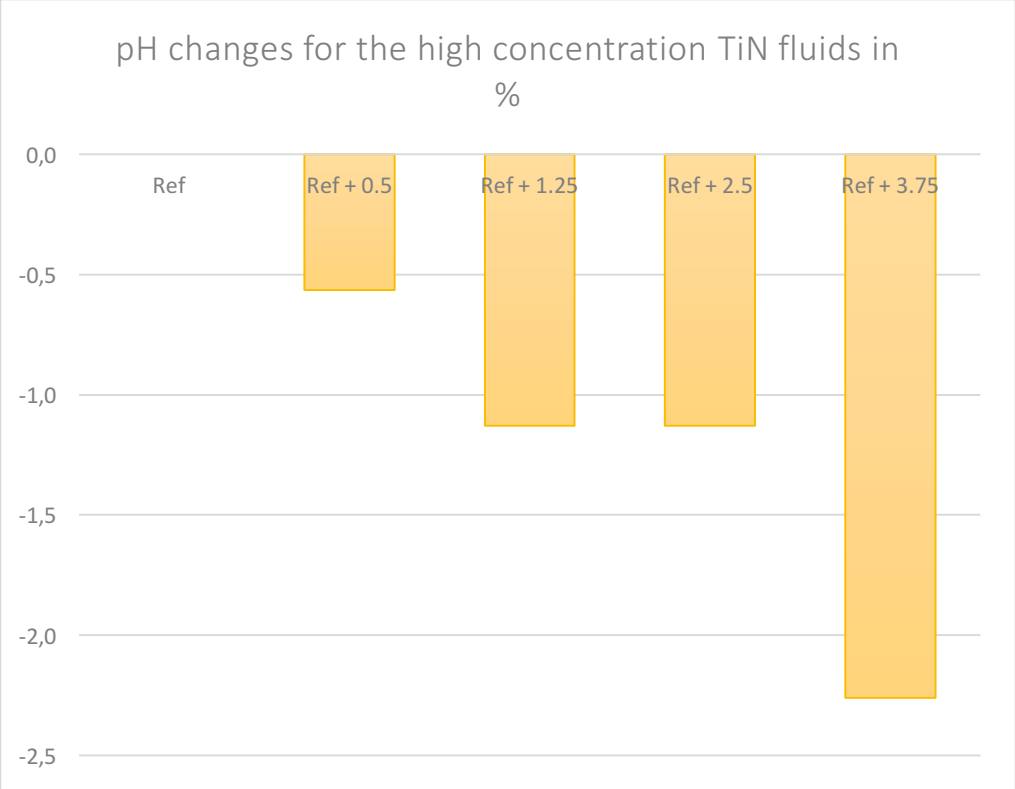

Figure A.4: pH changes for the high concentration TiN fluids in %

Weight % table for the TiN drilling fluids	
Drilling fluid	Weight %
Ref	0.00%
Ref + 0.05	0.01%
Ref + 0.10	0.02%
Ref + 0.15	0.03%
Ref + 0.20	0.04%
Ref + 0.50	0.10%
Ref + 1.25	0.25%
Ref + 2.50	0.50%
Ref + 3.75	0.75%

Table A.3: Weight % table for the TiN drilling fluids

Appendix A.2 – Rheological Tests of MoS_2

MoS2 Viscometer data							
RPM	Ref	Ref + 0.20	Ref + 0.50	Ref + 0.80	Ref + 1.25	Ref + 2.50	Ref + 3.75
600	41	40	39	40.5	40.5	42	37
300	35	34	33	34.5	34.5	36	31.5
200	32	31	30	31.5	31.5	34	27.5
100	28	27	26	27.5	27.5	30	24
60	26	25	24	25.5	25.5	28	22.5
30	24	23	22	23.5	23.5	26	20
6	20	20	19	20	20	21.5	16.5
3	19	18	17.5	18	18	20.5	15
pH	8.75	8.85	8.85	8.85	8.75	8.7	8.55
Filtrate	7	6.25	6.75	7	7.5	7.5	7.5

Table A.4: Viscometer data, pH data and filtrate data of the MoS_2 drilling fluids

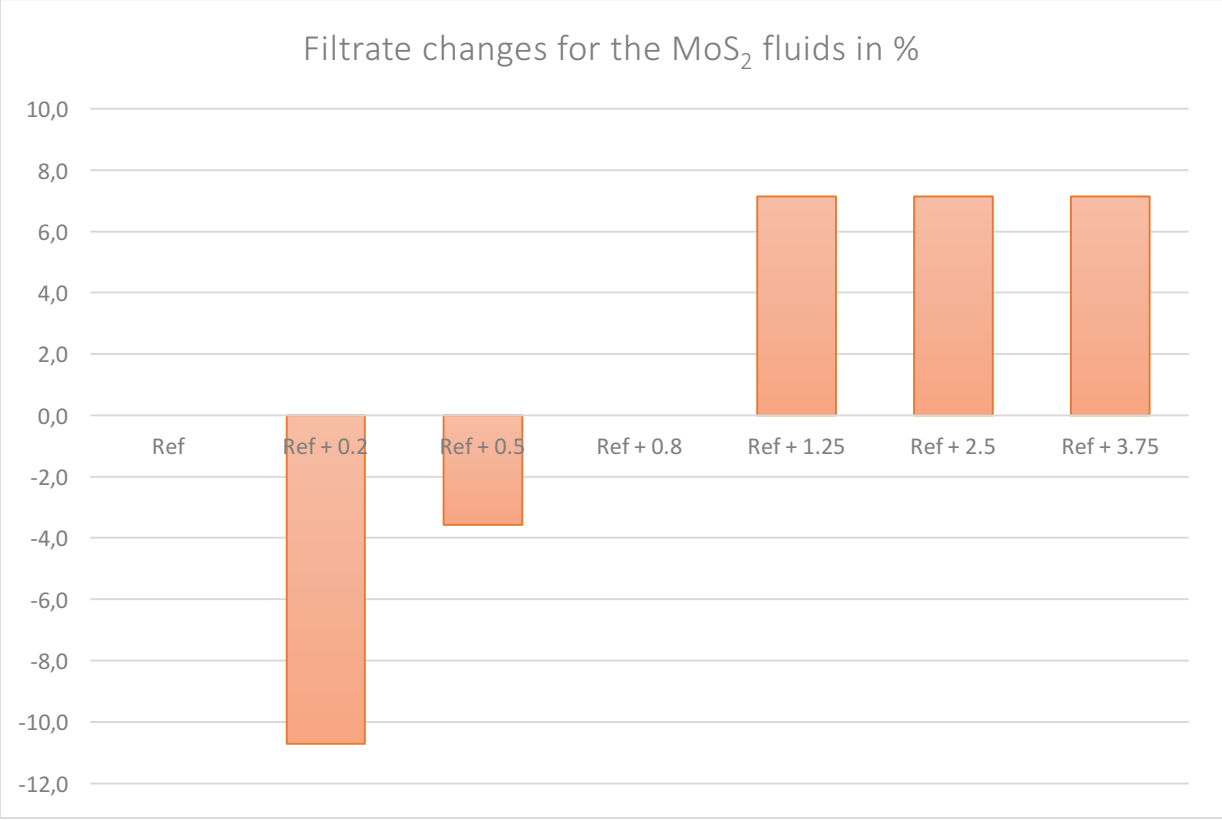

Figure A.5: Filtrate changes for the MoS_2 fluids in %

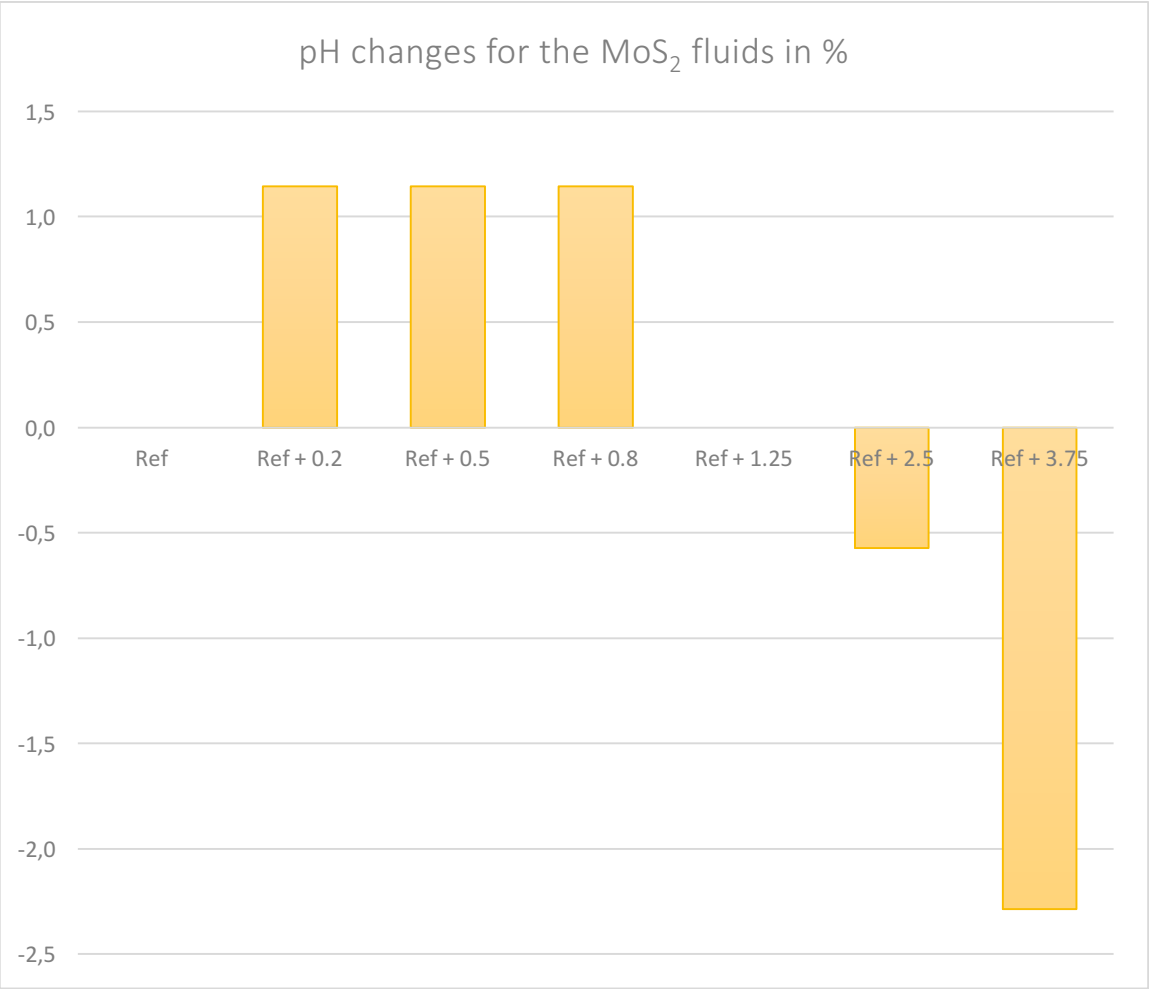

Figure A.6: pH changes for the MoS_2 fluids in %

Weight % table for the MoS_2 drilling fluids	
Drilling fluid	Weight %
Ref	0.00%
Ref + 0.20	0.04%
Ref + 0.50	0.10%
Ref + 0.80	0.16%
Ref + 1.25	0.25%
Ref + 2.50	0.50%
Ref + 3.75	0.75%

Table A.5: Weight % table for the MoS_2 drilling fluids

Appendix A.3 – Rheological Tests of Graphene

Graphene viscometer data					
RPM	Ref	Ref + 0.05	Ref + 0.10	Ref + 0.20	Ref + 0.40
600	17	25	27	17	16.5
300	12	19	22	12	12
200	10	16	19	10	10
100	7	13	15	7	7.5
60	6	11.5	13	6	6.5
30	5	9	11	5	5
6	3	5.5	6.5	3	3.5
3	3	4	5.5	3	3
pH	8.95	8.95	8.95	8.95	8.95
Filtrate	6.5	7	7.75	6.75	7.5
RPM	Ref + 0.60	Ref + 0.80	Ref + 1.25	Ref + 2.50	Ref + 3.75
600	15	11,5	17	15,5	15
300	10	7	13	11	10
200	9	6	11	8.5	8.5
100	7	4	8	6.5	6
60	6	3	6.5	5	5
30	4	2	5.5	4	4
6	3	1	4	3	2.5
3	2.5	1	3.5	2	2.5
pH	8.95	8.95	8.95	8.95	8.95
Filtrate	6.75	6.75	6.75	7	8

Table A.6: Viscometer data, pH data and filtrate data of the Graphene drilling fluids

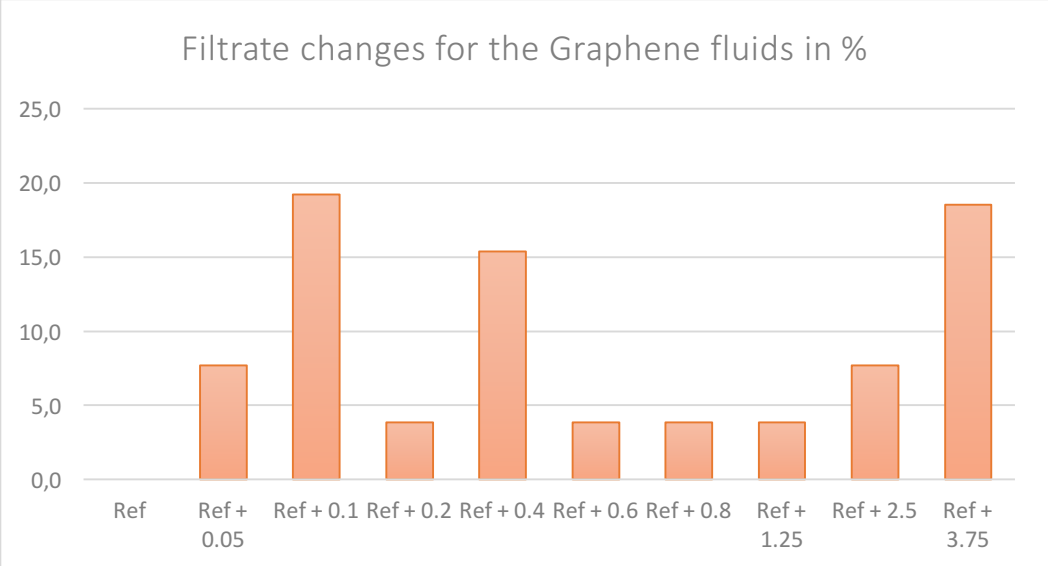

Figure A.7: Filtrate changes for the Graphene fluids in %

Weight % table for the Graphene drilling fluids	
Drilling fluid	Weight %
Ref	0.00%
Ref + 0.05	0.01%
Ref + 0.10	0.02%
Ref + 0.20	0.04%
Ref + 0.40	0.08%
Ref + 0.60	0.12%
Ref + 0.80	0.16%
Ref + 1.25	0.25%
Ref + 2.50	0.50%
Ref + 3.75	0.75%

Table A.7: Weight % table for the Graphene drilling fluids

Appendix B – Friction tests

Appendix B.1 – Friction Test for the Reference Fluids

Mean friction test values for the Reference with XG fluid			
Measurement	22 degrees C	50 degrees C	70 degrees C
1	0.253	0.224	0.319
2	0.237	0.263	0.319
3		0.246	

Table B.1: Mean friction values for the Reference with XG fluid

Mean friction test values for the Reference with CMC fluid			
Measurement	22 degrees C	50 degrees C	70 degrees C
1	0.417	0.581	0.547
2	0.460	0.582	0.511
3	0.445	0.533	

Table B.2: Mean friction values for the Reference with CMC

Appendix B.2 – Friction Test for The TiN Drilling Fluids

Degrees C	Reference	Reference + 0.1	Reference + 0.15	Reference + 0.2	Reference + 2.5
22	0.245	0.271	0.187	0.237	0.239
50	0.244	0.267	0.207	0.204	0.404
70	0.319	0.329	0.223	0.232	0.346

Table B.3: Averaged mean values of the TiN drilling fluids

Mean friction test values for the Ref + 0.1 TiN fluid			
Measurement	22 degrees C	50 degrees C	70 degrees C
1	0.268	0.283	0.336
2	0.274	0.251	0.309

Table B.4: Mean friction test values for the Ref + 0.1 TiN fluid

Mean friction test values for the Ref + 0.15 TiN fluid			
Measurement	22 degrees C	50 degrees C	70 degrees C
1	0.237	0.180	0.256
2	0.177	0.203	0.222
3	0.150	0.237	0.190
4	0.182		

Table B.5: Mean friction test values for the Ref + 0.15 TiN fluid

Mean friction test values for the Ref + 0.2 TiN fluid			
Measurement	22 degrees C	50 degrees C	70 degrees C
1	0.253	0.204	0.247
2	0.221	0.204	0.266
3			0.184

Table B.6: Mean friction test values for the Ref + 0.2 TiN fluid

Mean friction test values for the Ref + 2.5 TiN fluid			
Measurement	22 degrees C	50 degrees C	70 degrees C
1	0.184	0.409	0.349
2	0.272	0.398	0.343
3	0.262		

Table B.7: Mean friction test values for the Ref + 2.5 TiN fluid

Appendix B.3 – Friction Test for the MoS_2 Drilling Fluids

Degrees C	Reference	Reference + 0.2	Reference + 0.8
22	0.245	0.144	0.131
50	0.244	0.160	0.156
70	0.319	0.223	0.160

Table B.8: Averaged mean values of the MoS_2 drilling fluids

Mean friction test values for the Ref + 0.2 MoS_2 fluid			
Measurement	22 degrees C	50 degrees C	70 degrees C
1	0.149	0.157	0.231
2	0.143	0.148	0.214
3		0.175	

Table B.9: Mean friction test values for the Ref + 0.2 MoS_2 drilling fluid

Mean friction test values for the Ref + 0.8 MoS_2 fluid			
Measurement	22 degrees C	50 degrees C	70 degrees C
1	0.142	0.185	0.161
2	0.120	0.142	0.147
3		0.143	0.172

Table B.10: Mean friction values for the Ref + 0.8 MoS_2 drilling fluid

Appendix B.4 – Friction Test for the Graphene Drilling Fluids

Degrees C	Reference	Reference + 0.05	Reference + 0.1	Reference + 0.2	Reference + 1.25
22	0.441	0.398	0.423	0.480	0.527
50	0.565	0.499	0.484	0.603	0.606
70	0.529	0.511	0.473	0.576	0.615

Table B.11: Averaged mean values of the Graphene drilling fluids

Mean friction test values for the Ref + 0.05 Graphene fluid			
Measurement	22 degrees C	50 degrees C	70 degrees C
1	0.384	0.499	0.511
2	0.412	0.499	
3	0.398		

Table B.12: Mean friction test values for the Ref + 0.05 Graphene fluid

Mean friction test values for the Ref + 0.1 Graphene fluid			
Measurement	22 degrees C	50 degrees C	70 degrees C
1	0.413	0.492	0.482
2	0.433	0.475	0.464

Table B.13: Mean friction test values for the Ref + 0.1 Graphene fluid

Mean friction test values for the Ref + 0.2 Graphene fluid			
Measurement	22 degrees C	50 degrees C	70 degrees C
1	0.454	0.606	0.586
2	0.507	0.599	0.565
3	0.479		

Table B.14: Mean friction test values for the Ref + 0.2 Graphene fluid

Mean friction test values for the Ref + 1.25 Graphene fluid			
Measurement	22 degrees C	50 degrees C	70 degrees C
1	0.530	0.613	0.634
2	0.523	0.599	0.595

Table B.15: Mean friction test values for the Ref + 1.25 Graphene fluid

Appendix C – Rheological Modelling

Appendix C.1 – Rheological Modelling of the TiN Ref + 2.5 System

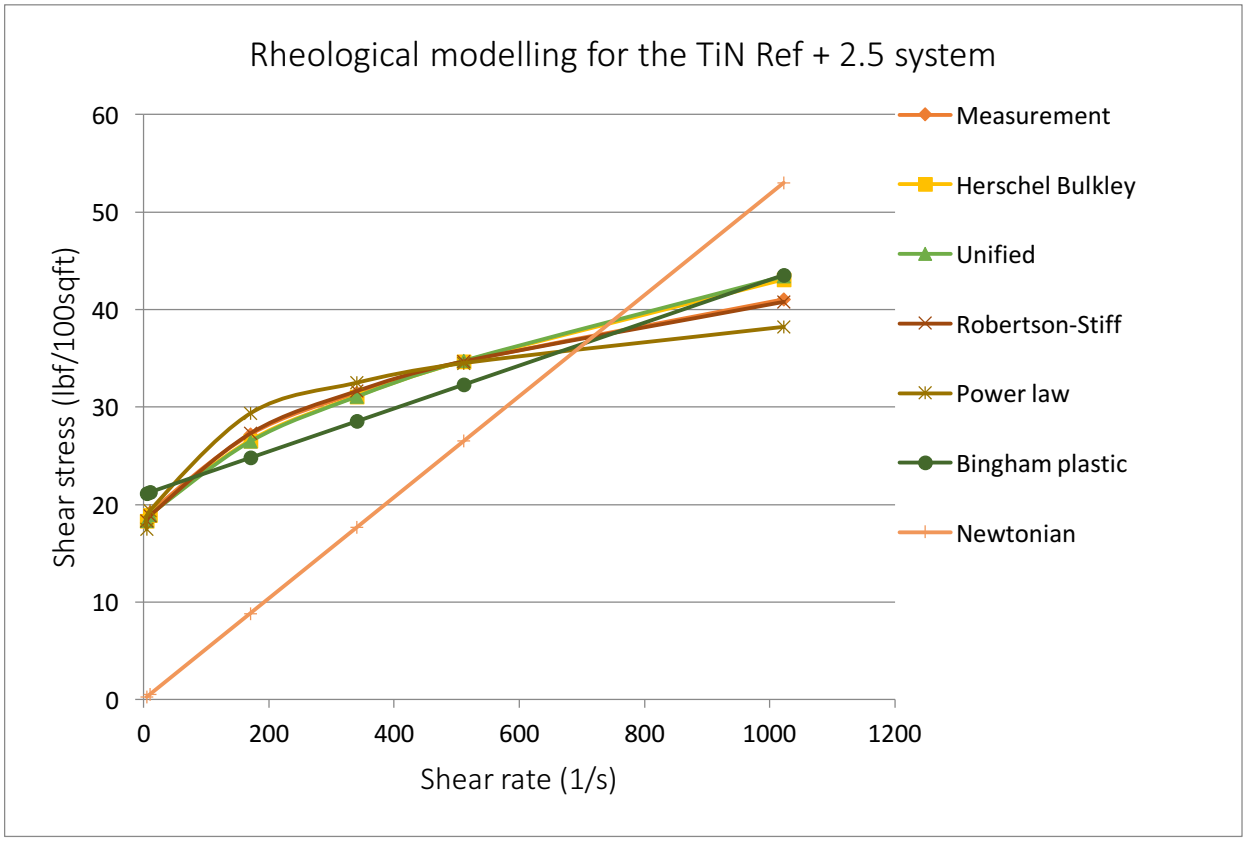

Figure C.1: Modelled trend-lines for the TiN Ref + 2.5 system

		Parameters					
Model	Equation	τo,τy, A	k, C	n, B	μp, μ	Error	cP
Herschel Bulkley	$13.870 + 2.0304\dot{\gamma}^{0.39790}$	13.870	2.0304	0.3979		2.46	
Unified	$13.871 + 2.0296\dot{\gamma}^{0.3979}$	13.871	2.0296	0.3979		2.46	
Power Law	$13.046\dot{\gamma}^{0.1712}$		13.046	0.1712		3.77	
Bingham	$0.0264\dot{\gamma} + 21.708$	21.708			0.0264	11.77	12.640
Newtonian	$0.0572\dot{\gamma}$				0.0572	59.15	27.387
Robertson and Stiff	$8.4331(18.7494 + \dot{\gamma})^{0.2405}$	8.4331	18.7494	0.2405		3.15	

Table C.1: Modelled equations for the TiN Ref + 2.5 system

According to the error of deviation, the best suited rheological model for the TiN Ref + 2.5 system is set to be either the Herschel Bulkley model or the Unified model, as they both deviated with a percentage of 2.46%. The equations are presented in Table C.1.

Appendix C.2 – Rheological Modelling of the MoS_2 Ref + 0.5 Fluid

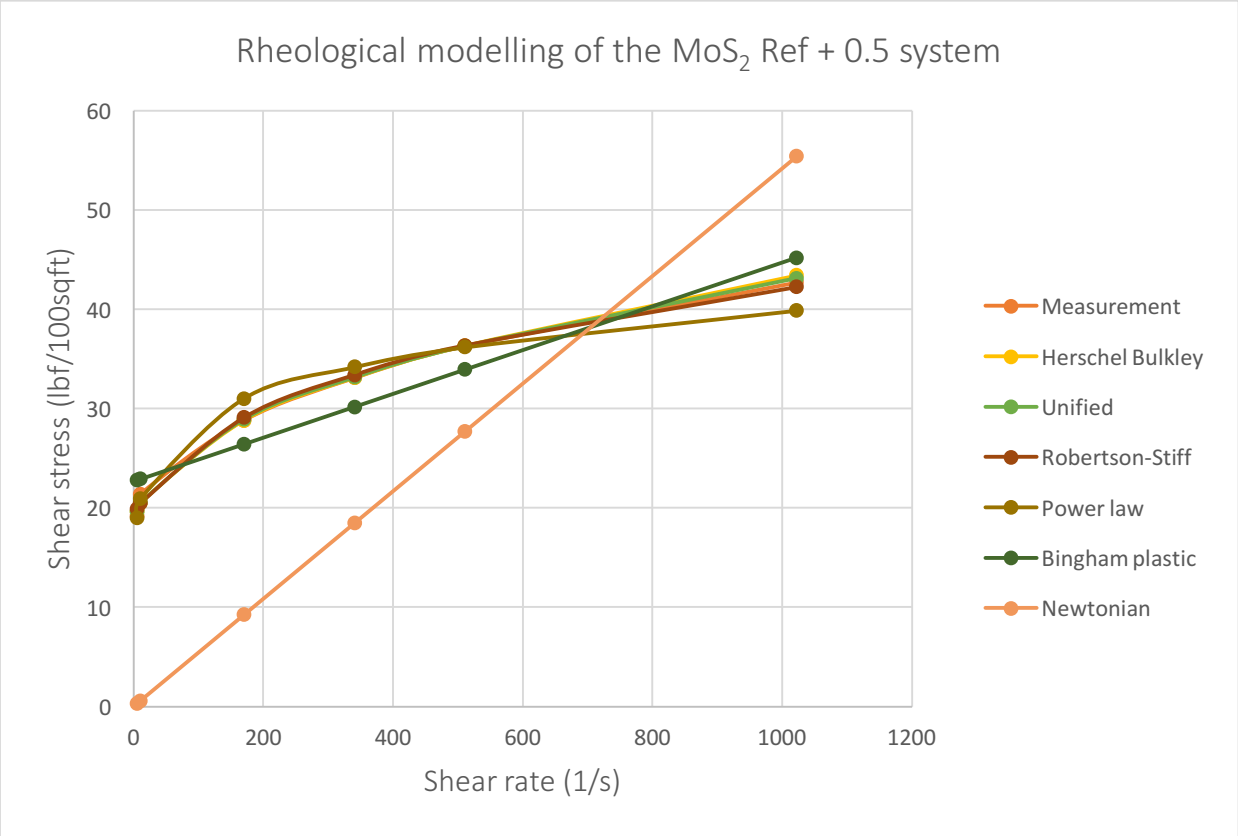

Figure C.2: Modelled trend-lines for the MoS_2 Ref + 0.5 system

		Parameters					
Model	Equation	τo,τy, A	k, C	n, B	μp, μ	Error	cP
Herschel Bulkley	$17.224 + 0.7647\gamma^{0.50640}$	17.224	0.7647	0.5064		1.39	
Unified	$17.072 + 0.8493\gamma^{0.4907}$	17.072	0.8493	0.4907		1.19	
Power Law	$14.44\gamma^{0.1422}$		14.44	0.1422		3.72	
Bingham	$0.0218\gamma + 21.775$	21.775			0.0218	9.17	10,438
Newtonian	0.0527γ				0.0527	60.07	25.233
Robertson and Stiff	$7.8943(36.3811 + \gamma)^{0.2373}$	7.8943	36.3811	0.2373		1.35	

Table C.2: Modelled equations for the MoS_2 Ref + 0.5 system

According to the error of deviation, the best suited model for the MoS_2 Ref + 0.5 system is the Unified model with a deviation error of 1.19%. The equation is presented in Table C.2.

Appendix C.3 – Rheological Modelling of the Graphene Ref + 0.2 Fluid

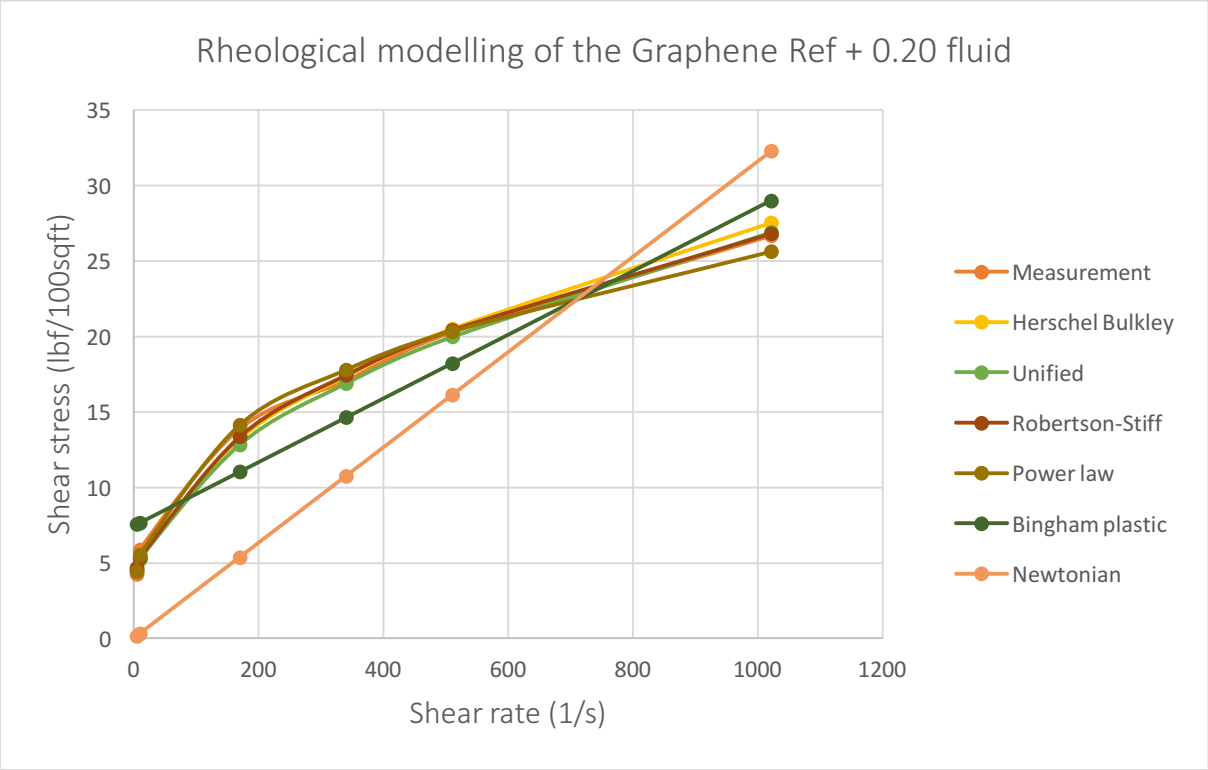

Figure C.3: Modelled trend-lines for the Graphene Ref + 0.2 system

		Parameters					
Model	Equation	τo,τy, A	k, C	n, B	μp, μ	Error	cP
Herschel Bulkley	$2.966 + 0.0458\gamma^{0.86030}$	2.966	0.0458	0.8603		6.04	
Unified	Not definable						
Power Law	$1.6329\gamma^{0.3279}$		1.6329	0.3279		9.62	
Bingham	$0.0148\gamma + 4.176$	4.176			0.0148	17.78	7.086
Newtonian	00207γ				0.0207	51.80	9.911
Robertson and Stiff	$0.3846(38.1363 + \gamma)^{0.5555}$	0.3846	38.1363	0.5555		1.74	

Table C.3: Modelled equations for the Graphene Ref + 0.20 system

According to the error deviation, the best suited model for the Graphene Ref + 0.20 system is the Robertson and Stiff model, as the deviation error is of 1.74%. The equation is presented in Table C.3.

Appendix C.4 – Rheological Modelling of the Graphene Ref + 1.25 Fluid

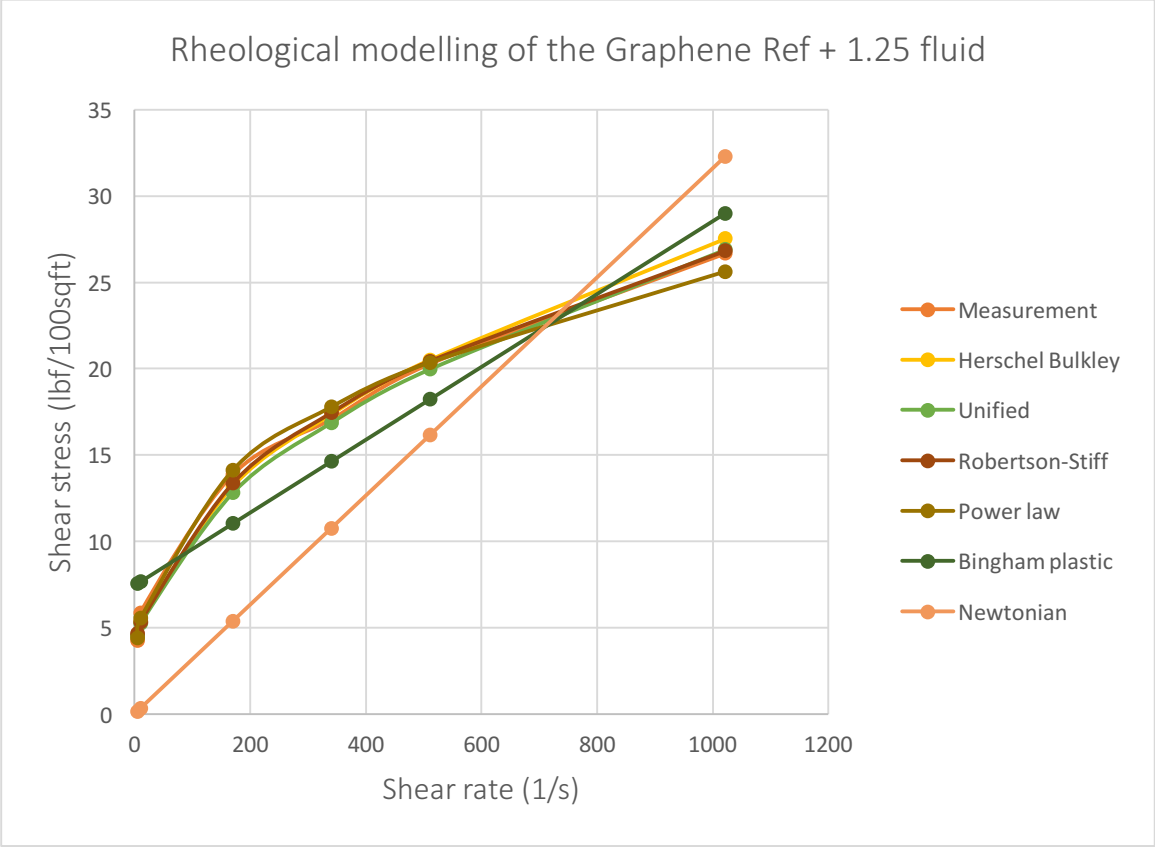

Figure C.4: Modelled trend-lines for the Graphene Ref + 1.25 system

		Parameters					
Model	Equation	τo,τy, A	k, C	n, B	μp, μ	Error	cP
Herschel Bulkley	$3.275 + 0.197\gamma^{0.6366}$	3.257	0.197	0.6366		3.14	
Unified	$3.201 + 0.2217\gamma^{6182}$	3.201	0.2217	0.6182		2.73	
Power Law	$2.1879\gamma^{0.2921}$		2.1879	0.2921		5.87	
Bingham	$0.014\gamma + 5.227$	5.227			0.014	18.63	6.703
Newtonian	0.0215γ				0.0215	54.76	10.294
Robertson and Stiff	$0.7874(28.2129 + \gamma)^{0.4537}$	0.7874	28.2129	0.4537		2.34	

Table C.4: Modelled equations for the Graphene Ref + 1.25 system

According to the deviation error, the best suited model for the Graphene Ref + 1.25 system is the Robertson and Stiff model with a deviation of 2.34%. The equation is presented in Table C.4.

Appendix C.5 – Comparison of the best rheological model and measurements

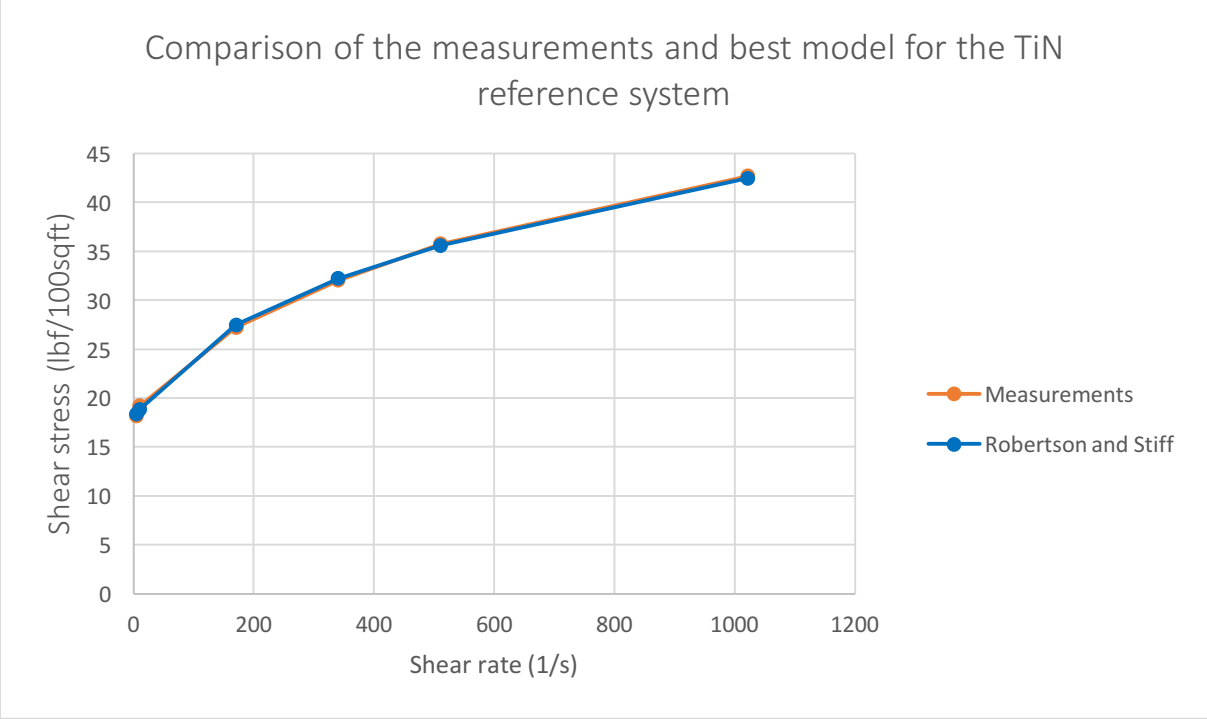

Figure C.5: Comparison of the measurements and best model for the TiN reference system

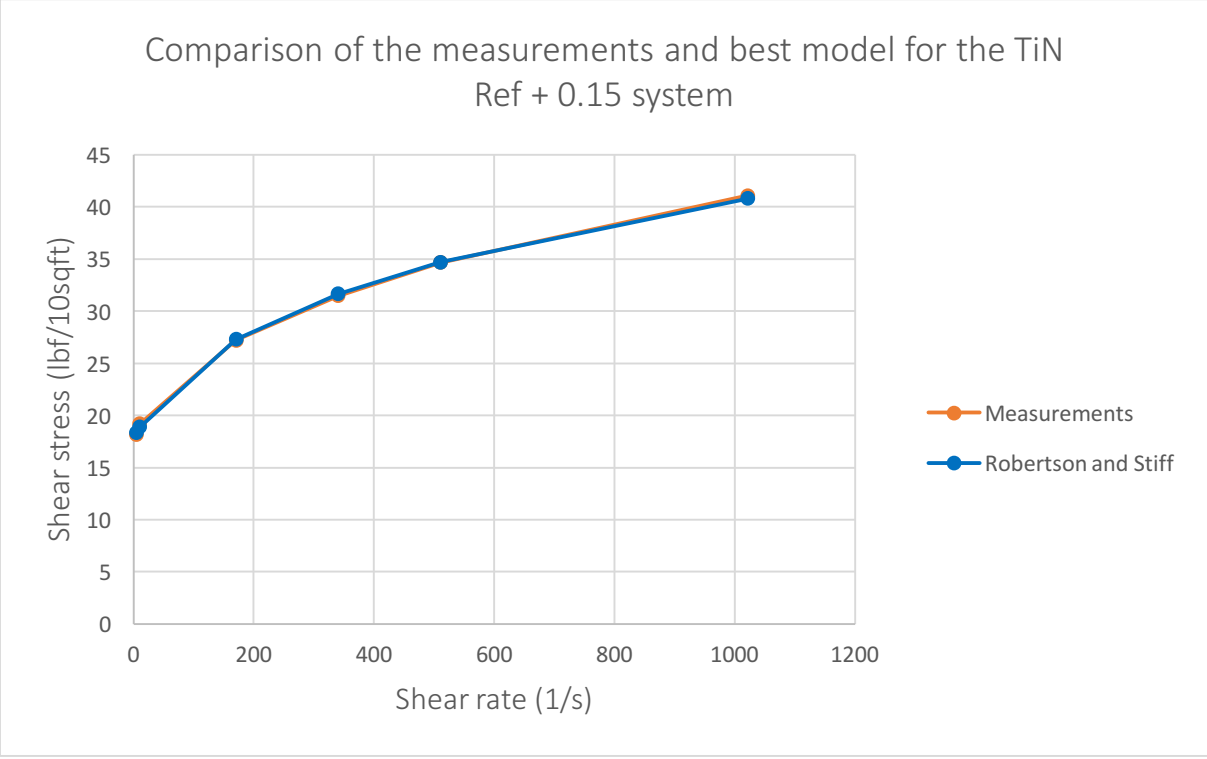

Figure C.6: Comparison of the measurements and the best model for the TiN Ref + 0.15 system

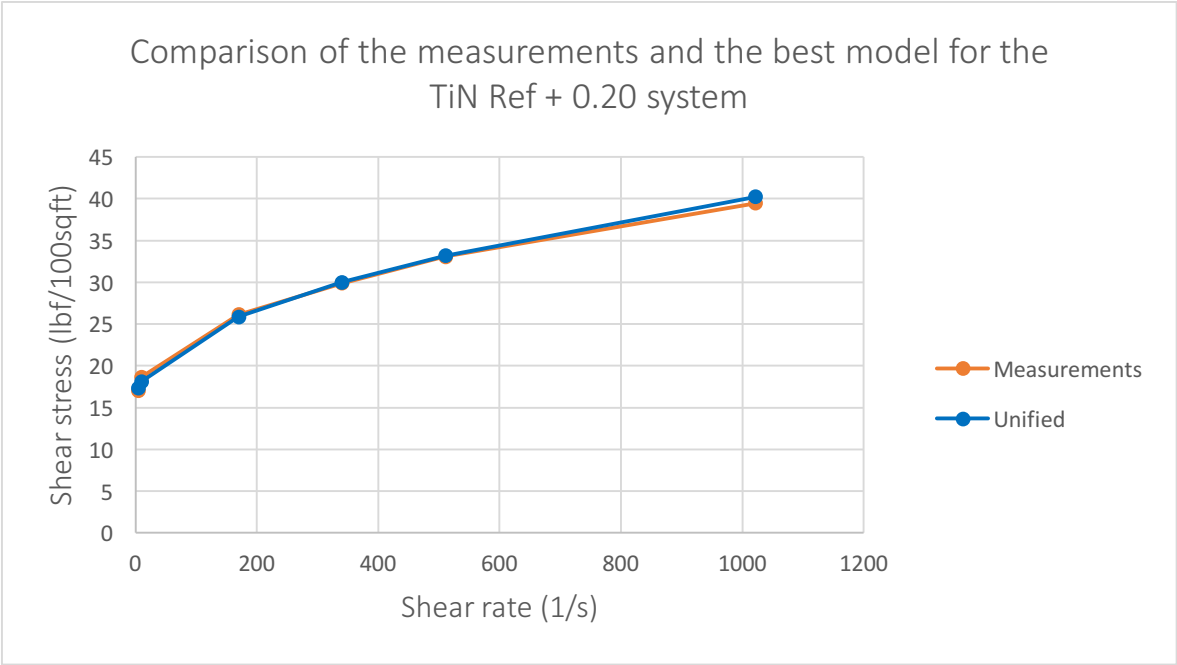

Figure C.7: Comparison of the measurements and the best model for the TiN Ref + 0.20 system

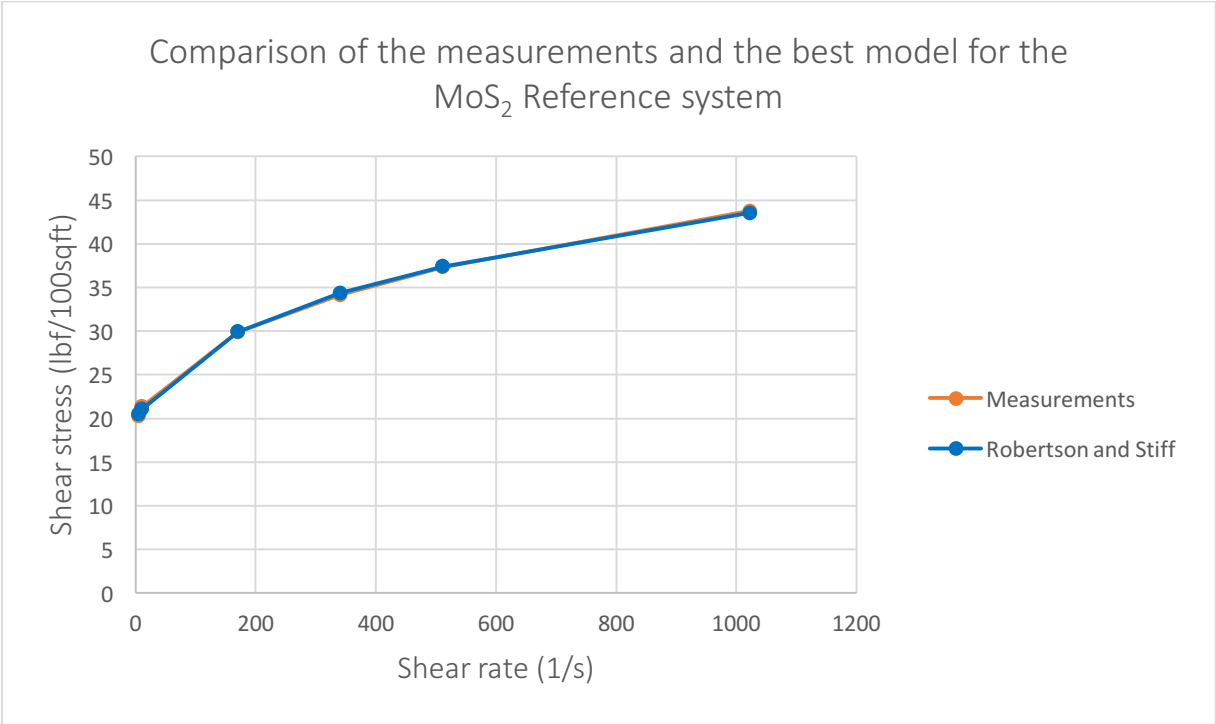

Figure C.8: Comparison of the measurements and the best model for the MoS_2 Ref system

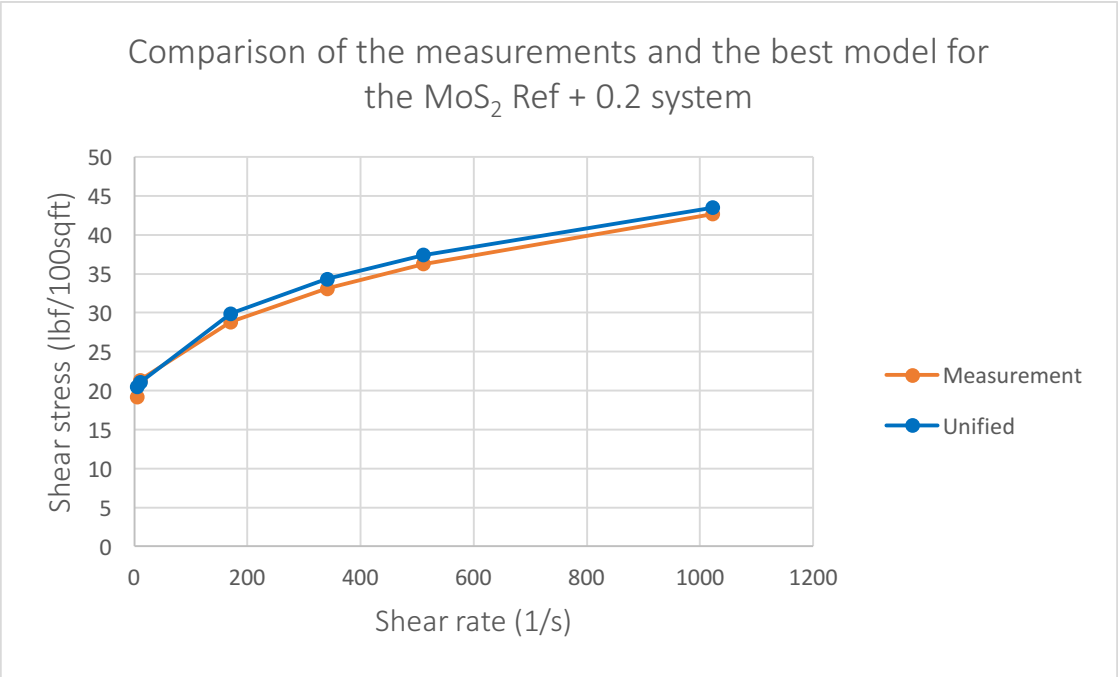

Figure C.9: Comparison of the measurements and the best model for the MoS_2 Ref + 0.2 system

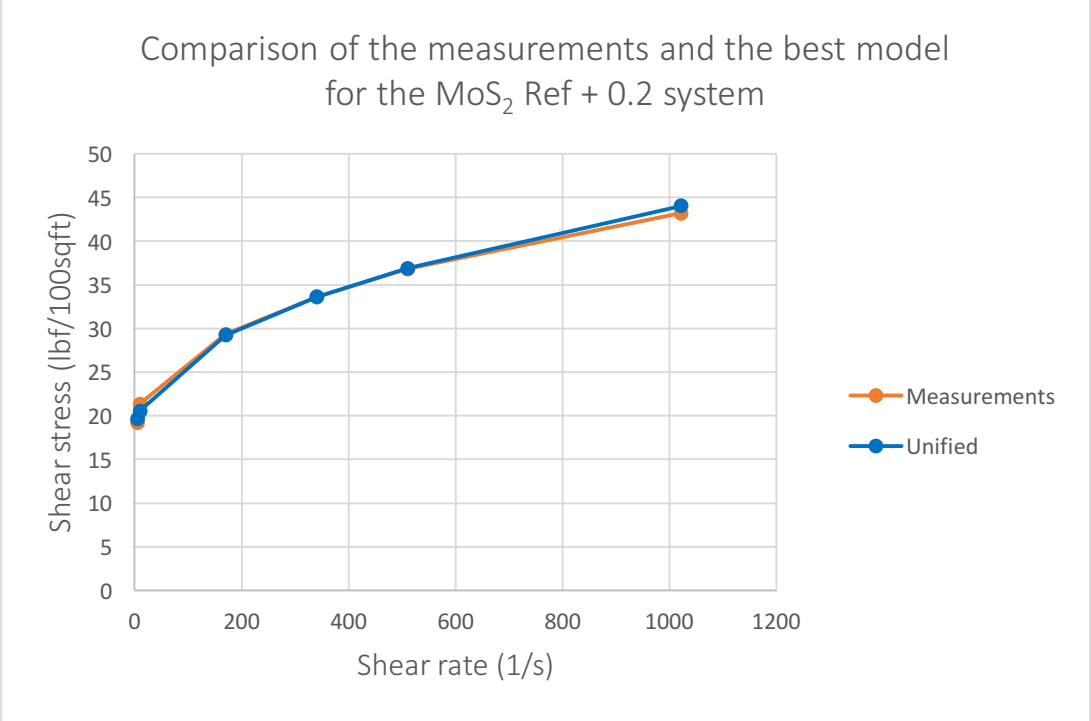

Figure C.10: Comparison of the measurements and the best model for the MoS_2 Ref + 0.8 system

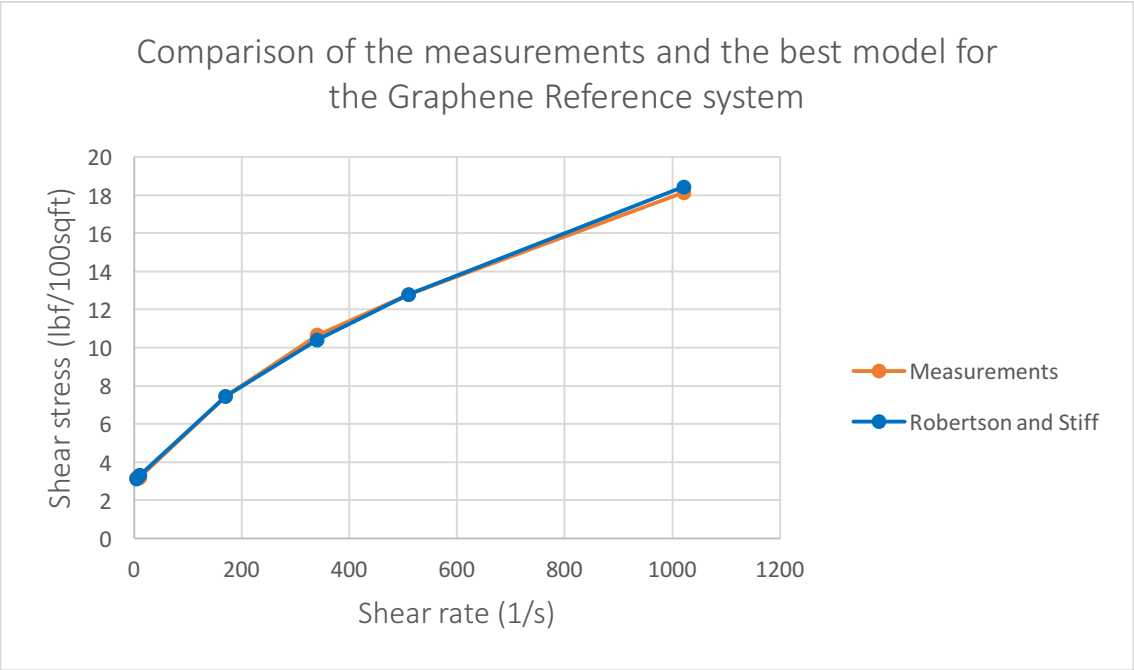

Figure C.11: Comparison of the measurements and the best model for the Graphene Ref system

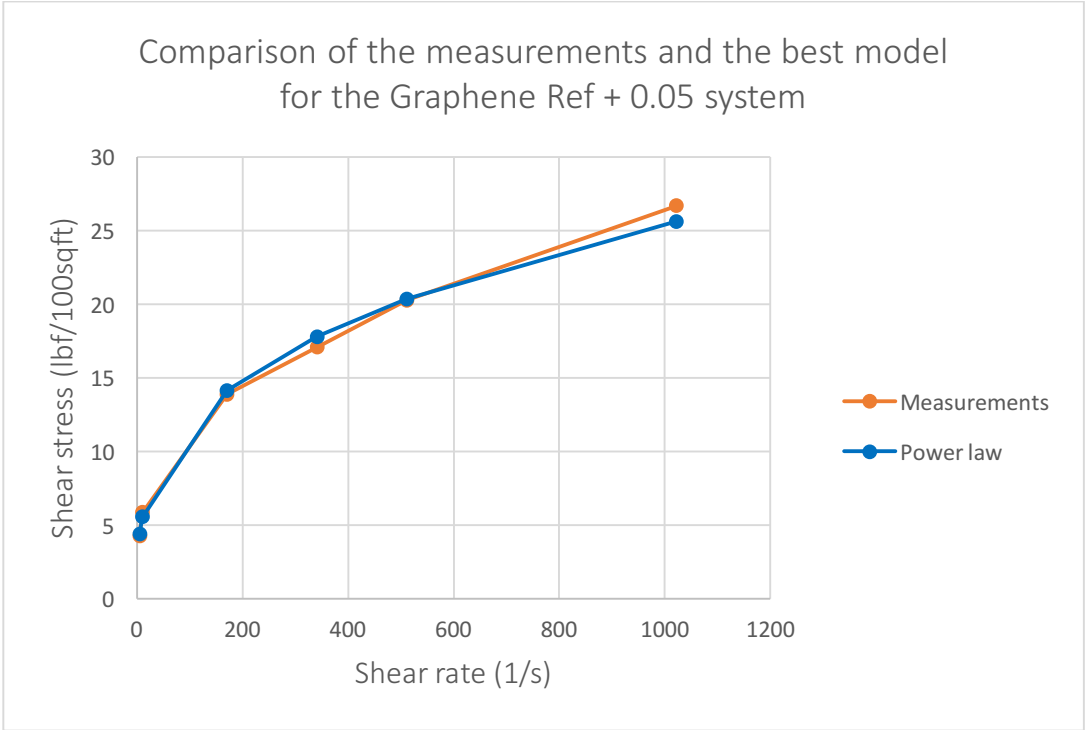

Figure C.12: Comparison of the measurements and the best model for the Graphene Ref + 0.05 system

Appendix D – Torque and Drag simulation

Appendix D.1 – Torque and Drag Simulation for the TiN Drilling Fluids

Comparisons of the Torque and drag simulations for the TiN drilling fluids			
Parameters	Ref	Ref + 0.15	Ref + 0.2
MD (ft)	13123	15020	14423
Change length (ft)		1897	1300
% Change		14.5	9.9
Torque tripping in (ft-lb)	17431.2	13527.9	14639.4
% Change		22.4	16.0
Torque tripping out (ft-lb)	20242.3	15162.3	15572.4
% Change		25.1	23.1
Drag tripping in (kip)	259.2	264.2	262.8
% Change		1.9	1.4
Drag tripping out (kip)	307.5	301	302.8
% Change		2.1	1.5

Table D.1: Comparisons of the Torque and drag simulations for the TiN drilling fluids

Appendix D.2 – Torque and Drag Simulation for the MoS_2 Drilling Fluids

Comparisons of the Torque and drag simulations for the MoS_2 drilling fluids			
Parameter	Ref	Ref + 0.2	Ref + 0.8
MD (ft)	13123	15123	16523
Change length (ft)		2000	3400
% Change		15.2	25.9
Torque tripping in (ft-lb)	17371.3	11651.2	9935.9
% Change		32.9	42.8
Torque tripping out (ft-lb)	20161.5	12843.6	10790.2
% Change		36.3	46.5
Drag tripping in (kip)	259.3	266.6	268.8
% Change		2.8	3.7
Drag tripping out (kip)	307.4	298	295.4
% Change		3.1	3.9

Table D.2: Comparisons of the Torque and drag simulations for the MoS_2 drilling fluids

Appendix D.3 – Torque and Drag Simulation for the Graphene Drilling Fluids

Comparisons of the Torque and drag simulations for the Graphene drilling fluids			
Parameter	Ref	Ref + 0.05	Ref + 0.1
MD (ft)	9923	10323	10393
Change length (ft)		400	470
% Change		4.0	4.7
Torque tripping in (ft-lb)	16684.5	15426.9	15124.7
% Change		7.5	9.3
Torque tripping out (ft-lb)	20079.3	18286	17863.1
% Change		8.9	11.0
Drag tripping in (kip)	201.8	203.4	203.8
% Change		0.8	1.0
Drag tripping out (kip)	248.4	246.1	245.6
% Change		0.9	1.1

Table D.3: Comparisons of the Torque and drag simulations for the Graphene drilling fluids

Appendix E – Hydraulic performance simulation

Appendix E.1 – Hydraulic Performance of the TiN Drilling Fluids

Annular pressure loss (psi)				
Q (gpm)	Ref	Ref + 0.15	Ref + 0.2	Ref + 2.5
1	304.9	294.4	276.2	251.8
50	353.9	344.9	323.8	318.0
100	376.7	367.6	345.6	347.9
150	394.1	384.6	362.1	370.4
200	408.6	398.8	375.9	389.2
250	421.3	411.1	387.9	405.5
300	432.8	422.2	398.7	420.2
350	443.3	432.3	408.6	433.6
400	453.1	441.7	417.8	446.1
450	462.2	450.4	426.4	457.7
500	470.9	458.7	434.5	468.6
550	479.0	466.5	442.2	479.0
600	486.9	473.9	449.5	488.8

Table E.1: Calculated annular pressure loss values for the TiN drilling fluids in the simulation well

Pump pressure loss (psi)				
Q (gpm)	Ref	Ref + 0.15	Ref + 0.2	Ref + 2.5
1	476.7	464.3	433.0	390.9
50	602.7	590.3	551.9	533.1
100	650.8	637.2	597.1	589.9
150	686.9	672.3	631.2	632.6
200	717.8	702.3	660.5	669.1
250	746.1	729.6	687.3	702.2
300	772.9	755.5	712.7	733.4
350	798.9	780.7	737.5	763.3
400	824.6	805.6	762.1	792.7
450	850.2	830.5	786.7	821.8
500	876.2	855.7	812.1	851.5
550	904.5	883.4	842.3	890.7
600	940.8	917.7	882.4	946.8

Table E.2: Calculated total pressure loss values for the TiN drilling fluids in the simulation well

Appendix E.2 – Hydraulic Performance of the MoS_2 Drilling Fluids

Annular pressure loss (psi)				
Q (gpm)	Ref	Ref + 0.2	Ref + 0.5	Ref + 0.8
1	340.4	303.4	303.6	303.6
50	389.8	360.4	353.8	363.9
100	412.2	385.0	376.5	389.5
150	429.0	403.2	393.5	408.3
200	443.0	418.2	407.6	423.8
250	455.2	431.3	419.9	437.2
300	466.2	442.9	431.0	449.1
350	476.3	453.5	441.1	460.0
400	485.5	463.3	450.4	470.0
450	494.2	472.4	459.2	479.2
500	502.4	481.0	467.4	487.9
550	510.2	489.1	475.2	496.2
600	517.6	496.8	482.6	504.0

Table E.3: Calculated annular pressure loss values for the MoS_2 drilling fluids in the simulation well

Pump pressure loss (psi)				
Q (gpm)	Ref	Ref + 0.2	Ref + 0.5	Ref + 0.8
1	539.4	482.8	479.2	484.9
50	671.1	619.3	606.4	626.1
100	718.9	669.0	653.5	677.0
150	754.5	705.6	688.7	714.4
200	784.8	736.8	718.8	746.1
250	812.3	765.0	746.1	774.7
300	838.4	791.7	772.1	801.7
350	863.7	817.5	797.3	827.8
400	888.7	842.9	822.2	853.4
450	913.7	868.2	847.1	879.0
500	938.9	893.8	872.3	904.7
550	964.8	920.6	899.4	931.5
600	993.4	951.8	932.1	962.1

Table E.4: Calculated total pressure loss values for the MoS_2 drilling fluids in the simulation well

Appendix E.3 - Hydraulic Performance of the Graphene Drilling Fluids

Annular pressure loss (psi)					
Q (gpm)	Ref	Ref + 0.05	Ref + 0.1	Ref + 0.2	Ref + 1.25
1	60.8	56.6	100.9	60.8	60.6
50	76.3	109.5	169.5	76.3	88.7
100	85.9	132.9	195.6	85.9	102.1
150	93.9	150.4	214.3	93.9	112.4
200	101.0	164.9	229.3	101.0	121.0
250	107.4	177.5	242.2	107.4	128.6
300	113.5	188.8	253.4	113.5	135.5
350	119.1	199.1	263.6	119.1	141.8
400	124.5	208.6	272.8	124.5	147.6
450	129.8	217.5	281.4	129.8	153.1
500	138.8	225.8	289.4	138.8	158.3
550	161.3	233.8	296.9	161.3	164.0
600	187.3	241.3	303.9	187.3	174.1

Table E.5: Calculated annular pressure loss values for the Graphene drilling fluids in the simulation well

Pump pressure loss (psi)					
Q (gpm)	Ref	Ref + 0.05	Ref + 0.1	Ref + 0.2	Ref + 1.25
1	89.0	86.4	159.0	89.0	92.0
50	120.9	173.1	275.7	120.9	144.0
100	140.0	211.6	319.3	140.0	168.4
150	156.8	241.8	351.8	156.8	188.3
200	173.1	268.4	379.6	173.1	206.5
250	206.7	293.2	404.9	206.7	224.7
300	255.8	321.1	429.0	255.8	263.7
350	301.7	374.9	452.7	301.7	141.8
400	350.4	427.8	484.5	350.4	351.4
450	402.5	481.8	529.5	402.5	398.4
500	461.7	538.2	579.7	461.7	448.0
550	537.7	597.1	632.9	537.7	500.9
600	620.5	658.6	688.4	620.5	560.9

Table E.6: Calculated total pressure loss values for the Graphene drilling fluids in the simulation well

11 List of Figures

12 List of Tables

13 List of Abbreviations

WBM	Water Based Mud
OBM	Oil Based Mud
ROP	Rate of Penetration
HPHT	High Pressure High Temperature
NCS	Norwegian Continental Shelf
NPT	Non Productive Time
ECD	Equivalent Circulation Density
CMC	Carboxymethylcellulose
XG	Xanthan Gum
PAL	Palygorskite
LPLT	Low Pressure Low Temperature
BHA	Bottom Hole Assembly
LCM	Loss Circulation Material
PV	Plastic Viscosity
YS	Yield Strength
YP	Yield Point
LSYS	Lower Shear Yield Stress
LVER	Linear Viscoelastic Region
POOH	Pulling Out of Hole
RIH	Running into Hole
RPM	Rounds per Minute
Ref	Reference
MD	Measured Depth
OD	Outer Diameter
ID	Inner Diameter
kip	1000-pounds force
gpm	Gallon per minute
ft-lb	Foot-Pound (energy unit)

14 List of Nomenclature

ΔP	Differential Pressure
P_m	Hydrostatic Well Pressure
P_{ff}	Formation Fluid Pressure
F_p	Pull Force
μ_f	Coefficient of Friction
A_c	Contact Area between Pipe and Filtrate Cake
τ	Shear Stress
γ	Shear Rate
μ	Fluid Viscosity
Re	Reynolds Number
ρ	Fluid Density
$\overline{V}$	Mean Fluid Velocity
D	Pipe Diameter
θ	RPM
θ_{600}	600 RPM
θ_{300}	300 RPM
θ_{200}	200 RPM
θ_{100}	100 RPM
θ_{60}	60 RPM
θ_{30}	30 RPM
θ_6	6 RPM
θ_3	3 RPM
V	Reading in Field Units
μ_p	Plastic Viscosity
τ_y	Yield Point
k	Consistency Index
n	Flow Behaviour/Power Law Index
τ_0	Yield Stress
τ^*	Geometric Mean of the Shear Stress

γ^*	Geometric Mean of the Shear Rate
τ_{yL}	Lower Shear Yield Point
A	Consistency Index for the Robertson and Stiff Model
B	Flow Behaviour Index for the Robertson and Stiff Model
C	Correction Factor for the Robertson and Stiff Model
G'	Elastic/Storage Modulus
G''	Viscous/Loss Modulus
δ	Phase Angle
θ	Inclination of Plane
F	Tangential Force
φ	Azimuth
ω	Axial Weight Components
β	Buoyance Factor
S	String segments
F_i	Bottom Weight
ΔT	Increment Torque
r	Rotating Radius
ΔS	Length Change
N_i	Contact Force
ΔP_{surf}	Pressure Loss Through Surface Equipment
$\Delta P_{drillstring}$	Pressure Loss Through Drill-string
ΔP_{bit}	Pressure Loss Through Drill Bit
$\Delta P_{annulus}$	Pressure Loss Through Annulus
$\Delta P_{dsannulus}$	Pressure Loss Through Drill-string Annulus
ΔP_{tot}	Total Pressure Loss
D_{TVD}	Total Vertical Depth
MW	Mud Weight
T	Temperature

15 List of Chemical Compounds

KCl	Potassium Chloride
TiN	Titanium Nitride
MoS_2	Molybdenum Disulphide
CuO	Copper Oxide
ZnO	Zinc Oxide
CO_2	Carbon Dioxide
N_2	Nitrogen in gas state
$CaCO_3$	Calcium Carbonate